Dynamic Mechanical Regulation of Cells in 3D Microtissues

Matthew Walker

Thesis submitted to the University of Ottawa in partial fulfillment of the requirements for Doctor of Philosophy in Biology.

Department of Biology
Faculty of Science
University of Ottawa

Abstract

It has been well established that the fundamental behaviors of mammalian cells are influenced by the physical cues that they experience from their surrounding environment. With respect to cells in our bodies, mechanically-driven morphological and phenotypic changes to our cells have been linked to responses critical to both normal development and disease progression, including lung, heart, muscle and bone disorders, and cancer. Although significant advancements to our understanding of cell behavior have been made using 2D cell culture methods, questions regarding how physical stretch guides cell behavior in more complex 3D biological systems remain unanswered. To address these questions, we used microfabrication techniques to develop vacuum-actuated stretchers for high throughput stretching and dynamic mechanical screening of 3D microtissue cultures. This thesis contains five research chapters that have utilized these devices to advance our understanding of how cells feel stretch and how it influences their behavior in a 3D matrix. In the first research chapter (chapter 2), we characterized how stretch is transferred from the tissue-level to the single-cell level and we investigated the cytoskeletal reinforcement response to long-term mechanical conditioning. In the second research chapter (chapter 3), we examined the effects of an acute dynamic stretch and found that 3D cultures soften through actin depolymerization to homeostatically maintain a mean tension. This softening response to stretch may lengthen tissues in our body, and thus may be an important mechanism by which airway resistance and arterial blood pressure are controlled. In the third and forth research chapters (chapter 4-5), we investigated the time dependencies of microtissues cultures and we found that their behavior differed from our knowledge of the rheological behavior of cells in 2D culture. Microtissues instead followed a stretched exponential model that seemed to be set by a dynamic equilibrium between cytoskeletal assembly and disassembly rates. The difference in the behavior from cells in 2D may reflect the profound changes to the structure and distribution of the cytoskeleton that occur when cells are grown on flat surfaces vs. within a 3D environment. In the fifth and final research chapter (chapter 6), we examined how mechanical forces may contribute to the progression of tissue fibrosis through activating latent TGF-β1. Our results suggest that mechanical stretch contributes to a feed forward loop that preserves a myofibroblastic phenotype. Together these investigations further our understanding of how cells respond to mechanical stimuli within 3D environments, and thus, mark a significant contribution to the fields of mechanobiology and cell mechanics.

Statement of Originality

To the best of the author's knowledge, the work presented throughout this thesis is, in its entirety, original. Research was performed and the manuscript was prepared under the supervision of Dr. Andrew Pelling in the Center for Interdisciplinary Nanophysics Laboratories in the Department of Physics at the University of Ottawa. The thesis starts with an introductory review briefly covering the topics prudent to the reader's understanding of the thesis. It is followed by experimental research manuscripts (Chapters 2-6) that have been published or prepared for peer-review at scientific journals. Each of these chapters begins with a brief overview of the motivation, and objectives. Lastly, this thesis ends with a discussion of future directions and implications of this work (Chapter 7).

Manuscripts included in this thesis:

- **Walker, M.,** Godin, M. & Pelling, A. E. A vacuum-actuated microtissue stretcher for long-term exposure to oscillatory strain within a 3D matrix. *Biomed. Microdevices* **20,** 43 (2018).

- **Walker, M.,** Rizzuto, P., Godin, M. & Pelling, A. E Structural and mechanical remodeling of the cytoskeleton maintains tensional homeostasis in 3D microtissues under acute dynamic stretch. (Manuscript accepted at Scientific Reports)

- **Walker, M.,** Godin, M., Harden, J., & Pelling, A. E. Time dependencies in the dynamical mechanical behavior of 3D microtissue cell cultures. (Manuscript under review at APL Bioengineering)

- **Walker, M.,** Godin, M., Harden, J., & Pelling, A. E. The rheological behavior of microtissues under oscillatory loading is consistent with a stretched exponential. (Manuscript prepared for submission to APL Bioengineering)

- **Walker, M.,** Godin, M., & Pelling, A. E. Mechanical stretch sustains myofibroblast phenotype and function in microtissues through latent TGF-β1 activation. (Manuscript under review Integrative Biology)

Conference presentations:

- **Walker, M.,** Godin, M. & Pelling, A. E. Time-Scale and Other Dependencies in 3D Cell Culture Mechanics. BMES Annual Meeting. 2018. (Talk)

- **Walker, M.,** Godin, M. & Pelling, A. E. Dynamic Mechanics of Microtissues Investigated Using a Novel Vacuum Actuated Stretcher. BMES Annual Meeting. 2018. (Poster)

Other Contributions

Contributions to other manuscripts (not covered in this thesis):

- **Walker, M.**, Chagnon-Lessard, S., Godin, M., Pelling, A.E. Intercellular calcium dynamics following targeted cell wounding. (Manuscript in preparation)

- Gullekson, C., **Walker, M**., Harden, J. L. & Pelling, A. E. Measuring mechanodynamics in an unsupported epithelial monolayer grown at an air-water interface. *Mol. Biol. Cell* **28,** 111–119 (2017).

Statement of Contributions

I, Matthew Walker, contributed the vast majority of the work presented in this thesis. The work involved includes the microstretcher designs, microfabrication (photolithography, soft lithography and assembly), electronic vacuum regulator setup and programming (Labview), cell culture, experiments using the microstretchers, confocal microscopy, image and data analysis (with custom written Matlab and Labview programs for measuring the strain field, tissue mechanics, and cytoskeletal remodeling), and statistical analysis. I am the first author and primarily wrote the scientific manuscripts included here (Chapters 2-6).

This work could not have been completed if it were not for the contributions of other researchers. Dr. Andrew Pelling contributed to the direction and editing of all manuscripts. Dr. Michel Godin lent me the use of his microfabrication facilities and contributed to editing of all manuscripts. Dr. James Harden aided in experimental design and edited the manuscripts regarding the time dependencies of 3D cell cultures (Chapters 4-5). Pauline Rizzuto, a visiting summer student from the University of Côte d'Azur, collected strain-softening data with myoblast cell cultures under my supervision (Chapter 3).

Acknowledgements

First, and foremost, I would like to thank Dr. Andrew E. Pelling for giving me the opportunity to join his group and for his mentorship throughout my development as a researcher. I consider myself extremely fortunate to have spent these past years in such a diverse exploratory environment under his supervision. His fearlessness to challenge dogmas and his curiosity-driven investigative approach were vital to the completion of this work. I would also like to thank Dr. Michel Godin and Dr. James Harden for their encouragement and input they gave to me throughout my journey.

Of course, I would like to sincerely thank all of the members of the Pelling Lab. You made these years spent inside a dimly lit room over a microscope not just tolerable, but fun. I deeply cherish the friendships that we have built.

To my family, I thank you so much for your loving support and encouragement throughout the (too) many years of my education. I am lucky to have you.

Most importantly, I would I like thank Adriana, for showing me how to make PFA on a Saturday morning. Meeting you was one of the best things to have happened to me and I am very grateful that we are sharing our lives together. I cannot thank you enough for all that you have done for me.

List of Abbreviations

- AFM – atomic force microscopy
- ADP – adenosine diphosphate
- ATP – adenosine triphosphate
- CytoD – cytochalasin D (actin polymerization inhibitor)
- C2C12 – myoblast cell line
- DMEM – Dulbecco's Modified Eagle's medium
- DMSO – dimethylsulfoxide
- D_p – poroelastic diffusion constant
- D12 – HASM cell line
- ECM – extracellular matrix
- E – elastic or Young's modulus
- eGFP/GFP – enhanced green fluorescent protein
- FA – focal adhesion
- F-actin – filamentous actin
- FAK – focal adhesion kinase
- FBS – fetal bovine serum
- FC – focal complex
- FFT – Fourier transform
- FILGAP - filamin-GTPase-activating protein
- fps – frames per second
- G – shear modulus
- G-actin – globular actin
- GAP - GTPase-activating proteins
- GDP – guanosine diphosphate
- GEF –guanosine nucleotide exchange factor
- GTP – guanosine triphosphate
- GW – GW788388 (TGF-βRI inhibitor)
- HASM – human airway smooth muscle
- IF – intermediate filaments
- K – hydraulic permeability
- k - stiffness
- LAP – Latency-associated peptide
- LARG - Leukemia-associated Rho GEF
- LSCM – laser scanning confocal microscopy
- LTBP – Latent TGFβ binding protein
- mDia – mammalian diaphanous
- MHC – myosin heavy chain
- MLC – myosin light chain
- MLCK – myosin light chain kinase
- MT – microtubules
- m – meter (unit)
- NA – numerical aperture
- NIH3t3 – fibroblast cell line
- Noco – nocodazole (microtubule polymerization inhibitor)
- N – newton (unit)
- OMTC –optical magnetic twisting cytometry
- Pa - Pascal (unit)
- PBS – phosphate buffered saline
- PDMS – polydimethylsiloxane
- PFA – paraformaldehyde
- q – filtration velocity
- RhoA – ras homolog gene family (member A)
- Rock – Rho-associated protein kinase
- ROI – region of interest
- SEM – standard error of the mean
- SD – standard deviation
- SGR – soft glassy rheology
- SLS – standard linear solid
- TGFβ-1 – transforming growth factor Beta1
- TX – triton X-100 (reagent)
- α-SMA – α-smooth muscle actin
- x – noise temperature
- B –power law constant (dimensionless)
- δ - phase lag
- Γ – gamma function
- ε - strain
- η –viscosity
- ν – Poisson's ratio
- ξ –pore radius
- σ - stress
- τ – time constant
- ω – radian frequency
- φ – porosity

Table of Contents

ABSTRACT ..... **II**

STATEMENT OF ORIGINALITY ..... **III**

OTHER CONTRIBUTIONS ..... **IV**

STATEMENT OF CONTRIBUTIONS ..... **V**

ACKNOWLEDGEMENTS ..... **VI**

LIST OF ABBREVIATIONS ..... **VII**

TABLE OF CONTENTS ..... **VIII**

LIST OF FIGURES ..... **X**

LIST OF TABLES ..... **XIII**

CHAPTER 1| INTRODUCTION **1**

FORWARD 1

1.1 A PART LIST FOR CELL MECHANICS AND MECHANOSENSING 3

1.2 MICRO-RHEOLOGY 6

1.3 MECHANICAL MODELS OF CELL BEHAVIOR 7

1.4 THEORETICAL FOUNDATIONS OF MICRORHEOLOGY MODELS 11

1.5 THE EXTRACELLULAR ENVIRONMENT AND 3D CELL CULTURE TECHNIQUES 14

1.6 MECHANOTRANSDUCTION: ASSEMBLING THE PARTS 15

1.7 PERSPECTIVES ON OUR UNDERSTANDING OF MECHANOTRANSDUCTION 18

1.8 MECHANICAL FORCES IN FIBROSIS: APPLICATIONS OF MECHANOSENSING 19

1.9 CONCLUSIONS AND THESIS OUTLINE 20

CHAPTER 2| A VACUUM-ACTUATED MICROTISSUE STRETCHER FOR LONG-TERM EXPOSURE TO OSCILLATORY STRAIN WITHIN A 3D MATRIX **24**

2.1 ABSTRACT 24

2.2 INTRODUCTION 24

2.3 METHODS 26

2.4 RESULTS 30

2.5 DISCUSSION 35

2.6 CONCLUSIONS 36

CHAPTER 3| STRUCTURAL AND MECHANICAL REMODELING OF THE CYTOSKELETON MAINTAINS TENSIONAL HOMEOSTASIS IN 3D MICROTISSUES UNDER ACUTE DYNAMIC STRETCH **38**

3.1 ABSTRACT 38

3.2 INTRODUCTION 39

3.3 METHODS 41

3.4 RESULTS 44

3.5 DISCUSSION 52

3.6 CONCLUSIONS 56

CHAPTER 4| TIME DEPENDENCIES IN THE DYNAMICAL MECHANICAL BEHAVIOR OF 3D MICROTISSUE CELL CULTURES **57**

4.1 ABSTRACT 57

4.2 INTRODUCTION 58

4.3 METHODS 59
4.4 RESULTS 61
4.5 DISCUSSION 70
4.6 CONCLUSIONS 73

CHAPTER 5| THE RHEOLOGICAL BEHAVIOR OF MICROTISSUES UNDER OSCILLATORY LOADING IS CONSISTENT WITH A STRETCHED EXPONENTIAL 75
5.1 ABSTRACT 75
5.2 INTRODUCTION 75
5.3 METHODS 77
5.4 RESULTS 79
5.5 DISCUSSION 87
5.6 CONCLUSIONS 91

CHAPTER 6| MECHANICAL STRETCH SUSTAINS MYOFIBROBLAST PHENOTYPE AND FUNCTION IN MICROTISSUES THROUGH LATENT TGF-B1 ACTIVATION 93
6.1 ABSTRACT 93
6.2 INTRODUCTION 94
6.3 METHODS 95
6.4 RESULTS 97
6.5 DISCUSSION 103
6.6 CONCLUSIONS 105

CHAPTER 7| CONCLUSIONS & FUTURE DIRECTIONS 106

APPENDIX A| SUPPLEMENTARY INFORMATION OF CHAPTER 2 109
SUPPLEMENTARY NOTE 109
ADDITIONAL FIGURES 110
ELECTRONIC SUPPLEMENTARY INFORMATION 111

APPENDIX B| SUPPLEMENTARY INFORMATION OF CHAPTER 3 112
ADDITIONAL FIGURES 112
SUPPLEMENTARY NOTE 117
ELECTRONIC SUPPLEMENTARY INFORMATION 119

APPENDIX C| SUPPLEMENTARY INFORMATION OF CHAPTER 4 120
ADDITIONAL FIGURES 120

APPENDIX D| SUPPLEMENTARY INFORMATION OF CHAPTER 5 127
ADDITIONAL FIGURES 127

APPENDIX E| SUPPLEMENTARY INFORMATION OF CHAPTER 6 130
ADDITIONAL FIGURES 130

REFERENCES 131

List of Figures

Fig. 1.1 The cytoskeleton in mammalian cells 4

Fig. 1.2 Models of the mechanical behavior of the cell 8

Fig. 1.3 Cells feel forces through focal adhesions 16

Fig. 2.1: MVAS device assembly 27

Fig. 2.2: Representative microtissues after four days 30

Fig. 2.3: Bulk Strain Characterization 31

Fig. 2.4: Tissue strain field 32

Fig. 2.5: Cellular strain 33

Fig. 2.6: Cytoskeletal remodeling in response to chronic cyclic strain 34

Fig. 3.1: The MVAS-Force allows high throughput dynamic mechanical measurements of 3D cell cultures 41

Fig. 3.2: 3T3 fibroblast microtissues strain soften to maintain a constant mean stress 46

Fig. 3.3: Adaptation to oscillatory loading depends upon the loading frequency 47

Fig. 3.4: Softening requires an intact actin cytoskeleton 48

Fig. 3.5: Oscillatory stretch increases remodeling of actin filaments in living cells in 3D culture 48

Fig. 3.6: F-actin depolymerizes with stretching and repolymerizes upon stretch cessation 49

Fig. 3.7: Microtubules and myosin do not contribute to softening 50

Fig. 3.8: Strain softening is a conserved response among different microtissue cultures 52

Fig. 4.1: Microtissue tension dynamically relaxed and recovered with changes in length 62

Fig. 4.2: Stress relaxation and recovery in microtissues followed stretched exponential trajectories 63

Fig. 4.3: The rate of stress relaxation was nonlinear while recovery was strain invariant 65

Fig. 4.4: The locations of remodeling following changes to microtissue length were strain-dependent 67

Fig. 4.5: Stress relaxation and recovery varied with pharmacological disruption of the cytoskeleton and myosin inhibition 68

Fig. 4.7: The underlying relationships between microtissue dissipation and elasticity 71

Fig. 5.1: Microtissue cell cultures have a characteristic time-scale 80

Fig. 5.2: Fourier transforms of a stretched exponential for select time and power law constants 81

Fig. 5.3: The frequency response of microtissues shares the timescale dependencies of a stretched exponential model 83

Fig. 5.4: The time-scale behavior of microtissue cultures is produced by multiple components of the cytoskeleton 84

Fig. 5.5: The dynamic mechanical behavior of microtissues is strain-dependent 87

Fig. 5.6: Microtissues possess underlying relationships in their dynamic mechanical behavior throughout a range of pharmacological treatments 90

Fig. 6.1: TGF-β1 treatment contracts and stiffens microtissue cultures 98

Fig. 6.2: TGF-β1 induces myofibroblast differentiation of microtissues 99

Fig. 6.3: Myofibroblast differentiation is, in part, reversible but sustained through mechanical stretch 100

Fig. 6.4: TGF-β1 receptor inhibition prevents sustained myofibroblast differentiation through mechanical stretch 102

Fig. 6.5: Latent TGF-β1 is activated by mechanical stretch to promote myofibroblast differentiation 102

Fig. A.2: Single cell strain at 90kPa 110

Fig. A.3: Out of plane motion 111

Fig. B.1: The force-sensing cantilever spring constant and validation of MVAS-Force 112

Fig. B.2: MVAS-force assembly 113

Fig. B.3: Microtissue recovery shares similar dynamics across pharmacological treatments and cell types 114

Fig. B.4: Pharmacological responses 115

Fig. B.5: Strain softening does not depend upon myosin activity 116

Fig. B.6: Microtubules remodel under oscillatory stretching but polymerization does not change 117

Fig. C.1: MVAS-force validation for step strain measurements 120

Fig. C.2: Microtissue viscoelastic behavior is highly repeatable 121

Fig. C.3: Microtissue creep does not effect assessment of stress relaxation behavior 122

Fig. C.4: Microtissue stress recovery rate is strain independent 123

Fig. C.5: The fitting constants for microtissue stress relaxation at various step sizes 124

Fig. C.6: The fitting constants for microtissue stress recovery at various step sizes 124

Fig. C.7: Remodeling in the longitudinal direction following changes to microtissue length 125

Fig. C.8: Remodeling in the longitudinal direction following changes to microtissues length varies with pharmacological treatments …… 126

Fig. D.1: Strain amplitude characterization and validation of dynamic mechanical measurements with the MVAS-Force …… 127

Fig. D.2: The characteristic timescale of oscillatory measurements lies between the characteristic timescales of stress relaxation and recovery …… 128

Fig. D.3: The timescale behavior of microtissue prestress under various pharmacological treatments and strain amplitudes …… 129

Fig. E.1: Cyclic stretch does not contribute to myofibroblast differentiation in microtissues …… 130

List of Tables

Table 4.1: The stress relaxation and recovery fitting constants (N=79) …… 62

Table 4.2: The changes to stress relaxation fitting constants measured at 10.9% vs. 3.3% strain …….. 64

Table 4.3: The changes to stress recovery fitting constants measured at 10.9% vs. 3.3% strain …… 64

Table 4.4: The pharmacologically induced changes to stress relaxation and recovery fitting constants …….. 67

Table 5.1: The fitting constants to the frequency response of microtissues under small strain amplitudes …… 79

Table 5.2: The fitting constants to the frequency response following pharmacological disruption of the cytoskeleton or myosin inhibition …… 82

Table 5.3: The fitting constants to the frequency response under small and large amplitude strains …… 83

CHAPTER 1| INTRODUCTION

Forward

Our lives would be quite different if it were not for the physical abilities of our cells to dynamically contract, divide, and migrate. Arguably such physical and dynamic tasks have been the greatest necessity for all living matter from the time when life first wriggled through the mud on the floor of a shallow ocean three billion years ago. Because these distinguishing features of living matter are gained from the continuous turnover of the cytoskeletal structure and through active force generation by motor proteins, these abilities form a fundamental link between mechanics and biology. More to that point, it is now well recognized that cell behavior is not only a product of biochemical signaling, but rather, it is also determined by a vast assortment of mechanical stimuli, including tension, stiffness, shear and stretch [1–3]. This ability for cells to feel and react to mechanical stimuli in their microenvironment has been linked to crucial events in normal development and function, as well as the progression of numerous diseases [4–6]. The goals of this thesis were to work towards developing new tools to study mechanobiology, and in using these tools, gain insights into how the dynamic physical properties of cells in tissues are determined from specific cytoskeletal proteins and how cell behavior is regulated by physical forces in both health and disease.

In the body, cells experience a dynamic assortment of tissue-specific physical stimuli, which along with biochemical signaling regulate their behaviors to maintain homeostasis. These mechanical regulators include the passive characteristics of the extracellular matrix (ECM), such as stiffness and topography, and as well dynamic signals from stretching, shearing and compressing [1–3]. For example, cyclic stretch is felt by airway cells due to lung expansion during breathing [7–9], as well as cells in the vasculature from pulsatile blood flow [10,11]. In addition whole body movements, such as walking, also apply compression and tensile loads to cartilage, muscles, tendons and bone. There are countless other examples (ie. shear stress from blood flow along vessel walls and sound waves in our inner ear, and compression from touch etc.). In fact, most cells in the body experience stretch or compression to a certain degree [12].

In the current paradigm, cells sense these abovementioned forces through conformational changes in their proteins [1,13–15]. For example, forces open membrane ion channels in cardiomyoctes to regulate cellular electrical activity in response to changes in the contractile function or volume load of the heart [16]. Forces may also be sensed through changes to binding affinities for proteins that interact with matrix adhesions and the cytoskeleton, and thereby, regulate further signaling cascades that control cell behavior [1,3,13,17]. This process through which mechanical forces are converted into biochemical signals is referred to as mechanotransduction.

This ability for cells to feel and react to mechanical stimuli in their environment has been linked to crucial events in normal development and function. In particular, it is now commonly believed that tissue morphogenesis and patterning in embryos is, in part, driven by mechanical cues [4,18]. For example, high shear fluid flow stresses have been shown critical in various stages of heart development in zebrafishes, and conversely, deformities similar

to congenital cardiac diseases in humans, such as defective valves or abnormal chamber growth, may result from changes to the flow pattern [19]. Stem cell differentiation into cells with specialized functions is also directed by the stiffness, topology and strain in the ECM [20–23]. There are numerous examples of forces regulating cell function in mature organisms as well. To name a few: our bones grow and remodel according to compressive loads [24]; cyclic stretching from breathing decreases airway smooth muscle contractility, which leads to increased airway diameters [7,8]; and lastly, endothelial cell migration during angiogenesis, the creation of new blood vessels, is directed by intravascular pressure and shear stress [25]. In more general terms, mechanical stimuli are regulators of fundamental cell functions, including protein synthesis, apoptosis, proliferation, migration, differentiation, and contractility [1,2,4,18,21].

Conversely, dysregulation of the ability for cells to feel mechanical forces is now believed to be a common feature shared in the pathogenesis of a number of diseases, including bone, muscle, heart and lung disorders, and cancer [5,6]. For instance, increased ECM stiffness contributes to the activation of myofibroblasts in fibrotic tissues [26–28]. Increased ECM stiffness, and dynamic stretch and has also been linked to smooth muscle hyperplasia and increased contractile function in asthmatic airways[29,30]. Because mechanical stimuli play such a prevalent role in health and disease, there is an urgent need to identify the underlying molecular mechanisms of how cells sense forces. However, despite increasing efforts to integrate mechanics with biological and medical research, much remains to be discovered. Continued investigation into mechanotransduction is required, as these force-sensing mechanisms may provide pivotal molecular targets for new therapeutic approaches.

In addition to mechanical forces, the 3D network of structural and signaling molecules that make up the ECM is critical to regulating cell behavior in the body. Within this network cells interact and form adhesions with their environment in 3D dimensions. In turn, the cytoskeleton is fundamentally different compared to conventional 2D culture techniques[31]. The binding of structural ECM proteins and its ability to sequester growth factors also provides pivotal ligand-receptor mediated signaling that regulates cell-type specific gene expression [32]. Furthermore, changes to the ECM and the remodeling capability of cells are a fundamental aspect to many diseases, including asthma and fibrosis. Together these arguments contend that a physiological 3D ECM is often a prerequisite for meaningful cell culture research in general and in mechanobiology[32–34].

In order to perform cell-level mechanobiology experiments, our field is faced with many technical challenges. First, we need tools that are able to micromanipulate cells and apply precise dynamic mechanical cues. Secondly, these tools must be sensitivity enough to be able to measure forces from cells (ie. in the nN range). Lastly, cell behaviors need to be assessed in complex microenvironments that as closely as possible replicate *in vivo* conditions while maintaining necessary experimental control. One approach that has had success to study the effects of mechanical forces on cells, is to shrink the laboratory to their scale using lab-on-a-chip devices. This approach utilizes microfabrication techniques to miniaturize and mimic *in vivo* conditions. Other advantages of lab-on-a-chip devices include the ability to parallelize many experiments (increased throughput) and reduced reagent use (lower experimental cost). On the other hand, a major challenge of using these devices is that this approach is

relatively novel, and, therefore, the continued development of new platforms and improving capabilities goes hand-in-hand with conducting mechanobiology research.

The objective of the first chapter is to introduce key concepts in cell mechanics and mechanotransduction that are relevant to the research presented in this thesis. It briefly covers the elements of cell mechanobiology, current techniques used to assess cell mechanics, our understanding of the mechanical behavior of cells, the role of the ECM and 3D culture techniques, and mechanotransduction pathways. This chapter concludes with a perspective on the field of mechanotransduction, a review of mechanobiology in fibrosis, and an outline of the remaining thesis chapters.

1.1 A Part list for cell mechanics and mechanosensing

When first discovered, the cytoskeleton was considered as an uninteresting gel-like substance that only existed to anchor organelles. Since then, much research has shown that the cytoskeleton also plays central roles in cell migration, division, contraction, adhesion, vesicle transport and processes such as endocytosis. Because of these many roles, the cytoskeleton is incredibly dynamic – it is continuously polymerizing and depolymerizing, and is remodeled by molecular motors – and in turn, it gives cells their unique mechanical properties that are unlike any other soft matter. These mechanical properties are not only critical to understanding how cells deform, but also to the pathways through how cells sense forces. The main cellular components of the cytoskeleton (fig. 1.1) and the links between them and the mechanical regulation of cell behavior are discussed below.

Actin microfilaments. Inside a eukaryotic cell, actin microfilaments form a mesh-like structural network to control and maintain the cell shape. Filamentous actin (F-actin) is a thin double helical polymer formed by globular actin molecules (G-actin). In living cells, actin filaments are under a state of dynamic flux - subunits are continuously added and removed to its ends. Whether or not assembly and disassembly occurs depends upon the cytosolic concentration of available monomer subunits. Although assembly and disassembly can occur at both the positive (contains ATP) and minus (ATP has been hydrolyzed to ADP) ends of the filament, the dynamics differ because monomer addition to the minus end requires a conformational change. The concentrations at which neither addition or removal of monomers occurs at the ends are called the critical concentrations. The critical concentration at the minus end is greater than at the plus end. When the concentration of G-actin is higher than both critical concentrations, monomers are added to both ends; while when the concentration of G-actin is lower than both critical concentrations, monomers are removed at both ends. At intermediate concentrations that are higher than the critical concentration of the plus end but lower than the critical concentration at the minus end, subunits are added to the plus end and removed at the minus end, and there is no net change in the length of the filament. This is referred to as treadmilling. Actin formation and stability are further influenced by RhoA effector proteins, such as profilin, formin, and cofilin [36–38]. While the continuous dynamic turnover of actin comes at a great energy cost (as great as 50% of the entire ATP hydrolysis in some cells) [39], it is necessary for cell migration, and

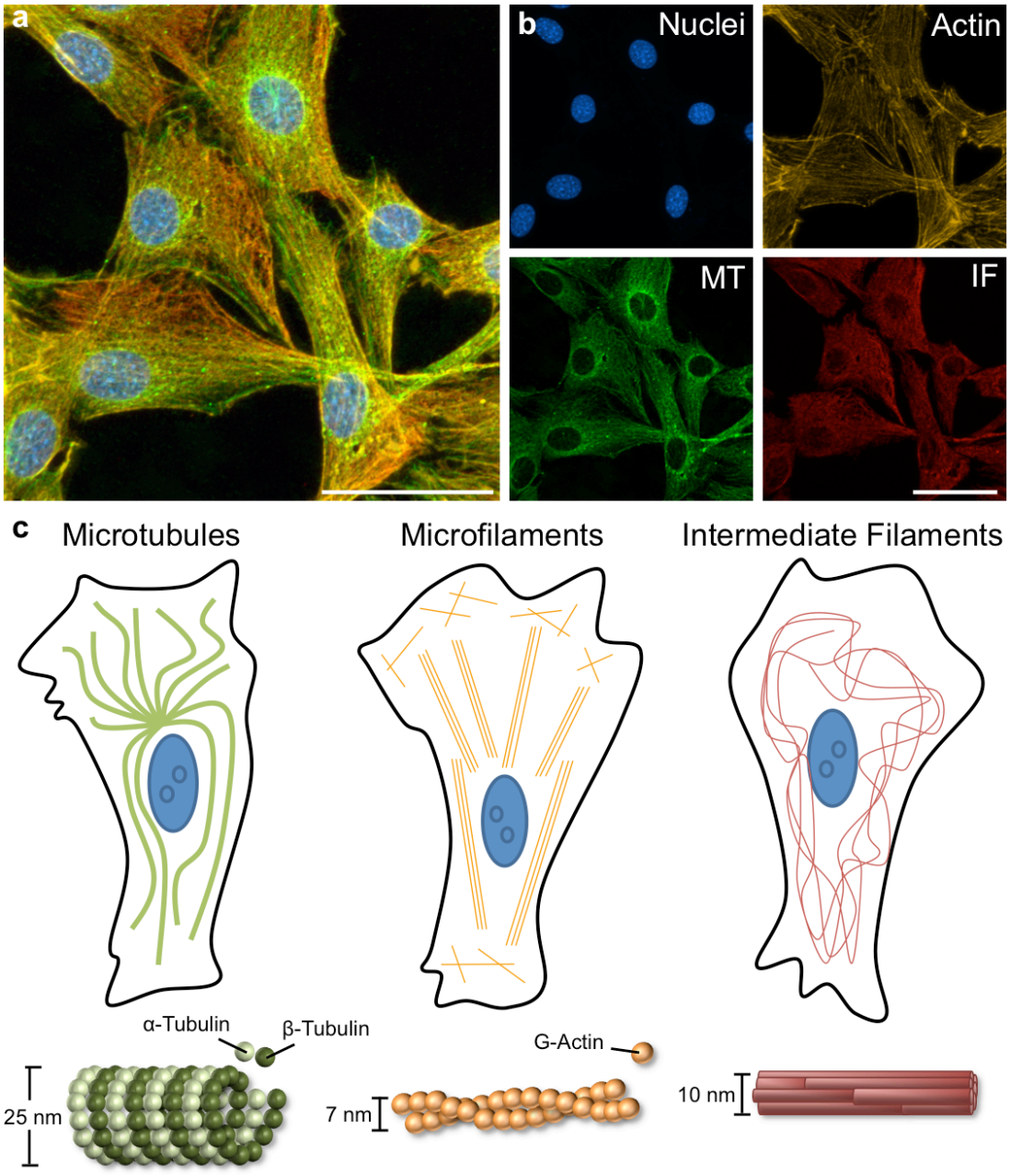

Fig. 1.1 The cytoskeleton in mammalian cells. Nuclei, actin microfilaments, microtubules (MT) and vimentin intermediate filaments (IF) of NIH-3T3 cells are shown in (a) and (b). Cells were fixed with PFA and permeabilized with triton-X. Nuclei and F-actin were stained with dapi (Fisher, D1306) and phalloidin conjugated to Alexa fluor 546 (Fisher, A22283), respectively. IFs were labeled with a rabbit anti-vimentin primary (Abcam, AB92547) and a goat anti-rabbit secondary conjugated to Alexa fluor 647 (Invitrogen, A32733). MTs were labeled with a mouse anti-α-tubulin primary (Sigma, T6074) and a rabbit anti-mouse secondary conjugated to Alexa fluor 488 (Invitrogen, A11059). (c) MTs are stiff hollow tubes consisting of tubulin subunits, which radiate from the centrosome. 'Rope-like' microfilaments bundle with myosin motors into stress fibers that run the length of the cell body to generate a 'prestress' or tension in the cytoskeleton. At the cell periphery, actin forms lattice-like networks that support the membrane. Lastly, extensible IFs form a cage around the nucleus and protect the cell against large deformations.

division, as well as processes like endocytosis and vesicle trafficking. Actin polymerization itself can also be a means that cells use to generate 'protrusion' forces as growing filaments provide a 'push' to advance the plasma membrane forward during cell migration [40].

F-actin is stiff under tensile forces but relatively flexible when compressed or bent [35]. To further impart mechanical behaviors to the cell, actin microfilaments are bound together by a number of crosslinking molecules. For example, Arp2/3 acts as a nucleation site to form branches ('daughter' microfilaments) off the sides of preexisting ('mother') actin. In addition at the cell periphery filamin forms a flexible cross-hatchet bridge between two actin filaments, and thereby imparting loose or gel-like mechanical qualities to a lattice-like actin network [41]. Lastly, α-actinin and non-muscle myosin II can bundle actin into dense, contractile stress fibers that span the length of the cytoplasm.

Microtubules. In contrast to actin microfilaments, microtubules are mechanically rigid under compressive loads and they are formed by α and β tubulin subunits that radiate as hollow tubes from the centrosome [35]. Microtubules are involved in cell movement, cell division, and act as a vesicle transport system. As with actin microfilaments, the formation of microtubules is highly dynamic. Their free end (the plus end) rapidly switches between periods of catastrophe (depolymerization) and rescue (polymerization) [42,43]. This phenomenon is termed 'dynamic instability' and it helps to generate pushing forces during cell migration and pulling forces to separate chromosomes during mitosis through rapid polymerization and depolymerization, respectively [44]. Although the exact role of microtubules in governing cell mechanics is still controversial [45], it is largely believed that they counter inward contraction forces from actomyosin activity, as depolymerization of microtubules has routinely been shown to increase cell traction and stiffness [46,47].

Intermediate filaments While F-actin and microtubules are polarized and dynamically regulated from nucleotide (ATP and GTP, respectively) hydrolysis occurring along their lengths, intermediate filaments are relatively stable α-helical chains that lack polarity. Although not as frequently researched as actin or microtubules, intermediate filaments are thought to enhance the mechanical integrity of cells by protecting against large deformations [48]. This role comes from their ability to be compliant at small deformations but stiffen drastically with stretch (ie. strain stiffen). They are also rather deformable, being able to be stretched several times their initial lengths [49]. These key features come from the hierarchical structure of intermediate filaments, which supports a cascade of deformation mechanisms depending upon the level of strain [50].

Myosin motors. Myosin II provides the 'pulling' forces on actin filaments to contract the cell, and thereby plays a central role in migration, cytokinesis, cell adhesion and control of cell shape [51]. In non-muscle cells, myosin II exists with densely polymerized actin in stress fibers [52]. It is composed of two heavy chains (MHC) and light chains (MLC). MHCs have globular heads with ATPase activity that walk along actin filaments and interact with other myosin II

motors through their coiled-coiled domains to crosslink multiple actin filaments. Myosin is activated by phosphorylation of the regulatory MLCs by myosin light chain kinase (MLCK).

Focal adhesions. It is thought that cells feel their external environment, at least in part, through special transmembrane structures called focal adhesions (FA) [3,13,53–57]. These structures provide a physical link between the internal cytoskeleton to the cell's external environment, and thereby act as a bridge to connect physical and biochemical events. Their ability to act as mechanoreceptors for transmitting mechanical forces to the cytoskeleton was first revealed by applying twisting forces on magnetic beads bound directly to FAs, and in showing that the measured stiffness from this approach (ratio of stress to strain) required intact microtubules, intermediate filaments and microfilaments [58].

Although much remains to be discovered about their structure and regulatory functions, FAs are basically large macromolecular assemblies of force sensors that vary in composition and activation as a result of mechanically induced conformational changes [3,13,53–57]. Their transmembrane portion consists of heterodimeric integrins. Outside the cell, integrin α and β subunits bind to specific amino-acid sequences (ie. Arginyl-glycyl-aspartic acid, RGD, in fibronectin etc.) in the ECM. Inside the cell, talin and tensin anchor the integrin β-subunit to actin filaments. This initial assembly is referred to as a focal complex (FC), a precursor to a mature FA, and its assembly is not reliant on mechanical tension [59]. Maturation from FCs to FAs follows the recruitment of vinculin caused by a mechanosensitive unfolding of talin [60]. The binding of vinculin not only further solidifies the link between the growing FA and the cytoskeleton, but, also controls the clustering of multiple integrins to the FA [61]. Vincluin, in itself, also acts as a force sensor that undergoes mechanically induced conformation changes to allow binding of Paxillin [62]. In mature FAs, many other mechanosensitive proteins are recruited, including Focal adhesion kinase (FAK), Src, and p130Cas, to form a regulatory hub that controls cell behavior. In particular, FAs have been shown to initiate Rho signaling via activation of Guanine nucleotide exchange factors (GEF), and thereby control actin formation and myosin contractility [63].

1.2 Micro-rheology

Technical advances have made it possible to measure the mechanical behavior of cells with high degrees of spatial and temporal resolution. For instance in atomic force microscopy (AFM), a cantilever beam can be used to assess local compressive stresses by essentially poking isolated cells [64,65]. Then based on the deflection of the cantilever and its known spring constant, the stiffness of the cell can be measured. Optical magnetic twisting cytometry (OMTC) is another prominent example [66–68]. In this method, ferrous beads adhered to integrins on the cell surface are twisted by a magnetic field. Then from knowing the torque applied to the beads and their measured displacement, the shear modulus of the cell can be measured. Other examples of micro-rheology techniques used in cell mechanics research includes optical tweezers [69,70], magnetic tweezers [71,72], and microplate rheometers [73–75].

It is well recognized that cells are viscoelastic – they possess the ability to both store and dissipate energy, and these behaviors are time-scale dependent [64,68,76,77]. For this reason, it is necessary to measure the mechanical properties of cells and tissues across multiple time-scales.

Stress relaxation. One common method to quantify viscoelastic properties is to measure the stress relaxation following a step increase in length (ie. a strain). The mathematical function through which the stress (ie. the force per cross-sectional area) is dissipated gives an understanding of the dissipation and elasticity at specific timescales over a broad time range.

Dynamic Modulus. The polymerization of the cytoskeleton and myosin motor activity, in themselves, are regulated by dynamically fluctuating strain [78–83]. Therefore, it is also common to evaluate the mechanical behavior of cells under sinusoidally oscillating strains. In this regard when dynamically loaded, viscoelastic materials characteristically display hysteresis in their loading and unloading curves, indicating energy expenditure. The area between the loading and unloading curves gives the amount of energy lost while the area under the unloading curve gives the amount of energy elastically stored. To characterize the elastic and dissipative properties at a given time-scale (ie. the loading frequency), the storage (E') and loss modulus (E") can be calculated according to equations 1.1 and 1.2, respectively, using the amplitudes of stress (σ) and strain (ε), and the phase lag (δ) between stress and strain. Furthermore, the ratio of energy dissipation to energy stored, also known as the loss tangent (ie. the tangent of the phase lag between stress and strain), indicates how viscous fluid-like (loss tangent approaches infinity) or elastic solid-like (loss tangent approaches 0) the cell is behaving (equation 1.3).

$$E' = \frac{\sigma}{\varepsilon}\cos(\delta) \quad 1.1$$

$$E'' = \frac{\sigma}{\varepsilon}\sin(\delta) \quad 1.2$$

$$\tan(\delta) = \frac{E''}{E'} \quad 1.3$$

1.3 Mechanical models of cell behavior

> …'if we were compelled to suggest a model (of cell mechanics) we would propose Mother's Work Basket – a jumble of beads and buttons of all shapes and sizes with pins and threads for good measure, all jostling about and held together by colloidal forces' - Crick and Hughes (1950)

For nearly a hundred years, our field has been studying the mechanical properties of cells [84], and with thanks to technological advancements in biophysics and biochemistry, we can name and characterize many of the 'beads, buttons and threads' in Crick and Hughes' description of the cytoskeleton [85]. Yet a single agreed-upon universal model that encompasses nonlinear mechanics and time-dependences still currently eludes us. Defining these mechanical behaviors is critical to a full understanding of the pathways through which cells sense and respond to forces from their external environment. This section briefly reviews current models (fig. 1.2) and the mechanical behaviors that they describe.

Tensegrity. Tensegrity is an architectural term for structures (eg. tents) made from stiff rods (eg. the tent poles) and tensed cables (eg. the tent fabric) (fig. 1.2a). They tend to be lightweight, yet fairly robust to mechanical stress as locally applied forces are distributed throughout the structure via compressive loads bore by the stiff rods and tensile loads bore by the cables.

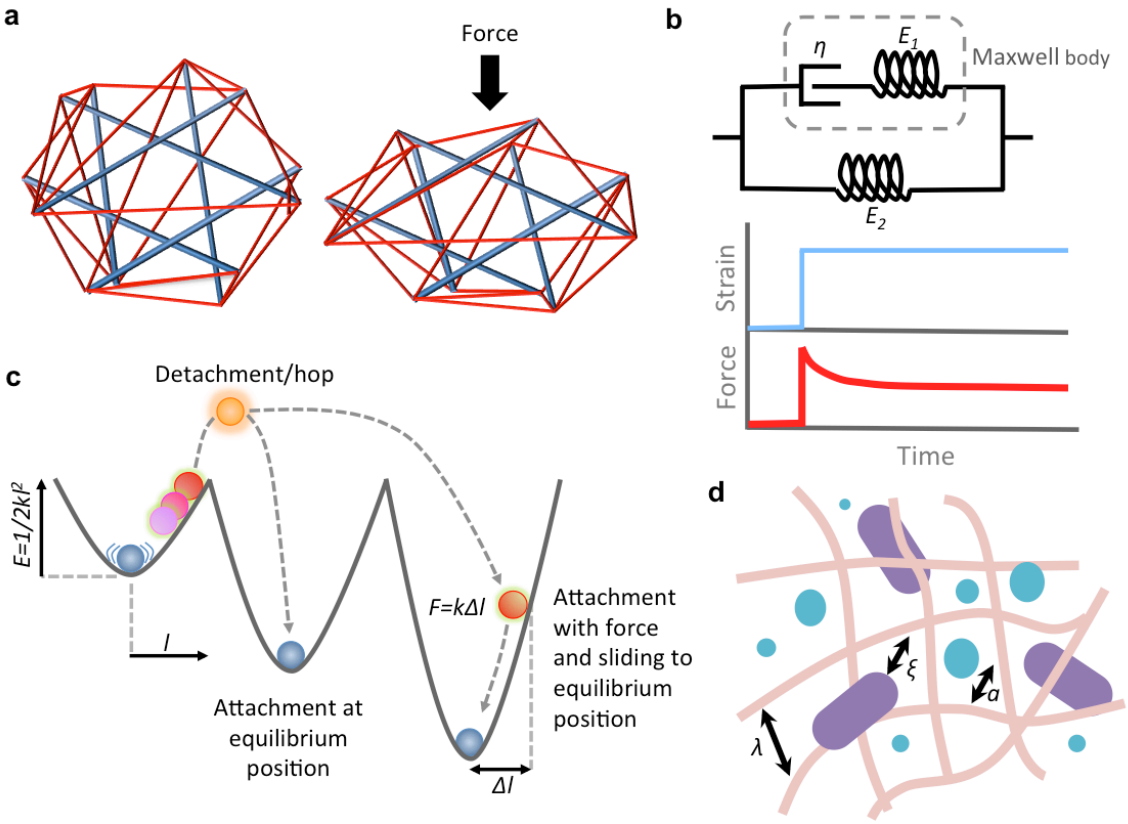

Fig. 1.2 Models of the mechanical behavior of the cell. (a) A tensegrity model considers that cells achieve their rigidity through a balance of forces between tensile stresses in actin microfilaments (red) and generated by myosin motor contractility, and opposing compressive loads in stiff microtubules (blue), as well as tension in ECM adhesions (not shown). When an external force is applied, stresses are distributed throughout the cytoskeleton as tensile and compressive loads. (b) Classically viscoelastic effects are modeled with a series of springs, described by their elastic moduli, E, and dashpots, described by their viscosity, η. Shown here is a standard linear solid (SLS) configuration. Following a step strain, the stress in the Maxwell body relaxes and the total stress in the SLS model heads towards at set point given by E_2. (c) SGR imagines the cytoskeleton as a series of quadratic potential traps with different depths containing elastic elements. When agitated, these elements overcome the potential energy barrier, $E=1/2kl^2$, and are able to hop between the wells. If attachment occurs on the side of the well, a force, $F=k\Delta l$, is generated as the element slides towards the equilibrium position (adapted from [76]). (d) Poroelasticity describes mechanical behaviors that are generated from cytosolic fluid flow through an elastic network of cytoskeletal filaments. The elastic and dissipative properties of these models depend upon the moduli of the network and the rate of fluid flow, which is determined by the size of the filaments and macromolecules, a, the entanglement length of the network, λ, and the hydraulic pore size, ξ (adapted from [64,86]).

For a cell, the tensegrity model predicts that microtubules and actin microfilaments act as the rods and cables, respectively. Thereby inward pulling myosin motor proteins acting on actin filaments are opposed by compression-bearing microtubules and adhesion proteins that anchor the cell to the ECM [87–89]. This balance of forces leads to tension or pre-stress in the cytoskeleton, and analogous to the strings on a guitar: the greater the tension the cell generates, the stiffer it is.

In support of this model, the level of pre-stess in individual cells is known to be directly related to their stiffness, and both are controlled through actomyosin activity [87]. Tensegrity also correctly predicts that the stiffness of a cell is proportional to the stress at which it is probed (ie. cells strain stiffen) [58,75,87]. Further it explains how local loads are carried throughout the interconnectedness of the cytoskeleton to distant regions of the cell [58]. Microtubules have also been shown to be compression-bearing elements that counter actomyosin contraction in cells. In that regard, depolymerization of microtubules rapidly leads to increased cell prestress and stiffness [47], and microtubules in cells visibly buckle under compressive loads [90].

Although tensegrity offers an intuitive understanding that may directly reflect the physiological contributions of cytoskeletal proteins, the acceptance of this model remains controversial [45]. In that regard, the link between actin and microtubules, which is a prerequisite of tensegrity models, has not been established on a molecular-level. Furthermore, tensegrity also does not offer an explanation for the timescale-dependent behavior of cells [68,73,76] or the widely reported strain softening response from dynamic loading [80,82,91,92].

Standard linear solid (springs and dashpots). It is widely known that the mechanical behavior of a cell depends upon the rate at which it is probed [68,73,76]. In engineering this timescale-dependent behavior, referred to as viscoelasticity, is traditionally described using a network of elastic springs, and viscous dashpots. These basic elements allow materials to both store energy like an elastic spring, and to dissipate energy like a viscous liquid.

In one variation, termed a standard linear solid (SLS), a spring and a dashpot in series (ie. a Maxwell body) are in parallel with another spring (fig. 1.2b). Solving the constitutive equations for an SLS model following a step change in length gives an exponential decay in stress (or a decaying exponential increase in length for a step change in stress) with a time constant depending upon the elastic modulus of the spring and viscosity of the dashpot [93]. For inert materials, this behavior is related to an equivalent response in the frequency domain by the Fourier transform. In this representation, these models display a peak in dissipative stresses at a characteristic frequency, corresponding to their time constant.

In early work, investigators tried to link the elements in these models (ie. springs and dashpots) to specific processes that occur in the cell (ie. myosin crossbridge cycling) [73,94]. However, as the time resolution of their methods improved, more Maxwell bodies were needed to fit the data. Because the number of parameters varied with the experimental acquisition rate, investigators concluded that the elements could not be linked to specific processes and perceived these models as an ineffective method to describe cells [76].

Furthermore, these models, with basic springs and dashpot, lack the complexity to describe nonlinearities are commonly seen in cells, including strain stiffening and dynamic strain softening [76,87,91,92,95,96]. With that said,

more complex ideas have been recently introduced with this type of model, such as the dissociation and recruitment of dashpots, to capture some nonlinearities (ie. quasi-linear viscoelasticity) and more complex rheological behaviors (ie. power-law rheology) [97,98].

Soft glassy rheology. In contrast to the characteristic timescale behavior from exponential spring-dashpot models, the frequency response of cells in 2D culture, measured from locally applied shear forces (ie. OMTC), was observed to follow a featureless weak power law with a single exponent [66,68,99]. In that regard, both dissipative and elastic stresses increased monotonically with the oscillation rate with the same weak power law. Stress relaxation, measured by local compression (ie. AFM), has also confirmed that an equivalent behavior exists in the time-domain [65]. Therefore, under these experimental conditions, the ratio of dissipative to elastic stresses was deemed to be timescale invariant, following the structural damping law [68]. This behavior is consistent with the hypothesis that dissipation arises from molecular friction generated by cytoskeletal filaments smoothly gliding passed one another [100].

In addition to power law behavior, several investigators have shown that cells share a seemingly universal response to dynamic stretch, the cytoskeleton softens (decreased elasticity) and becomes more fluid-like [92,101–103]. Then upon stretch cessation, it slowly regains its stiffness and resolidifies [92]. Although the molecular mechanism(s) behind strain softening remains unclear, stretching of cells has been reported to depolymerize actin filaments [78–80], and also, strain softening in reconstituted actin-myosin networks has been attributed to the disruption of myosin crosslinks [81–83]. In the body, this response is believed to play a role in both the maintenance of airway caliber [7,8] and the regulation blood pressure [104], but is absent from certain pathological disorders, such as in asthmatic airways [105].

Seemingly universal observations of power law rheology and fluidization across different cell types, techniques and following a range of cytoskeletal drugs, has since given traction to the hypothesis that cells belong to a class materials called soft glasses [106]. The rheological behavior of these materials (eg. foams, dense emulsions, pastes and slurries) was first described by Peter Sollich (1997) [107]. In his theory on soft glassy rheology (SGR), Sollich (1998) modeled their behavior as elastic elements that are agitated by an effective temperature or noise level (x), which can cause them to overcome an energy barrier and hop between traps of different potential energy depths (fig. 1.2c) [108]. While Sollich's SGR model describes inert slurries and colloids, this approach may also capture active force generation from actomyosin crossbridge cycling if elements are permitted to reattach outside of the equilibrium position at the bottom well. It is important to understand, that SGR is a purely theoretical model, and thus, it does not offer any mechanistic explanation for the actual physiological behavior of cells. Furthermore, unlike the cytoskeleton [58,75,87], soft glasses do not strain stiffen.

Poroelasticity. A poroelastic model considers a material to be biphasic, consisting of a porous elastic medium bathed in a viscous fluid. It describes the interactions between fluid flow and the deformation of the solid medium [109]. For a cell, poroelastic effects are thought to arise from the redistribution of the viscous cytosolic fluid between

local regions within the network of cytoskeletal filaments (fig. 1.2d) [86]. In that way, dissipation through fluid flow is tied to the porosity of the cytoskeleton and how it deforms. Re-enforcing (or disrupting) the cytoskeleton effectively decreases (or increases) the pore size and/or increases (or decreases) the volume fraction of the network. Decreasing (or increasing) the pore size and/or increasing (or decreasing) the volume fraction of the network, in turn increases (or decreases) the effective viscosity leading to greater energy expenditure. At the same time, the elastic deformation of the cytoskeleton depends upon its hydrodynamic drag through the cytosol. Therefore, poroelasticity imparts a timescale behavior that depends upon the diffusion constant of the cytosol through the cytoskeleton. For cells, poroelasticity has been linked to the initial (<1sec) exponential behavior in response to a large volumetric compression [86]. In addition to time-dependencies, poroelastic materials are characteristically nonlinear with respect to stress.

1.4 Theoretical foundations of micro-rheology models

Standard linear solid. The viscoelasticity of the SLS model in fig. 1.2b can be described by a system of equations. The stress, σ, produced at a given strain, ε, in the springs are given by:

$$\sigma_1 = E_1\varepsilon_1 \quad 1.4$$

$$\sigma_2 = E_2\varepsilon_2 \quad 1.5$$

where E_1 and E_2 are the elastic moduli of spring 1 and spring 2, respectively. The stress in the dashpot is given by:

$$\sigma_3 = \eta\frac{d\varepsilon_\eta}{dt} \quad 1.6$$

where η is the viscosity of the dashpot. The total stress, σ, is given by the sum of the stresses between the two parallel branches:

$$\sigma = \sigma_1 + \sigma_2 = \sigma_\eta + \sigma_2 \quad 1.7$$

where σ_1, σ_2, σ_η are the stresses in spring 1, spring 2 and the dashpot, respectively. The total strain, ε, is equal to the sum of the strains in either of the parallel branches:

$$\varepsilon = \varepsilon_1 + \varepsilon_\eta = \varepsilon_2 \quad 1.8$$

where ε_1, ε_2, ε_η are the strains in spring 1, spring 2 and the dashpot, respectively. Solving this system gives the following constitutive equation:

$$\frac{\eta}{E_1}\frac{d\sigma}{dt} + \sigma = \frac{\eta E_2}{E_1}\frac{d\varepsilon}{dt} + E_2\varepsilon + \eta\frac{d\varepsilon}{dt} \quad 1.9$$

This expression maybe further simplified using $\tau = \eta/E_1$:

$$\frac{d\sigma}{dt} + \frac{\sigma}{\tau} = E_2\frac{d\varepsilon}{dt} + \frac{E_2\varepsilon}{\tau} + \frac{\eta}{\tau}\frac{d\varepsilon}{dt} \quad 1.10$$

where τ is a time constant.

For a step strain, $\frac{d\varepsilon}{dt} = 0$. Substituting this condition into equation 1.10 yields:

$$\frac{d\sigma}{dt} + \frac{\sigma}{\tau} = \frac{E_2\varepsilon}{\tau} \quad 1.11$$

Solving this ordinary differential equation gives a simple exponential decay function:

$$E(t) = E_2 + E_1 e^{-t/\tau} \quad 1.12$$

When considering oscillatory conditions, the SLS model can be transformed into the frequency domain by performing a Fourier transform on its constitutive equation, giving:

$$E'(\omega) = E_2 + E_1 \frac{\omega^2\tau^2}{1+\omega^2\tau^2} \quad 1.13$$

$$E"(\omega) = E_1 \frac{\omega\tau}{1+\omega^2\tau^2} \quad 1.14$$

where ω is the radian frequency. This model predicts that the storage modulus, E', follows a sigmoidal curve while the loss modulus, E", follows a bell-shape, peaking at the characteristic time constant.

Power law rheology. In cells under certain experimental conditions, the stress following a step deformation relaxes according to a power law with elapsed time:

$$\frac{\sigma(t)}{\varepsilon} = E_o\left(t/\tau_o\right)^{\beta} \quad 1.15$$

where the prefactor E_o characterizes the initial stiffness; β is a dimensionless power law exponent; and the time, t, is normalized by an arbitrary timescale, τ_o, giving this model timescale-invariant behaviors. For a sinusoidally varying force, the Fourier-transformation of equation 1.15 gives an equivalent response as a function of the radian frequency, ω:

$$E' = E_o(\omega\tau)^{\beta}\cos\left(\frac{\pi\beta}{2}\right)\Gamma(1-\beta) \quad 1.16$$

$$E" = E_o(\omega\tau)^{\beta}\sin\left(\frac{\pi\beta}{2}\right)\Gamma(1-\beta) \quad 1.17$$

where *Γ* denotes the gamma function. From these equations, the storage and loss modulus follow the same power law with frequency, hence:

$$E'(\omega) \sim E"(\omega) \sim \omega^{\beta} \quad 1.18$$

Therefore, the loss tangent, or the ratio of the amount of the energy dissipated for a given amount stored is independent of the oscillation rate, and follows, the structural damping law.

In the power law rheological behavior of cells a range of viscoelastic responses is captured solely through varying the power law exponent, β (E_o, τ_o are considered constants for a given cell type) [66]. If β approaches zero, then equation 1.15 simplifies to $\frac{\sigma(t)}{\varepsilon} = E_o$, which is Hooke's law of elastic deformation. Thus all the energy is elastically stored. On the other hand, if β approaches unity, then equation 1.15 simplifies to $\frac{\sigma(t)}{\varepsilon} = E_o t$, which is equivalent to Newton's law of viscous deformation. Thus all the energy is lost. At intermediate values of β, both elastic and dissipative behaviors coexist. In cells, β ranges between 0.1 and 0.5 [76]. Remarkably this also means that cells cannot change their elastic and dissipative properties independently but only along a specific trajectory governed by changes in the exponent β.

As mentioned previously, soft glassy materials are a class of soft (kilopascal range) matter that are not at thermodynamic equilibrium and their rheological behavior follows weak power laws (β is on the order of 0.1) with a near constant loss tangent for a wide range of frequencies. In this context, the power law exponent β signifies

the noise temperature minus unity (x-1); the prefactor, E_o is the highest stiffness, which occurs at the glass transition temperature (x=1); and the timescale, τ_o, is the residence time of an element before it hops out of a well. When x>1, the elements are sufficiently agitated and may hop between the potential energy wells in Sollich's model. Consequently, the system becomes disordered and can flow as a whole. However, when x approaches 1, the elements are trapped in sufficiently deep wells with energy barriers that are not overcome by the noise temperature. Consequently, the system is stabilized and behaves like an elastic solid.

Poroelasticity. Biot (1941) first proposed a theory of poroelasticity to further consolidation models of fluid-saturated porous ground soil [109]. This theory makes the following assumptions: 1) there is an interconnected pore system that is uniformly saturated with fluid, 2) the material is isotropic, and 3) the total volume of the pore system is small compared to the volume of the solid network material. More recently, investigators have applied poroelastic models to describe cytosolic fluid motion within the cytoskeleton [86]. Presented below is the theoretical basis for poroelasticity.

For an isotropic fully saturated poroelastic medium, the constitutive equation relates the strain tensor (σ) to the infinitesimal strain tensor (ε) of the solid matrix and the pore fluid pressure (p):

$$\sigma = 2G_s\varepsilon + \frac{2G_s\upsilon_s}{(1-2\upsilon_s)}\{tr\ \varepsilon\}I - pI \qquad 1.19$$

where G_s is the shear modulus and υ_s is Poisson ratio of the drained matrix, I is the identity tensor, tr is the trace operator and $\theta = tr\ \varepsilon$ is the variation in fluid content. The first two terms on the right side of this equation is equivalent to the constitutive equation for a single-phase linear elastic material. The third, and last, term on the right accounts for the time dependent properties by acting as a fluid pressure acting on the solid phase. Under quasi-static conditions, using the equilibrium condition $div\ \sigma = 0$, equation 1.19 becomes:

$$G_s\nabla^2 u + \frac{G_s}{(1-2\upsilon_s)}\nabla div\ u - \nabla p = 0 \qquad 1.20$$

where u is the vector of solid displacement for small deformations $\varepsilon = 0.5\nabla u + \nabla u^T$, and div, ∇, and ∇^2 are the divergence, gradient and Laplacian operators, respectively. Next we consider fluid transport inside the porous medium by combining the continuity equation ($div\ q = -{}^{d\theta}/_{dt}$) and Darcy's law ($q = -K\nabla p$ where q is the filtration velocity and K the hydraulic permeability) to yield:

$$\frac{d\theta}{dt} = K\nabla^2 p \qquad 1.21$$

The diffusion equation for θ can then be obtained by combining equations 1.20 and 1.21 into what is called the consolidation equation:

$$\frac{d\theta}{dt} = D_p\nabla^2\theta \qquad 1.22$$

where D_p is the poroelastic diffusion coefficient, which is given by:

$$D_p = \frac{2G_s(1-\upsilon_s)}{(1-2\upsilon_s)}K \qquad 1.23$$

Thereby the mechanical properties of the cytoplasm are characterized by three independent parameters: G_s, v_s and D_p. The hydraulic permeability, K, can be related to the microstructure of the cell by assuming Poiseuille flow through an average pore radius of ξ with a porosity of ϕ:

$$K = \frac{\varphi}{4\kappa}\frac{\xi^2}{\eta} \quad 1.24$$

where η is the viscosity of the cytosolic fluid and κ is a constant taking into account the irregularity, interconnectivity and tortuosity of the pores. Substituting equation 1.24 into 1.23 with the relationship between shear and elastic moduli ($E = 2G_s(1 + \upsilon_s)$) gives:

$$D_p = \left(\frac{(1-\upsilon_s)}{(1+\upsilon_s)(1-2\upsilon_s)}\frac{\varphi}{4\kappa}\right)\frac{E\xi^2}{\mu} \quad 1.25$$

As a first approximation, the parameters inside the parenthesis can be assumed to be constant giving the following relationship between the diffusion constant, and the elasticity of the cytoskeleton, pore size, and cytosolic fluid:

$$D_p = \alpha\frac{E\xi^2}{\eta} \quad 1.26$$

1.5 The extracellular environment and 3D cell culture techniques

In the body, cells exist within a 3D, dynamic environment consisting of: (1) an ECM composed of a scaffold of collagens and other structural proteins that is interlaced with proteoglycans; (2) mechanical stimulation; and (3) soluble mediators from neighboring cells. Through receptor-mediated signaling and mechanotransduction pathways, this environment provides critical mechanical and biochemical stimuli for regulating cell behavior. For example, TGF-β1, an inflammatory cytokine, induces myofibroblast activation, which leads to increased collagen deposition at sites of injury [110]. The resulting increased matrix stiffness, in turn, further enhances the myofibroblast phenotype through mechanosensing pathways [111,112]. This example also demonstrates that gene expression in cells and remodeling of their microenvironment are intimately linked in the body through an ongoing, bidirectional interaction referred to as dynamic reciprocity [113,114]. Yet, in contrast to *in vivo* conditions, our understanding of cell mechanobiology has been largely influenced by *in vitro* studies done on isolated single cells, grown on static, stiff 2D substrates void of natural ECM proteins and soluble mediators [1,3,13,58,65,66,68,115]. For this reason, techniques that allow the assessment of cell behavior while recapitulating the microenvironment a cell would experience in the body - through a mechanically active, multicellular, 3D matrix - are of increasing interest to our field [32–34,116].

Collagen is the most abundant protein composing the ECM. Its precursor, pro-collagen, is secreted by resident cells as a triple helix, and through covalent cross-linking, forms into a fibular network to support cell adhesion, growth, proliferation, and migration[117]. Collagen binds integrins directly and indirectly through fibronectin, and thereby cells can exert forces to remodel this network and receive mechanical stimuli (ie. stiffness, stretch) from the ECM [58]. Collagen also influences gene expression and thus cell behavior through, in itself, acting as a ligand for many receptors on the cell surface [118].

To partially replicate the ECM in the lab, culturing cells in reconstituted 3D collagen gels has become standard practice for many laboratories [116,119]. Although arguably still far from the cellular microenvironment in the

body, such 3D cell culture techniques have been shown in many cases to elevate cell-type specific gene expression and functionality, which is typically lost while harvesting cells onto 2D plates from donor tissues [32,120–122]. For that reason, many in our field believe that mammalian cells may require signals from a 3D environment to form physiologically relevant structures in-vitro [32–34]. Moreover, 3D quasi-organ culture techniques will likely have an increasingly important role in applications such as screening new drugs for efficacy and safety in humans before clinical trials [123].

In terms of mechanobiology, culturing cells within a 3D matrix vs. on a 2D substrate is known to fundamentally change the distribution and structure of the cytoskeleton, because 2D culture forces un-natural apical-basal polarity of adhesion complexes [31]. One method that has been used previously to study contractile forces generated by cells within a 3D ECM are microfabricated tissue gauges (microtissues) [124]. In the microtissue model, cells in a collagen matrix form around pairs of flexible vertical cantilevers into an array of dense, organized structures. From the visible deflection of the cantilevers, relatively high-throughput tensile force measurements can then be calculated. Microtissues have been shown to share comparable morphology and functionality as connective tissue [124], and skeletal [125], airway [120] and cardiac [126] muscle layers. Although static force and quasi-static stiffness measurements of microtissues have recently received a lot of attention [120,124–129], the dynamic mechanical behaviors of 3D cell cultures has largely gone unexamined outside of the work presented in this thesis.

In addition to a 3D collagen matrix and mechanical forces, cellular behavior in the body is further influenced by other matrix proteins (proteoglycan, fibronectin, laminin etc.) [130], electric signals [131], and communication between multiple cell types through cell-to-cell adhesions (cadherins, connexins, claudins, occludins etc.) [132] and soluble mediators (ions, enzymes, growth factors etc.) [133]. As such, in order to fully recapitulate the *in vivo* microenvironment in the lab, more complex cell culture techniques must be developed to include realistic matrix compositions, electrical stimulation and co-cultures.

1.6 Mechanotransduction: assembling the parts

Mechanotransduction refers to the process through which mechanical forces (ie. stretch, stiffness, shear) are transformed into chemical signals to ultimately guide cell behavior. In perhaps the most famous example Engler *et al.* 2006 showed that the fate of mesenchymal stem cells can be directed down different lineages based solely upon the stiffness of the substrate on which they were grown [20]. In that regard, the cells either became neurons when plated on soft substrates that mimicked the brain, myoblasts when plated on an intermediate stiffness that was consistent with muscle, or osteocytes when plated on rigid substrates that recapitulate collagenous bone. In addition to differentiation, mechanical forces are a powerful stimulus crucial for a variety of other fundamental cell functions that have important biological implications. For instance, cells remodel their cytoskeleton to tune their contractility and stiffness in direct accordance to the rigidity of their substrate (ie. cells on stiffer substrates are also stiffer and more contractile) [134,135]. Matrix stiffness has also been shown to directly impact cell migration [136,137]. As a final example, cyclic mechanical stretching is known to routinely cause cells in 2D

culture to reorient themselves perpendicular to the principal strain direction, and thereby exerts organizational control over cells [95,138]. Curiously, in contrast, cells have been shown to reorient preferentially parallel to the stretching direction in 3D cultures, indicating that the ECM may alter how these forces are perceived by cells [139].

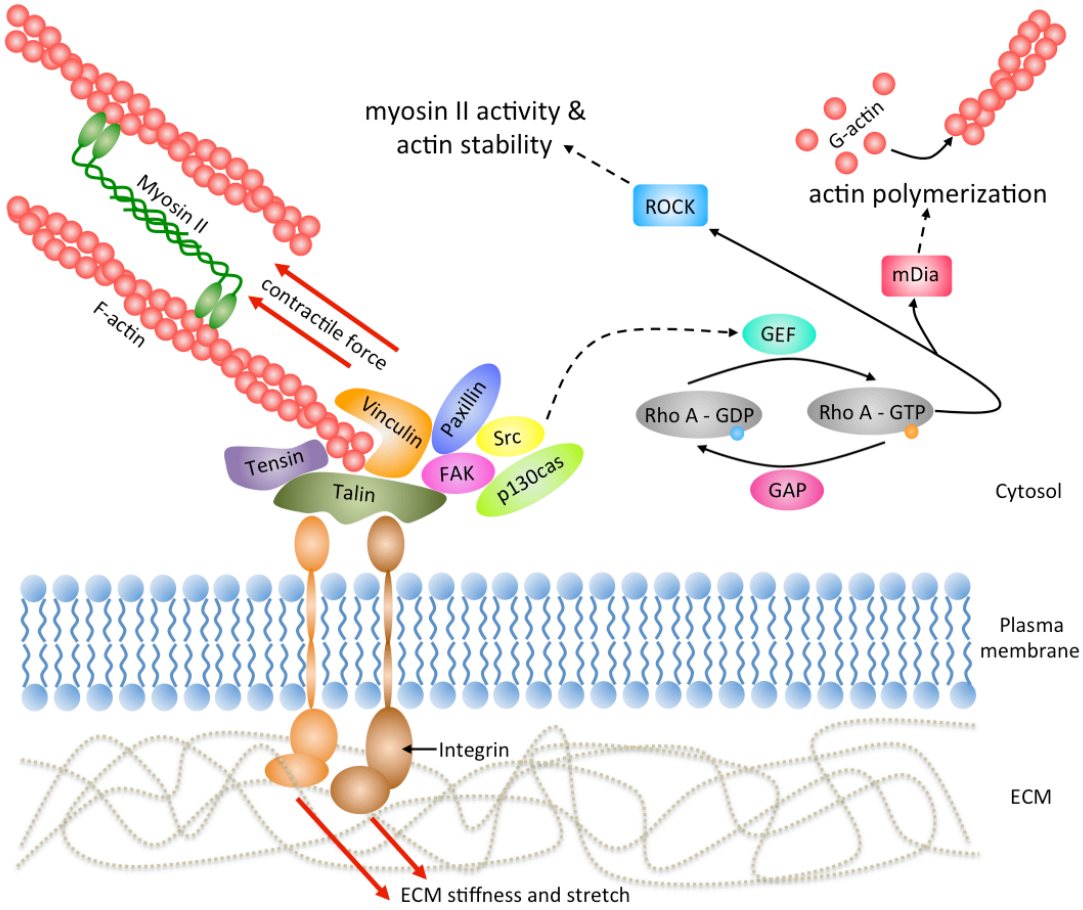

Fig. 1.3 Cells feel forces through focal adhesions. Within a FA, transmembrane integrins link the ECM to the inside of the cell, and through adaptor proteins, such as tensin and talin, connect to actin filaments. When a force is felt, either generated by myosin contraction during ECM rigidity sensing or an externally applied load, conformational changes allow vinculin and subsequently a number of other signaling molecules to bind, including FAK, paxillin, Src, and p130cas. In turn the recruitment of these molecules initiates various signaling cascades that regulate cell behavior. In particular, external stretch and stiff substrates are known to activate GEF. GEFs switch the GDP for GTP in the regulatory domain of RhoA, and in doing so, activates it. Two downstream effectors of RhoA, ROCK and mDia, then lead to actin polymerization and increased stability, as well as myosin II contraction.

In early stages, mechanobiology research largely focused on stretch-activated transmembrane ion channels in specialty sensory cells [140]. These channels open in response to increased membrane tension caused by external forces, and they allow ions to flow into and out of the cell, which in turn alters the electrical potential across the membrane. In a classic example, sound vibrations are sensed through Ca^{2+} influx in stretch-activated channels on stereocilia that protrude from the membrane of hair cells into the cochlea in the inner ear [141,142]. These channel have also been implicated in a mechanoelectrical feedback loop in heart muscle cells to dynamically regulate their

contractile function in accordance to cardiovascular demands [16]. In more a more general example, it has been proposed that these mechanosensitive channels may indicate to a cell where its cytoskeleton is absorbing the most load, and initiates locally remodeling to reinforces those areas [142]. Looking beyond stretch-activated channels, our field has more recently identified numerous other mechanisms through which cells perceive mechanical stimuli.

FAs have taken a central focus in mechanotransduction research because it is known that FAs act as signaling hubs, and that they transduce mechanical forces between the cytoskeleton and the external environment. In the case of substrate stiffness sensing, myosin motors generate fluctuating tugging forces that are carried through actin microfilaments to FAs and out to the ECM so that cells may actively probe their environment [56]. On the other hand, when cells encounter external mechanical loads (ie. the stretch in airways), the ECM transmits that stress through FAs to the cytoskeleton. In both cases, forces are felt by cells through directly causing conformational changes in focal adhesions (fig 1.3)[1,13,17]. In turn, these conformational changes alter the binding affinity for further proteins (ie. vinculin, FAK, paxillin) to interact with FAs, which triggers signaling cascades that regulate cell behavior [13,14,143].

Force-sensing at focal adhesions has long been thought to include activation of Rho GTPases in the Ras superfamily [144]. Their active forms interacts with numerous downstream effectors to regulate a wide variety of cell functions, including cell growth, gene expression, and membrane trafficking [144]. In response to mechanical forces, family members RhoA, Rac1 and Cdc42 lead to remodeling of cell adhesions and the actin cytoskeleton [145,146]. In particular, RhoA has two major downstream effectors that influence stress fiber formation and actomyosin cycling: Rho kinase (ROCK) and mDia. First, ROCK promotes myosin II-mediated contractility by directly phosphorylating MLC and deactivating myosin phosphatase [147]. ROCK also stabilizes actin microfilaments by indirectly inhibiting the depolymerization through cofilin [148]. Secondly, mDia, a formin, promotes actin polymerization through stimulating nucleation and processively adding actin monomers to the elongating plus end[36].

Rho GTPases are activated by a conformation change in their effector domain that occurs upon exchanging bound GDP for GTP. This exchange is governed by GEFs (GEFs) and GTPase-activating proteins (GAPS), which activate and deactivate RhoA, respectively [149]. Applying mechanical forces to integrins through fibronectin-coated beads has been shown to recruit GEFs (GEF-H1 and LARG) to the vicinity of FAs [150]. Once there, GEFs are activated through various pathways. For example LARG is activated by the tyrosine-protein kinase Fyn, while GEF-H1 is controlled through a FAK/RAS/ERK signaling pathway [150]. In particular, cyclic stretch induced RhoA activation has been shown through the recruitment of a number of GEFs, including GEF-H1 [151], Vav2 [152], and Solo [153].

In addition to mechanosensing at FAs, there is also evidence in support that the cytoskeleton itself may be mechanosensitive. For example stretch has been shown to both depolymerize [91,92] or reinforce [91,154,155] actin fibers and alter the ability of crosslinkers to bind [8,156–158]. The actin crosslinker filamin is also believed to sense mechanical shear and myosin driven contraction itself, because it has been shown that changes in actin lattice binding angles switches its binding affinity between filamin-GTPase-activating protein (FilGAP) and the cytoplasmic tail of β-

integrins [156]. GEFs interacting with microtubules and intermediate filaments are also thought to coordinate mechanotransduction between the different components of the cytoskeleton. For instance, microtubule depolymerization has been shown to lead to higher levels of GEF-H1 for RhoA activation[159]. However, whether this is a direct effect of microtubule depolymerization, or it may simply be secondary to the change in the forces at focal adhesions, remains to be addressed. Like microtubules, intermediate filaments, such as keratins and vimentin, also interact with RhoA-GEFs (Solo and GEF-H1, respectively) to control actin stress fiber assembly [160,161].

In high-density cell populations, external stresses may also be transferred through cell-cell adhesions (cadherins) to the cytoskeleton, in addition to ECM-cell integrins [162]. For example, cyclically stretching endothelial cell monolayers has been suggested to lead to RhoA activation mediated by GEFs (Solo) at cadherins [153]. Mechanosensing through cadherins has also been shown to lead to a number of changes that reinforce intercellular junctions in a positive feedback loop, including force dependent remodeling [163], and altered mechanical properties, such as adhesion strength [164,165], cell traction forces [166], and stiffness [167].

1.7 Perspectives on our understanding of mechanotransduction

At the most basic understanding of mechanotransduction, a mechanical force stretches-out the proteins that make up FAs and the cytoskeleton. These conformational changes in turn alter the binding affinity and association of other proteins, and thereby, control numerous signaling cascades that regulate cell behavior. In other words, extracellular forces alter biochemical interactions, and in turn the biology. A complete understanding of mechanosensing pathways is, however, lacking due to a few unresolved questions that are fundamental to these mechanisms.

Firstly, as mechanotransduction occurs through physical conformational changes in proteins, we need a foundation of how cells and their cytoskeleton behave and deform under loads in order to truly understand mechanosensing pathways [1,3,55,58,89]. To fulfill this need, a great effort has been carried out to characterize the mechanical properties of cells and the role of individual cytoskeletal proteins through micro-rheology methods, such as AFM and OMTC. Results from these investigations have revealed a number of seemingly universal behaviors that describe the cytoskeleton, including strain softening [76,77,92]. Often as a field, however, we have been focused on describing the basis for these behaviors using theoretical models (ie. SGR) that lack direct experimental observations and mechanistic explanations [76]. For this reason, investigations that visualize cytoskeletal remodeling and link these observations with mechanical properties are, and will continue to be, incredibly impactful [168,169]. Moreover, the local compression from an AFM tip and local shear from OMTC, likely has little physiological significance, and therefore, it is unclear whether the deformations studied with these techniques provide any relevance to mechanosensing in the body [170]. Conversely, our understanding of how stresses are transferred from the soft ECM to cells in tissues under physiologically loading has also not been well characterized. Indeed, our understanding of mechanotransduction is largely limited by the currently available techniques to apply mechanical stimulation at the cell and tissue levels, and measure biomechanical and biochemical responses [171].

Secondly, the structural conformational changes and binding of proteins are in themselves inherently rate and strain dependent [13,172], yet the effects of these dependencies on mechanosensing pathways has been largely unexplored [55]. For example, if loaded too slowly, stress can be dissipated through remodeling events in the cytoskeleton or cell adhesions rather than causing conformational changes to mechanosensitive proteins. Conversely, if loaded under a cyclic frequency that is too fast, the mechanosensitive proteins will not have enough time to undergo a conformational change during the loading cycle. To add to that point, myosin driven forces inside some FAs are known to fluctuate at regular time intervals, which suggests that cells have a preferred timescale for sensing substrate stiffness [56]. Further evidence of the timescale dependence of cellular mechanosensing and the influence of ECM viscoelasticity on cellular phenotype has come from a recent study that showed that substrate viscosity controls cell morphology and differentiation independently from substrate elasticity [173].

Thirdly, cell mechanics and mechanosensing have been mostly studied in 2D culture on flat, rigid substrates rather than the soft, 3D matrix a cell would experience were it in the body. We know, however, that the physical environment in which a cell is investigated alters its mechanical behavior and response to mechanical and biological stimuli. For example, cells grown on stiff substrates tend to have their actin cytoskeleton arranged into dense stress fibers, and are stiffer, more solid-like and under higher tension (prestress) compared to cells on softer substrates [134–137]. In addition to matrix stiffness, it is also suspected that the mechanical behavior of a cell may be further altered by the dimensionality of its environment. In support of this growing hypothesis, culturing cells on a 2D substrate vs. within a more physiologically relevant 3D matrix fundamentally changes the distribution and structure of the cytoskeleton by forcing un-natural apical-basal polarity of adhesion complexes [31]. These observations have raised important questions about how cells sense and react to mechanical factors in their environment, and whether observations made in rigid 2D dishes actually reflect how cells behave in the body.

1.8 Mechanical forces in fibrosis: applications of mechanosensing

As part of a normal healing response, myofibroblast activation is essential for rapid wound contraction and de novo matrix deposition following tissue injury found throughout the body [174–178]. However, if myofibroblast activation goes unchecked, tissues can progressively lose their functionality to potentially life-threatening fibrotic remodeling [174]. Fibrosis is a leading cause of death in developed countries, and justifiably so, has become central focus for lung, heart, vasculature, liver, renal, and eye research [177,179–182]. Yet, the factors that contribute to persistent myofibroblast activation remain unclear [177,182]. Identifying these factors and the mechanisms through which they influence myofibroblast activation may provide new therapeutic targets to prevent the development and arrest the progression of fibrosis.

Along with biochemical inflammatory mediators, mechanical stimuli are thought to be key determinants in the development and progression of tissue fibrosis through controlling fibroblast to myofibroblast differentiation. For example, several investigators have shown that culturing fibroblasts on stiffer substrates with

TGF-β1 promotes a transition to a myofibroblastic phenotype [111,112]. Conversely culturing on substrates with a much lower stiffness, to approximate the mechanical properties of a soft tissue, has been shown to reduce myofibroblast activation in the presence of TGF-β1 from fibroblast pools [183,184]. Also without any biochemical signals, a fraction of fibroblasts cultured on standard polystyrene dishes will spontaneously express α-smooth muscle actin (α-SMA), a characteristic marker of myofibroblasts [111].

Although it is generally agreed that mechanical tension from increased substrate stiffness favors fibroblastic differentiation into myofibroblasts, the role of cyclic stretching, as cells would encounter in airways and vasculature, is less clear. There have been conflicting reports as to whether cyclic stretch activates myofibroblast differentiation or serves as a protective role promoting a quiescent fibroblastic phenotype. Curiously it seems that studies where uniaxial strain has been applied favors a myofibroblastic transition in precursor cells [185] whereas biaxial strain may provide a protective effect [186]. Further in support of this hypothesis, enhanced anisotropy when under biaxial loading has been shown to augment myofibroblast activation [187]. Difference in the ECM stiffness may have also in part contributed to the contradictory role of stretch in myofibroblast activation. In that regard, stretching has been shown to promote the expression of the myofibroblastic phenotype in lung fibroblasts cultured on stiff (30kPa) gels, while stretching on soft (2kPa) gels had no affect over static conditions [188]. Other explanations may lie in the duration of their experiments, strain amplitude, cell types, matrix composition and oscillatory frequency.

Mechanical stretch has also been hypothesized to contribute to maintaining the myofibroblastic phenotype through activating TGF-β1, which is secreted as a latent complex by myofibroblasts in an autocrine feedforward loop [189–191]. This inactive form consists of the latent TGF-β1 binding protein (LTBP), which associates with the ECM, and the latency-associated peptide (LAP), which non-covalently sequesters a TGF-β1 polypeptide and binds to integrins on the cell's membrane. Mechanical stretch, such as in lung tissue from breathing or cell contractile forces, are thought to directly induce a conformational change in the LAP to release active TGF-β1 into the ECM [189,192–194]. Therefore latent TGF-β1 may be activated through a mechanosensitive pathway to maintain and encourage further myofibroblast activation.

From this brief review, mechanical forces and stretch are clearly intimately related to myofibroblast activation. Furthermore fibrosis is, in itself, clinically characterized by a progressive deterioration in the mechanical behavior of tissues. Therefore developing new approaches for conducting cell mechanics research, and further understanding of mechano-sensitive pathways may lead to new targets for urgently needed fibrosis treatments.

1.9 Conclusions and thesis outline

An approach that has been used before to understand the effect of external forces on cell behavior is to deform the 2D substrate on which they are cultured [9,195]. Additionally the current tools used for assessing the mechanical properties of cells largely require that they be grown on a 2D substrate. Environmentally speaking, these conditions are quite distant from the conditions cells would experience in the body. The objectives of this

thesis were to develop experimental techniques for mechanobiology, and to assess the mechanical and biological behavior of cells in a 3D environment exposed to stretch. This was achieved through 1) the development and characterization of lab-on-a-chip devices capable of stretching 3D cell cultures; 2) measuring of the effect of stretch on cell mechanics and remodeling in the cytoskeleton; 3) quantifying the timescale dependencies of 3D cultures in both the time and frequencies domains; and 4) investigating the effect of stretch on myofibroblast activation in 3D cultures. An outline of the remainder of the thesis is presented below:

Chapter 2. Although several macroscale stretching systems and a handful of microdevices have been previously developed to investigate the response to strain of both 2D and 3D cultures, a significant effort was carried out to fabricate a platform that could answer the specific research questions posed by this work. The general requirements for our platform included: 1) a microenvironment that was suitable for long-term (days) conditioning of cells; 2) reconstituting both the physical loading that cells experience *in vivo* and their 3D ECM; and 3) compatibility with high resolution live-cell imaging. We hypothesized that a pneumatically driven lab-on-a-chip device could meet these requirements. Our approach was validated for biophysical investigations through assessing how strain was transmitted from the tissue to the single cell-level. We also demonstrated here that our pneumatic device was a suitable approach for conducting biological research by assessing the effect of long-term stretch on actin remodeling. This manuscript was published in *Biomedical Microdevices* in 2018 [196].

Chapter 3. A number of studies have shown that cells on 2D substrates respond to dynamic loading by acutely softening and behaving more fluid-like. Yet this remodeling response of the cytoskeleton is poorly understood at the molecular-level, and the extent of this response is unclear at the tissue-level. We hypothesized that 3D cultures would also soften when acutely stretched through depolymerization and remodeling of their cytoskeleton. The objective of this chapter was to quantitatively link dynamic loading-induced structural remodeling of the cytoskeleton to mechanical changes at the tissue-level. This was achieved by modifying our pneumatic device to allow the assessment of forces. This investigation confirmed that the actin cytoskeleton of cells in 3D cultures is also regulated by dynamic stress, and thereby mechanical loading confers changes to the physical behavior of at the tissue-level. However, in contrast to other work in 2D culture and simplified gel networks, myosin cycling did not affect responses, and neither did remodeling in microtubules. These findings provide new insights on the mechano-sensing response of cells within physiological tissues. This manuscript was published in *Scientific Reports* in 2020.

Chapter 4. Force-sensing in cells involves physical conformational changes that are determined by their elastic and dissipative properties. Therefore defining the mechanical behavior of cells is necessary to fully understand these pathways. Prior to this work, our understanding of cell mechanics largely came from delivering unrealistic local shear and compressive loads on isolated cells grown on 2D substrate. Yet, we knew that growing cells in a 2D

environment vs. within a 3D ECM fundamentally changes the structure and distribution of the cytoskeleton. Furthermore, it was not known how local measurements scaled up to the entire cell behavior because of the complex, heterogeneous cytoskeletal structure. For these reasons, we hypothesized that the mechanical behavior of 3D cultures would exhibit time-scale dependencies that differed from the featureless rheological behavior that had been previously reported in cells in 2D culture. The objectives of this chapter were to measure the stress relaxation and recovery behaviors of microtissues, and to quantify the contributions of specific cytoskeletal proteins. This investigation found that, unlike previous results from 2D culture, the rheological behavior of microtissues follow stretched exponentials that are predominately determined by remodeling in actin microfilaments but also influenced by the presence of microtubules and myosin activity. This investigation provided new insights into how cytoskeletal proteins determine the dynamic mechanical behavior of cells and their collective behavior in tissues, which is necessary to understanding how cells sense forces in both health and disease. This manuscript was submitted to APL Bioengineering in 2020 and is currently under review.

Chapter 5. The results from chapter 4 raised important questions on the rheological behavior of cells within 3D environments in response to step changes to their length (ie. their behavior in the time domain). Many cells in the body, however, experience dynamic cyclic length changes, such as in our lungs and vasculature. Therefore, we asked whether there was an equivalent behavior under dynamic cyclic loading (ie. their behavior in the frequency domain). Our hypothesis was that the frequency response of microtissues would be a Fourier transform of their stretched exponential stress relaxation and recovery behaviors. We found that the frequency response was broadly distributed around a characteristic timescale, and thus, could be approximated by a stretched exponential. Furthermore the characteristic timescale corresponded to the difference in stress relaxation and recovery time constants. This suggests that, under cyclic loading, cells reach an equilibrium state set by the separate dynamics of these processes. Specifically we believe that stress relaxation and recovery measurements reflect assembly and disassembly rates of actin because the timescale dependencies largely disappeared upon pharmacological depolymerization of microfilaments. These findings further our understanding of the dynamic regulation of the cytoskeleton in cells in 3D environments. This manuscript has been prepared for submission to APL Bioengineering upon the publication of Chapter 4.

Chapter 6. In the body, persistent myofibroblast activation leads to the progressive deterioration in tissue mechanics that characterizes fibrotic disease. In this chapter, we used our microdevice to assess the effect of cyclic stretching on the phenotypic and mechanical changes to microtissues during fibroblast to myofibroblast differentiation and dedifferentiation. Specifically, we consider the hypothesis that cyclic stretch may be a stimulus that will maintain myofibroblast differentiation in microtissues through activating endogenously produced latent TGF-β1. We investigated this hypothesis by assessing α-SMA expression and microtissue mechanics. As expected, TGF-β1 treatment promoted a myofibroblast phenotype and microtissues became stiffer and possessed increased

contractility. These changes were partially reversible upon TGF-β1 withdrawal, however, as hypothesized, long-term cyclic stretching maintained myofibroblast activation. A receptor block and differentiation with a latent source further suggested that this effect was caused by endogenous TGF-β1 activation. These results link cell-level phenotypic changes to the functional changes that characterize the clinical manifestation of fibrotic disease, and provide insights into a mechanism through how myofibroblasts are regulated through mechanical stretch. Continued investigation with our microdevice and further knowledge of this mechanism may reveal new therapeutic targets to treat fibrosis. This manuscript has been submitted for publication to *Integrative Biology* in 2020 and is currently under review.

Chapter 7. This chapter concludes the thesis with future directions and a broad discussion of the implications of the thesis findings.

CHAPTER 2| A VACUUM-ACTUATED MICROTISSUE STRETCHER FOR LONG-TERM EXPOSURE TO OSCILLATORY STRAIN WITHIN A 3D MATRIX

Authors: **Matthew Walker**, Michel Godin, Andrew E. Pelling

This manuscript was published in Biomedical Microdevices in 2018 (doi: 10.1007/s10544-018-0286-4):

Walker, M., Godin, M. & Pelling, A. E. A vacuum-actuated microtissue stretcher for long-term exposure to oscillatory strain within a 3D matrix. *Biomed. Microdevices* **20,** 43 (2018).

The supplementary information is contained in Appendix A.

Motivation & Objective| For many cells, stretch and a 3D ECM are a key regulators of their biological function in the body. However, our understanding of cell behavior has largely come from investigations carried out on static 2D cultures. In this chapter, we developed a stretcher for 3D cell cultures, and validated the effectiveness our approach through biophysical assessments with live-cell microscopy and long-term mechanical conditioning in an incubator.

2.1 Abstract

Although our understanding of cellular behavior in response to extracellular biological and mechanical stimuli has greatly advanced using conventional 2D cell culture methods, these techniques lack physiological relevance. To a cell, the extracellular environment of a 2D plastic petri dish is artificially flat, extremely rigid, static and void of matrix protein. In contrast, we developed the microtissue vacuum-actuated stretcher (MVAS) to probe cellular behavior within a 3D multicellular environment composed of innate matrix protein, and in response to continuous uniaxial stretch. An array format, compatibility with live imaging and high-throughput fabrication techniques make the MVAS highly suited for biomedical research and pharmaceutical discovery. We validated our approach by characterizing the bulk microtissue strain, the microtissue strain field and single cell strain, and by assessing F-actin expression in response to chronic cyclic strain of 10%. The MVAS was shown to be capable of delivering reproducible dynamic bulk strain amplitudes up to 13%. The strain at the single cell level was found to be 10.4% less than the microtissue axial strain due to cellular rotation. Chronic cyclic strain produced a 35% increase in F-actin expression consistent with cytoskeletal reinforcement previously observed in 2D cell culture. The MVAS may further our understanding of the reciprocity shared between cells and their environment, which is critical to meaningful biomedical research and successful therapeutic approaches.

2.2 Introduction

Cellular behavior is highly influenced by biological and mechanical stimuli from the surrounding extracellular environment [1,33,34,134,135]. Whereas in the body cells receive stimuli in three dimensions, conventional cell culture techniques limit these interactions to two dimensions. In doing so, adhesion complexes and the

cytoskeleton are forced into an unnatural apical-basal polarity [31]. Conventional cell culture in petri dishes further disrupts adhesion-signaling pathways by offering an extremely rigid substrate void of natural matrix adhesion ligands, which greatly impacts cellular morphology and phenotype [134,135].

In addition to a soft 3D matrix, many cells in the body also experience cyclic mechanical stretch. Examples include the expanding of airways during inspiration or of blood vessels during systole. These forces create continually unstable and unevenly distributed strain at focal adhesion complexes, across the cell membrane, along cytoskeleton filaments and through the nucleus. Many ligand-receptor affinities that regulate cellular phenotype and function are known to be responsive to these forces [1,17].

The differences between the *in vivo* extracellular environment and a 2D static, rigid petri dish may account for observed disparities in cellular behavior and could explain how many drugs developed using conventional 2D cell culture are found to be ineffective in costly clinical trials [33,34,123,197]. Thus there is a need for novel high-throughput, low resource intensive cell culture techniques capable of probing cellular behavior and drug screening while providing a physiologically relevant environment.

To recapitulate the 3D *in vivo* environment, cells have often been cultured in bulk soft gels of innate extracellular matrix proteins. These methods have been extensively reviewed elsewhere [116,119]. It is also becoming an increasingly common practice, particularly in airway and vascular cell biology, to chronically stretch 3D cell cultures using either in-house built bioreactors [123,198–203] or commercially available systems (eg. Tissue Train®, Flexcell; MCFX, CellScale). Due to their scale, these methods are, however, resource intensive and low throughput, while leading to a high diffusive barrier for pharmacological treatments and nutrients. The ability to image through the sample is also often limited. The disadvantages of large-scale 3D cell cultures led to the development of a sub-millimeter 3D cell culture model called microfabricated tissue gauges (microtissues) [124]. The microtissue model consists of an array of wells each containing two flexible polydimethylsiloxane (PDMS) cantilevers spaced approximately 500mm apart. Cells in a collagen solution are introduced into each well, and self-assemble around the tops of the cantilevers into an organized 3D structure highly comparable to *ex vivo* tissue.

Recently, the Magnetic Microtissue Tester (MMT) was developed to deliver cyclic stretch to microtissues. In the MMT, magnetic microspheres are manually fixed under a microscope one at a time to one of the cantilevers in each well. A microtissue can then be actuated by using magnetic tweezers to attract the microsphere [128,129]. The MMT was later adapted to stretch multiple microtissues simultaneously with an array of electrodeposited bar magnetics [204]. This method, however, still required manually fixing the microspheres to one cantilever at a time, which limits high-throughput fabrication, and the strength of the electrodeposited magnetics limited the bulk strain amplitude to 4%. More importantly, although Xu *et al.* (2015) highlighted the importance of chronic mechanical conditioning to microtissue development, the ability of their device to operate within a humid and highly corrosive incubator for a long period (days) has yet to be demonstrated.

Here we present an alternative method, the Microtissue Vacuum-Actuated Stretcher (MVAS), which utilizes vacuum actuation to produce bulk strain amplitudes up to 13%, and is fabricated by high-throughput mold

replication and alignment steps. It consists of an array of wells each with a set of cantilevers on a thin membrane bordered by vacuum chambers. When a vacuum is applied, the walls of the wells deform, stretching the thin membrane and the microtissue in plane allowing simultaneous live-cell imaging. Similar vacuum actuation systems have previously been shown to be reliable for 2D cell culture [9,138,195]. We show that this vacuum actuation system is reliable for long term conditioning of 3D cell cultures. In this paper, we describe the fabrication steps of the MVAS and we characterized the bulk microtissue strain, the microtissue strain field and single cell strain. As a final demonstration of our approach, we assessed changes in F-actin expression in response to chronic cyclic strain, which has commonly been observed in cells in 2D culture [205].

2.3 Methods

Device design

The MVAS consists of five independently controllable rows of ten microtissue wells. As with the original microtissue design [124], each well has an open top for cell loading and cantilevers spaced apart by 500mm around which the microtissues are formed. The wells are bordered by enclosed vacuum chambers, which are connected to an external electronic regulator (SMC, ITV0010) and controller via Labview software. When a vacuum is applied, the flexible PDMS material deforms to separate the cantilevers to stretch the microtissues along their longitudinal axes.

The MVAS is composed of a top support and three photolithographic layers all entirely polydimethylsiloxane (PDMS) (Dow Corning, Sylgard 184). An expanded view is shown in fig. 2.1(a) and the assembled device is shown in fig. 2.1(b). The top support contains the vacuum and fluidics inlets, and encloses the fifty-microtissue wells within a single shared media well. During fabrication, the top support reduces shrinking and warping of the top layer so it retains the geometry of its mold. The top layer contains cell and vacuum chambers. The middle membrane is a thin layer with the cantilevers around which the microtissues compact. The bottom layer contains vacuum chambers with identical geometry to the top layer, and empty bottom chambers that equalize the pressure on either side of the membrane to minimize out of plane motion.

Device fabrication

The masters for the top layer, middle membrane, and bottom layer were fabricated using common photolithographic techniques. Briefly, SU-2075 photoresist (Microchem) was spin coated onto plasma-cleaned silicon wafers (University Wafers, UW3MEC). The photoresist was then UV polymerized through a photomask (CAD Art Services Inc.), transferring the features of the photomask to the wafer. Non-polymerized photoresist was then removed with SU-8 developer (Microchem). Spin rates, baking, and energy exposure were kept consistent with manufacturer's recommendations. Two photolithography steps were used for the top layer to create open top wells, and for the through-holes in the middle membrane.

Devices were quickly (<1hr/device not including curing time) fabricated through mold replication from the reusable photolithographic masters. The top and bottom layers were cast with a 10:1 monomer to curing agent ratio, whereas the middle membrane was cast with a 15:1 ratio. Fabrication steps of one well are illustrated in fig. 2.1(c). PDMS was applied over the features on the bottom layer master. For the middle membrane and top layer, PDMS was spin coated to 30mm and up to the feature height, respectively. The bottom layer was removed from its master and plasma bonded onto the middle membrane (green arrow). The top support (also PDMS) was bonded onto the top layer (blue arrow). The two halves of the device were then removed from the middle membrane and top layer masters, respectively, and bonded together (red arrows).

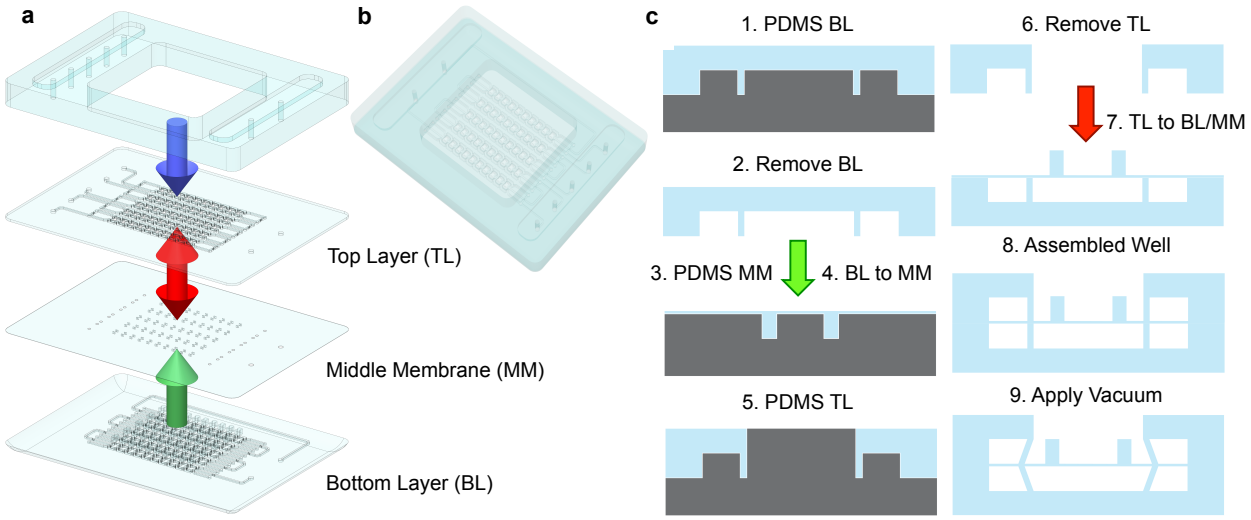

Fig. 2.1: MVAS device assembly. The MVAS consists of 4 layers: 1) a top support; 2) a top channel and vacuum layer; 3) a middle membrane with the cantilevers; and 4) a bottom channel and vacuum layer. An exploded view is shown in (a) and the assembled device is shown in (b). Cross-sections of fabrication steps of one well are illustrated in (c). For the bottom layer, PDMS is applied over top of the features on the SU-8 photolithography master and removed. For the middle membrane and top channel layers, PDMS is spin coated to 30mm and up to the top of the features, respectively. The bottom layer is then plasma bonded onto the middle membrane (green arrow) and the top support is bonded onto the top layer (blue arrow). The two are then removed from the middle membrane and top layer masters, respectively, and bonded together (red arrow). When vacuum is applied, the middle membrane is strained in plane moving the cantilevers apart stretching the microtissue.

Cell culture

NIH3T3 (ATCC) and NIH3T3-GFP (Cedarlane, AKR-214) cells were cultured in DMEM (Dulbecco modified eagle medium) with 10% fetal bovine serum (FBS), 50mg/ml streptomycin and 50U/ml penicillin antibiotics (all from Hyclone Laboratories Inc.), and maintained at 37°C with 5% CO_2 on 100mm tissue culture dishes (Fisher) until 80-90% confluent.

Tissue fabrication

Microtissue fabrication was performed as described previously [120,124], with some modifications. Briefly, the device was sterilized by three washes with 70% ethanol, and treated with 0.2% Pluronic F-127 (Invitrogen, P6866) for two minutes to reduce cell adhesion to the PDMS. 300,000 cells were resuspended in 1.5mg/ml rat tail collagen type I (Corning, 354249) substituted with 1x DMEM (Hyclone, SH30003.02), 44 mM $NaHCO_3$, 15 mM d-ribose (Sigma Aldrich, R9629), 1% FBS and 1 M NaOH to achieve a final pH of 7.0-7.4. The d-ribose was added to cross-link collagen fibrils through non-enzymatic glycation to improve the matrix stability. The cell-collagen solution was pipetted into the MVAS and centrifuged to load ~800 cells into each well. Once the excess collagen was removed, the device was transferred into the incubator for 15min to initiate collagen polymerization. Cell culture media was added and changed every 24 hours. To measure the cell strain within the microtissue, one NIH3T3-GFP cell was included for every 200 non-labeled 3T3 cells. For all other experiments, solely non-labeled cells were used.

Imaging

To estimate the tissue strain field, phase contrast videos were captured on a TiE microscope (Nikon) at 10 frames per second and 8-bit resolution. All other images were acquired on a TiE A1-R laser scanning confocal microscope (LSCM) (Nikon). 12-bit images were acquired with standard LSCM configurations with appropriate laser lines and filter blocks. To assess morphology, microtissues were fixed *in situ* with paraformaldehyde for 10 minutes and permeabilized with Triton-X for 3 minutes. The actin cytoskeleton was stained with Alexa Fluor 546 Phalloidin (Fisher, A22283) and the nuclei were stained with DAPI (Fisher, D1306).

Bulk strain

The bulk axial microtissue strain was calculated from measurements of cantilever motion. The locations of the cantilevers were tracked using pattern matching in Labview. To be consistent with previous work [129,204], the bulk strain was defined as the percent change in the distance between the inner most edges of the cantilevers. This measurement, however, does overestimate strain values if the microtissues are not perfectly anchored at the inner edges of the cantilevers. The peak dynamic bulk strain was determined from the magnitude at the fundamental frequency of the Fourier transform.

Tissue strain field

Local strains were estimated across microtissues while undergoing a 0.1Hz sinusoidal stretch. A detailed example of how the strain fields were estimated can be found in Appendix A.1. The inter-frame displacements were estimated at five-pixel spacing across a region of interest (530x315 pixels) encompassing the microtissue using Labview's pyramid based Lucas and Kanade algorithm [206] with four levels, sub-pixel precision and a window size of 17x17 pixels. The inter-frame strain tensor was calculated from the gradient of the displacement field after

it had been smoothed with a LOWESS surface-fitting algorithm in Matlab. Starting at 0% strain, the inter-frame strain field was integrated to estimate the local total strain field.

Cell strain

To measure the cell strain within the microtissue, randomly distributed GFP labeled cells were imaged at 2 days post seeding immediately following static loading at 0%, 3%, 7% and 14% strain. These strains were chosen empirically to provide measurements that cover the physiological range [11,29,207,208]. Individual cell lengths were measured in Matlab using adaptive thresholding on maximum intensity projections of confocal stacks. The cell length was defined as the largest distance between any two points on the cell perimeter. Only cells between the cantilevers were used in the analysis.

The cell strain, e, was defined as the change in the length, L, divided by the initial length irrespective of cell orientation (equation 2.1).

$$Cell\,\varepsilon = \frac{L_2 - L_1}{L_1} \tag{2.1}$$

To account for reorientation of the cells caused by loading, the axial strain produced by cell lengthening and reorientation (Total Cell e_x) was calculated according to equation 2.2. The angle, θ, was measured between the cell length and the longitudinal axis of the microtissue.

$$Total\ Cell\,\varepsilon_x = \frac{L_2 * cos\,(\theta_2) - L_1 * cos\,(\theta_1)}{L_1 * cos\,(\theta_1)} \tag{2.2}$$

The contributions of cell lengthening (Cell e_x) and cell rotation (Angle e_x) to axial strain were calculated according to equation 2.3 and 2.4, respectively.

$$Cell\,\varepsilon_x = cos(\theta_1) * \frac{L_2 - L_1}{L_1} \tag{2.3}$$

$$Angle\,\varepsilon_x = Total\ Cell\,\varepsilon_x - Cell\,\varepsilon_x \tag{2.4}$$

To compare the individual measurements of cell strain to the tissue strain, the axial tissue strain for each cell location was calculated from the gradient of the cell displacement field after it had been smoothed with LOWESS surface fitting algorithm.

F-actin expression in response to chronic strain

After microtissue fabrication, both the control and stretched groups were left to compact for two days under static condition. The stretched group then received a 10% 0.1Hz bulk strain for another two days while the control group was left under static condition. At four days post seeding, the nuclei and the F-actin cytoskeleton of both groups were stained with the same protocol, and imaged with identical laser and camera settings. The average integrated intensities of confocal stacks normalized to the control group were used as measures of cell number and actin polymerization. To assess the spatial distribution of changes in nuclei and F-actin, integrated confocal projections were aligned and averaged to give a percent change between stretched and control groups.

Data analysis

Linear regression and t-tests were performed where indicated. $P<0.05$ was considered significant. SE: standard error; SD: standard deviation, R^2: coefficient of determination; n: sample size; P: p-value.

Data availability

The datasets generated during and/or analyzed during the current study are available from the corresponding author on reasonable request.

2.4 Results

Microtissue morphology

Cells in a collagen solution were pipetted into the device, which was then centrifuged to load 770±30 (SD, n=8) cells into each well. Microtissue formation occurred as previously shown [124]. The cells compacted the collagen matrix away from the F-127 coated sides and bottoms of the wells, and around the cantilevers into dense, organized, freely suspended, three-dimensional microtissues. The MVAS contains fifty individual microtissue wells enabling high content manipulations for cellular mechanics and pharmaceutical discovery (fig. 2.2(a)). At four days post seeding, microtissue survival rates were greater than 80% with the large majority of cells contained within the microtissues.

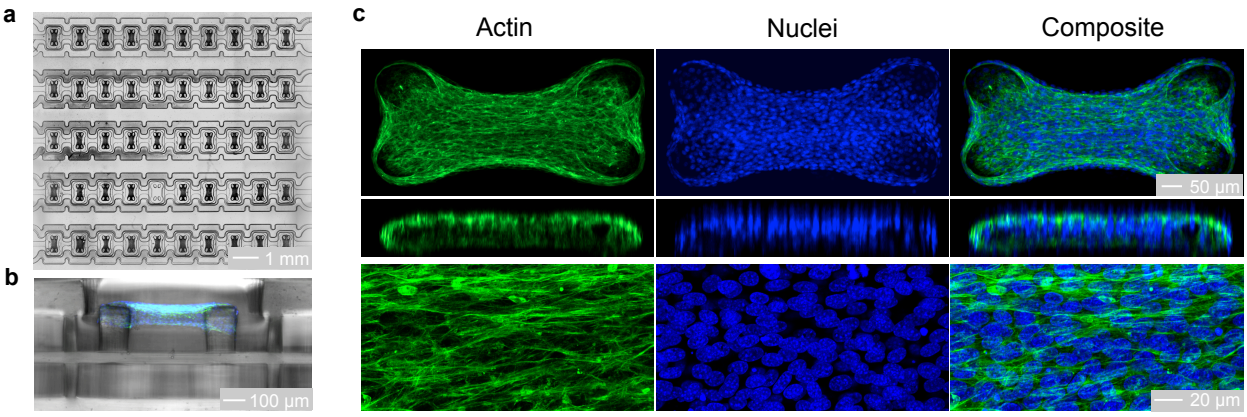

Fig. 2.2: Representative microtissues after four days. Microtissues are dense, organized, three-dimensional cell cultures freely suspended around cantilevers. The MVAS contains an array of fifty microtissues (a). A cross-sectional view of the MVAS and a microtissue is shown in (b). Max projections and an orthogonal slice of representative confocal stacks are shown in (c). The actin cytoskeleton is in green and the nuclei are in blue. Both the actin cytoskeleton and nuclei possess a high degree of organization, aligning between the cantilevers.

A cross-sectional view of a fully compacted representative microtissue in the MVAS is shown in fig. 2.2(b). Maximum intensity projections of confocal stacks with an orthogonal slice at 10X magnification, and centrally-

located maximum intensity projections of a 10mm-thick section at 60X magnification are shown in fig. 2.2(c). The actin cytoskeleton was highly polymerized and organized into dense stress fibers that were oriented with the length of the microtissue. The cell nuclei were evenly distributed in three dimensions and mostly aligned with the microtissue.

Bulk strain characterization

When a vacuum is applied to the chambers bordering the cell culture wells, the cantilevers move apart, stretching the microtissues (fig. 2.3(a) and Appendix A: movie A.1). The motion is largely planar (Appendix A.3), allowing real-time imaging of the deformation. When using a computer-controlled regulator to apply a 0.1Hz sinusoidal vacuum, the bulk strain, measured from cantilever motion, was smooth and continuous with submicron resolution and high repeatability (fig. 2.3(b)). The average (n=9) peak dynamic bulk strain was directly related to the applied vacuum with some nonlinearity at higher pressures (fig. 3c). At 90 kPa, the peak strain was 13.0 ± 0.9 (SD)%, which covers the physiological range [11,29,207,208], and was highly reproducible.

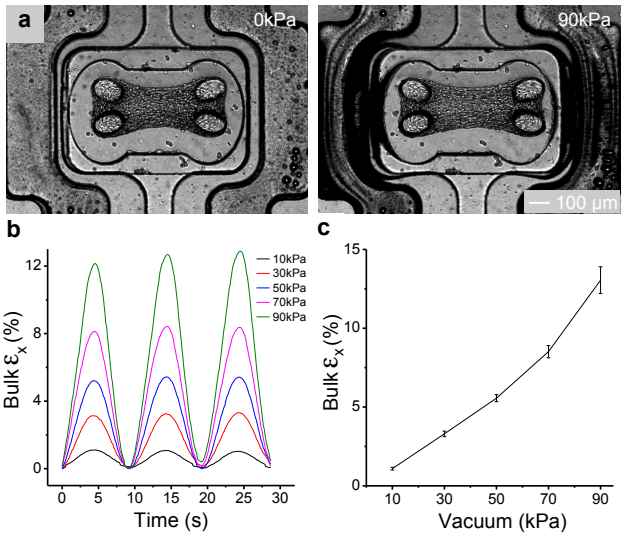

Fig. 2.3: Bulk strain characterization. When a vacuum is applied, the cantilevers move apart stretching the microtissue in plane. Representative images of a microtissue in the MVAS are shown in (a). With a 0.1Hz sinusoidal vacuum, the bulk strain is smooth, continuous and repeatable (b). The average (n=9) bulk strain increased reproducibly with vacuum pressure (c). At 90kPa, the peak bulk strain was 13± 0.9(SD)%. Error bars represent the standard deviation.

Tissue strain field

To estimate the dynamic axial strain distribution, microtissues (n=10) were stretched at 0.1Hz to a maximal bulk strain of 10.7±0.9 (SD)%. As expected the bulk microtissue strain measured from the cantilever motion and the spatial average of the axial strain field followed the sinusoidally applied vacuum (fig. 2.4(a) and (b), respectively). The maximal spatially averaged strain field was 8.3±0.7 (SD)%. The difference in amplitude from the

bulk strain can be accounted by an over estimation in the bulk strain measurement caused by imperfect anchoring of cells at the inner edges of the cantilevers.

Axial strain fields of a representative microtissue are shown in fig. 2.4(c). Qualitatively, there are local maxima in the axial strain field near each cantilever indicating strain heterogeneity. The maximum axial strain during one cycle averaged across multiple (n=10) microtissues is plotted as a function of axial position in fig. 2.4(d). Strain heterogeneity near the cantilevers is again evident. The maximum axial strain field was reproducible across multiple microtissues (n=10) with a standard deviation of 1.5 ± 0.5%. The average (n=10) and standard deviation of axial strain fields are shown in Appendix A: movies A.2-3, respectively. The maximum standard deviation (n=10) of the axial strain field during one cycle was 2.8 ± 0.4%. The transverse and shear strain fields were comparably smaller (Appendix A: movies A.4-7).

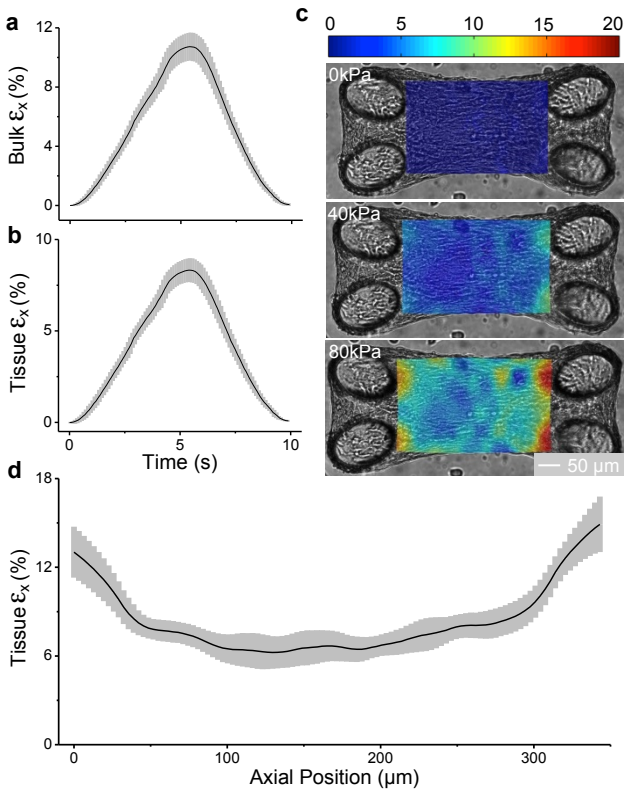

Fig. 2.4: Tissue strain field. The time courses of tissue bulk strain measured from the inter-cantilever distance (a) and the average (n=10) of estimated axial strain fields (b) followed the sinusoidal change in vacuum. The estimated axial strain field of a representative microtissue is shown in (c). The strain field was inhomogeneous and concentrated around the cantilevers. The average (n=10) peak axial strain values are plotted against axial position in (d). The estimated strain field was highly reproducible between tissues. Error bars on all graphs represent the standard deviation.

Cell strain

To measure the strain experienced by individual cells, changes in length of GFP labeled cells were assessed immediately following static loading within the MVAS (fig. 2.5(a)). The average (n=79) cell length increased linearly (R^2=0.999, P<0.001) with tissue axial strain measured from the gradient of the cellular displacement field fig. 2.5(b)). The degree of cell lengthening was significantly, albeit weakly, related to the initial cell length, with shorter cells undergoing greater strain (R^2=0.07, P<0.05) (Appendix A.2 (a)).

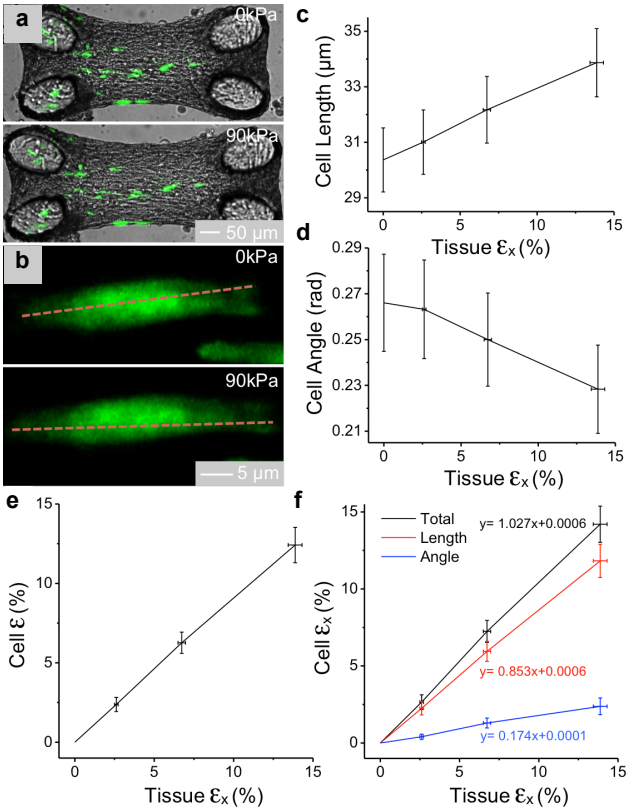

Fig. 2.5: Cellular strain. A representative microtissue with GFP labeled cells (green) under 0% and ~15% strain is shown in (a). A GFP labeled cell located within the microtissue is shown in (b) with the measured cell length drawn in red. The average (n=79) cell length increased linearly with tissue axial strain (c) and the average absolute cell angle decreased (d). Due to cellular reorientation, the average cell strain was attenuated 10% compared to the tissue axial strain (e). Accounting for reorientation, the axial cell strain was approximately equal to the axial tissue strain (f). The axial cell strain due to cell lengthening accounted for 85% of the axial tissue strain, and reorientation accounted for 17%. Error bars represent the standard error.

The average absolute angle between the cell and the longitudinal axis of the microtissue decreased (R^2=0.987, P<0.005) with tissue axial strain (fig. 2.5c). At a tissue strain of 13.9±0.4(SE)%, the average cell had reoriented 0.04±0.03(SE) rad to better align with the tissue. The degree of alignment was weakly related to the initial cell angle in that poorly aligned cells had a greater degree of reorientation (R^2=0.26, P<0.001) (Appendix A.2

(b)). There were no relationships between initial cell angle and the cell or tissue strains (P>0.05) (Appendix A.2 (c,d)).

The average cell strain was 89.6% (R^2=0.9996, P<0.001) of the tissue axial strain (fig. 2.5(d)). This difference is attributable to cellular reorientation (fig. 2.5(e)). When accounting for reorientation, the axial strain produced by cell lengthening and rotation was 102.7% (R^2=0.9996, P<0.001) of the axial tissue strain. The axial cell strain due to cell lengthening accounted for 85.3% (R^2=0.9996, P<0.001) of the axial tissue strain, and reorientation accounted for 17.4% (R^2=0.994, P<0.005). Interestingly, the relative contributions of cell lengthening and reorientation to tissue axial strain were both constants at all strains tested.

Chronic stretch increases f-actin expression in microtissues

To assess the effect of long-term stretch on F-actin expression, microtissues (n=6) were cyclically stretched at a bulk strain of 10.3±0.3(SE)% for 48 hours and compared to a static control group (n=6). The normalized integrated fluorescence of nuclei and F-actin is shown in fig. 2.6(a). Although there was no significant change in total nuclei fluorescence (P>0.05, t-test), chronic stretch significantly increased F-actin (P<0.01, t-test). On a per cell basis, actin polymerization increased by 35±5(SE)%. The average nuclei and F-actin spatial distributions of percent change comparing stretched to control are shown in fig. 2.6(b) and (c), respectively. Qualitatively, compared with the control, the nuclei appear slightly more concentrated in the center of stretched microtissues, and the F-actin fluorescence is greater throughout.

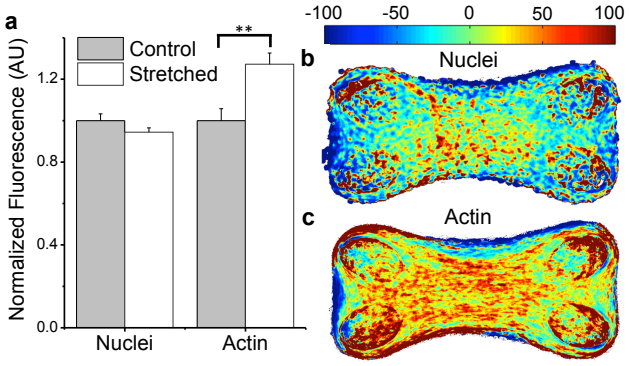

Fig. 2.6: Cytoskeletal remodeling in response to chronic cyclic strain. The average (n=6) normalized total fluorescence of nuclei did not change between non-stretched control and stretched groups while F-actin fluorescence significantly increased with stretch (a). Chronic stretch caused a 35% increase in F-actin per cell. Error bars represent the standard error. The spatial distribution of percent change between stretched to control of average (n=6) nuclei and F-actin fluorescence are shown in (b) and (c), respectively. Stretch increased F-actin expression throughout the microtissues. (**: P<0.01)

2.5 Discussion

It is widely accepted that biological and mechanical stimuli from the surrounding extracellular environment influences cellular behavior [1,33,34,134,135]. Yet traditionally, cell culture for biomedical research and pharmaceutical discovery has been carried out in petri dishes, which to a cell, is a 2D, rigid, static substrate with little physiological relevance. Although our understanding of cellular behavior has advanced tremendously using these conventional cell culture techniques, it is unknown whether cellular behavior studied in the lab truly reflects cellular behavior in the body. To answer this question, there is currently a need for cell culture methods with improved physiological relevance. To fulfill this need, cells in our device are cultured within a 3D collagen matrix and self-organize into a densely compacted microtissue comparable to *ex vivo* tissue. Importantly, cells grown in similar 3D collagen matrices better express their differentiated functions when compared to cells grown in 2D culture [33,34,123,197].

In addition to offering relevant 3D cell-matrix interactions, our device enables investigations into chronic cyclic stretch. The uniaxial stretch is applied along the longitudinal axis of the microtissues, with which the cells are mostly aligned. The cellular orientation with respect to the strain direction recapitulates the circumferential stretch in airways or blood vessels, and the longitudinal stretch in muscle.

We found long-term (2 days) stretch significantly increases F-actin expression per cell. Cytoskeletal reinforcement in response to stretch is consistent with previously published findings in 2D culture [78,155,205,209–212]. Although the added complexity of a 3D matrix often makes direct comparisons with 2D culture difficult, we have now confirmed that cytoskeletal reinforcement in response to long term conditioning occurs in cells grown in a physiological 3D cell culture. With that said, further work is needed to investigate whether the change in F-actin was produced from increased actin production and/or increased recruitment of actin into stress fibers.

In addition to regulating F-actin, stretch has been shown in 2D culture to be a potent regulator of protein interactions within focal adhesion complexes that govern cell behavior [11,29,207,208]. For two reasons it is critical to continue this work using 3D cell culture. First, a third dimension for cell adhesion significantly affects integrin/adhesion distribution and the cytoskeletal structure [31], which may alter how mechanical inputs are perceived. It has been speculated that stretching 3D tissue constructs may induce more biomimetic effects than 2D cell culture [213]. Second, the presence of a soft, viscoelastic matrix may alter the strain field felt by the cells. To that end, we found that the average cell strain was 10.4% less than the microtissue strain. Although very little is known about strain magnitudes experienced by cells in tissue, attenuation from tissue-level to cell-level has been observed previously in fibrous tissues [214]. In our microtissues, we found the attenuation could be explained fully by the initial cell angle and rotation. After accounting for initial cell angle and rotation, we found the axial cell strain was equal to the axial microtissue strain. Importantly, this mechanism of attenuation is not captured in 2D culture systems.

Biological and mechanical differences between 2D cell culture and the *in vivo* environment have cost pharmaceutical companies immensely in failed clinical trials creating a strong demand for more relevant 3D cell

culture techniques [33,34,123,197]. Although many large-scale bioreactors have combined a 3D cell matrix and stretch, these techniques often require months of cell culture, and due to their size, large drug doses to be synthesized [123,202,203]. The multi-well capability and sub-millimeter scale makes the MVAS a high-content, low resource intensive alternative, and importantly, all fabrication steps can be quickly replicated to meet the demands of the pharmaceutical industry.

The MVAS is capable of delivering large oscillatory strain to an array of microtissues while allowing live imaging with minimal (<10μm) out of plane motion (Appendix A.3). Because of the planar stretch, the MVAS is suited for assessing biomechanics of cells and tissues. As a demonstration of this capability, we quantified the bulk tissue strain, the tissue strain field and the cellular strain. The axial strain field was homogeneous apart from strain concentrations around the cantilevers. Strain gradients are important consideration for when examining local cell behavior [138], and should be improved in future work through a better method of anchoring. Our device was capable of delivering a bulk tissue strain greater than 13% with a 90kPa vacuum. Although higher strain may be achievable through increased vacuum pressure or further optimizing device dimensions and materials, this strain sufficiently covers the physiological range in airways and blood vessels and is a sufficient stimulus to produce measurable differences in cell behavior [11,29,207,208].

In this paper, we provided proof of concept for a device to stretch an array of lab grown microtissues consisting of fibroblasts and a 3D collagen matrix. Although this is a significant step forward in terms of physiological relevance compared to 2D cell culture, much is still needed to fully recapitulate the *in vivo* environment on a chip. Future work with using this device should be focused on culturing tissue specific cells, such as airway smooth muscle, vascular smooth muscle or skeletal muscle, and with a matrix composition that better matches health and disease states. To further the physiological relevance, each microtissue could be surrounded by a monolayer of epithelial or endothelial cells. Genetically modified cells may also be used in the device to mimic a specific disease, allowing investigations into tissue-level mechanobiology without creating and harvest samples from transgenic organisms. With these future developments, combined with rapid gene expression and immunofluorescence techniques, the MVAS would be a leading platform to perform high-content analysis for chronic biomedical research and drug development in blood vessel, airway and muscle cell cultures.

2.6 Conclusions

We developed a device to probe cellular behavior for biomedical research and pharmaceutical discovery while maintaining a physiologically relevant environment. Our device offers: 1) a soft, 3D multicellular environment composed from innate matrix protein; 2) the ability to apply large amplitude, long-term, cyclic mechanical stretch; 3) a micro-array format for high-content analysis; 4) compatibility with live imaging with limited out of plane motion; and 5) quickly replicable fabrication steps. These features of our platform mark a significant improvement over other methods currently used to study cellular behavior in biomedical research and the pharmaceutical industry. Future investigations using the MVAS to chronically manipulate mechanical and

biological cues may unveil how interactions between cells and their environment contribute to normal and pathophysiological behavior, which is critical to meaningful biomedical research and successful therapeutic approaches.

CHAPTER 3| STRUCTURAL AND MECHANICAL REMODELING OF THE CYTOSKELETON MAINTAINS TENSIONAL HOMEOSTASIS IN 3D MICROTISSUES UNDER ACUTE DYNAMIC STRETCH

Authors: **Matthew Walker**, Pauline Rizzuto, Michel Godin, Andrew E. Pelling

The manuscript was accepted for publication at Scientific Reports on April 21 2020 and is accessible on the preprint server BioRXIV (doi: https://doi.org/10.1101/780312). The supplementary information is contained in Appendix B.

Motivation & Objective| Whereas it has been well reported that cells grown on 2D substrates mechanically soften under acute dynamic stretch, the remodeling behavior of the cytoskeleton remains poorly understood. Also the extent of the response in tissues and 3D cell cultures is unclear. In this chapter, we addressed these research questions through assessing the mechanical response of microtissue cultures during cyclic loading by modifying our device in chapter 2 for force measurements. We then linked this behavior to direct visual evidence of remodeling and quantified the contribution to the softening response from distinct cytoskeletal elements.

3.1 Abstract

When stretched, cells cultured on 2D substrates share a universal softening and fluidization response that arises from poorly understood remodeling of well-conserved cytoskeletal elements. It is known, however, that the structure and distribution of the cytoskeleton is profoundly influenced by the dimensionality of a cell's environment. Therefore, in this study we aimed to determine whether cells cultured in a 3D matrix share this softening behavior and to link it to cytoskeletal remodeling. To achieve this, we developed a high-throughput approach to measure the dynamic mechanical properties of cells and allow for sub-cellular imaging within physiologically relevant 3D microtissues. We found that fibroblast, smooth muscle and skeletal muscle microtissues strain softened but did not fluidize, and upon loading cessation, they regained their initial mechanical properties. Furthermore, microtissue prestress decreased with the strain amplitude to maintain a constant mean tension. This adaptation under an auxotonic condition resulted in lengthening. A filamentous actin cytoskeleton was required, and responses were mirrored by changes to actin remodeling rates and visual evidence of stretch-induced actin depolymerization. Our new approach for assessing cell mechanics has linked behaviors seen in 2D cultures to a 3D matrix, and connected remodeling of the cytoskeleton to homeostatic mechanical regulation of tissues.

3.2 Introduction

With every breath, heartbeat and movement, cells in our body experience cyclic mechanical stretch, which in turn, creates continually unsteady forces at focal adhesions, across the cell membrane, along cytoskeletal filaments and through the nucleus [1,17]. In a cell, these forces direct functional and phenotypic behaviors by generating conformational changes, and thereby, alter ligand-receptor affinities [1,17]. Importantly, this ability of cells to feel and adapt to mechanical forces has been linked to crucial events in normal development and function, as well as disease progression, including bone, muscle, heart and lung disorders, and cancer [4,5].

In particular, the well-conserved structural elements that make up the cytoskeleton of eukaryotic cells are in themselves mechanosensitive; in response to dynamic stretch, the cytoskeleton softens (decreased elasticity) and becomes more fluid-like [92,101–103]. Then upon stretch cessation, it slowly regains its stiffness and resolidifies [92]. Currently the molecular mechanism(s) behind strain softening remains unclear as there is limited visual-based evidence quantifying cytoskeletal remodeling following cyclic stretching [78–80]. Furthermore, whereas softening and fluidization has been observed in response to deformation at the subcellular [101,102] and single cell levels [92,103], the extent of the response remains poorly understood at the tissue-level [7,8,215]. Nevertheless, in the body, this response has been linked to the maintenance of airway caliber [7,8] and the regulation of blood pressure [104], but for unknown reasons, it is absent in certain pathological disorders. For example, unlike in healthy lungs, stretch from a deep inspiration does not dilate asthmatic airways [105].

While studying the mechanical behaviors of intact tissues has furthered our knowledge of how cells respond to stretch [7,8], these methods possess poor resolution for elucidating subcellular remodeling. Investigations may also be hindered by inter-donor variability and low availability of tissue samples. On the other hand, subcellular cytoskeletal remodeling responses and mechanotransduction pathways have been investigated in large part by growing cells on rigid, flat surfaces. Yet it is known that the physical environment in which a cell is grown alters its mechanical properties and behavior. For example, cells grown on stiff substrates tend to have their actin cytoskeleton arranged into dense stress fibers, and are stiffer, more solid-like and under greater pre-stress when compared to cells on softer substrates [134,135,137].

In addition to matrix stiffness, it is suspected that the mechanical behavior of cells may be further altered by the dimensionality of their environment. In support of this growing hypothesis, culturing cells on a 2D substrate vs. within a more physiologically relevant 3D matrix fundamentally changes the distribution and structure of the cytoskeleton by forcing un-natural apical-basal polarity of adhesion complexes [31]. The difference between a rigid, flat, petri dish and a soft 3D extracellular matrix (ECM) may also explain observed disparities in cellular behavior, and the loss of efficacy in costly clinical trials that often occurs when pharmaceutical treatments are developed using conventional 2D cell culture techniques [33,34,123,197]. Thus, there exists a need for new high-throughput cell culture techniques capable of probing cell mechanical behavior while maintaining a physiologically relevant soft 3D environment.

To address this need, techniques that allow assessment of the mechanical behavior of cells within reconstituted 3D collagen gels have been a keen interest to the fields of mechanobiology, pharmacology, and tissue engineering [116]. These methods have furthered our understanding of how tissue-level forces are collectively generated by cells and the ECM [216–218]. In regards to their response to stretch, it is known that cells within 3D cultures respond to static changes in matrix tension through altering their contractility in the opposite direction so to maintain a tensional homeostasis throughout the cell culture [219,220]. In other publications these behaviors following step length changes have been linked to actin depolymerization and reinforcement responses [221,222]. Although the responses to static strains have been well documented [219–222], the mechanical and cytoskeletal remodeling responses under cyclic stretching in 3D cultures is less clear. That said, during dynamic stretching of 3D cultures, the peak force of subsequent loading cycles has been shown to decrease towards a plateau [223], which is suggestive of an adaptive strain softening behavior. However, our field lacks a complete characterization of this mechanical response in 3D cell cultures and an investigation of the physiological cytoskeletal remodeling mechanism behind it.

In addition, the centimeter scale of the bulk gels used in previous investigations limits the experimental throughput, causes imaging difficulties, produces a high diffusive barrier for nutrients and may slow dynamic responses to soluble factors. These limitations of bulk 3D cell cultures can largely be overcome by shrinking the cell culture size through adopting a Lab-on-a-chip approach. For example, Legant *et al.'s* (2009) Microfabricated Tissue Gauges (microtissues) allowed for relatively high-throughput assessment of the rapid dynamics and force generation during cell contraction [124]. In their model, cells are cultured within a matrix composed of collagen and form around pairs of flexible vertical cantilevers into an array of dense, organized structures comparable to *ex vivo* tissue. High-throughput tensile force measurements can then be calculated from the visible deflection of the cantilevers. More recently, investigators fixed a magnetic microsphere to one of the cantilevers in each microtissue well, and with magnetic tweezers stretched one microtissue at a time for quasi-static stiffness measurements [128,129]. The limitations in experimental throughput and actuation range of magnetically driven devices were addressed by our recently published Microtissue Vacuum-Actuated Stretcher (MVAS) [196]. In that publication, the MVAS allowed for high-throughput visualization of cellular remodeling during stretching due to a mostly planar deformation and following chronic (several days) conditioning.

We now present a new microtissue stretcher, the MVAS-force, which enables measurements of tensile force and dynamic mechanical analysis. In contrast to our previous design, only one of the cantilevers in the MVAS-force is actuated through a regulated vacuum pressure while forces are measured simultaneously from the passive bending in the other cantilever. In this article, this new approach allowed us to assess the mechanical properties of microtissues during dynamic loading and upon loading cessation, and to link the changes in mechanics to sub-cellular remodeling using responses to pharmacological treatments and by directly imaging the cytoskeleton. The findings that can be gained from our approach on a cell's ability, or impaired ability to sense mechanical forces are critical to understand pathways of development, normal function and disease progression in the body.

3.3 Methods

Device design

Our original MVAS device [196] was modified to allow *in situ* measurements of microtissue tension and dynamic stiffness. The MVAS-Force consists of six independently controllable rows of ten microtissue wells (fig. 3.1). Vacuum chambers border one side of each row of wells. Within each well, there are two cantilevers spaced apart by 500µm. One cantilever is secured on a flexible membrane that deforms to stretch the microtissue when a vacuum is applied through an external electronic regulator (SMC ITV0010) controlled via Labview software (Appendix B: movie B.1). The other cantilever acts as a passive force sensor. Its deflection is optically tracked and converted into a force measurement using a spring constant of $k_{cantilever}$=0.834N/m estimated with Euler-Bernoulli beam theory and verified with atomic force microscopy (Appendix B.1).

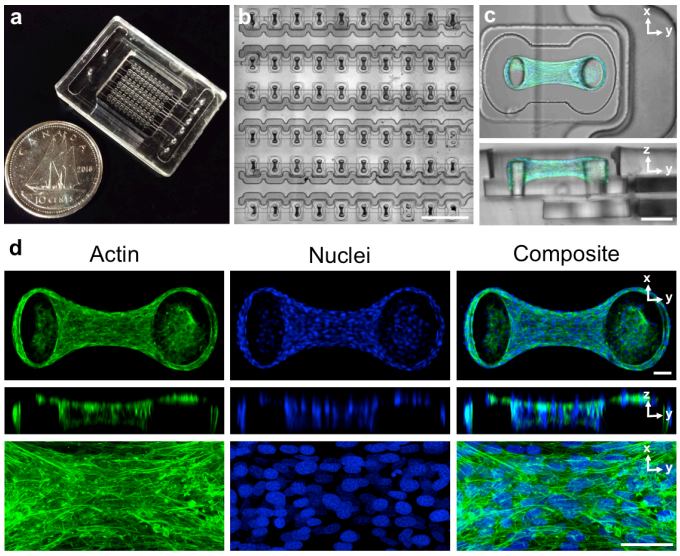

Fig. 3.1: The MVAS-Force allows high throughput dynamic mechanical measurements of 3D cell cultures. The MVAS-force was microfabricated from three photolithographic masters (a). It comprises of an array of microtissue wells each bordered by a controllable vacuum chamber (b). A top-down and cross-section view of a microtissue is shown in (c). Microtissues are dense, organized, three-dimensional cell cultures that are freely suspended around the cantilevers. Max projections of confocal stacks, orthogonal views and high magnification images are shown in b). The actin cytoskeleton is in green and the nuclei are in blue. Both the cytoskeleton and nuclei show a high degree of organization, aligning between the cantilevers. Scale bars in b,c and d, represent 1mm, 100µm and 50µm, respectively.

Device fabrication

Devices were fabricated as previously described [196] with slight modifications and detailed assembly steps are illustrated in (Appendix B.2). Briefly, the MVAS-Force consists of three layers fabricated through mold replication from SU8 (Microchem) masters made with standard photolithographic methods on polished silicon wafers (Universitywafers.com). All photomasks were ordered from CAD Art Services Inc. The top layer of the

MVAS-Force comprises the open-top microtissue wells and enclosed vacuum chambers. The thin middle membrane is fabricated with the cantilevers around which the microtissues compact. Finally the bottom layer contains vacuum chambers that match the top layer, and bottom chambers that equalize the pressure on either side of the membrane to minimize out of plane motion. All three layers were cast in polydimethylsiloxane (PDMS) from the SU-8 negatives with a 10:1 monomer to curing agent ratio and then plasma bonded together. To aid in tracking the bottom of the cantilevers, the middle membrane was fluorescently dyed with Rhodamine B (RhoB).

Cell culture

NIH3T3 fibroblast (ATCC) and C2C12 skeletal muscle (ATCC) cells were cultured in Dulbecco's Modified Eagle's Medium (DMEM) (Hyclone Laboratories Inc.). Human ASM cells (Donor 12) (previously characterized by Gosens *et al.* [224]) immortalized by stable transfection with human telomerase reverse transcriptase were obtained as a generous gift from Dr. William Gerthoffer (University of South Alabama) and maintained in DMEM/F12 (Invitrogen 11330). All culture media was supplemented with 10% fetal bovine serum (FBS), 100mg/ml streptomycin and 100U/ml penicillin antibiotics (all from Hyclone Laboratories Inc.). Cells were grown at 37℃ with 5% CO_2 on 100mm tissue culture dishes (Fisher) until 80-90% confluent.

Microtissue fabrication

Microtissue fabrication was performed as described previously [120,124], with modifications. Briefly, the device was sterilized with 70% ethanol, and treated with 0.2% Pluronic F-127 (P6866, Invitrogen) for two minutes to reduce cell adhesion. 250,000 cells were resuspended in 1.5mg/ml rat tail collagen type I (354249, Corning) solution containing 1x DMEM (SH30003.02, Hyclone), 44 mM $NaHCO_3$, 15 mM d-ribose (R9629, Sigma Aldrich), 1% FBS and 1 M NaOH to achieve a final pH of 7.0-7.4. The cell-collagen solution was pipetted into the MVAS-Force and centrifuged to load ~650 cells into each well. The excess collagen was removed and the device was transferred into the incubator for 15 minutes to initiate collagen polymerization. An additional 50,000 cells were added and allowed to adhere to the top of the tissues. Excess cells were washed off. Cell culture media was added and changed every 24 hours.

Force measurements

Microtissue mechanics were deduced from the visible deflection of the force-sensing cantilever while under dynamic loading at 0.25Hz (Appendix B: movie B.1). Prior to measurements, microtissues were preconditioned until subsequent loading loops were superimposable. All measurements were completed at 37^{o}C and 5% CO_2.

To track cantilever deflection, images of both the tops and bottoms of the cantilevers were captured at 15 frames per second for one minute. The bottom positions were measured by finding their centroids on thresholded fluorescent images of the Rho-B dyed cantilevers. The top of each cantilever was tracked using pattern matching with adaptive template learning in Labview on brightfield images. The deflection of the force sensor was calculated

from the difference in the top and bottom positions after accounting for the phase lag caused by the camera delay between the top and bottom images. The deflection was then converted into a force measurement using the cantilever spring constant, $k_{cantilever}$.

Microtissue strain, ε, was defined as the percent change in the length between the innermost edges of the tops of the cantilevers (equation 3.1):

$$\varepsilon(t) = \frac{length(t) - length_o}{length_o} \times 100 \tag{3.1}$$

The phase lag, δ, between force and strain was defined as the difference in the phase angles, Φ, at the oscillatory frequency (equation 3.2):

$$\delta = \{\phi_{force} - \phi_{strain}\}_{0.25hz} \tag{3.2}$$

The storage, k', microtissue stiffness was defined as the ratio of the magnitudes of the Fourier Transforms of force and strain at the oscillatory frequency multiplied by the cosine of the phase lag between force and strain (equations 3.3):

$$k' = \left\{\frac{|FFT[force(t)]|}{|FFT[\varepsilon(t)]|}\right\}_{0.25Hz} cos\ \delta \tag{3.3}$$

k' describes the amount of energy that is elastically stored for a given deformation, and δ describes the ratio of energy dissipated to energy stored where in purely elastic samples tan(δ)=0 and in purely viscous samples tan(δ)=inf.

The tension offset or prestress, T_o, was defined as the magnitude of the Fourier transform of the microtissue force at 0Hz minus the half of the peak-to-peak magnitude of the Fourier transform at 0.25Hz (equation 3.4).

$$T_o = \{|FFT[force(t)]|\}_{0Hz} - \frac{\{|FFT[force(t)]|\}_{0.25Hz}}{2} \tag{3.4}$$

The noise floor for calculating microtissue mechanics and measurements of an elastic standard with our approach are given in Appendix B.1.

To assess the response of microtissue mechanics to stretch, measurements were taken at progressively higher strains. After completing measurements at the largest strain, the recovery response was measured by promptly decreasing the strain amplitude. Stiffness recovery was measured by performing Fourier transforms on intervals spanning three loading cycles.

To assess the role of individual cytoskeletal proteins in contributing to the mechanical properties of microtissues and the strain softening behavior, measurements were taken following 20 minute incubations with either 10μM nocodazole (Noco), a microtubule polymerization inhibitor, 5μM blebbistatin (Bleb), a myosin-II inhibitor, or 10 μM cytochalasin D (CytoD), an actin polymerization inhibitor. As mechanical properties can vary between microtissues, each microtissue was compared to its own pre-treatment value where indicated. To prevent crossover in responses from multiple drugs, only a single treatment was administrated to a microtissue.

Quantification of cytoskeletal remodeling and polymerization

Images were acquired on a TiE A1-R laser scanning confocal microscope (LSCM) (Nikon) with standard LSCM configurations using appropriate laser lines and filter blocks. To assess actin and microtubule remodeling in living microtissues in response to stretch, cells were loaded with either 0.1μM SiR-actin or SiR-tubulin with 1μM verapamil 6-12 hours before imaging. Z-stacks were taken before and following 4 seconds (one stretch), one minute and five minutes of static resting and then ~9% stretching at 0.25hz. Imaging was completed with a 60x 1.2NA water immersion objective to give a centrally located field of view of 212x106μm (1024x512 pixels). Z-stacks were flattened by integrating slices, divided into sub images with a size of 100x100 pixels with 10-pixel spacing, and compared with cross-correlation. The correlation coefficient is a measure of how closely images matched before and after a given condition, and thus is inversely proportional to the amount of remodeling (ie. a low correlation coefficient corresponds to a high degree of remodeling).

To assess f-actin expression and microtubule polymerization, microtissues were fixed *in situ* with 3.5% paraformaldehyde for 15 minutes and permeabilized with 0.5% Triton-X in HEPES buffer for 5 minutes. Microtissues were left in blocking buffer (5% FBS in PBS) for 40 minutes. Microtubules were labeled with 1:200 (in PBS) α-tubulin primary antibody produced in mouse (Sigma, T6074) over night at 4^{o}C and 1:500 (in PBS) rabbit anti-mouse IgG secondary antibody conjugated to Alexa Fluor 488 for 1 hour at room temperature (Invitrogen, A11059). The actin cytoskeleton was stained with Alexa Fluor 546 Phalloidin (Fisher, A22283), and the nuclei were stained with DAPI (Fisher, D1306). All images were captured with identical laser power, detector sensitivity, resolution and scan speeds. To quantify f-actin expression per cell, Z-stacks were flattened by integration, averaged and normalized to DAPI fluorescence. Microtubule polymerization was quantified with the same method except images were first thresholded to remove any signal from nonpolymerized tubulin.

Data analysis and statistics

All numerical data are presented as mean ± standard error unless indicated otherwise. Statistical tests, as described in the results, were performed using Originlab 8.5 (Northampton, MA), with $p<0.05$ considered statistically significant. Post hoc testing of ANOVAs were all completed with Tukey's HSD test after verifying the assumption of homogeneity of variances.

3.4 Results

Microtissue morphology

Within the MVAS-Force, 3T3 fibroblast cells self-assembled around the cantilevers into dense, highly organized, three-dimensional constructs that morphologically resemble tissue. Top-down and cross sectional views of a fully compacted, representative microtissue are shown in fig. 3.1c. As been shown previously [120,124,196], the cells compacted the collagen matrix away from the bottom and sides of the well into a tissue freely suspended

around the tops of the cantilevers. The average microtissue thickness measured at its center after four days was 97 ± 2 μm (n=5) and was qualitatively uniform along the longitudinal axis.

Maximum intensity projections with orthogonal slices and centrally located magnified views of F-actin and cell nuclei within a representative microtissue at four days are shown in fig. 3.1d. Actin was highly polymerized into dense stress fibers that were oriented with the longitudinal axis of the microtissue. The cell nuclei were also mostly aligned with the microtissue and evenly distributed in three dimensions.

Microtissues strain soften to maintain their mean tension

It has been widely reported that acute dynamic stretching changes the mechanical properties of cells grown on 2D surfaces; they become softer (decreased elasticity) and more fluid-like (increased phase lag) [80,92,95]. In that regard, we started by investigating whether or not 3D microtissues composed of 3T3 fibroblasts share this behavior by assessing their dynamic mechanical properties under progressively larger strains at 0.25Hz.

Microtissue storage stiffness decreased in a strain-dependent manner (N=22, linear regression: R^2= 0.97, p<0.001), (fig. 3.2a). Comparing 9% to 1% strain, the average storage stiffness decreased by 26 ± 2% (repeated measures t-test: p<0.001). Unlike previously published findings on cells in 2D culture, where softening is accompanied with a more fluid-like behavior (or fluidization) [92], the phase lag of microtissues decreased with the strain amplitude (linear regression: R^2= 0.95, p<0.01) (fig. 3.2b), indicating a greater amount of energy stored for a given amount dissipated at higher levels of strains. Therefore in contrast to cells in 2D, fibroblast microtissues become more elastic-like as they soften. The softening response in microtissues was also accompanied with a decrease to their prestress (linear regression: R^2=0.97, p<0.001) (fig. 3.2c). Comparing 9% strain to 1% strain, the average prestress decreased by 2.7 ± 0.3μN (N=22, repeated measures t-test: p<0.001).

Together the softening response and the decrease to the prestress generated a mean tension that was invariant with respect to the strain amplitude (linear regression: p>0.5) (fig. 3.2c). This behavior occurred despite a linear increase to the mean microtissue length (linear regression: R^2=0.99, p<0.001) (fig. 3.2d) and is indicative of an intrinsic tensional homeostatic response that cells and tissues possess [219,220]. Moreover, since we considered an auxotonic condition, the minimum microtissue length of a loading cycle (ie. the offset length) increased with the stretch amplitude (linear regression: R^2=0.99, p<0.001) (fig. 3.2d). Thus, the tension regulating ability of microtissues under dynamic stretching resulted in their lengthening.

The strain softening response was reversible upon returning to small amplitude oscillations (fig. 3.2e). The stiffness and prestress recoveries are shown in fig. 3.2f,g, respectively (N=8). After 160 seconds, microtissue stiffness recovered to 99± 3% of its initial value and the prestress agreed well with initial measurements. The recovery curves followed stretched exponential functions (equation 3.5) with agreeing time (τ) (38 ± 1 vs. 35 ± 6 seconds) and power law constants (β) (0.87 ± 0.01 vs. 0.92 ± 0.08) (Appendix B.3). The offset microtissue length recovered as well with the same dynamics (data not shown).

$$F(t) = a * e^{-t/\tau^{\beta}} + d \tag{3.5}$$

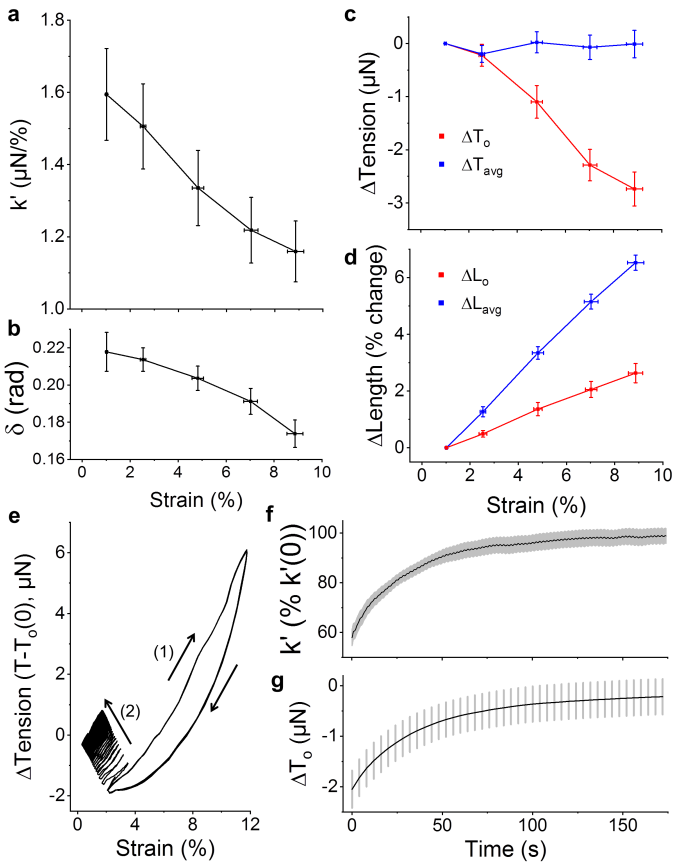

Fig. 3.2: 3T3 fibroblast microtissues strain soften to maintain a constant mean stress. The storage stiffness, k', (a), phase lag between stress and strain, δ, (b) and prestress, T_0, (c) all decreased with increasing oscillatory strain amplitude (N=22). Importantly, the decrease to the stiffness and prestress led to a constant mean stress, T_{avg}, (c) despite a linear increase to mean microtissue length, L_{avg} (d). Under an auxotonic condition, these behaviors increased the offset microtissue length, L_o, beyond its initial length. To see whether these responses were reversible, microtissues were oscillated under a large amplitude strain until subsequent loading loops overlapped (1) and then suddenly switched to a small amplitude strain (2) (e). Both the storage stiffness (f) and prestress (g) fully recovered to their initial values over 160 seconds with similar rates (N=8). In this figure, the prestress and mean stress are expressed as the difference from the smallest strain amplitude.

To determine how the softening behavior developed within microtissues during cyclic loading, the conditioning cycles from a static state were examined in fig. 3.3. At a loading frequency of 0.25 Hz, the mechanical behavior of microtissues adapted over the first couple of loading cycles (fig. 3.3a). Over these cycles, the prestress decreased towards a new set value (fig. 3.3c), while the mean tension promptly increased and then stabilized back to the resting tension (fig. 3.3d). As we considered an auxotonic load, these changes resulted in progressive tissue lengthening (fig. 3.3e). In contrast, when the loading period (400 seconds) was much slower than the recovery time constant ($1/f >> \tau$), the degree of the mechanical adaptation was reduced and predominately occurred over the first loading cycle (fig. 3.3b-e). Furthermore, when oscillated around an offset strain at 0.0025 Hz, the mean tension did not stabilize to its resting tension (fig. 3.3d).

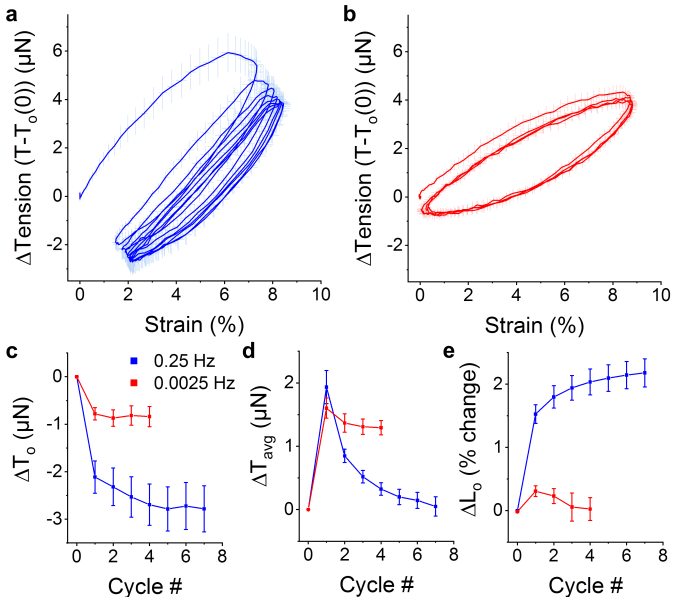

Fig. 3.3: Adaptation to oscillatory loading depends upon the loading frequency. Average conditioning cycles from rest at 0.25Hz and 0.0025Hz are shown in (a) and (b), respectively. In both cases, the prestress decreased with subsequent loading towards a new set point but to a greater extent with faster loading frequencies (c). While the mean tension remained elevated when oscillations were slowly applied, it decreased with the cycle number towards the resting tension with a loading 0.25Hz (d). Under an auxotonic condition and when the oscillation frequency was faster than the recovery time constant, these behaviors resulted in a progressive lengthening response (e). However, this lengthening response was absent when the oscillation frequency was slower than the recovery time constant.

In this section, we have shown that, as with cells in 2D culture, 3D microtissue cultures strain soften. Depolymerization of actin filaments [78–80,92] and perturbing of myosin motor binding [7,8,81–83] are previously hypothesized mechanisms of this response for cells in 2D culture. On the other hand, the involvement of microtubules has been largely overlooked despite their contributions to overall cell mechanics [47,58,88,225] and their dynamic instability [42]. Accordingly, we investigated the roles of these three cytoskeletal proteins to microtissue strain softening. We begin with examining the involvement of actin microfilaments.

Dynamic stretch remodels and depolymerizes actin

To assess the role of the actin cytoskeleton in strain softening, f-actin was depolymerized with Cytochalasin D (CytoD). As expected, CytoD treatment reduced the resting tension, stiffness and phase lag (fig. 3.4a and Appendix B.4). Importantly, CytoD treatment also muted the softening response (N=16 repeated measures t-test, $p<0.001$) (fig. 3.4b). In fact the stiffness of CytoD treated microtissues was independent from the strain amplitude (repeated measures t-test, $P>0.05$). Upon stretch cessation, CytoD treatment also prevented tension recovery; further demonstrating that CytoD treated microtissues do not soften (fig. 3.4c). These results indicate that strain softening is dependent upon changes to a densely polymerized actin cytoskeleton.

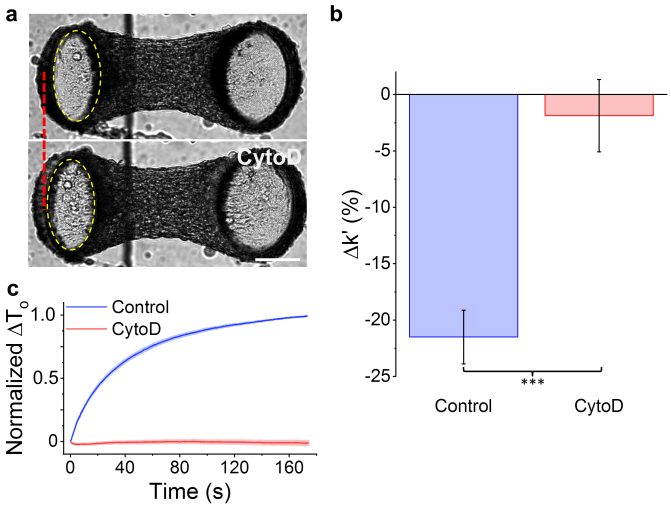

Fig. 3.4: Softening requires an intact actin cytoskeleton. Images of a microtissue prior to and following CytoD treatment are in panel (a). As shown by the dotted red line and the dotted yellow ellipse that outlines the top of the force-sensing cantilever (left), depolymerization of F-actin with Cytochalasin D (CytoD) visibly moved the cantilever outward, indicating a lower resting tension. Importantly, CytoD treatment reduced the stiffness change under large vs. small amplitude stretching (ie. the amount of strain softening) (b). There was also no tension recovery following stretch cessation (c). The scale bar in (a) represents 100µm.

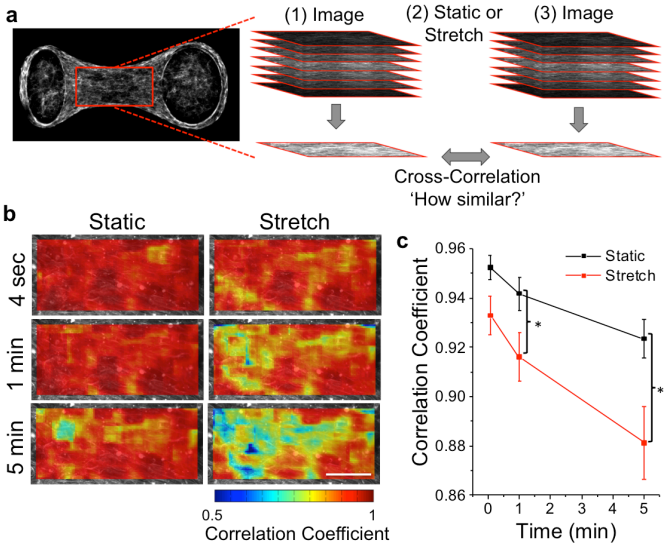

Fig. 3.5: Oscillatory stretch increases remodeling of actin filaments in living cells in 3D culture. The effect of oscillatory stretch on the actin remodeling rate was measured across centrally located regions (212x106µm; red rectangle) in living microtissues using live-cell staining and comparing confocal stacks taken immediately before and after various durations of stretching or static culture (a). Representative heat maps of cross-correlation coefficients show that actin remodeling was spatially heterogeneous and increased with large amplitude stretching vs. static conditions (b). The average correlation coefficient was significantly reduced (ie. a greater amount of remodeling had occurred) when stretching vs. static after 1min and 5min (b). The scale bar in (b) represents 50µm. (*P<0.05; N=6 repeated measures t-test)

We have shown that f-actin is required for strain softening in microtissues. To further link the softening response to changes in the cytoskeleton, we labeled actin filaments with a live-cell stain. Then by comparing images taken before and following various durations of static resting or oscillatory stretching, we assessed whether stretching increases the rate of actin remodeling. Heat maps of correlation coefficients showing actin remodeling (areas with low correlation coefficients indicate high remodeling) within a centrally located region of the microtissue are in fig. 3.5a. Actin remodeling was spatially heterogeneous throughout the microtissue and increased with time under both static and loading conditions. Importantly, compared to the static condition, oscillatory loading significantly increased remodeling of actin filaments (decreased the average correlation coefficient) after one and five minutes (N=6, repeated measures t-test, $P<0.05$) (fig. 3.5b).

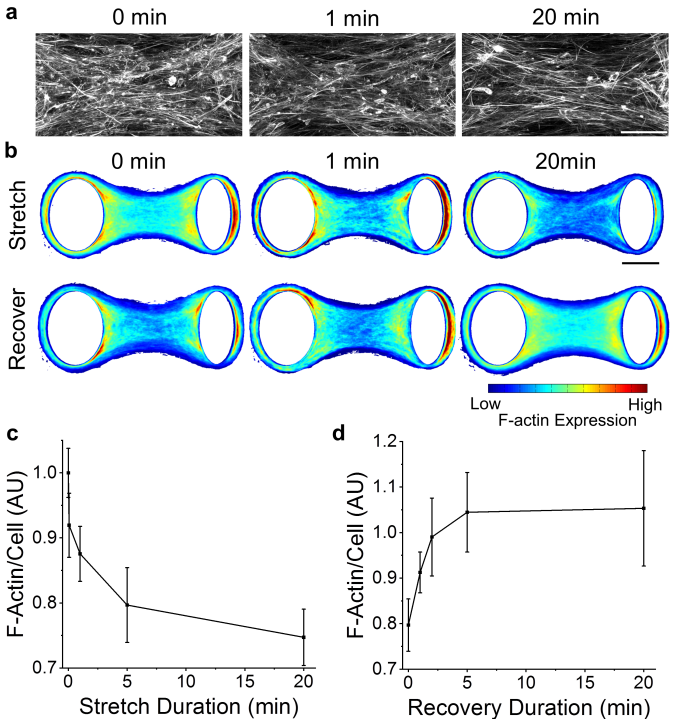

Fig. 3.6: F-actin depolymerizes with stretching and repolymerizes upon stretch cessation. Representative images after different durations of stretching show that there were fewer actin filaments with longer stretch durations (a). F-actin staining intensity in average heat maps was similarly reduced with stretch duration (b) (N>14 microtissues per time point). Moreover, f-actin intensity recovered to initial values upon stretch cessation (N>11 microtissues per time point). The average actin expression normalized to the number of cells under various durations of stretching and recovery are shown in (c) and (d), respectively. The scale bars in (a) and (b) represent 50 and 100μm, respectively.

To investigate whether remodeling arose simply from organizational changes or depolymerization/repolymerization of filaments, microtissues were fixed and stained immediately following various durations of stretching at 9% strain. Representative images, average heat maps and average f-actin expression per cell (fig. 3.6a-c, respectively) all indicated that f-actin rapidly depolymerized with oscillatory

stretching (N>14). Then to show that f-actin also repolymerizes following stretch cessation, microtissues were fixed and stained after various durations of recovery following five minutes of stretching. Average heat maps and f-actin expression per cell (fig. 3.6b,d) show complete recovery to initial expression values (t-test P>0.05) (N>11). Although our time resolution of f-actin expression was poor and the uncertainties are large, the rate of f-actin recovery appeared to be within the same order of magnitude (tens of seconds) as the rate of tension and stiffness recovery, suggesting that the mechanical measurements reflect actin repolymerization.

Myosin and microtubules do not contribute to strain softening

We have identified that actin filaments play a major role in the strain softening response of 3D microtissues, however, the mechanical behavior of cells [47,51,58,88,225] and microtissues is also highly dependent upon myosin activity and microtubules (fig. 3.7a and Appendix B.4). To assess the contribution of myosin and microtubules to strain softening, we examined the response following myosin inhibition with blebbistatin (Bleb) and microtubule depolymerization with nocodazole (Noco).

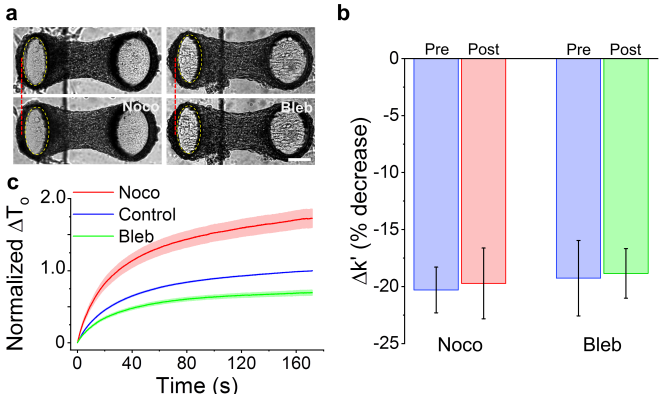

Fig. 3.7: Microtubules and myosin do not contribute to softening. Microtissues prior to and following nocodazole and blebbistatin treatments are shown in (a). Microtubule depolymerization with nocodazole moved the force-sensing cantilever inward, indicating increased prestress. In contrast, myosin-II inhibition with blebbistatin moved the cantilever outward, indicating decreased prestress. Neither treatment changed the amount of strain softening in terms of percent change (b). Furthermore, microtubule depolymerization increased the tension recovery while myosin inhibition decreased recovery (c) but neither treatment changed the time constant of the recovery response. The scale bar in (a) represents 100μm.

Myosin inhibition with blebbistatin decreased microtissue stiffness (N=10, repeated measures t-tests, P<0.05) and prestress (p<0.01) (Appendix B.4). Myosin inhibition, however, did not affect strain softening (N=10, repeated measures t-test, P>0.05). As expected, it did reduce the tension recovery (fig. 3.7c) because of the decrease in prestress that unsurprisingly accompanied myosin inhibition. However, as there was no change in the rate of recovery, myosin cycling was not likely responsible for the recovery following softening (Appendix B.3). Although it is possible that there was incomplete inhibition of myosin motors, it is unlikely according to

blebbistatin's measured dose-response curve (Appendix B.5). Moreover, even with incomplete inhibition, one would still expect a decrease in the softening response if perturbing of myosin binding were responsible for the strain softening response of microtissues.

In keeping with the hypothesis that microtubules are mainly compressive elements that oppose acto-myosin activity [47,58,88,225], microtubule depolymerization increased microtissue stiffness (N=15, repeated measures t-tests, P<0.001), and prestress (P<0.001) (Appendix B.4). Microtubule depolymerization, however, had no effect on strain softening in terms of the percent change to the storage stiffness (P>0.05) (fig. 3.7b). It did increase the absolute tension recovery (fig. 3.7c) as expected, because of the increase in prestress that accompanied microtubule depolymerization. However, again the molecular mechanism for softening was not likely affected by microtubule depolymerization, as there was no change to the rate of recovery (Appendix B.3). Interestingly, oscillatory stretching did increase remodeling in microtubules with significant differences from static conditions after one and five minutes of stretching (Appendix B.6) (N=7, repeated measures t-tests, p<0.01 and p<0.05, respectively). However, stretching did not change the degree of microtubule polymerization per cell (Appendix B.6) (N>14, 1-way ANOVA: P>0.05).

Strain softening is a conserved response for microtissues

We have shown that microtissues composed of 3T3 fibroblasts, mimicking connective tissue, strain soften through actin depolymerization. To assess whether this behavior is unique to fibroblasts or is shared among other cell types, we assessed the strain-softening responses in microtissues composed of human airway smooth muscle cells (HASM) or skeletal muscle cells (C2C12). Both smooth and skeletal muscle microtissues strain softened (linear regression: R^2= 0.99, 0.98 P<0.001, 0.001, respectively) (fig. 3.8a). The phase lag of skeletal muscle microtissues decreased with strain (linear regression: R^2=0.99, P< 0.001), whereas in smooth muscle microtissues it did not (R^2=0.43, P=0.14) (fig. 3.8b).

As with fibroblast microtissues, HASM and C2C12 microtissues shared strain-dependent decreases to their prestress (linear regression: R^2= 0.98, 0.94 P<0.001, 0.01, respectively) (fig. 3.8c). Furthermore, the decrease in their stiffness and prestress led to a constant mean stress (linear regression: P>0.05) (fig. 3.8d) despite a linear change to their mean lengths (linear regression: both R^2=0.99, P<0.001) (data not shown). Again, these adaptations resulted in microtissue lengthening (ie. L_o increased with strain amplitude) (linear regression: linear regression: both R^2=0.95, P<0.01) (fig. 3.8e).

Upon decreasing the strain amplitude, the stiffness and tension of HASM and C2C12 microtissues recovered as previously observed with the fibroblast cultures (fig. 3.8f,g). The offset microtissue length recovered as well (data not shown). The time constant for stiffness recovery in HASM cells was statistically greater than either 3T3 or C2C12 microtissues (1-way ANOVA: P<0.05) (Appendix B.3). On the other hand, the time constants for tension recovery agreed well with each.

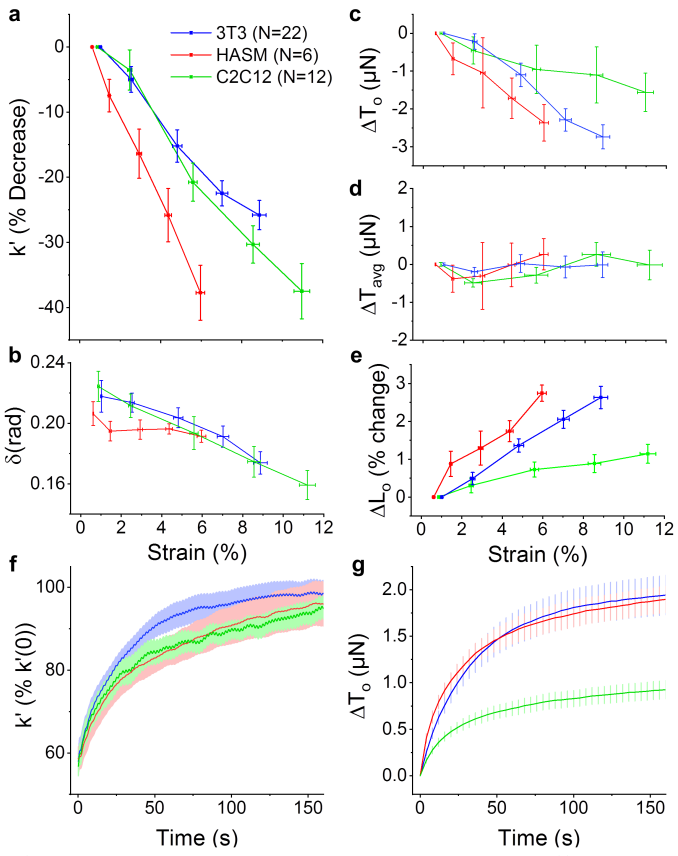

Fig. 3.8: Strain softening is a conserved response among different microtissue cultures. Microtissues composed of fibroblast (3T3), human airway smooth muscle (HASM), or skeletal muscle (C2C12) cells all strain softened with similar changes to their stiffness (a), phase lag (b), and prestress (c). For all cell types, the mean tension was invariant with the stretch amplitude (d) despite a linear increase to their mean lengths (data not shown). Together these behaviors led to an increased offset microtissue length (e). 3T3, HASM and C2C12 microtissues also shared similar recovery dynamics upon stretch cessation in terms of the rates of their storage stiffness (f) and prestress (g) recovery.

3.5 Discussion

We aimed at assessing the response to acute oscillatory stretch in cells grown in conditions that mechanically and biologically recapitulate the 3D environment that a cell would experience were it in the body. In order to fulfill this goal, we developed a novel approach to allow high throughput measurements of dynamic mechanical properties and direct visualization of the cytoskeleton in 3D microtissue cell cultures. Our approach consists of an array of vacuum-driven actuators to stretch microtissues and optically tracked force-sensors to measure their mechanical behavior. Advantages and limitations of our approach are summarized in Appendix B.7. In using our approach, we showed that microtissues soften under dynamic stretching through actin depolymerization. Furthermore, through this softening behavior, tissues homeostatically maintain their mean tension, which results in stretch-induced tissue lengthening. These results are further discussed the sections that follow.

Microtissues soften under dynamic loading

We showed that the prestress and storage modulus of living 3D microtissue cultures composed of three different contractile cell types decreased with the dynamic strain amplitude. This finding agrees well with previous reports in cells in 2D culture [91,92,95], and ex vivo tissue strips [7,8]. Furthermore, it reflects an important mechanism through which tissues maintain homeostasis throughout the body. For example, strain softening may explain how a large tidal stretch from a deep inspiration can open contracted airways in healthy lungs [7,8] and could contribute to the regulation of blood pressure in arteries [104].

In addition to softening, cells in 2D have long been reported to exhibit a more fluid-like behavior when stretched [226–228]. More recently this fluidization response of cells has been associated with that of a class of inert materials called soft glasses (eg. foams, dense emulsions, pastes and slurries) [92]. In contrast to these reports and the soft glassy rheology hypothesis, skeletal muscle and fibroblasts microtissues actually became more elastic-like with greater strain amplitudes, and smooth muscle microtissues did not phase transition. Although this apparent contradiction could arise from environment differences between growing cells in our 3D microtissues and past reports done in 2D culture, it is more likely that the fluidization response was hidden by the elasticity of the ECM. After removing most of the cellular component to the mechanical behavior of the microtissue with CytoD treatment, the remaining behavior, primarily describing the contribution of the matrix, is elastic and contributes little to energy dissipation (Appendix B.4). In turn, a more elastic-like behavior could be perceived as the cells soften (and perhaps fluidize) because the cellular contribution to the overall mechanical behavior becomes less important compared to the elasticity of the matrix. It would, however, still be of interest in future work to assess whether or not microtissues follow the same time-scale invariance [66] that has given traction to the hypothesis that the mechanical behavior of cells follow Sollich's (1997) theory on soft glassy rheology [107].

Upon strain cessation, we showed that microtissue stiffness returned to pre-intervention values along well-conserved trajectories that could be modeled over three magnitudes of time with a stretched exponential. Stretched exponentials have previously been used to describe relaxation processes in disordered systems [229,230] and can appear from a linear superposition of simple exponential functions with a nontrivial distribution of relaxation times [231]. It, therefore, should not be overly surprising that such a function can appear from the complex nature of the cytoskeleton and the added intricacies that arise when considering an aggregate of cells. In spite of this, we found that the recovery time constants for prestress and stiffness were between 35 and 43 seconds for all tested treatments that showed a recovery response and cell types (except for stiffness recovery in HASM microtissues). This time constant appears to be within the same order of magnitude as previously reported recoveries in cortical actin stiffness following transient stretching cells in 2D culture [92]. Unfortunately the authors of that work did not fit their curves to stretched exponentials. They did, however, concede that recovery occurs with timescales that grow with the elapsed time since stretch cessation and is slower than an exponential process, which are characteristic features of stretched exponentials.

We believe that these findings are related to the tensional homeostasis behavior that has been widely reported in 3D cell cultures in response to quasi-static loading [219,220]. In that regard, it is known that cells will change their internal contractility to oppose external mechanical loads to maintain a set point tension. In keeping with this concept, we found that the decrease in the prestress and stiffness of well-adapted microtissues was sufficient to maintain a constant mean tension across increasingly larger strain amplitudes with increasingly greater mean lengths. Thereby our work extends tensional homeostasis to conditions of cyclically applied loading. In addition we found that the adaptation response occurred at a physiological loading rates but was absent when loading was slower than the tension and stiffness recovery time constants.

Under auxotonic conditions, these behaviors led to tissue lengthening. For our approach, the auxotonic resistance is set by the bending stiffness of the force-sensing cantilever. This resistive force is analogous to the parenchymal tethering stiffness in the lung. A loss of these tethering force [232] may explain why the normal dilating response from a deep inspiration does not occur in asthmatic airways [105].

In the literature strain softening exists in a paradox with a large number of studies reporting strain stiffening and actin reinforcement in response to stretch [233]. Under a sustained stretch or examining different locations along the stress-strain curve, reconstituted crosslinked actin gels [96,234], cells [235], and 3D cell cultures [216,236] have all been shown to strain stiffen. This nonlinear effect arises from reorganization of actin filaments [96,234] and, for tissues, reorientation of cells and percolation of these local effects across the cell culture [236]. Although our loading loops were mostly linear, strain stiffening can be observed to a degree at large strain amplitudes (the total harmonic distortion from nonlinearities increased from 0.041 ± 0.002 at 1% strain to 0.152 ± 0.004 at 9% strain ($P<0.0001$, repeated measures t-test)). However, this effect was still much smaller than the softening behavior produced by dynamic loading. On the other hand, downstream signaling cascades have been reported to cause mechanical stiffening through actin microfilament reinforcement [91,155,237–240] as a sort of negative feedback to maintain localized mechanical stress [241,242]. Microtissues have previously been shown to stiffen following 15 minutes of dynamic stretching [128,204] and we have also reported actin reinforcement in microtissues under chronic (2 days) conditioning [196]. Importantly in those investigations quasi-static stiffness measurements and f-actin expression were evaluated following loading and after a period much greater than the time-scale of stiffness recovery and actin repolymerization we report here. That said, over our relatively short experimental window, we did not observe any differences between initial and fully recovered stiffness, prestress, length and f-actin expression measurements.

Stretch depolymerizes actin in microtissues

Although strain softening of cells and tissues has been widely reported [7,8,91,92,95], the molecular mechanism(s) behind this response remains unclear. Here we investigated the contributions of actin microfilaments, myosin II motors and microtubules.

Firstly, in a cell, the actin cytoskeleton is a filamentous network that gives the cell its shape and opposes tensile forces. In 2D culture, stretching of cells has been reported to depolymerize actin filaments [78–80]. Our results in 3D cultured microtissues agree with those observations. We found that 1) f-actin was necessary for strain softening and the recovery response; 2) actin remodeling in living cells increased with stretch; 3) short-term stretch lowered f-actin expression; and 4) upon stretch cessation, f-actin expression recovered along the same timescale as tension and stiffness recovery. These findings strongly suggest that strain softening, at least in part, arises from actin depolymerization. Our observed timescale of actin repolymerization following cyclic stretch cessation also agreed well with a previous report that measured actin recovery following a step length change in 3D cell cultures [221].

Strain induced actin depolymerization has been recently linked to increased cofilin activity. In that regard knocking down this actin-severing molecule in cells in 2D culture, reduced softening and their actin filaments remained largely intact following a transient stretch [243]. In addition, myosin Ib has recently been shown to act as a catch-bound actin depolymerase (its affinity for actin, and thus its stress fiber severing capability, strongly increases with the applied load) [244], and thus may also promote the strain softening behavior of cells and tissues. On the other hand, the actin recovery response was perhaps mediated in part by zyxin facilitated stress fiber repair. In that regard, it has been previously shown that zyxin localizes to sites of stress fiber fragmentation, and knockdown of zyxin reduces the recovery of contractile force in single cells and leads to more rapid dilation in precision cut lung slices following stretch [245]. Assessing these molecules in our MVAS-force device may further our understanding of their contributions to the dynamic regulation of the cytoskeleton and the mechanical properties of tissues, and thus, should be a focus of future investigations.

Secondly, myosin II motors regulate the mechanical behavior of cells by generating tension through crosslinking and actively pulling on actin filaments. Furthermore, strain softening in reconstituted actin-myosin networks has been attributed to the disruption of myosin crosslinks [81–83]. Perturbing of the binding of myosin has also been implicated in the softening response in airway tissue strips [7,8]. In contrast, we found that softening in microtissues was invariant on myosin activity and that there was no change to the rate of the recovery response following strain cessation. This strongly suggests that myosin has no role in the softening response of cells in 3D culture.

Lastly, although our understanding of the role of microtubules in cell mechanics is still being refined [45], it is thought that they act as compressive struts to oppose actin-myosin contractility, as in tensegrity architecture [47,58,88,225]. Accordingly, and in keeping with several other investigations measuring cell traction forces and stiffness in 2D [46,47], we found that depolymerization of microtubules with nocodazole increased microtissue stiffness and prestress (Appendix B.4). Comparably fewer studies have assessed how stretching cells and tissues affects microtubule remodeling and polymerization. That said, microtubules have visually been seen to buckled while cells deform [225], and in axons grown in 2D culture, microtubules have been shown to disassemble under large (75%) dynamic loading [246]. In contrast, we did not observe any changes to microtubule polymerization and nocodazole

treatment had no affect on the softening response. Dynamic stretching did, however, increase microtubule remodeling. Whether stretching directly caused disassembly/assembly of microtubules or they simply remodeled in accordance with actin depolymerization, and whether or not the observed microtubule remodeling contributes to changes in the mechanical behavior of cells are interesting questions for future investigations.

3.6 Conclusions

In this article, we presented a new high-throughput approach for assessing both dynamic cell mechanics and for visualization of remodeling at the sub-cellular level in response to stretch within physiologically relevant 3D microtissue cultures. Our approach offers the ability to link behaviors observed in 2D culture to cells within a soft 3D matrix comparable to human tissue, and to connect visual remodeling of the cytoskeleton to changes in mechanical properties. In that regard, we found that fibroblast, smooth muscle, and skeletal microtissue cultures all shared a conserved softening response when dynamically stretched and recovery following stretch cessation. Microtissues responded to maintain a constant mean stress, and under an auxotonic condition, their response led to tissue lengthening. Furthermore, by directly quantifying cytoskeletal remodeling, these behaviors appeared to arise from rapid actin depolymerization. This suggests that actin microfilaments are sensors of mechanical stretch in cells, and in turn, form a feedback loop to control the mechanical behavior of tissues. The ability of cells to feel and react to mechanical stimuli from their environment is an important mechanism for maintaining homeostasis in the body and is a critical aspect to a full understanding of many pathological disorders.

CHAPTER 4| TIME DEPENDENCIES IN THE DYNAMIC MECHANICAL BEHAVIOR OF 3D MICROTISSUE CELL CULTURES

Authors: **Matthew Walker**, Michel Godin, James L. Harden, Andrew E. Pelling

The manuscript was submitted to APL Bioengineering in January 2020 (under review) and is accessible on the preprint server BioRXIV (doi: https://doi.org/10.1101/780312). The supplementary information is contained in Appendix C.

Motivation & Objective| Growing cells in a 3D ECM vs. on a 2D substrate is known to fundamentally alter the structure and distribution of the cytoskeleton, but the effects of these changes on the mechanical behavior of the cell is not understood. Furthermore, whereas mechanical properties under local shear and compressive loading have been well characterized, tensile loading at the length-scale of the entire cell is poorly understood. This chapter shares insights into these research questions by characterizing the rheological behavior of microtissues under tensile step strains and by quantifying the contributions from distinct cytoskeletal elements.

4.1 Abstract

Characterizing the elastic and dissipative properties of cells is not only necessary to determine how they deform, but also to fully understand how external mechanical forces trigger biochemical-signaling cascades to govern their behavior. Presently mechanical properties are largely assessed by applying local shear or compressive forces on single cells in isolation grown on non-physiological 2D surfaces. In comparison, our microfabricated vacuum actuated stretcher measures tensile loading of 3D multicellular 'microtissue' cultures. With our approach, we assessed here the time-dependency of microtissue mechanics and quantified the spatial remodeling that follows step length changes. Unlike previous results from other micro-rheological techniques, stress relaxation and recovery in microtissues followed stretched exponential behaviors that shared similar amplitudes but differed in their dynamics. In that regard, relaxation time constants changed with an inverse power law with step size, while recovery rates were invariant. Pharmacological responses, however, indicated that the contributions of individual cytoskeletal elements did not qualitatively differ from our existing understanding of their roles. The elasticity and dissipation of microtissues were mainly determined by the actin cytoskeleton but also augmented by myosin motor activity and reduced by the presence of microtubules. These results were reflected in changes to remodeling dynamics and spatial distributions of the integrated strain field. This assessment of microtissues offers insights into how the collective behavior of cells and their cytoskeletal proteins generate the dynamic mechanical properties of tissues, which is necessary for a full understanding of how cell behaviors are regulated in both health and disease.

4.2 Introduction

The requirements of crawling, dividing and contracting demand that the cell's cytoskeletal network of structural and motor proteins be tremendously dynamic. This behavior is unique from other soft materials and gives cells and tissues their distinct elastic and dissipative properties. Defining these properties is not only necessary for an understanding of how cells deform, but also how cells sense and transduce external mechanical forces into biochemical signals that direct cell behavior. In that regard, when cells are stretched or come in contact with a stiffer matrix, there are time-scale dependent conformational changes to adhesion and cytoskeletal proteins, which in turn alter ligand-receptor binding affinities to trigger biochemical signaling cascades [1,3]. Through this regulation of biochemical signaling, mechanical forces have been linked to normal development and function, as well as disease progression, including bone, muscle, heart and lung disorders and cancer [4,5].

Cells have long been shown to exhibit both solid-like elastic and fluid-like viscous properties depending upon the time-scale at which they are measured [85]. Traditionally this behavior, called viscoelasticity, is described using a network of elastic springs, and viscous dashpots. Solving the constitutive equations for these types of models following a step change in length gives an exponential decay in stress with characteristic time constants depending upon the elastic modulus of the springs and viscosity of the dashpots [247].

Many studies have set out to define the viscoelastic behavior of cells and to link them to specific processes that occur within the cell. Although initial experimental data could be fit with a single time constant [73,94,248,249], as the resolution of techniques has improved, fitting the resulting data has required more model parameters [76]. Moreover, exponential-like behavior is not always observed. In particular, a power law with a single exponent was shown to accurately describe both the frequency response and viscoelastic stress relaxation of cells grown on 2D substrates [65,66,68,99]. Seemingly universal observations of power law rheology across different cell types, techniques and following a range of cytoskeletal drugs, has since given traction to the hypothesis that cells belong to a class materials called soft glasses [66,68].

Perhaps rather importantly, yet under appreciated, this current understanding of cell mechanics has been mainly shaped by growing cells on 2D substrates with probes applying local shear and compressive loads [65,66,68,99]. First in that regard, it is known that forcing un-natural apical-basal polarity of adhesion complexes by growing cells on 2D substrates causes vast differences in the distribution and structure of the cytoskeleton when compared to cells grown within more physiologically relevant 3D environments[31]. It is reasonable to suspect that these fundamental changes to cytoskeletal structure caused by the dimensionality of the cell's environment may alter their mechanical behavior. Secondly, it is reasonable to suspect that an inhomogeneous network of actin, microtubules and cross-linkers will transfer loads differently when probed locally in shear and compression vs. globally in tension. Indeed when cells have been probed previously in tension at their length-scale, they have exhibited time-scale dependencies that are not captured by power laws typical of other micro-rheological methods[73,216,250].

For these reasons, 3D cell culture methods that enable the assessment of tensile forces have become a keen interest to the field of cell mechanics[116]. In that regard, both the frequency and stress relaxation response of cells within bulk reconstituted collagen gels have previously been fit with a standard linear spring-dashpot models[216,218]. Due to their centimeter-scale, however, these cultures tend to have poor cellular organization and low cell density, suffer from slow experimental throughput, are hard to image, and possess a high diffusive barrier for nutrients. In contrast to bulk 3D cultures, previous microtissue models have been fabricated, consisting of a high throughput array of flexible cantilevers around which cells in a collagen matrix form sub millimeter-scale structures with comparable cell alignment and density to human tissue [124]. Although quasi-static mechanics (i.e. contractility and stiffness) of microtissues have already received attention [120,124,128,204], the time-dependencies in these systems remain unclear.

In this article we investigated the viscoelastic stress relaxation of microtissue cultures using a microfabricated device that we have developed called the Microtissue Vacuum Actuated Stretcher (MVAS) [196]. The MVAS enables large deformations, and simultaneous measurements of tension and live imaging. The description of the dynamic behavior of 3D microtissue cultures that follows in this article qualitatively differs from local measurements on cells in 2D culture, and thus, raises important questions on how as a field we measure cell mechanics and the models that we use to describe them.

4.3 Methods

MVAS device

MVAS devices were fabricated out of polydimethylsiloxane (PDMS) using mold replication and plasma bonding steps outlined previously[196] from three masters created with standard photolithographic techniques. Masters were modified from our previous article[196] to allow measurements of tension. The MVAS now consists of 60 microtissue wells, each containing two cantilevers spaced apart by 500μm around which the 3D microtissues form (Fig. 4.1a). A vacuum chamber borders one side of each well and is connected to an external electronic regulator (SMC ITV0010) controlled through Labview software. When a vacuum is applied, the cantilever closest to the vacuum chamber moves to stretch the microtissue, while the other cantilever is used as a passive force sensor by optically tracking its deflection and utilizing its known spring constant ($k_{cantilever}$=0.834N/m). The dimensions of the force sensing cantilever were empirically chosen to be stiff enough to reduce the amount of creep that inherently occurs during stress relaxation because of our method of force measurement, yet also soft enough in order to have a sufficient signal to noise ratio in tension measurements.

Cell culture

NIH3T3 fibroblast (ATCC) cells were cultured in Dulbecco's Modified Eagle's Medium (DMEM) (Hyclone Laboratories Inc.) supplemented with 10% fetal bovine serum (FBS), 50mg/ml streptomycin and 50U/ml penicillin

antibiotics (all from Hyclone Laboratories Inc.). Cells were grown at 37℃ with 5% CO_2 on 100mm tissue culture dishes (Fisher) until 80-90% confluent.

Microtissue fabrication

Microtissues consisting of 3T3 fibroblasts in a 3D collagen matrix were cultured as previously described [124,196]. Briefly, the MVAS was sterilized with 70% ethanol, and treated with 0.2% Pluronic F-127 (P6866, Invitrogen) for two minutes to reduce cell adhesion. 250,000 cells were resuspended in 1.5mg/ml rat tail collagen type I (354249, Corning) solution containing 1x DMEM (SH30003.02, Hyclone), 44 mM $NaHCO_3$, 15 mM d-ribose (R9629, Sigma Aldrich), 1% FBS and 1 M NaOH to achieve a final pH of 7.0-7.4. The cell-collagen solution was pipetted into the MVAS and centrifuged to load ~650 cells into each well. The excess collagen was removed and the device was transferred into the incubator for 15 minutes to initiate collagen polymerization. An additional ~130 cells were centrifuged into each well and allowed to adhere to the top of the tissues. Excess cells were washed off. Cell culture media was added and changed every 24 hours.

Imaging

All images were acquired on a TiE A1-R laser scanning confocal microscope (LSCM) (Nikon) with standard LSCM configurations using appropriate laser lines and filter blocks. To assess morphology, microtissues were fixed *in situ* with paraformaldehyde for 10 minutes and permeabilized with 0.5% Triton-X for 3 minutes. The actin cytoskeleton was stained with Alexa Fluor 546 Phalloidin (Fisher, A22283) and the nuclei were stained with DAPI (Fisher, D1306).

Force measurements

After three days of static culture, we measured both stress relaxation of microtissues following a step strain and stress recovery after a subsequent return to initial length at 37^{o}C and 5% CO_2. Changes in microtissue tension were deduced from the visible deflection of the force-sensing cantilever. Bright field images of the tops of the cantilevers were captured at 15 frames per second during both stress relaxation and recovery. The cantilever tops were tracked using pattern matching with adaptive template learning in Labview. To aid in tracking the bottom position of the force-sensing cantilever, the middle device layer was fluorescently labeled by doping the PDMS mixture with Rhodamine-B prior to curing. Fluorescent images of the bottom of the cantilevers were captured before and after stress relaxation and recovery experiments. After thresholding, the bottom position of the force-sensing cantilever was measured from these images with a simple centroid algorithm in Matlab. The deflection of the force sensor was then calculated by subtracting the difference in the top and bottom positions. A validation of our approach with a elastic standard and characterization of the noise floor are in Appendix C.1.

To investigate nonlinearities in the viscoelastic behavior of microtissues, stress relaxation and recovery were measured for various step strain values. The strain, ε, was defined as the percent change in the length

between the innermost edges of the tops of the cantilevers once the microtissue had fully relaxed or recovered (equation 4.1).

$$\varepsilon(t) = \frac{length(t) - length_o}{length_o} \times 100 \quad (4.1)$$

To assess the role of individual cytoskeletal proteins in contributing to the viscoelasticity of microtissues, measurements were taken following 20 minute incubations with either 10μM nocodazole (Noco), a microtubule polymerization inhibitor, 5μM blebbistatin (Bleb), a myosin-II inhibitor, 10 μM cytochalasin D (CytoD), an actin polymerization inhibitor, or 0.5% Triton-X, to decellularize microtissues. 0.5% DMSO was used a loading control. As mechanical properties varied between microtissues, each microtissue was compared to its own pre-treatment value where indicated. To prevent crossover in response from multiple drugs, only a single treatment was administrated to any given microtissue.

Quantification of microtissue remodeling

To quantify the spatial distribution of remodeling that occurs following a change in length, local strains were estimated across microtissues using a method described previously [196]. Briefly, starting at the frame immediately following the step change in length, inter-frame displacements were estimated every one second for 100 seconds in Labview at two-pixel spacing across a region of interest using a four level-pyramid based Lucas and Kanade algorithm[206] with sub-pixel precision and a window size of 17x17 pixels. In Matlab, the displacement field was first smoothed with a LOWESS surface-fitting algorithm, then the inter-frame strain tensor was calculated by finding the gradient of the smoothed displacement field, and finally the inter-frame strain tensor was integrated to estimate the local total strain field.

Data analysis and statistics

All numerical data are presented as mean ± standard error. Statistical tests as described in the results were performed using Originlab 8.5 (Northampton, MA), with $p<0.05$ considered statistically significant. Fits to stress relaxation data were performed using Matlab's curve fitting toolbox.

4.4 Results

Microtissues are viscoelastic

In the MVAS, cells in a collagen matrix compacted around the cantilevers into freely suspended 3D microtissues with high cell density and organization (fig. 4.1). In contrast to bulk 3D cell cultures[216,251], the cells in microtissues are mostly aligned with the direction of tension development shown by both the longitudinally oriented actin cytoskeleton and the nuclei in fig. 4.1b. After three days of static culture, fibroblast microtissues developed a resting tension of 8.7±0.4μN (N=79).

In addition to static tensile measurements, the MVAS enables the assessment of dynamic mechanical behavior through a vacuum-driven planar stretch and by visibly tracking the deflection of the force-sensing

cantilever (fig. 4.1a). Following a step change in length, microtissue tension rose sharply and then relaxed through well-conserved dynamics to a new equilibrium point as commonly seen in viscoelastic solids (fig. 4.1c). Upon returning the microtissue to its initial length, the tension dropped past and then slowly recovered to its original resting value (P>0.05, repeated measures t-tests). This behavior was highly repeatable as subsequent steps were superimposable (Appendix C.2). These results indicate that cells within microtissues work to maintain unique tension equilibriums at any given strain.

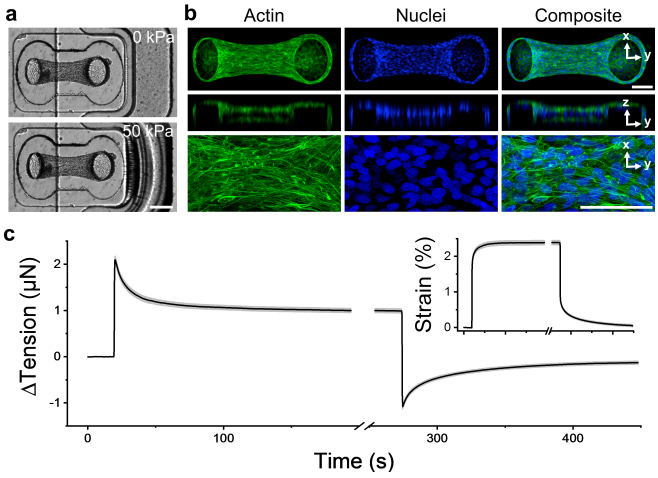

Fig. 4.1: Microtissue tension dynamically relaxed and recovered with changes in length. Microtissues were grown in our MVAS-force device (a). In the MVAS-force, changes to microtissue length are driven by applying a regulated vacuum pressure to a chamber that borders one side of each microtissue well. The cantilever closest to the vacuum chamber (shown here on the right) is actuated to stretch the microtissue in plane while changes in tension can then be measured by tracking the deflection of the opposing cantilever (on the left). Microtissues are organized 3D cell cultures freely suspended between the cantilevers. Max projections of confocal stacks, orthogonal views and high magnification images are shown in (b). Both the actin cytoskeleton (green), and the nuclei (blue) are predominately aligned between the cantilevers. Scale bars in (a) and (b) represent 200μm and 100μm, respectively. Following a step in strain (insert), microtissue tension (N=79) sharply increased and then relaxed to a new set point as expected in a viscoelastic solid (c). Then upon returning the microtissue to its original length, the tension recovered.

In order to further characterize the viscoelastic behavior of microtissues, we searched for an appropriate model to describe their tension (T) relaxation and recovery behavior (fig. 4.2a and 4.2b, respectively). First, we tested the standard linear solid (SLS) viscoelasticity model (equation 4.2) as it has been commonly applied to isolated cells[73,94,249], 3D cell cultures[216] and ex vivo tissue strips[93]. A SLS model, where k_1 and k_2 are spring constants and τ is a time constant, fits the data well at short time-scales but fails to capture the long time tail in both relaxation and recovery responses.

$$T_{SLS}(t) = \varepsilon\left(k_1 e^{-t/\tau} + k_2\right) \tag{4.2}$$

In contrast to an exponential model, slow relaxation and recovery at long timescales is exemplified in power law rheological models (equation 4.3), which been widely reported in single cells[65,68,99] and tissues [252,253].

For microtissues, a power law, where β is dimensionless constant describing the viscoelastic behavior, fits the slow relaxation at long-timescales but predicts faster than experimental dynamics at shorter times.

$$T_{PL} = \varepsilon\left(k_1 t^{\beta} + k_2\right) \tag{4.3}$$

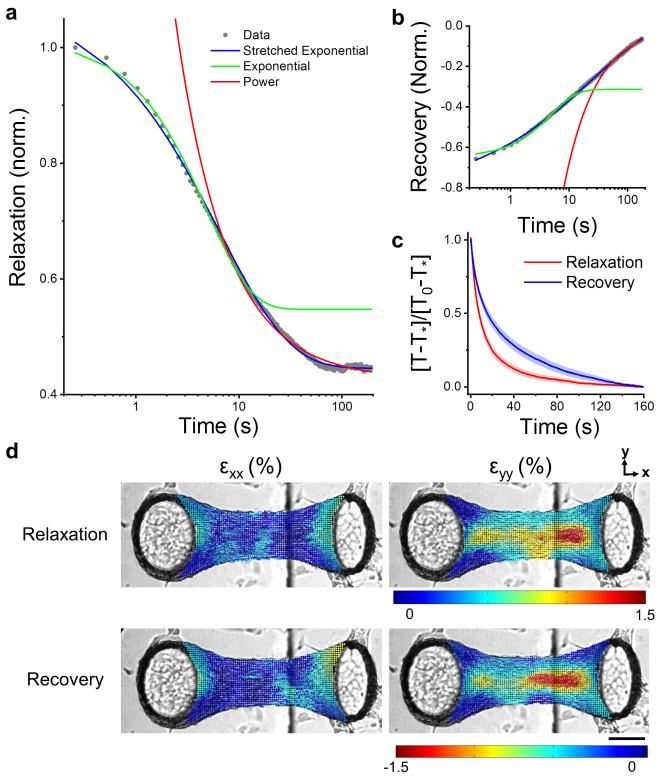

Fig. 4.2: Stress relaxation and recovery in microtissues followed stretched exponential trajectories. Microtissue stress relaxation fitted to various viscoelastic models is shown in (a) and stress recovery is shown in (b). Stretched exponentials capture relaxation and recovery behaviors over three decades of time. Responses are normalized to their amplitudes in (c), showing that relaxation occurred much quicker than stress recovery. Yet, stress relaxation and recovery appeared to share the same spatial locations within a given microtissue in terms of both remodeling in the longitudinal (ε_{xx}) and transverse (ε_{yy}) directions immediately following the change in length (d). The scale bar represents 100μm.

From these models it was clear that in order to capture both the exponential stress decay at short-time scales and the slow relaxation at long time-scales, we needed a model that first appeared as an exponential but crossed over to a more slowly relaxing tail behavior at long times. This behavior is characteristic of a stretched exponential (equation 4.4). Although we have not come across previous reports that have modeled the viscoelastic behavior of cells or tissues with stretched exponentials, they have been widely used to describe relaxation in glassy, disordered systems[254,255]. For microtissues, a stretched exponential fits both stress relaxation and recovery data over three decades of time (R^2>0.99). The average fitting constants are summarized in table 4.1. Importantly, the creep that inherently accompanied our method of measuring microtissue tension relaxation was insufficient to

significantly change either the type model or the fitting constants (Appendix C.3). While we likely could have fit the data just as well by adding additional exponential time constants to a SLS, as in a Wiechert model[256], this method is an ineffective use of variables compared to a single stretched exponential.

$$T(t) = \varepsilon\left(k_1 e^{-(t/\tau)^{\beta}} + k_2\right) \tag{4.4}$$

The spring elements, k_1, describing the amplitudes of stress relaxation and recovery, agreed well each other. Moreover, the spatial distributions of strain, describing the locations of stress relaxation and recovery, were well correlated (fig. 4.2d). This indicates that the regions in the tissue that underwent stress relaxation were also responsible for stress recovery.

Table 4.1: The stress relaxation and recovery fitting constants (N=79).

	k_1 (μN/%)	k_2 (μN/%)	τ (s)	β
Relaxation	0.55 ± 0.03	0.42 ± 0.02	14 ± 1	0.70 ± 0.03
Recovery	0.5 ± 0.02	-0.02 ± 0.02	31 ± 2	0.59 ± 0.02

The second spring constant (k_2) in equation 4.4 describes the residual elastic stress in the tissue once fully relaxed or recovered. The source of this elasticity is unclear. It may arise from the contribution of the matrix, or perhaps indicates of the existence of a stress threshold up to which cytoskeletal elements can behave elastically but beyond which they yield. In recovery curves k_2 is approximately equal to zero, indicating that microtissues fully recovered to their original prestress upon returning to their initial length. In other words, any remodeling done to relax the increase in tensile stress that accompanies a step strain, is undone once microtissues are returned to their initial lengths.

In fig. 4.2c microtissue tension, T, during stress relaxation and recovery was normalized to the respective amplitudes of the responses. By normalizing the curves in this manner, it was clear that relaxation occurred much quicker than stress recovery. Therefore the dynamics of these viscoelastic responses are imbalanced.

In this section we have described the viscoelasticity of microtissues and found that this behavior can be captured through a relatively efficient stretched exponential model. In the rest of this article, we aimed to gain further insight into how the mechanics of microtissues are controlled by underlying molecular and structural mechanisms in the cells by first examining how this behavior is affected by strain, and secondly, how microtissue viscoelasticity changes under a range of pharmacological treatments targeting specific cytoskeletal elements.

Microtissue viscoelasticity is nonlinear

To assess whether there are nonlinearities in the viscoelastic behavior of microtissues, stress relaxation and recovery measurements were performed at various step strain amplitudes on the same tissues. Shown in fig.

4.3a are average response curves for 3.3 ± 0.2 % and 10.9 ± 0.8% step strains. Using the same method of normalization as above, fig. 4.3b shows that stress relaxation occurred much more quickly following larger step strains. In contrast, the rate of stress recovery was step strain amplitude invariant (fig. 4.3c) and it did not depend upon the strain at which the microtissue recovered (Appendix C.4). Therefore the rate of stress relaxation in microtissues was nonlinear with strain for large amplitudes, while stress recovery was linear for the same range of amplitudes.

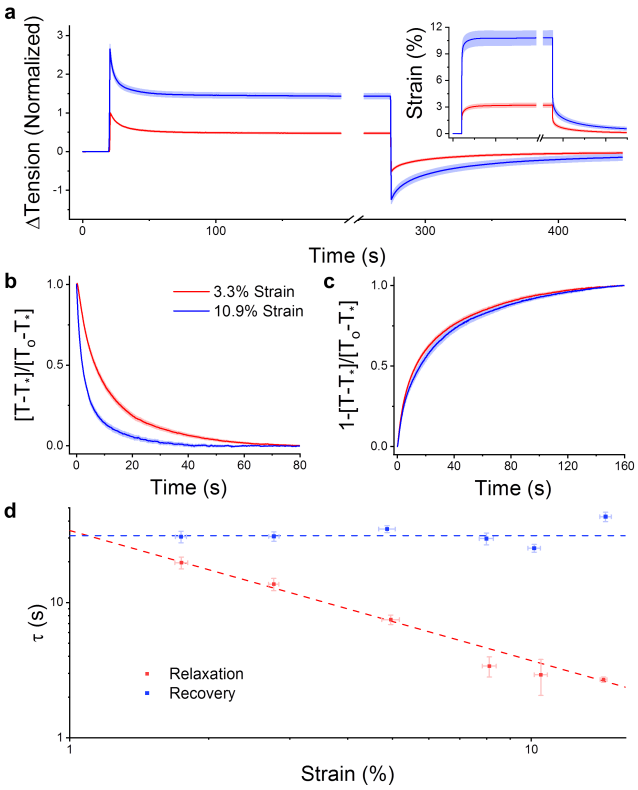

Fig. 4.3: The rate of stress relaxation was nonlinear while recovery was strain invariant. To assess viscoelastic non-linearity, the step size was varied (insert). Stress relaxations for a 3.3 and 10.9% step are shown in (a) (N=17). After normalizing for response amplitude, (b) shows that the rate of stress relaxation increased with strain. In fact, the time constant for stress relaxation appeared to follow an inverse power law with a near unity exponent (d). In contrast, the rate of recovery was invariant on the step size (c and d).

The changes to fitting constants for stress relaxation and recovery for these strain amplitudes are summarized in tables 4.2 and 4.3 respectively. For stress relaxation, a larger step strain decreased both of the spring constants (repeated measures T-tests; for k_1: $P<0.001$, for k_2: $P<0.05$), the time constant ($P<0.001$) and the power law constant ($P<0.001$). In comparison, for stress recovery, applying a larger step strain only significantly reduced the k_1 spring constant ($P<0.001$). Recovery responses shared the same time, and power law constants, and the tissue tension fully recovered under both small and large step strain sizes (all $P>0.05$).

To further highlight these nonlinearities, the viscoelastic responses in 160 microtissues were analyzed with step strains ranging from 1.75 ± 0.06% to 14.3 ± 0.2%. As reported above, the recovery time constant stayed relatively strain-invariant (fig. 4.3d). On the other hand, the relaxation time constant decreased with what appeared to be a power law dependence on strain amplitude (non-linear regression: R^2=0.96 P<0.001), although the range of strain only spanned a single decade. The remaining fitting constants are summarized in Appendix C.5 and C.6. As with our repeated-measurement findings, k_1 relaxation and recovery values were weakly correlated to strain (linear regression: R^2=0.78 P<0.001 and R^2=0.66 P<0.05, respectively), indicating that on fast time-scales, microtissues strained softened. However, in contrast to repeated-measurements, neither k_2 nor the power law relaxation constant were dependent on strain (linear regression: P>0.05), possibly because inter-tissue variance may have outweighed these trends. k_2 and power law constants were also seemingly invariant for stress recovery data (linear regression: P>0.05).

Table 4.2: The changes to stress relaxation fitting constants measured at 10.9% vs. 3.3% strain. Values were compared with repeated measures t-tests (N=17) (* P<0.05, ***P<0.001).

Δk_1 (%)	Δk_2 (%)	$\Delta\tau$ (%)	β (%)
-24 ± 4 (***)	-12 ± 5 (*)	-58 ± 5 (***)	-19 ± 5 (***)

Table 4.3: The changes to stress recovery fitting constants measured at 10.9% vs. 3.3% strain. Values were compared with repeated measures t-tests (N=17) (** P<0.01).

Δk_1 (%)	$\Delta\tau$ (%)	β (%)	$\Delta T_{f\text{-}l}$ (μN)
-28 ± 5 (**)	15 ± 7	-2 ± 3	-0.4 ± 0.2

In addition to the fitting constants, the spatial distribution of microtissue remodeling following a step change in length varied considerably with strain. Fig. 4.4a and b show, respectively, the raw and normalized remodeling in the transverse direction in representative microtissues after 100 seconds. Remodeling during stress relaxation and recovery in the transverse direction increased with step size and became transversely focused to the center of the tissue but longitudinally diffuse, spanning the entire tissue length.

Transverse strain fields were averaged across the region of interest to compute a mean metric of the integrated remodeling response through time (fig. 4.4c and d, respectively). During stress relaxation following a small step strain (1.7 ± 0.2%), microtissues showed little remodeling in the transverse direction. With an intermediate step strain (3.4 ± 0.2%), microtissues relaxed to reach a new equilibrium. Lastly, with a large step strain (10.4 ± 0.5%), microtissues quickly relaxed, then contracted to a smaller degree, and eventually reached an equilibrium strain.

Mean recovery curves showed slower dynamics (fig. 4.4d) compared to relaxation curves. Yet, relaxation and recovery following small and intermediate step strains shared similar spatial distributions and amplitudes but with opposing signs, indicating that the gross structural remodeling that occurred after a step strain is in part reversible. In contrast however, recovery amplitudes following a large step strain were comparably higher than the final equilibrium in relaxation curves. This suggests that large steps sizes may cause permanent remodeling in microtissues through a stretch activated contraction.

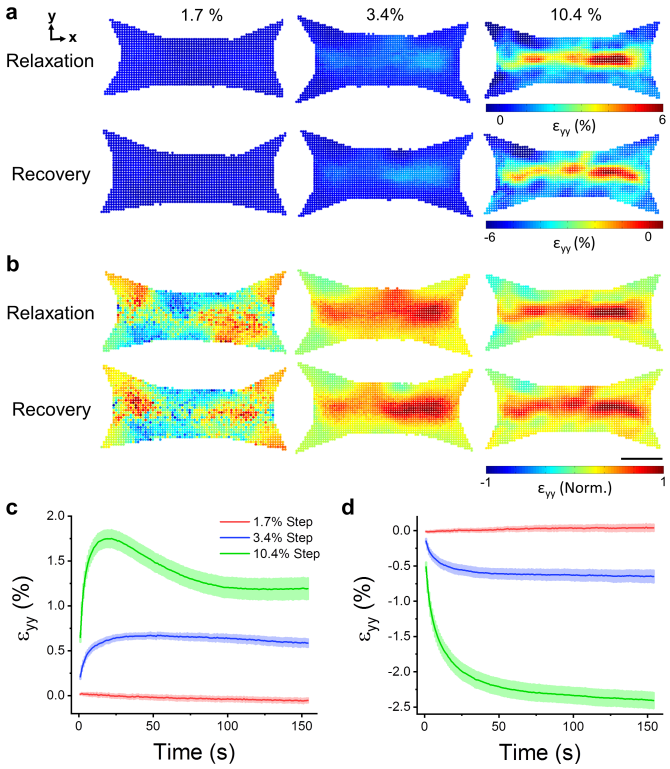

Fig. 4.4: The locations of remodeling following changes to microtissue length were strain-dependent. Spatial distributions of relaxation and recovery in the y-direction immediately after various step sizes are shown in (a). The distributions are normalized to three standard deviations outside of the absolute mean value in (b). The scale bar represents 100µm. The average (N=6) strain in the transverse direction that occurred during stress relaxation and recovery is plotted against elapsed time in (c) and (d), respectively.

In comparison with the remodeling in the transverse direction, remodeling in the longitudinal direction was less extensive being constrained by the cantilevers. Longitudinal remodeling was also highly tissue-specific and mainly located near the fronts of the cantilevers rather than the body of the tissue. This behavior likely was not indicative of tissue detachment from the cantilevers but rather reflected the heterogeneity and anisotropy within microtissue cultures as final relaxation and recovery longitudinal strain fields shared similar mean amplitudes for all tested step sizes (Appendix C.7).

Pharmacological behaviors

To assess the role of several key cellular proteins in governing microtissue viscoelasticity, stress relaxation and recovery were measured following various pharmacological treatments meant to either disrupt the cytoskeleton or alter actomyosin activity. Normalized responses and fitting constants are shown in fig. 4.5a and table 4.4, respectively. Each fitting constant was normalized and compared with paired t-tests to their own pre-treatment control. DMSO was used as a loading control and did not affect either relaxation or recovery curves. Furthermore none of the treatments caused a difference between the initial tension prior to a step strain and the final tension following stress recovery, indicating that there was no plastic change to the microtissues and that the incubation periods for the treatments were sufficient to reach an equilibrium state.

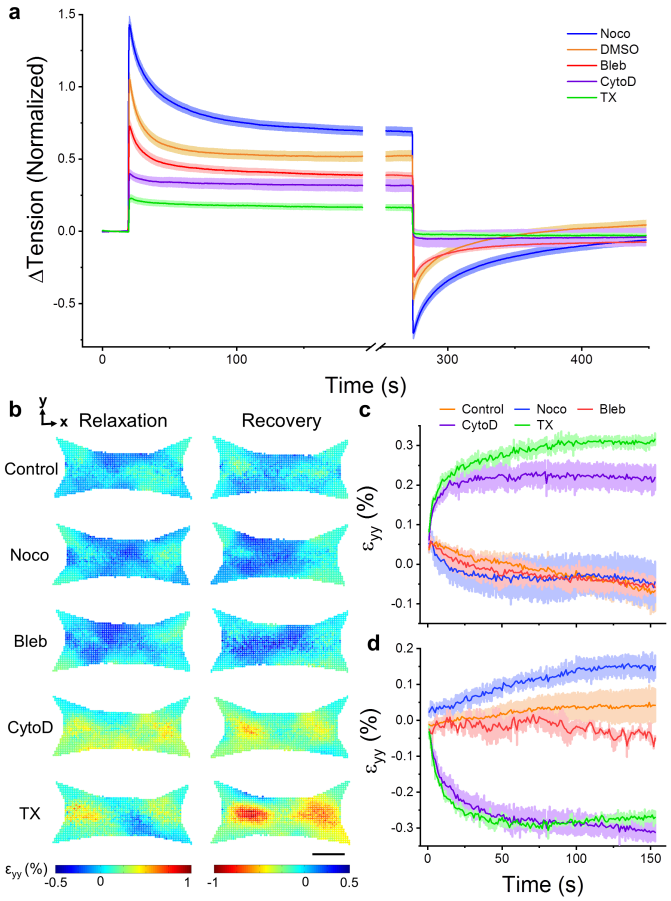

Fig. 4.5: Stress relaxation and recovery varied with pharmacological disruption of the cytoskeleton and myosin inhibition. Depolymerization of microtubules (Noco) increased stress relaxation and recovery responses, whereas myosin inhibition (Bleb), actin depolymerization (CytoD) and decellularization (TX) decreased relaxation and recovery (a). DMSO, a loading control, had no difference compared to no treatment. Microtissues only ever received a single treatment and each treatment was normalized to its pretreatment control. The spatial distributions of relaxation and recovery in the transverse direction following a small (1.7%) change in length are shown in (b). The scale bar represents 100µm. The average (N=3) strains in the transverse direction during stress relaxation and recovery are shown in (c) and (d), respectively.

Consistent with our understanding that microtubules act as compressive struts that oppose actomyosin activity [225], microtubule depolymerization with nocodazole increased the resting tension in microtissues by 3.7 ± 0.4μN (P<0.001). Microtissue spring constants for stress relaxation (k_1 and k_2 both P<0.001) and recovery (k_1 P<0.001) responses increased as well. Microtubule depolymerization did not effect either the time or power law constants for stress relaxation (τ and β both P>0.05). However, in contrast, nocodazole treatment increased the time constant, τ, and decreased the power law constant, β for stress recovery (P<0.01 and P<0.05, respectively). This suggests that the recovery rate may be altered through the regulatory action of microtubules on acto-myosin activity, but that relaxation rates are unchanged.

Myosin inhibition (blebbistatin), actin depolymerization (cytochalasin D) and decellularization (triton-X) all decreased resting microtissue tension (by -2.8 ± 0.5 μN, -5.0 ± 0.4μN and -8.8 ± 0.8μN, respectively; all P<0.001), relaxation k_1 and k_2, and recovery k_1 (various P values). Blebbistatin treatment did not affect the relaxation time constant but did decrease the recovery time constant (P<0.01), indicating again that myosin motor activity, in part, determines the recovery speed. There was no observable stress relaxation or recovery upon either actin depolymerization or decellularization, and for this reason, it was not possible to accurately fit time and power law constants to these treatments. Nevertheless, these curves show that remodeling in actin microfilaments is chiefly reasonable for the viscoelastic behavior of microtissues.

Table 4.4: The pharmacologically induced changes to stress relaxation and recovery fitting constants. Each treatment was compared to its pretreatment control using paired t-tests (* P<0.05, ** P<0.01, ***P<0.001).

	ΔT_{base} (μN)	Relaxation				Recovery			
		Δk_1 (%)	Δk_2 (%)	$\Delta\tau$ (%)	$\Delta\beta$ (%)	Δk_1 (%)	$\Delta\tau$ (%)	$\Delta\beta$ (%)	$\Delta T_{f\text{-}i}$ (μN)
Noco (N=24)	3.7 ± 0.4 (***)	40 ± 9 (***)	37 ± 9 (***)	10 ± 12	11 ± 5	96 ± 14 (***)	87 ± 25 (**)	-7 ± 4 (*)	0.03± 0.07
DMSO (N=21)	-0.1 ± 0.2	6 ± 6	8 ± 7	4 ± 9	8 ± 8	10 ± 9	5 ± 13	8 ± 5	0.17 ± 0.09
Bleb (N=16)	-2.8± 0.5 (***)	-27 ± 7 (**)	-15 ± 5 (*)	14 ± 10	-2 ± 9	-32 ± 5 (***)	-27 ± 8 (**)	7 ± 4	-0.1 ± 0.06
CytoD (N=8)	-5.0 ± 0.4 (***)	-74 ± 10 (***)	-47 ± 12 (***)	-	-	-112 ± 6 (***)	-	-	-0.1 ± 0.1
TX (N=7)	-8.8 ± 0.8 (***)	-86 ± 6 (***)	-65 ± 7 (**)	-	-	-109 ± 10 (***)	-	-	-0.1 ± 0.2

To examine how microtissue remodeling during relaxation and recovery was affected by microtubules, actin microfilaments, myosin motor activity and the extracellular matrix, strain fields were assessed at the same

small step strain (1.7 ± 0.2%) following pharmacological treatments. Microtubule depolymerization and myosin inhibition behaved similarly to control microtissues in their transverse (fig. 4.5b-d) and longitudinal (Appendix C.8) remodeling responses. In contrast, actin depolymerization and decellularization induced remodeling responses that were more consistent with a larger step strain in terms of the spatial distribution, amplitude and dynamics of the strain fields. This finding implicates the depolymerization of actin and the contribution from the matrix in the gross remodeling behavior and nonlinear dynamics observed with large strains.

4.5 Discussion

In this article, we assessed the dynamic mechanical behavior of physiologically relevant 3D microtissue cell cultures. As expected, microtissues displayed timescale-varying mechanics. In response to a step increase in length, the tension quickly rose and then relaxed to a new equilibrium point as in a viscoelastic solid. When microtissues were returned to their initial lengths by a recovery strain, their tension quickly dropped below initial measurements, and then slowly, yet fully, recovered. These responses, however, differed greatly in their dynamics. Whereas recovery rates were strain independent, relaxation was a highly nonlinear function of strain, following with what appeared to be an inverse power law with strain amplitude. Both these responses differed from the weak power laws that describe the relaxation of cells in 2D culture typically observed with other micro-rheological techniques [66,68,99]. Therefore, our findings raise important questions about how we characterize the mechanical behavior of cells (globally vs. locally or tension vs. shear vs. compression) and the environment in which they are assessed (2D vs. 3D culture) [170].

In particular, unlike previous work in 2D cell culture, which predominately have used power law models [66,68,99], we found that tensile stress relaxation and recovery in microtissues followed stretched exponential functions. To the best of our knowledge, stretched exponentials have not been previously used to describe the viscoelastic behavior of cells or cell cultures. Still, however, our findings are in close agreement with previous reports from bulk fibroblast populated collagen gels [216,250]. In that regard, we both reported characteristic time constants of similar magnitudes with time-dependencies that are more broadly distributed than what can be explained by a single exponential function (ie. a SLS model). With this said, much work is still needed to show that this behavior exists in other cell types besides fibroblasts. Furthermore, although the cells greatly remodeled the initially glycated collagen gel and likely secreted additional ECM proteins, the ECM composition, and in turn, its mechanical behavior still differed from intact tissues. Proteoglycans, for example, control the mass transport of water, and therefore, are a key determinant of energy dissipation [130] that we did not intentionally incorporate into our microtissues. That being said, since the decellularized response was primarily elastic and there was no recovery, these stretch exponential processes can be solely attributed to the active mechanics of the cytoskeleton and how the cells interact with their matrix.

In the contrary to biological samples, there does exist a strong precedent for the use of stretched exponentials to describe relaxation in disordered condensed matter physics. In fact both polymer networks [257] and

glasses near their transition temperature [254,255] relax according to stretch exponentials. Such glassy polymer response has already been linked to the mechanical behavior of the cytoskeleton [76]. Furthermore, our average values of β (0.64 ± 0.01 and 0.61 ± 0.01 for relaxation and recovery, respectively) are in close agreement with an universal experimental value of 0.6 in glasses dominated by Brownian motion [258], which is theoretical justified by a so-called 'trapping model' [259]. Mathematically this model is beyond the scope of this work but it is relatively easy to conceptualize. In a trapping model, the material consists of randomly distributed traps. During relaxation, these traps capture molecules that diffuse through the material, and as the traps are filled, the remaining molecules must travel longer to find unoccupied traps. Thereby, the relaxation rate falls with a power law given by the dimensionality of the model.

Although a trapping model can be a great tool to conceptualize stretched exponentials, the question remains whether we can draw out any physiological meaning or link any mechanism(s) to account for the stretched exponential relaxation and recovery in microtissue behavior. Similar to power laws, stretched exponentials can be expanded into a superposition of simple exponential functions with a nontrivial distribution of relaxation times [231]. It should also not be overly surprising that relaxation processes exist across a broad spectrum of timescales in something as complex and heterogeneous as the network of cytoskeletal proteins inside single cells, and in a more collective sense, when considering an aggregate of cells and extracellular matrix. Thus, our fitting constants may be interpreted as a general description of microtissue behavior reflecting the broad viscoelastic heterogeneity in the cytoskeleton and amongst cells rather than capturing a specific process.

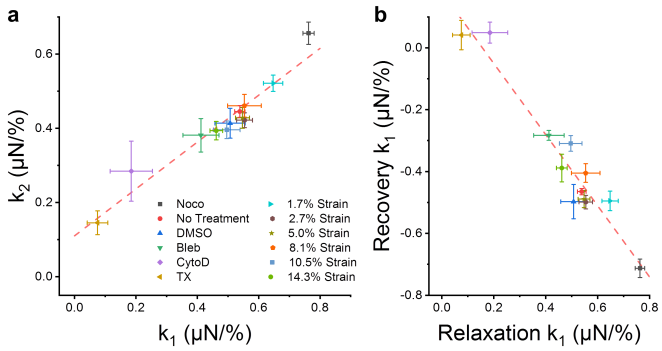

Fig. 4.6: The underlying relationships between microtissue dissipation and elasticity. The k_1 and k_2 stress relaxation spring constants were linearly coupled throughout an assortment of pharmacological treatments and step lengths (a) (linear regression; $P<0.001$ $R^2=0.94$). The amplitude of stress relaxation was also coupled to the amplitude of stress recovery (b) (linear regression; $P<0.001$ $R^2=0.92$).

In spite of the generality of stretched exponentials, the relaxation spring constants in our model (k_1 and k_2) were tightly coupled throughout an assortment of pharmacological treatments targeting specific proteins, and as well in measurements at different step strain amplitudes; in particular, all treatments followed a single linear relationship (fig. 4.6a). This coupling behavior has previously been interpreted as evidence suggesting that elastic

and dissipative stresses are borne from the same origin(s) [260,261]. Even so, it is surprising that targeting different cytoskeletal elements can produce responses that seemed to follow a single universal relationship, unless an understanding of mechanisms at a hierarchy beyond the single protein-level is required. Rather than following responses in single molecules, as our field has been studying in a traditional reductionist approach, the viscoelasticity of cells and tissues is perhaps more influenced by the association and interaction of proteins with each other [106]. Further evidence in support of this view has been reported through various universalities in single cell mechanics [66,92,225,262].

Dissipative stresses during microtissue relaxation were also strongly coupled to the stress regained during recovery (fig. 4.6b). Furthermore, for the most part, microtissue remodeling during relaxation and recovery occurred with similar spatial distributions and comparable amplitudes. These results suggest that stress relaxation and recovery depended upon reversible remodeling in the same cells within the microtissue. On the other hand, the dynamics of the relaxation and recovery responses were, for the most part, very different. Relaxation rates were nonlinear with step strain amplitude, decreasing with what appeared to be a power law, but were relatively invariant with microtubule depolymerization or myosin inhibition. In contrast, recovery rates were invariant with step strain amplitude but increased with microtubule depolymerization and decreased with myosin inhibition. This suggests that myosin contributed only as a passive cross-linker during relaxation, while active myosin crossbridge cycling was partially responsible for stress recovery. Still however, the actin cytoskeleton was the principal source of elasticity and dissipation since depolymerization of actin filaments had the biggest effect on microtissue viscoelasticity outside of decellularization. There also appeared to be some passive component to the recovery as there was remodeling upon returning samples with actin-depolymerized cells and as well as in decellularized microtissues to initial lengths. Interestingly, this remodeling was consistent with larger step strains, suggesting that the loss of the actin cytoskeleton and how the cells associate with the matrix may be in part be responsible for the non-linear relaxation rates.

It is not uncommon for relaxation in soft biological tissues to be nonlinear. Perhaps, it is more surprising that stress recovery was so linearly independent of the step strain. Indeed nonlinearities have been previously reported in lung[263], heart valve[264], ligament[265], and muscle[266]. Recently, nonlinear relaxation rates in cells were argued to arise from a poroelastic effect occurring through the redistribution of the viscous cytosolic fluid between local regions within the network of cytoskeletal filaments[86]. It is, however, debatable that the same effect is the main determinant in our measurements, as there is a difference of more than a decade in time-constants between our findings and those of the poroelastic model. Moreover, poroelasticity does not offer an explanation as to why the recovery rates were linear with strain amplitude and much slower than relaxation rates.

An alternative mechanism conceives stress relaxation in cells as a friction force produced by cytoskeletal filaments sliding smoothly past one another [100]. The main support for this hypothesis is that local shear measurements on cells in 2D culture follow the structural damping law; the ratio of dissipative to elastic stresses is invariant of the time-scale at which they are assessed [66,68]. This hypothesis, however, does not offer any

explanation as to the nonlinearity observed in relaxation rates and the imbalance with recovery dynamics. Furthermore it is not compatible with either standard linear solid viscoelasticity or a stretched exponential, as both models produce characteristic rate-dependencies that contradict structural damping. Interestingly, in contrast with local shear measurements, characteristic rate-dependencies similar to our observations in microtissues have been previously reported in individual cells[73] and 3D cultures[216] when probed in tension at a length-scale of the entire cell/culture. It would still be of interest, however, in future work to show that the frequency response of microtissues is consistent with their stretched exponential relaxation in the time domain.

A last possible mechanism to explain the viscoelastic response in microtissues is that stress relaxation and recovery reflects the rupturing and reforming of bonds within the cytoskeleton (i.e. within actin filaments and between actin and its crosslinkers), and between the cells and the extracellular matrix. In support of this hypothesis, there is a strong precedent that mechanical stretch depolymerizes actin filaments[78–80,92] and perturbs myosin binding[7,8,81–83]. Indeed, we have shown here that microtissues strain-soften. Further in regard to this hypothesis, the imbalance in microtissue relaxation and recovery rates can simply be explained by differences in bond destruction and formation rates; it is not unreasonable to suspect that it takes less time to pull bonds apart than for proteins in a cell to diffuse through Brownian motion, correctly reorient themselves, and then lastly reform chemical bonds, especially if additional enzymes (ie. profilin) and molecules (ie. ATP) are needed. Furthermore, nonlinearities in relaxation behavior have previously been captured by models in which stress is relieved through sequential rupturing of Maxwell bodies, where each micro-yield event passes the stress on to other regions of the tissue [97,98]. Results from these models give an exponential with a long-tail power law, however it is possible that chemical bonds have a finite yield strength, and therefore in actuality curves may flatten, behaving as stretched exponentials. Admittedly, however, this model is currently unable to explain nonlinearities beyond quasi-linearity, such as the inverse power law between relaxation rate and strain amplitude that we observed.

4.6 Conclusions

The viscoelastic behavior of microtissues likely does not come down to a single physiological mechanism, but rather it is an amalgamation of many physical remodeling events occurring at different time and length scales. Therefore, the measured stress relaxation and recovery of microtissues are generalized responses, and perhaps unsurprisingly differ from local measurements in 2D culture. In that regard, we found that the viscoelastic behavior of microtissues followed a stretched exponential, and that stress relaxation rates were nonlinear and imbalanced with a linear recovery response. On the other hand, the contributions of specific cytoskeletal elements (actin, myosin, microtubules) to microtissue mechanics did not qualitatively differ from our previous understanding of their roles in the mechanical behavior of cells grown on 2D substrates. Importantly, all our results, collapsed onto a single relationship between elastic and dissipative stresses, indicating that the cytoskeleton of cells within microtissues may follow an universal behavior set not by the role of individual proteins

but rather by the physical architecture of cells and their surrounding matrix as a whole. To conclude, the assessment of dynamic mechanics of microtissues has yielded further insights into how tissues gain their mechanical properties from cells, and from the distribution and interaction of their cytoskeletal proteins. This knowledge is critical to a full understanding of how physical forces are sensed and regulate cell behavior in health and disease.

CHAPTER 5| THE RHEOLOGICAL BEHAVIOR OF MICROTISSUES UNDER OSCILLATORY LOADING IS CONSISTENT WITH A STRETCHED EXPONENTIAL

Authors: **Matthew Walker**, Michel Godin, James L. Harden, Andrew E. Pelling

The manuscript has been prepared for submission to APL Bioengineering following the publication of chapter 3. The supplementary information is contained in Appendix D.

Motivation & Objective| The time-domain rheological behavior of microtissues presented in chapter 4 differed from our field's understanding of cells studied in 2D culture. To investigate whether microtissues exhibit an equivalent frequency domain behavior, in this chapter we assessed the mechanical properties of microtissues under cyclic loading across a broad frequency range. The findings contained here give insights into how the cytoskeleton is regulated by dynamic stretch.

5.1 Abstract

Microtissue cell cultures offer the ability to investigate the mechanical behavior of the cytoskeleton within a physiologically relevant 3D environment. In contrast to other work in 2D cell cultures, we previously reported that stress relaxation and recovery responses of microtissues could both be captured by stretched exponentials. This behavior is consistent with a theoretical understanding of disordered systems, perhaps reflecting the disordered glassy-like nature of actin microfilaments. To follow that work, we assessed here whether microtissues possess a Fourier equivalent under oscillatory loading. We found that the frequency response of microtissues displayed a broadly distributed characteristic timescale that appears to be determined from a dynamic equilibrium set by a difference in cytoskeletal assembly and disassembly rates. We further demonstrated that a stretched exponential could fit responses following an assortment of pharmacological treatments and at various strain amplitudes, indicating that it robustly approximates the dynamical mechanical properties of microtissues. We also linked the strain-softening response of microtissues to their rheological behavior, demonstrating that this mechanotransduction mechanism is time-scale dependent. To conclude, investigating the behavior of microtissues under oscillatory loading furthers our understanding of the time-dependent forces that cells experience in the body, which is needed in order to fully comprehend mechano-sensing pathways in normal development and disease progression.

5.2 Introduction

External mechanical forces (ie. stiffness, stretch, shear, compression) have been widely linked to cellular behavioral changes that are critical in both normal development and disease progression, including lung, heart, muscle and bone disorders, and cancer [4,5]. Therefore a closer look at how mechanical forces are transduced into

chemical signals in cells, may help us better understand these diseases and improve treatment options. In the current paradigm, mechanical loading generates conformation changes in focal adhesions and cytoskeletal proteins that in turn alter the binding affinities for additional signaling molecules [1,3]. As these force-sensing pathways are ultimately reliant on the physical deformation of proteins, an understanding of cell mechanics is a fundamental aspect to these mechanisms. With respect to this paradigm, however, it is often overlooked that cells posses a spectrum of mechanical behaviors depending upon the rate at which they are probed [88,89], and thus, importantly force-sensing pathways, themselves, are likely timescale-dependent based upon the rheological properties of the cell.

Accordingly, our field has set out to define the viscoelastic behaviors of cells and to link them to specific processes occurring in cytoskeletal elements. Early on investigators studied the mechanical behavior of cells under tensile loads with deformations occurring at relatively large length-scales (ie. micropipette aspiration and microplates), and found characteristic timescales and modeled cell behavior as a standard linear solid (SLS) with a simple exponential function [73,94,249].

In contrast, however, more recent local shear and compression measurements (ie. optical magnetic twisting cytometry (OMTC) and atomic force microscopy (AFM)) have been characterized with weak power laws [65,66,68,99,267]. Under these experimental conditions, dissipation arises according to structural damping (ie. the ratio of dissipative to elastic stresses is time-scale invariant) presumably from molecular friction between cytoskeletal elements sliding passed one another [66,68]. Seemingly universal observations of power law rheology across a wide range of pharmacological treatments and cell types has since given traction to the hypothesis that cells belong to a class of soft glassy materials [66,68,81,106].

In addition, at very short timescales (~0.5s), dissipation may be produced through a poroelastic effect caused when cytosolic fluid redistributes throughout the cytoskeleton [86]. While at long timescales (>30s), the mechanical behavior may in part reflect the consumption of ATP during active remodeling of the cytoskeleton and myosin cross-bridge cycling [268].

This understanding of cell mechanics, however, has mainly originated from investigations that have grown cells on 2D substrates rather than within a more physiologically relevant 3D environment. Yet, we know 2D cell culture forces an unnatural apical-basal polarity of cell adhesions, and thus, fundamentally changes the structure and distribution of the cytoskeletal [31]. To address how the mechanical behavior of cells may be affected by the dimensionality of their environment, techniques that allow assessment of cells within reconstituted 3D collagen gels have been a keen interest to our field [116]. In that regard, while investigating tensile loading in bulk 3D cell cultures, exponential-like behavior and a characteristic time constant has been found within the same order (tens of seconds) as earlier measurements at the single cell-level [216,250]. However, the breadth of timescales over which the rheological behavior changed was noticeably greater than their simple model expected.

In comparison to centimeter-scale bulk 3D cultures, microtissues offer a high-throughput, highly organized alternative with a low diffusive barrier and better imaging capabilities [124]. In a previous publication we

developed a microtissue vacuum actuated stretcher (MVAS) that is capable of deforming an array of microtissues while simultaneously measuring dynamic mechanical properties [269]. In characterizing the dynamic mechanical response of microtissues to step length changes, we reported that both stress relaxation and recovery responses were captured by stretched exponentials [270] with a power law constant that is consistent with a so-called "trapping model" dominated by short-range Brownian forces [258,259]. This model may provide a theoretical understanding as to why viscoelastic effects during tensile loading of 3D cell cultures occurs over timescales that are wider than expected from a simple exponential and it may reflect a glassy disordered network of actin microfilaments [258,259] or simply the heterogeneity in the viscoelastic response from a collective cell population.

In this article, we continue that work by assessing whether microtissues display a Fourier equivalent of a stretched exponential behavior while under oscillatory loading. Our findings give insights into the mechanical behavior of the cytoskeleton while within a physiologically relevant 3D environment. Thereby studying the mechanical behavior of microtissues may establish an important link between our knowledge of mechano-sensing pathways and how forces govern cell behavior in the body under both healthy and diseased states.

5.3 Methods

MVAS-Force fabrication

Devices were fabricated as previously described [196,269]. Briefly, the MVAS-force consists of six rows of ten wells (60 in total) each containing a 500μm in-length 3D cell culture suspended between two cantilevers (fig. 5.1a). Each row is bordered on one side by an independent vacuum chamber connected to an external electronic regulator (SMC ITV0010) controlled through Labview software. When a vacuum is applied, the cantilever closest to the vacuum chamber is actuated to stretch the microtissue, while forces can be measured through tracking the visible deflection in the opposing cantilever and its known spring constant, $k_{cantilever}$=0.834N/m.

The MVAS-force, itself, consists of three polydimethylsiloxane (PDMS) layers replicated from molds created by standard photolithographic techniques, which are then plasma bonded together. The top layer contains the open-top microtissue wells and enclosed vacuum chambers. The middle membrane has the cantilevers and is fluorescently dyed with Rhodamine B (RhoB) to aid in tracking. The bottom layer contains vacuum chambers with identical dimensions as the top layer and empty bottom chambers that equalize the pressure on either side of the middle membrane to minimize out-of-plane motion.

Cell culture and microtissue fabrication

NIH3T3 (ATCC) cells were cultured in Dulbecco's Modified Eagle's Medium (DMEM) with 10% fetal bovine serum (FBS), 100mg/ml streptomycin and 100U/ml penicillin antibiotics (all from Hyclone Laboratories Inc.), and maintained at 37°C with 5% CO_2 on 100mm tissue culture dishes (Fisher) until 80-90% confluent.

3T3-fibroblast microtissues were cultured as described previously[120,124]. Briefly, after sterilizing an MVAS-force device with 70% ethanol, it was treated with 0.2% Pluronic F-127 (P6866, Invitrogen) for two minutes to

reduce cell adhesion. 250,000 cells were resuspended and pipetted into the device in a solution containing final concentrations of 1.5mg/ml rat tail collagen type I (354249, Corning), 1x DMEM (SH30003.02, Hyclone), 44 mM $NaHCO_3$, 15 mM d-ribose (R9629, Sigma Aldrich), 1% FBS and 1 M NaOH to achieve a final pH of 7.0-7.4. The device was then centrifuged to load ~650 cells into each well. The excess collagen was aspirated and the device was incubated at 37^{o}C for 15min to initiate collagen polymerization. ~130 cells were then centrifuged into each well and allowed to adhere to the top of the tissues. Excess cells were washed off. Cell culture media was added and changed every 24 hours.

Imaging

All images were acquired on a TiE A1-R laser scanning confocal microscope (LSCM) (Nikon) with standard configurations using appropriate laser lines and filter blocks. To assess morphology, microtissues were fixed *in situ* with paraformaldehyde for ten minutes and permeabilized with Triton-X for three minutes. Actin microfilaments were stained with Alexa Fluor 546 Phalloidin (Fisher, A22283). Microtubules were labeled with α-tubulin primary antibody produced in mouse (Sigma, T6074) and a rabbit anti-mouse IgG secondary antibody conjugated to Alexa Fluor 488 (Invitrogen, A11059). Cell nuclei were stained with DAPI (Fisher, D1306).

Force measurements

After four days of static culture, dynamic mechanical properties of microtissues were measured at frequencies logarithmically ranging from 0.00125 to 5Hz by tracking the visible deflection of the force-sensing cantilever. The acquisition rate was adjusted to be a minimum of three times greater than the Nyquist frequency and so that the total acquisition period was an integer multiple of the oscillation period. At a minimum three loading loops were observed to give reasonable data set sizes (≥240 points/ measurement). Prior to measurements, microtissues were preconditioned until subsequent loading loops were superimposable. All measurements were completed at 37^{o}C and under 5% CO_2.

To track the cantilever deflection, focal plans at both the tops and bottoms of the cantilevers were captured. The bottom positions were measured by performing a centroid algorithm on thresholded fluorescent images of the Rho-B dyed cantilevers. The top positions were measured on brightfield images using Labview's pattern matching algorithm with adaptive template learning. The deflection in the force-sensing cantilever was calculated by subtracting the top and bottom positions after accounting for the phase shift caused by the camera delay between the two images. Lastly, the deflection was converted into a force measurement using the cantilever spring constant.

Microtissue strain, ε, was calculated as the percent change in the length between the innermost edges of the tops of the cantilevers (equation 5.1).

$$\varepsilon(t) = \frac{length(t) - length_o}{length_o} \times 100 \tag{5.1}$$

The phase lag, δ, between force and strain was calculated as the difference in the phase angles, Φ, at the oscillatory frequency (f_o) (equation 5.2). δ is a measurement of loop hysteresis, indicating how much energy is lost for a given amount stored. In purely elastic samples tan(δ)=0 and in purely viscous samples tan(δ)=inf.

$$\delta = \{\phi_{force} - \phi_{strain}\}_{f_o} \tag{5.2}$$

The storage, k', and loss, k", microtissue stiffnesses were calculated as the ratio of the magnitudes of the Fourier transforms of force and strain at the oscillatory frequency multiplied by either the cosine or sine of the phase lag between force and strain, respectively (equations 5.3 and 5.4). k' and k" describe the amount of energy that is elastically stored and dissipated for a given deformation, respectively.

$$k' = \left\{\frac{|FFT[force(t)]|}{|FFT[\varepsilon(t)]|}\right\}_{f_o} cos\ \delta \tag{5.3}$$

$$k'' = \left\{\frac{|FFT[force(t)]|}{|FFT[\varepsilon(t)]|}\right\}_{f_o} sin\ \delta \tag{5.4}$$

The tension offset or prestress, T_o, was calculated as the amplitude of the Fourier transform of the microtissue force at 0Hz minus the amplitude of the Fourier transform at the oscillatory frequency (equation 5.5). A noise floor characterization of our method is in Appendix D.1.

$$T_o = \{|FFT[force(t)]|\}_{0Hz} - \{|FFT[force(t)]|\}_{f_o} \tag{5.5}$$

To assess how stretch alters the frequency response of microtissue mechanics, measurements were first taken at 2% and then at 11% strain. To assess the role of individual cytoskeletal proteins, measurements were taken following a 20 minute incubation with either 0.5% dimethyl sulfoxide (DMSO), a loading control, 10μM nocodazole (Noco), a microtubule polymerization inhibitor, 5μM blebbistatin (Bleb), a non-myosin-II inhibitor, or 10 μM cytochalasin D (CytoD), an actin polymerization inhibitor. As mechanical properties can vary between microtissues, each microtissue was normalized to its own pre-treatment value where indicated. To prevent crossover in responses from multiple drugs, only a single treatment was administrated to a microtissue.

Data analysis and statistics

All numerical data are presented as mean ± standard error. Statistical tests as described in the results were performed using Originlab 8.5 (Northampton, MA), with $P<0.05$ considered statistically significant.

5.4 Results

Microtissues display a characteristic time-scale

We cultured microtissues consisting of 3T3 fibroblasts in a 3D collagen matrix in our MVAS-force device (fig. 5.1a). After four days of static culture, microtissues had highly compacted and developed appreciable resting tension indicated by inward deflections of the force sensing cantilevers.

As commonly seen in viscoelastic materials, microtissue strain lagged the change in tension (fig. 5.1b). This phase lag produced characteristic clockwise loading loops with considerable hysteresis, indicating energy dissipation. Loading loops of a representative microtissue at 0.02 and 5Hz are in figure 5.1c. Increasing the

oscillation rate increased the measured stiffness, given by the slope of the loading loop, and decreased loop hysteresis. Under relatively small sinusoidal oscillations, loading loops were largely linearly across the tested frequency window.

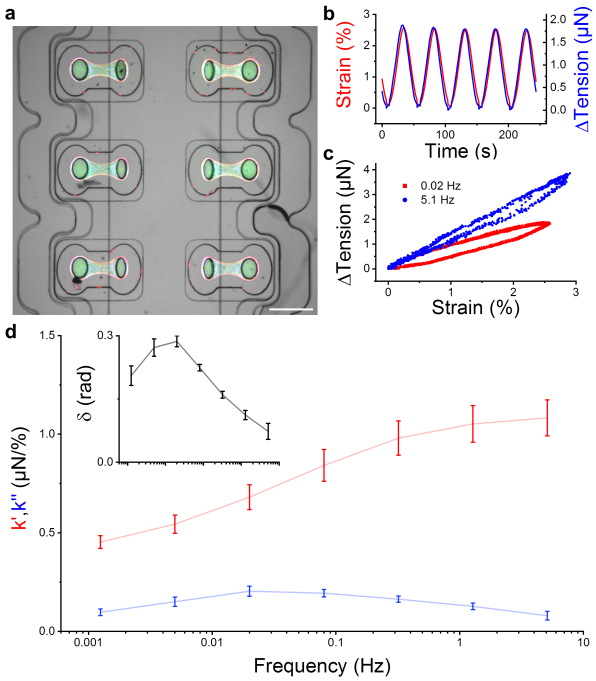

Fig. 5.1: Microtissue cell cultures have a characteristic time-scale. Microtissues consisting of 3T3-fibroblasts and a collagen I matrix were grown in our MVAS-force device. The MVAS-force consists of an array of 60 culture wells (six are shown) bordered on one side by a vacuum chamber (a). After four days of static culture, microtissues had densely compacted around the cantilevers and developed appreciable resting tension. Applying a vacuum to the device moves the cantilevers closest to the vacuum chamber outward to stretch the microtissues while changes in tension can be measured through tracking the passive deflection in the opposing cantilever. To examine the dynamic mechanical behavior at specific timescales, a frequency sweep of sinusoidal vacuum functions with identical strain amplitude was applied. As microtissues are viscoelastic, energy was dissipated each loading loop and consequently strain lags stress (b). Representative clockwise-running loading loops at 0.02Hz and 5Hz are shown in (c). The average (N=15) mechanical behavior under a strain amplitude of 2.4 ± 0.2 % is in (d). Microtissue elasticity (k') increased with frequency while energy dissipation (k") and the phase lag (δ) (insert) between stress and strain peaked at a characteristic timescale. The scale bar in (a) represents 500μm.

To further characterize the mechanical properties of viscoelastic materials, it is common to describe their behavior in terms the amount of energy elastically stored for a given deformation (k', the storage stiffness) and the amount of energy dissipated (k", the loss stiffness). The phase lag corresponds to the ratio of these measurements, and thereby gives a measurement of loop hysteresis. Microtissue k' increased with oscillation frequency, while k" and δ peaked somewhere between 0.02 and 0.08Hz where energy dissipation reached a maximum. Importantly these findings indicate that unlike cells cultured on 2D substrates probed with shear and compressive loads [65,68,99],

there is a characteristic timescale that describes microtissue mechanics. For standard linear viscoelastic fluids, this maximum coincides with the frequency at which k' and k" cross. However, we have shown in our previous report that in additional to their viscoelastic behavior, microtissues also possess the ability to residually store energy [270]. Therefore microtissues are consistent with viscoelastic solids, and their storage stiffness is shifted vertically by this stiffness term (k_2), and k' and k" do not cross.

The dynamic behavior of microtissues follows a stretched exponential

In previous work, we reported that stress relaxation and recovery in microtissues followed a stretched exponential (equation 5.6) [270]. This model has the same elements as a SLS viscoelastic model except the dashpot is described by both a time constant, τ, and as well, a power law constant, β (fig. 5.2a). Thereby stress relaxes and recovers with a characteristic timescale that increases with a power law with the elapsed time, leading to slower dynamics as time passes.

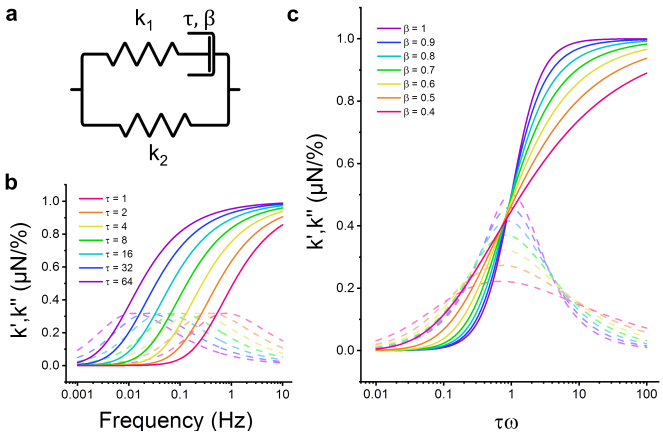

Fig. 5.2: Fourier transforms of a stretched exponential for select time and power law constants. In previous work, we found that the stress relaxation response of microtissues could be accurately captured by a stretched exponential. This function is similar to a standard linear solid viscoelasticity model except the dashpot is described by a time constant (τ) that grows with a power law with elapsed time (a). The effects of changing the time constant and power law exponent (β) on the frequency domain representation of this model are shown in (b) and (c), respectively. The solid lines represent the storage stiffness and the dotted lines give the loss stiffness. Lengthening the time constant shifts the response towards the left (b). Decreasing the power law exponent flattens out the responses over a wider range of frequencies (ω) and shifts the crossing frequency to a longer timescale (to the left) than the characteristic time constant (c). For simplicity, k_2 the residual elasticity, was kept at zero; values greater than zero, would simply translate the storage stiffness vertically by a fixed amount.

In linear systems, the time domain response is associated with expressions for k' and k" through the Fourier transformation. Unfortunately for a stretched exponential, there are no simple expressions for k' and k" in the frequency domain. Instead they can be approximated by numeric integration with any rational value for β and τ by solving the system of equations 5.6-5.8. We performed this integration in Matlab and results for various

values of τ and β are in figures 5.2b and c, respectively. For simplicity and to highlight the changes to the curves, k_2 was kept at zero for these simulations.

$$k(t) = k_1 e^{[-(\frac{t}{\tau})^{\beta}]} + k_2 \quad (5.6)$$

$$k'(\omega) = \omega \int_0^{\infty} k(t) \sin(\omega t)\, dt \; + k_2 \quad (5.7)$$

$$k"(\omega) = \omega \int_0^{\infty} k(t) \cos(\omega t)\, dt \; + k_2 \quad (5.8)$$

With longer values of τ, the expressions for k' and k" are shifted leftward (fig. 5.2b). In comparison decreasing β broadens the response over a wider range of frequencies and shifts the crossing frequency to a longer timescale than the characteristic time constant (Fig. 5.2c). When β=1 the model reverts back to a standard linear solid; the changes in the frequency response are more abrupt (they span only a few decades of time) and the crossing frequency corresponds to the characteristic time constant.

The oscillatory behavior of microtissues is compared to a stretched exponential in figure 5.3. When fitting the model, we assumed that k_1 and k_2 were linearly related as we had observed in stress relaxation experiments [270]. Under oscillatory stretching, τ differed from previously reported stress relaxation and recovery time constants (Appendix D.2) [270]. Instead, τ agreed well with the difference between these rates. In this way, the oscillatory response reflected an equilibrium state as in a biochemical rate equation described by forward and reverse reactions. Lastly, β was kept as 0.6 as in our previously reported stress relaxation and recovery experiments [270] and is predicted by a 3D trapping model [258,259]. Thereby the average frequency response was fit only through modifying k_1 to account for differences in the stiffness of the microtissues. The fitting constants are summarized in table 5.1.

Table 5.1: The fitting constants to the frequency response of microtissues under small strain amplitudes.

k_1 (μN/%)	k_2 (μN/%)	τ (s)	β
0.60	0.50	22	0.6

The model captured k' over the tested frequency range (MSE=0.0004) (fig. 5.3a). The mean behaviors for k" (MSE=0.003) and δ (MSE=0.006) could also be approximated by our model (fig. 5.3a and b). In that responses shared a characteristic maximum at 0.04Hz, but admittedly appeared more broadly distributed than our model predicts. Although decreasing β may aid in the fits for k" and δ, doing so would worsen the fit for k'. Instead this difference from the model is likely from an effect of averaging multiple responses with slightly different time constants.

The Cole-Cole plot of k' vs. k" followed the symmetric semi-circle that is predicted by the model but was shifted upwards (fig. 5.3c). This suggests that there may be additional sources of energy dissipation during oscillatory loading that were absent from step strain experiments. For example, k" values may have been

invariantly shifted by sliding friction, which has been reported in cells exposed to oscillatory shear in 2D culture [66,68].

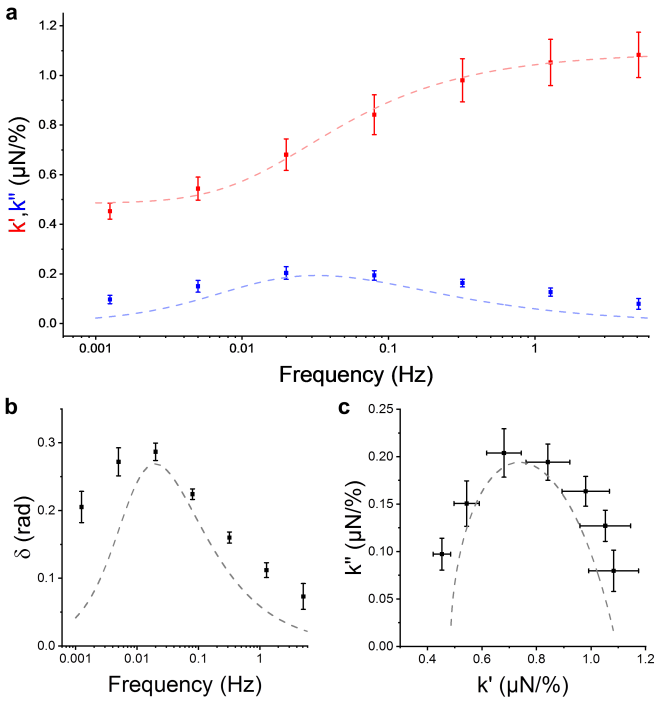

Fig. 5.3: The frequency response of microtissues shares the timescale dependencies of a stretched exponential model. The average (N=15) storage and loss stiffness and phases lag were fit to a stretched exponential in (a) and (b), respectively. The model described the average storage stiffness relatively well throughout the range of frequencies. The average phase lag and loss stiffness both peaked as the model predicted but appeared to change over a broader range of frequencies. Cole-Cole plots of the average microtissue response and the fitted model are in (c), and show that both follow a symmetrical semicircle.

Stretched exponential behavior is preserved across pharmacological treatments

The elastic and dissipative behavior of a cell is produced by a disordered tangle of structural cytoskeletal filaments, associated cross-linkers and motor proteins interacting with each other across a spectrum of length and time scales within a gelatinous cytosol. To differentiate the individual role of several key proteins to the overall viscoelastic behavior of microtissues, dynamic mechanical properties were measured following various pharmacological treatments designed to either disrupt the cytoskeleton or alter actomyosin activity. 0.5% DMSO was used as a loading control and produced no differences in the mechanical behavior from untreated microtissues (repeated measures, 1-way ANOVA $P>0.5$).

To begin, actin microfilaments are the preeminent structural components of the cytoskeleton and are relatively resistive to tensile loading but flexible under bending and compressive stress [35]. In microtissues, actin formed into densely polymerized stress fibers that primarily spanned in the direction between the cantilevers (fig. 5.4a-d). Consequently, actin depolymerization with CytoD decreased prestress, k', k'' and δ over the tested frequency range (Appendix D.3, fig. 5.4e,g,i, respectively). As these changes were quantitatively similar to

responses following decellularization with triton-X (one-way ANOVA, P>0.05), actin is the main cellular contributor to elasticity and dissipation in microtissues.

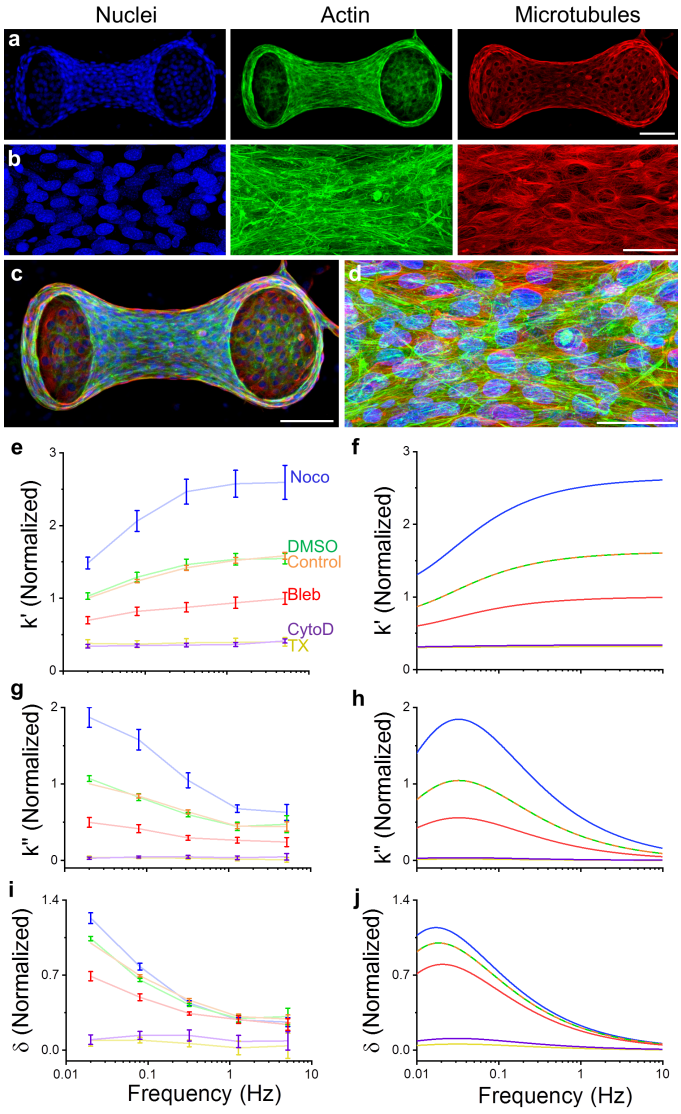

Fig. 5.4: The time-scale behavior of microtissue cultures is produced by multiple components of the cytoskeleton. Fluorescent images showing cell nuclei (blue), actin microfilaments (green) and microtubules (red) throughout whole microtissues and centrally magnified regions are in (a-d). Nuclei and a densely polymerized actin cytoskeleton are mostly oriented with the direction of tension development. Microtubules, on the other hand, do not show a preferred direction, radiating outward from microtubule-organizing centers. The frequency response after microtubule depolymerization (Noco; N=13), DMSO (a loading control; N=10), no treatment (N=39), non-muscle myosin-II inhibition (Bleb; N=17), actin depolymerization (CytoD; N=11) and decellularization (TX; N=9) are shown in (e), (g) and (i). Stretched exponentials fits to each response are shown in (f), (h), and (j). The scale bars in (a) and (c) represent 100μm, and in (b) and (d) represent 50μm.

The decellularized response of 3D cultures has been previously interpreted as the 'passive' contribution made by the extracellular matrix, and typically subtracted from the total response to calculate the 'active' contribution of the cells [128,216]. This interpretation would indicate that the matrix is relatively soft (k' is small) and it is largely elastic-like (δ is small). We, however, choose only to use this interpretation qualitatively, because cells inherently exert forces to bundle extracellular filaments and compact the matrix, which effectively increases its stiffness and in turn its share of the load bearing capacity. The use of this overly simplistic interpretation underestimates the contribution of the matrix and overestimates the contribution of the cells.

Table 5.2: The fitting constants to the frequency response following pharmacological disruption of the cytoskeleton or myosin inhibition.

	k_1 (Norm.)	k_2 (Norm.)	τ (s)	β
Noco	1.06	0.73	22	0.6
Control/DMSO	0.60	0.50	22	0.6
Bleb	0.32	0.36	22	0.6
CytoD	0.02	0.21	22	0.6
TX	0.01	0.2	22	0.6

Additionally in a cell, actin microfilaments are crosslinked and actively pulled on by the cycling of myosin motors, which prestresses the cytoskeleton, and in part, determines the cell's stiffness. Accordingly, inhibiting myosin-II activity with blebbistatin in microtissues decreased prestress, k', k" and δ (Appendix D.3, fig. 5.4e,g,i, respectively) but to a smaller extent as actin depolymerization.

Lastly unlike actin filaments, microtubules are relatively stiff under compressive and bending loads [35]. In microtissues, they radiated from microtubule-organizing centers without a prefer direction (fig. 5.4a-d). Although still controversial, microtubules are believed to oppose the inward tension created from acto-myosin cross-bridge cycling as in tensegrity structures [47,225]. In keeping with this hypothesis, microtubule depolymerization with nocodazole increased prestress, k', k" and δ (Appendix D.3, fig. 5.4e,g,i, respectively) over the tested frequency range.

Our stretched exponential model, using the same fitting method that was explained in the previous section, could approximate these behaviors (fig. 5.4f,h,j). The fitting constants for each treatment are summarized in table 5.2. During fitting, for simplicity, τ was assumed to be invariant with the treatment, β was kept at 0.6 based upon our previously reported step strain data [270] and a theoretical justification [259], and the same linear

relationship between k_1 and k_2 was used as mentioned above. This meant that the differences in the responses could largely be explained through only varying a single spring constant. Moreover, this demonstrates that a simple stretched exponential model can provide a robust understanding of microtissue mechanics across pharmacological treatments targeting a wide assortment of cytoskeletal targets.

Microtissue oscillatory mechanics are influenced by strain

Within a cell, the protein interactions that determine its mechanical properties, such as actin polymerization and actomyosin cross bridge cycling, are thought to be influenced by dynamic stretching [7,8,92,155,210]. Moreover, as cells are stretched to larger amplitudes, relatively soft structural rearrangements of cytoskeletal filaments are forgoed for stiffer protein unfolding events [96,234]. These effects lead to commonly observed nonlinearities in the elastic and dissipative behavior of cells [76]. When considering tissues, nonlinearities may also arises from cell rotation in the matrix [196] and percolation of local effects across the tissue's length [236].

In regards to these effects, in our previous article, we reported that stress relaxation had a non-linear rate constant that decreased with what roughly appeared to be a power law with strain [270]. We have also reported that oscillatory stretch can decrease the stiffness of microtissues through actin depolymerization [270]. For these reasons, we assessed here how the frequency response of microtissues changes when under different amplitudes of stretch.

Across the tested frequency range (0.02 to 5Hz), microtissues softened and became more solid-like when subjected to larger strain amplitudes (fig. 5.5a-c). The amount of softening was rate dependent, increasing with the logarithm of the loading rate (fig. 5.5d).

Table 5.3: The fitting constants to the frequency response under small and large amplitude strains.

Strain (%)	Δk_1 (μN/%)	Δk_2 (μN/%)	**τ** (s)	**β**
2.13 ± 0.08	0.60	0.50	22	0.6
11.0 ± 0.5	0.31	0.30	30	0.6

The responses were fit with stretched exponentials using constants summarized in table 5.3. In agreement with the nonlinear decrease in relaxation time that we had previously observed with step size [270] and our presumption that the oscillatory response reflects an equilibrium between cytoskeletal disassembly and reassembly rates, τ increased with the strain amplitude under oscillatory loading. β was kept as 0.6 for the same reasons as discussed before.

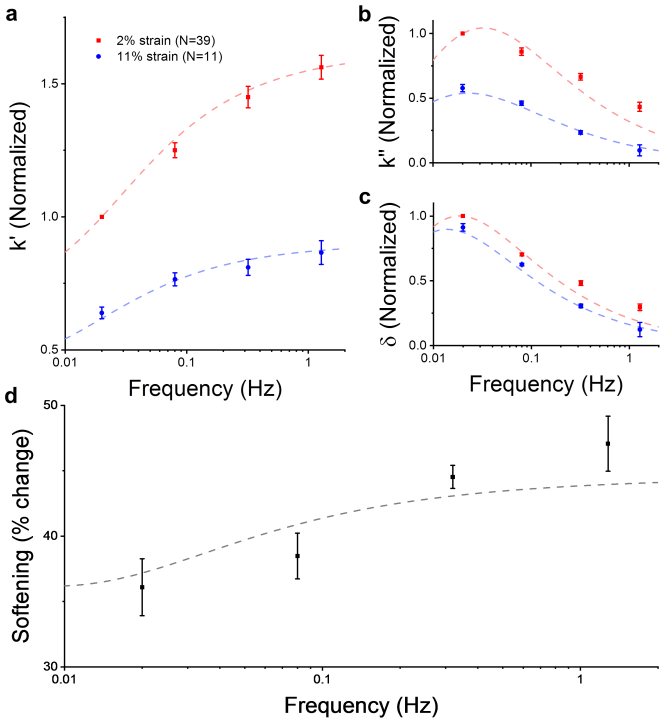

Fig. 5.5: The dynamic mechanical behavior of microtissues is strain-dependent. The frequency response of microtissue storage stiffness, loss stiffness and phase lag measured at 2% (N=39) and 11% (N=11) strain are plotted in (a-c), respectively. The dotted lines are stretched exponential fits. A stretched exponential captured the mechanical behavior of microtissues well at different strain amplitudes despite nonlinear elastic and viscoelastic behaviors. The model may also approximate the time-dependent softening (% decrease in k') response of microtissues (d).

As for the spring constants, the linear expression linking k_1 and k_2 that had been used until now, underestimated the dissipation at long timescales under large strain amplitudes (data not shown). As the only way to fit the data was through altering this relationship, perhaps the amplitude of oscillatory stretching affects how these spring constants are coupled. It is also possible that our interpretation of these results under large strain amplitudes has been skewed by the presence of nonlinear loading loops and our use of a linear method to approximate k' and k". Then again the total harmonic distortion of our measurements remained small, so presumably these effects were minor.

5.5 Discussion

In this article, we found that under oscillatory loading the dynamic rheological behavior of cells within 3D microtissues was consistent with a stretched exponential. In that regard, microtissues possessed a characteristic timescale where dissipation reached a local maximum as in a standard linear solid (SLS) model, but the changes to k' and k" were more broadly distributed in time than could be explained by a simple exponential function. Importantly these results tended to agree with our previous report on the stress relaxation and recovery responses

in microtissues following step length changes; both could be described by a stretched exponential with similar β, k' and k" constants.

As for the time constant during oscillatory loading, it did not match our previous reported value from a stress relaxation experiment as traditionally assumed but rather interestingly it followed the difference between the time constants for stress relaxation and recovery as in a biochemical equilibrium rate equation. This may suggest that, after preconditioning, the oscillatory behavior of microtissues is at a dynamic equilibrium state determined from both a cytoskeletal disassembly rate given by the relaxation time constant and a reassembly rate given by the recovery time constant. In regards to what part of the cytoskeleton is specifically remodeling, there exists a strong precedent in the literature that mechanical stretching causes depolymerization of actin filaments [78–80,92]. Similarly we have previously reported that microtissues strain soften through actin depolymerization [270]. Here we linked this mechanically induced softening effect in actin microfilaments to the rheological behavior of microtissues, demonstrating that this mechanotransduction mechanism is time-scale dependent. More to the point, stress relaxation and recovery [270], and the characteristic frequency behavior presented here all required an intact network of actin microfilaments. This is not to say that other cytoskeletal elements are not be involved in determining the viscoelasticity of cells. Clearly from our results, the elastic and dissipative behavior of cells and tissues are also regulated to a degree by the presence of microtubules and myosin motor activity.

Our observation that microtissues display a characteristic timescale is shared in earlier reports that investigated cells under tensile loads with deformations at relatively large length-scales. In that regard, single cells studied through either micropipette aspiration or microplates, were originally modeled as standard linear solids with simple exponential relaxation functions [73,94,249]. Tensile loading in bulk 3D cell cultures has also been previously modeled as a SLS with a characteristic time constant within the same order (tens of seconds) [216,250].

Contrary to our observations of a stretched exponential and these earlier reports, local shear and compression measurements of cells grown on 2D substrates have been largely characterized with weak power laws [65,66,68,99,267]. Apart from the featureless observation of structural damping that has given traction to a theoretical soft glassy rheological model of cell behavior[66,68], a power law may also reflect a generalized form of a distribution of exponential relaxation processes with a wide range of time constants [76].

Admittedly, like a power law, adding additional Maxwell elements to a SLS model could also fit our data. However a stretched exponential is more economical in terms of the number of fitting constants. In this way, a stretched exponential may be interpreted as a generalized form of a superposition of discrete exponential processes with a specific distribution of time constants that is described by β [231].

On the other hand, a stretched exponential in itself may indicate a deeper theoretical understanding of the mechanical behavior of cells. In that regard, in physics stretched exponential relaxation processes are described by so-called 'trapping models'. During relaxation in these models, randomly distributed traps capture molecules diffusing through Brownian motion, but, as the traps fill, the remaining molecules must travel longer to find unoccupied traps. Thereby, the exponential relaxation rate falls with a power law determined by the

dimensionality of the model. For a 3D model, the theoretical value for β (0.6) [259] is surprisingly close to what we have found in microtissues. Interestingly this relaxation behavior is commonly seen in glasses near their transition temperature that are dominated by short-range Brownian motion [258,259]. Therefore, our findings may still reflect a glass-like behavior seen in a network of actin filaments [81,106], even though this frequency behavior is quite different from the featureless rheological response of soft glasses [107].

Perhaps it should not be a surprise that probing an inhomogeneous network of actin, microtubules and cross-linkers transfers loads differently in shear and compression vs. tension, and when probed locally vs. globally. As our results in microtissues share comparable behavior with earlier reports that also probed cells in tension at their length-scale, this would suggest that the cytoskeleton could exhibit a characteristic timescale while being probed in this manner. More recently, however, cells probed in tension with a modified microplate setup have been shown to follow power law rheological models similar to local shear and compression measurements [74]. To the best of our knowledge, this behavior has only been reported by one research group in a single cell type during tensile loading thus far.

Alternatively the conflicting descriptions of the rheological behavior of cells and microtissues may instead lie in the dimensionality of the cell's environment. Culturing cells on a 2D substrate, which is necessary to study their behavior with OMTC and AFM, fundamentally changes the structure and distribution of their cytoskeleton when compared to cells cultured in more physiologically relevant 3D environments. In that regard, in 2D culture cell adhesions and in turn a large portion of the cytoskeleton is unnaturally polarized to the basal surface of the cell [31]. However, it is unclear how this explanation would extend to early reports from microplates and micropipette aspiration.

These plausible explanations as to why the viscoelastic behavior of microtissues may differ from power law rheology may lend to significant avenues for future investigations. Nevertheless, our present observations have revealed two underlying relationships to describe microtissue mechanics with timescale behaviors predicted by a stretched exponential. First, elastic and dissipative properties are linearly coupled, and second, prestress and elasticity are linearly related. These trends appear to exist at any given timescale but may be modified by nonlinear elastic and viscoelastic effects when the strain amplitude is large. The implications that these governing behaviors have upon our understanding of cell mechanics are examined in the remainder of this discussion.

Microtissue elastic and dissipative properties are coupled

In assessing responses to a range of pharmacologically induced modifications to the cytoskeleton, we found that changes to elastic and dissipative properties were linearly coupled (fig. 5.6a). At a given timescale, an increase (or decrease) in the amount of energy a microtissue could elastically store always coincided with a linear increase (or decrease) in the amount of energy that was lost. This coupling between elasticity and dissipation has been previously observed at both the cell [66,68] and tissue-levels [260,261]. In addition with regards to power law rheology, it has been shown that any change in dissipation and elasticity in response to a wide selection of

pharmacological treatments across several cell types can be captured solely by a change in the power-law exponent [66].

Similarly a stretched exponential model can approximate this behavior (dotted lines) when the spring constants are linearly tied to one another (ie. $k_2=m*k_1+b$) as we had shown in our previous report [270]. However, in contrast to step length changes, non-linear effects arising under dynamic oscillations may alter this relationship (fig. 5.5). Furthermore at high frequencies the data appears to deviate from the model, but remains linearly coupled, indicating that there exists additional means of dissipation during oscillatory loading, such as sliding friction. Although the precise molecular origin(s) of stress dissipation in a cell remains unknown, such strong coupling suggests that elasticity and dissipation are from the same molecular origin(s) [260,261]. Also perhaps, owning to the wide assortment of pharmacological treatments, cells and tissues seem to achieve their elasticity and dissipation not at the single protein level but through how these proteins interact with each other [106].

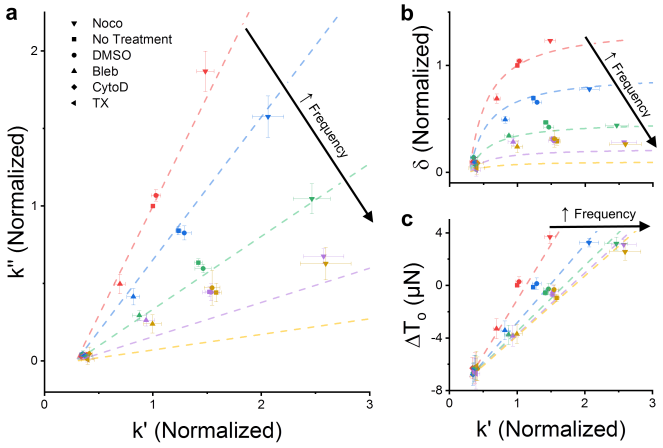

Fig. 5.6: Microtissues possess underlying relationships in their dynamic mechanical behavior throughout a range of pharmacological treatments. The linear mechanical behavior of microtissues collapses onto relationships predicted by our stretched exponential model. First, at a given timescale, the energy that was elastically stored in a microtissue was linearly coupled to the amount of energy that was dissipated, and the strength (ie. slope) of this relationship peaked at the characteristic frequency (a). Secondly, at a given timescale, the phase lag was nonlinearly related to the storage stiffness (b). Importantly these relationships are only produced when k_1 and k_2 remain linearly coupled. Nonlinear effects from varying strain amplitudes were not well predicted. Lastly, the tissue prestress was linearly related to the storage stiffness, but in contrast to tensegrity structures, this relationship was timescale variant (c). Each shape plotted here represents a different pharmacological treatment and each color is a different timescale ranging from 0.02 to 5Hz.

In addition to the coupling of elastic and dissipative stresses, we also found that the ratio of these stresses (the phase lag) varied with microtissue stiffness in a nonlinear, but predictable, manner (fig. 5.6b). As the elasticity of the tissue increased, there was a nonlinear relatively greater increase in the amount of energy lost for a given amount stored (or decreased stiffness, decreases energy lost for given amount stored). In other words, microtissues are more viscous fluid-like when they are stiffened and more elastic solid-like when made softer. This

finding challenges soft glassy rheology, which has been supported by local shear measurements that have shown increased stiffness accompanies a more elastic-like behavior (or decreased stiffness is more viscous fluid-like) [66,68,92,267]. Our results do, however, agree with observations made on *ex vivo* tissue strips. In that the delivery of a broad spectrum of contractile agonists to tissue strips has been shown to increase stiffness and the phase lag [261,271].

Microtissue prestress and stiffness are related

In an adherent cell there exists a balance of forces between inward pulling motor proteins acting on actin filaments, and opposing forces primarily generated by the elasticity of the extracellular matrix [87–89]. This balance of forces leads to tension or pre-stress in the cytoskeleton, and in turn, determines the cell's stiffness [87]. In keeping, we found that at any given timescale microtissue prestress and tension were linearly related (fig. 5.6c). For example, unsurprisingly actin depolymerization or myosin inhibition decreased both prestress and stiffness. This behavior could be predicted at different timescales (dotted lines) using a stretched exponential model to determined the expected elasticity while assuming that the prestress was timescale invariant (Appendix D.3).

The coupling between prestress and stiffness has been previously observed in individual cells [87] and is a critical aspect to the hypothesis that cells behave as tensegrity structures [225,248]. In this hypothesis, microtubules act as compressive struts to partially oppose tensile forces from actomyosin machinery [46,47,225,272]. Although the contribution of microtubules to the mechanical behavior of cells is controversial [45], several investigators have shown depolymerization of microtubules increases traction forces and stiffness of cells in 2D culture [46,47] and microtubules have visually been seen to buckled while cells deform [225]. Tensile force from fibroblasts in 3D cell cultures has also been shown to decrease >50% upon microtubule stabilization [272]. Consistent with those results, we found that microtubule depolymerization increased prestress and stiffness. With this said, tensegrity structures do not possess the timescale behavior of cells and tissues [45], and thus the tensegrity hypothesis does not correctly predict that the relationship between prestress and stiffness would change based on the oscillation rate.

5.6 Conclusions

In keeping with responses to step length changes, the dynamic mechanical behavior of microtissues under oscillatory loading displays characteristic features of a stretched exponential. In that regard, unlike previous reports measuring shear and compressive loads on cells in 2D culture, our observations suggest that there exists characteristic timescales for both cytoskeletal assembly and disassembly, and these exponential rates fall with a power law with elapsed time. Consequently in the corresponding response under oscillatory loading, the behavior reaches a dynamic equilibrium set by the difference in those time constants.

Pharmacological responses indicated, as expected, that this viscoelastic behavior arises predominately from remodeling in the actin cytoskeleton and is also influenced by both microtubules and myosin motors. Perhaps more interestingly, in spite of the large structural and mechanical changes to the cytoskeletal, two governing

relationships describing microtissue mechanics existed: at any given timescale 1) microtissue elasticity and dissipation are coupled, and 2) microtissue prestress and stiffness are linearly related.

To conclude, understanding the viscoelasticity of microtissues may reveal how cells determine the elastic and dissipative behavior of tissues in the body. Characterizing the timescale dependencies of these mechanical properties is essential to fully understanding the pathways through how forces are sensed by cells, and lead to critical behavioral changes in normal development and disease.

CHAPTER 6| MECHANICAL STRETCH SUSTAINS MYOFIBROBLAST PHENOTYPE AND FUNCTION IN MICROTISSUES THROUGH LATENT TGF-B1 ACTIVATION

Authors: **Matthew Walker**, Michel Godin, Andrew E. Pelling

The manuscript was submitted to Integrative Biology in January 2020 (under review) and is accessible on the preprint server BioRXIV (doi: https://doi.org/10.1101/2020.01.25.917179). The supplementary information is contained in Appendix E.

Motivation & Objectives| Dysregulation of myofibroblast activation leads to fibrotic disease. Static mechanical forces, such as matrix stiffness and tension, have previously been implicated as stimuli that promote myofibroblast differentiation from fibroblast precursor cells. This chapter investigates the role of dynamic stretch on myofibroblast activation and deactivation in microtissue cultures. Specifically we assess whether cyclic loading may activate latent TGF-β to maintain a myofibroblastic phenotype and functionality.

6.1 Abstract

Fibrosis is a leading cause of death in developed countries that is characterized by a progressive deterioration of tissue mechanical behavior. Developing methods to study tissue mechanics and myofibroblast activation may lead to new targets for therapeutic treatments that are urgently needed. Microtissue arrays are a promising approach to conduct relatively high throughput research into fibrosis as they recapitulate key biomechanical aspects of the disease through a relevant 3D extracellular environment. In early work, our group developed a device called the MVAS-force to stretch microtissues while enabling simultaneous assessment of their dynamic mechanical behavior. Here we investigated TGF-β1 induced fibroblast to myofibroblast differentiation in microtissue cultures using our MVAS-force device through assessing α-SMA expression, contractility and stiffness. By doing so, we linked cell-level phenotypic changes to functional changes that characterize the clinical manifestation of fibrotic disease. As expected, TGF-β1 treatment promoted a myofibroblastic phenotype and microtissues became stiffer and possessed increased contractility. Furthermore, these changes were partially reversible upon TGF-β1 withdrawal. In contrast, however, long-term cyclic stretching maintained myofibroblast activation. Furthermore stretching had no effect compared static cultures when TGF-β1 receptors were inhibited and stretching promoted myofibroblast differentiation when given latent TGF-β1. Together these results suggest that external mechanical stretch may activate latent TGF-β1 and might be a powerful stimulus for continued myofibroblast activation to progress fibrosis. Further exploration of this pathway with our approach may yield new insights into myofibroblast activation and more effective therapeutic treatments for fibrosis.

6.2 Introduction

Myofibroblast activation is a normal healing response following tissue injury found throughout the body, and is essential for rapid wound contraction and *de novo* matrix deposition [174–178]. However, when unchecked, continued myofibroblast activation may lead to chronic fibrosis, and potentially, a life-threatening loss of tissue functionality [174,273,274]. As one of the leading causes of death in developed countries, fibrosis has become an area of high interest for lung, heart, vasculature, liver, renal, and eye research [177,179–182]. Yet the contributing factors that determine whether myofibroblast activation persists and fibrosis progresses into a chronic illness, or whether restoration occurs and tissues regain their initial functionality, remain unclear [177,182]. Identifying these factors is not only necessary to understand how the activation of myofibroblasts is controlled, but importantly, may also provide valuable insights for future therapeutic approaches to prevent the development and arrest the progression of fibrosis.

Transforming growth factor (TGF)-β1, a biochemical inflammatory mediator, has been identified as a key determinant in the development and progression of tissue fibrosis, and as such, has become a central focus of research [110,275]. In that regard, TGF-β1 treatment is routinely used to induce fibroblast to myofibroblast differentiation *in vitro* in lieu of any other biochemical stimuli [276,277], and overexpression of TGF-β1 in animal models consistently exhibit marked fibrotic changes [278,279]. It is well recognized that TGF-β1 is a potent agonist of the SMAD2/3 pathway [276], which in fibroblasts leads to α-smooth muscle actin (α-SMA) expression, a commonly used biomarker of myofibroblast differentiation [175,177,178]. In addition to canonical SMAD2/3 signaling, TGF-β1 may also activate mitogen-activated protein kinase (MAPK) pathways to further regulate differentiation, proliferation, cell survival and apoptosis [280].

In an autocrine feedforward loop to drive further myofibroblast activation, inactivated TGF-β1 is secreted by myofibroblasts as a large latent complex (LLC) consisting of the latent TGF-β1 binding protein (LTBP), which associates with the extracellular matrix (ECM), and the latency-associated peptide (LAP), which non-covalently sequesters a TGF-β1 polypeptide and binds to integrins on the cell's membrane [189–191]. Mechanical stretch, such as encountered in lung tissue from breathing or internally produced by myosin contraction, has been previously proposed as a mechanism to activate this latent source by directly inducing a conformational change in the LAP to release active TGF-β1 into the ECM [189,192–194]. In doing so, this mechanosensitive pathway may maintain myofibroblast activation to advance the tissue towards of chronic fibrosis.

Although fibrosis and therapeutic treatments have often been investigated *in vitro* to reduce complexity and increased control, the effectiveness of this approach is often hindered by the lack of a biochemically and mechanically relevant environment when using standard 2D cell culture techniques [123,281]. Instead microtissue arrays, in which cells self-assemble within a collagen ECM around vertical cantilevers into sub-millimeter 3D organized structures, offer an appealing high-throughput alternative [124,282]. In addition to a relevant ECM, the microtissue method also enables direct assessment of tissue-level functional changes through tracking the visible deflection of the cantilevers for contractility measurements. Because these abilities, this method has been shown

to be especially appropriate for testing the efficacy of fibrosis treatments, as the clinical manifestation of fibrosis is stiff, chronically contracted tissues with a remodeled ECM [282].

In previous work, we developed a microtissue vacuum actuated stretcher (MVAS-force) that was capable of stretching an array of microtissues and simultaneous measurements of dynamic stiffness and contractility [269]. Here we used our MVAS-force device to link changes in α-SMA expression during TGF-β1 treatment to mechanical changes that are characteristic of tissue fibrosis. We then assessed whether microtissue mechanics and the quiescent fibroblastic phenotype is restored following TGF-β1 withdrawal. Finally, we tested the hypothesis that stretch may maintain myofibroblast differentiation during TGF-β1 withdrawal through endogenously produced latent TGF-β1 activation. These findings contribute to the field's understanding of the progression of fibrosis through TGF- β1 induced fibroblast to myofibroblast differentiation. We also established that MVAS-force devices are capable of investigating fibrosis development, and as such, may be a useful tool for pharmacological discovery. Lastly our findings further implicate that mechanical forces are stimuli that direct tissues away from normal healing pathways and towards fibrotic development, which may have important implications in therapeutic treatment development.

6.3 Methods

Cell culture

Prior to microtissue fabrication, NIH3T3 (ATCC) fibroblast cells were maintained on 100mm tissue culture dishes (Fisher) at 37℃ with 5% CO_2 until 80-90% confluent in feeder media composed of Dulbecco's Modified Eagle's Medium (DMEM) supplemented with 10% fetal bovine serum (FBS), 100mg/ml streptomycin and 100U/ml penicillin antibiotics (all from Hyclone Laboratories Inc.).

Microtissue fabrication

MVAS-force devices consist of 6 rows of 10 wells, each containing a microtissue formed around a pair of vertical cantilevers. To stretch the microtissues, vacuum chambers border each row, and are connected to independent external regulators (SMC ITV0010) controlled through Labview. When a vacuum is applied, the cantilevers closest to the vacuum chamber are actuated, while tissue tension can be measured through the visible deflection in the opposing 'force-sensing' cantilevers.

MVAS-force devices were fabricated from mold replication steps described previously [196,269]. Briefly, SU-8 masters for the three layers of the device were created with standard photolithographic techniques. The top layer contains the cell culture wells and vacuum chambers, the middle layer is a thin membrane with the cantilevers, and the bottom layer includes vacuum and empty bottom chambers. To fabricate devices, masters were cast with polydimethylsiloxane (PDMS) containing a 1:10 cross linker ratio and plasma bonded together.

Microtissues were cultured in MVAS-force devices as described previously [124,196,269]. Prior to seeding, devices were sterilized with 70% ethanol and treated with 0.2% Pluronic F-127 (P6866, Invitrogen) for two minutes

to reduce cell adhesion. ~650 cells were centrifuged into each well in a solution containing 1.5mg/ml rat tail collagen type I (354249, Corning), 1x DMEM (SH30003.02, Hyclone), 44 mM $NaHCO_3$, 15 mM d-ribose (R9629, Sigma Aldrich), 1% FBS and 1 M NaOH to achieve a final pH of 7.0-7.4. Excess collagen was removed and devices were incubated at 37^{o}C for 15min to initiate collagen polymerization. Lastly, an additional ~130 cells were then centrifuged on top of each tissue. Feeder media was added and changed every 24 hours. Microtissues were allowed to compact and secure themselves to the cantilevers under static conditions with feeder media for 2 days prior to experimentation.

Myofibroblast differentiation

To assess myofibroblast differentiation, the cell culture media was switched to a differentiation formulation containing DMEM, 5% FBS, 100mg/ml streptomycin, 100U/ml penicillin antibiotics, and 5ng/ml TGF-β1 (Peprotech, 100-21). Functional assessment of differentiation was assessed every 24 hours over a 3-day period. Because there was no change to microtissues beyond day 2, differentiation for subsequent experiments was kept to 2 days. To block the differentiation and to assess the contribution of Rho-signaling, the differentiation media was supplemented with 1μM Y27632 (Y27) (Y0503, Sigma Aldrich), a rock inhibitor.

We next investigated whether myofibroblast differentiation was reversible, by switching microtissues back to feeder media for 2 days following 2 days of differentiation. Once it was demonstrated that microtissue differentiation was in part reversible, we tested the hypothesis that long-term oscillatory mechanical stretch may maintain myofibroblast differentiation by cyclically loading microtissues at 0.5Hz 5% strain during dedifferentiation. Further in regards to this hypothesis, to assess whether stretch activates endogenously produced TGF-β1, TGF-β1 receptors were blocked with 10μM GW788388 (GW) (16255-1, Cayman Chemicals) during dedifferentiation, and lastly, differentiation was assessed with a latent source of 5ng/ml TGF-β1 (299-LT-005, R&D Systems) under both static and stretching conditions.

Functional assessment of differentiation

To assess how microtissues are functionally altered during myofibroblast differentiation, microtissue mechanics were assessed *in situ* using the MVAS-force at 37^{o}C and under 5% CO_2 [269]. Briefly, forces were measured through the visible deflection of the force-sensing cantilever and its known spring constant. To calculate the deflection, images were captured at focal planes containing both the top and bottom of the cantilevers. The bottom position of the cantilevers was measured using a centroid algorithm while the top was tracked using pattern matching with adaptive template learning in Labview. Static deflections, T_o, were calculated by subtracting the top and bottom positions and gave an assessment of the resting contractility.

To assess stiffness changes, the dynamic mechanical behaviors were measured at 0.5Hz with 3% strain. Images at both the tops and bottoms of the cantilevers were captured at 15fps for a minute. Tissue tension was calculated from the difference in the positions of the force-sensing cantilever in those images after accounting for

the phase shift caused by the camera delay between capturing the two focal planes. Microtissue strain, ε, was defined as the percent change in length measured from the innermost edges of the tops of the cantilevers (equation 6.1). The storage stiffness, a measurement of elasticity, was then calculated as the ratio of the magnitudes of the Fourier transforms of tension and strain multiplied by the cosine of the phase lag between force and strain (equation 6.2).

$$\varepsilon(t) = \frac{length(t) - length_o}{length_o} \times 100 \quad (6.1)$$

$$k' = \left\{ \frac{|FFT[tension(t)]|}{|FFT[\varepsilon(t)]|} \right\}_{f_o} cos\ \delta \quad (6.2)$$

Phenotypic assessment of differentiation

α-SMA was used as biomarker [175,177,178] to assess myofibroblast differentiation, and imaged with standard immunofluorescence techniques. Briefly microtissues were fixed and permeabilized *in situ* with ice-cold methanol for 10min. To prevent non-specific binding, microtissues were blocked for 30min with 5% FBS. α-SMA was labeled with 1:100 primary antibody produced in rabbit (Abcam, ab5694) at room temperature for two hours and then 1:200 Goat anti-rabbit IgG secondary antibody conjugated to Alexa Fluor 488 (Invitrogen, A11034) at room temperature for an addition two hours. Cell nuclei were stained with DAPI (Fisher, D1306).

Image stacks of microtissues were acquired on a TiE A1-R laser scanning confocal microscope (LSCM) (Nikon) with appropriate laser lines and filter blocks. To produce heat maps, images were flattened by integration, spatially aligned and averaged together. α-SMA fluorescence was normalized to the nuclei fluorescence to give a per cell measurement and to account for differences in proliferation.

Data analysis and statistics

All numerical data are presented as mean ± standard error. Statistical tests, as described in the results, were performed using Originlab 8.5 (Northampton, MA) with $p<0.05$ considered statistically significant.

6.4 Results

Myofibroblast differentiation in microtissue cultures

Myofibroblast differentiation has historically been characterized through biochemical assays of biomarker expression (ie. α-SMA) [175,177,178] in cells grown in 2D culture. Although there are other biomarkers for fibrosis (ie. pro-collagen), and as such reporting a single biomarker is an inherent limitation of our work, α-SMA expression is the predominately indicator of myofibroblast differentiation used in the literature. Comparably there have been much fewer *in vitro* investigations that have linked the appearance of a myofibroblastic phenotype to functional changes in mechanical behavior (ie. increased stiffness and contractility) at the tissue-level which are characteristic of fibrosis [282,283]. For that reason, we assessed both changes to static contractility (fig. 6.1a) and dynamic stiffness (fig. 6.1b) of microtissues during myofibroblast differentiation using our MVAS-force device.

As expected, TGF-β1 treatment increased the resting tension and stiffness over a 3-day period compared to the control group (fig. 6.1d and e, respectively) (t-tests). Functional changes largely occurred over the first 2 days of treatment, with no significant difference to either contractility or stiffness between days 2 and 3 (repeated measures t-tests p>0.05). For this reason, 2 days was used as the time point for all subsequent experiments. After 2 days of TGF-β1 treatment, there was a 4.4 ± 0.4μN increase in contractility and a 93 ± 10 % increase in stiffness.

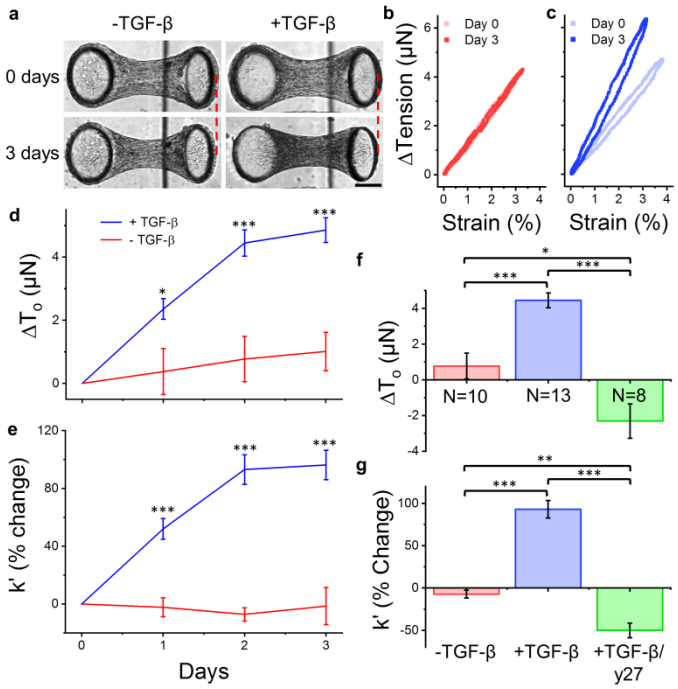

Fig. 6.1: TGF-β1 treatment contracts and stiffens microtissue cultures. At experimental day 0, once microtissues had compacted and were securely anchored to the cantilevers (2 days after seeding), they were either switched to a media containing TGF-β1 to promote myofibroblast differentiation or kept in normal feeder for an additional 3 days. TGF-β1 treatment increased the resting tension, T_o, compared to feeder media indicated by a greater deflection in the force-sensing cantilever (a). Additionally the dynamic stiffness of microtissues was measured *in situ* with the MVAS-force at 0.5Hz. Representative clockwise oriented tension-strain loops with normal feeder and differentiation media are in (b) and (c), respectively. While there was no difference in stiffness between experimental days 0 and 3 with feeder media, the stiffness markedly increased with TGF-β1 treatment. The average changes to the resting tension and stiffness over the 3-day period are in (d) and (e), respectively. The TGF-β1 induced increased tension and stiffness largely occurred over the first 2 days, leveling off by day 3. The effects of TGF-β1 treatment were completely blocked with concurrent treatment with y27, a ROCK inhibitor, indicating the role of Rho-induced stress fiber formation and myosin contraction during myofibroblast differentiation (f and g). The scale bar in (a) represents 100μm. *P<0.05, **P<0.01, ***P<0.001.

Inhibiting Rho-signaling with the ROCK inhibitor y27 blocked TGF-β1 induced functional changes (fig. 6.1f and g). In fact, concurrent treatment of TGF-β1 with y27 reduced microtissue contractility and stiffness below control microtissues maintained in feeder media (P<0.05 and <0.01, 1-way ANOVA). These results are not overly

surprising as Rho is known to direct the assembly and stabilization of the actin cytoskeleton [284] and control contractility through deactivation of myosin phosphatase and phosphorylation of myosin light chain [285]. Several studies have also shown the importance of Rho/ROCK signaling in controlling collagen synthesis [286–288], which would also contribute to increased microtissue stiffness.

To link functional changes in microtissues to a myofibroblast phenotype change, α-SMA was immunofluorescently imaged. Average heat maps of the distribution of cells and positive staining for α-SMA indicated that TGF-β1 treatment lead to myofibroblast differentiation predominately in cells directly associating with the relatively stiff PDMS cantilevers and around the perimeter of the tissue (fig. 6.2a). Moreover, the distribution of cells in the tissues became less uniform as TGF-β1 treatment increased the concentration of cells towards the center of the tissue. In contrast, however, there was no change to the total microtissue width on bright field images (data not shown, P>0.05, T-test). The spatial distributions were not greatly affected with concurrent treatment of TGF-β1 and y27 compared to TGF-β1 alone.

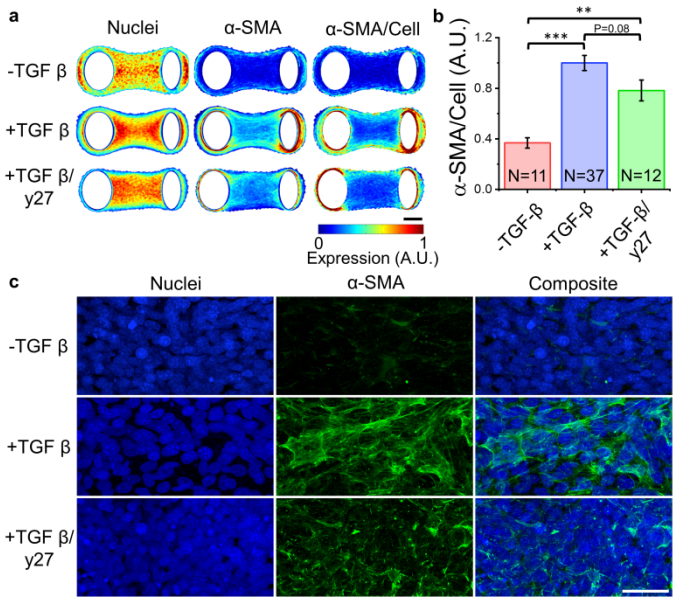

Fig. 6.2: TGF-β1 induces myofibroblast differentiation of microtissues. To quantify TGF-β1 induced myofibroblast differentiation, microtissues were stained for α-SMA. Average heat maps of cell nuclei, α-SMA and normalized fluorescence are in (a). Total α-SMA staining intensity normalized to the number of cells is in (b). TGF-β1 treatment significantly increased α-SMA staining intensity compared to the control. Concurrent treatment with y27 still had greater α-SMA staining than control but slightly, albeit not significantly, less than TGF-β1 alone. Images of representative centrally located magnified regions are in (c). TGF-β1 treatment promoted the expression and polymerization of dense α-SMA fibers. In microtissues that concomitantly received y27, α-SMA was not as densely polymerized into organized fibers, indicating the role of Rho in the recruitment of α-SMA into stress fibers. The scale bars in (a) and (c) represent 100 and 50μm, respectively. **P<0.01, ***P<0.001.

Overall, the total normalized α-SMA staining intensity increased by 120% with TGF-β1 treatment compared to the control (fig. 6.2b) (1-way ANOVA, p<0.001). α-SMA staining was also increased with concurrent

treatment of TGF-β1 and y27 (P<0.01). However, compared to TGF-β1 alone, y27 treatment seemed to decreased α-SMA staining, albeit the difference was not statistically significant (P=0.08). In representative images of centrally located regions, α-SMA is organized into polymerized fibers with TGF-β1 treatment (fig. 6.2c). Whereas in microtissues that concomitantly received y27, α-SMA was less densely polymerized into organized fibers. These findings demonstrate the involvement of Rho/ROCK pathways in the recruitment of α-SMA into stress fibers.

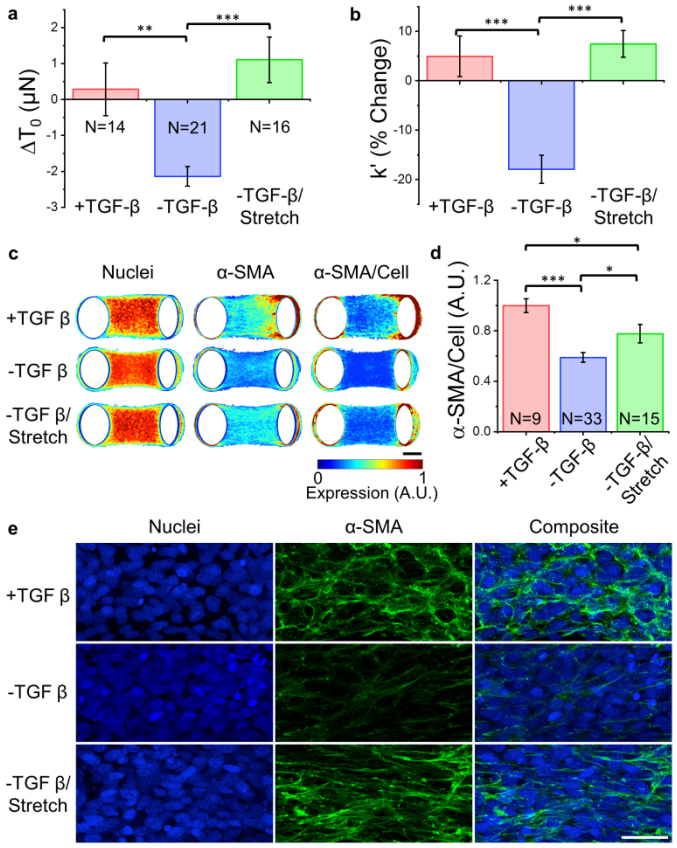

Fig. 6.3: Myofibroblast differentiation is, in part, reversible but sustained through mechanical stretch. To assess whether the activation of the myofibroblast phenotype could be reversed, microtissues were allowed to compact for 2 days in feeder media, then differentiated with TGF-β1 media for 2 days and finally switched back to feeder media. Compared to microtissues that were sustained in differentiation media, TGF-β1 withdrawal decreased resting tension and stiffness (a and b, respectively). In contrast, however, the tension and stiffness did not decrease in microtissues that were dynamically stretched at 5% 0.5Hz in addition to TGF-β1 withdrawal. These changes were mirrored in heat maps, normalized total, and representative images of α-SMA staining (c-e, respectively). TGF-β1 withdrawal decreased α-SMA staining and fiber formation. In contrast dynamic stretching, in part, prevented the loss of myofibroblast phenotype, but was still significantly reduced compared to continued TGF-β1 treated microtissues. These findings indicate that mechanical stretch may sustain myofibroblast differentiation. The scale bars in (c) and (e) represent 100 and 50μm, respectively. *P<0.05, **P<0.01, ***P<0.001.

Mechanical stretch sustains myofibroblast differentiation

The initial appearance of myofibroblasts is a normal physiological response following injury, contributing to wound contraction and collagen matrix deposition [174–178]. In tissues that are fully repaired, the myofibroblast phenotype disappears from the wound space and tissues regain their initial functionality. For reasons unknown, however, the presence of myofibroblasts may linger beyond normal wound healing, leading to a loss of tissue functionality and chronic fibrosis [174,273,274]. Accordingly we assessed whether microtissues may recover their initial fibroblastic phenotype and functionality if the TGF-β1 treatment was withdrawn following 2-days of differentiation.

Switching microtissues back to feeder media for 2 days decreased contractility by -2.1±0.3μN and stiffness by -18 ± 3% (1-way ANOVA, $P<0.01$ and $P<0.001$) (fig. 6.3a and b). Removing TGF-β1 also reduced α-SMA staining intensity by 40 ± 4% (1-way ANOVA, $P<0.001$) (fig. 6.3c-e). Importantly these findings show that the presence and functionality of myofibroblasts can in part be reversed in microtissues that were differentiated as in a normal wound healing process.

Mechanosensing pathways have been previously identified as key stimuli in myofibroblast differentiation [111,112,176,178], however, the role of dynamic stretch remains unclear. In that regard, stretching microtissues during TGF-β1 treatment produced no functional or phenotypic differences (Appendix E.1). In contrast, however, stretching microtissues upon TGF-β1 withdrawal prevented the decrease in contractility and stiffness that had been observed in static cultures that were also switched back to feeder media. In fact, stretching with TGF-β1 withdrawal sustained microtissue mechanics to the same extent as continued TGF-β1 treatment ($P>0.05$). This maintenance of microtissue mechanics was also mirrored by an increased α-SMA staining intensity compared to static conditions (1-way ANOVA $P<0.05$). Admittedly, however, the staining intensity was still lower than in microtissues kept in TGF-β1 ($P<0.05$). Nevertheless, these results suggest that cyclic stretching may in part be responsible for the maintenance of myofibroblastic phenotype, leading to chronic fibrosis.

Mechanical stretch activates latent TGF-β1 in microtissues

It has been previously hypothesized that dynamic stretching may contribute to myofibroblast differentiation through activating latent TGF-β1 sources sequestered by matrix proteins. This latent form can be produced and secreted into the extracellular environment by myofibroblasts in a feedforward loop, to drive further differentiation [189–191]. Therefore to assess whether mechanical stretching sustained myofibroblast differentiation through activating endogenous TGF-β1, we attempted to dedifferentiate microtissues while TGF-β1 receptors were blocked with GW to inhibit autocrine signaling.

As expected, blocking receptors did not affect the observed decrease to the stiffness or α-SMA straining intensity compared to TGF-β1 withdrawal only (1-way ANOVA, $p>0.05$) (fig 6.4a and c). Furthermore, when receptors were blocked, microtissue stiffness and α-SMA staining intensity, distribution and organization were no

different under static and stretching conditions (1-way ANOVA, p>0.05) (fig. 6.4 a-d). These results indicate that stretch maintains myofibroblast functionality and phenotype through an autocrine TGF-β1 signaling.

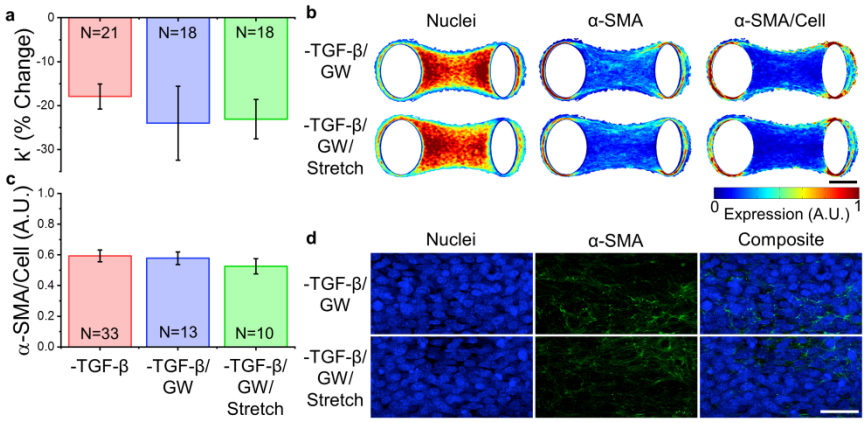

Fig. 6.4: TGF-β1 receptor inhibition prevents sustained myofibroblast differentiation through mechanical stretch. To assess whether dynamic stretching sustained myofibroblast differentiation through activation of endogenous latent TGF-β1 in an autocrine signaling pathway, TGF-β1 receptors were blocked with GW during exogenous TGF-β1 withdrawal. Upon blocking TGF-β1 receptors, dynamic stretching did not effect the reduction of microtissue stiffness (a) or α-SMA staining intensity (b-d) that accompanied exogenous TGF-β1 withdrawal. These findings suggest that the sustained differentiation with mechanical stretching is through endogenous TGF-β1 activation. The scale bars in (b) and (d) represent 100 and 50μm, respectively.

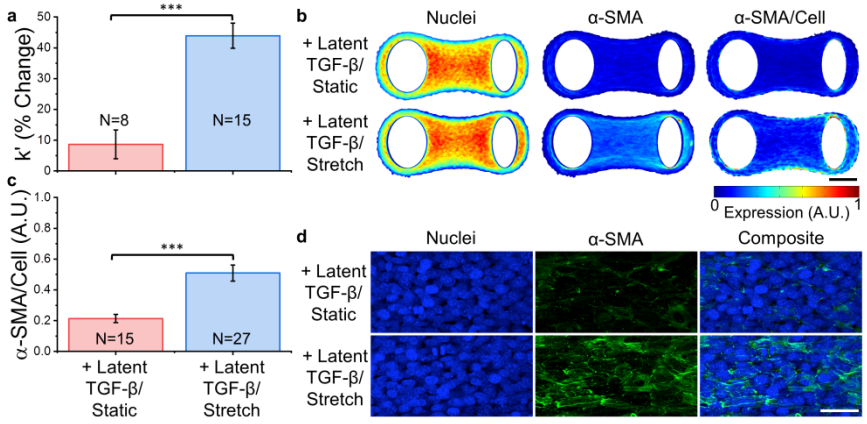

Fig. 6.5: Latent TGF-β1 is activated by mechanical stretch to promote myofibroblast differentiation. To demonstrate that a latent source of TGF-β1 can be activated by mechanical stretch, myofibroblast differentiation was assessed under static and stretching conditions with exogenous latent TGF-β1. Dynamic stretch significantly increased microtissue stiffness (a) and α-SMA staining intensity (c-d) compared to static conditions. These findings indicate that mechanical stretching can activate latent TGF-β1, further supporting its role in sustaining myofibroblast differentiation during TGF-β1 withdrawal. The scale bars in (b) and (d) represent 100 and 50μm, respectively. ***P<0.001.

In the latent form, TGF-β1 is non-covalently caged by the mechanosensitive latency-associated peptide (LAP), which effective decreases its bioavailability. It has been hypothesized that stretch may cause conformational changes to the LAP to free TGF-β1 to promote continued myofibroblast differentiation. Therefore to assess whether dynamic stretch was capable of causing this conformational change, microtissues were differentiated with 5ng/ml Latent TGF-β1 for 2 days.

Latent TGF-β1 alone produced no change in the stiffness (repeated measures t-test, $p>0.05$) and α-SMA staining remained low throughout microtissues (fig. 6.5). In contrast, dynamic stretch, in addition to latent TGF-β1, increased microtissue stiffness and α-SMA staining intensity (t-tests, $P<0.001$). Admittedly, the stiffness and staining intensity levels still remained lower than if the same concentration of activated TGF-β1 was given, likely because stretch did not activate 100% of the latent TGF-β1 given to the microtissues. Nevertheless, these results indicate that stretch can mechanically activate latent TGF-β1.

6.5 Discussion

Continued research and development of techniques are urgently needed to further our understanding of myofibroblast activation and to discover new drug targets to treat fibrosis. Not only do microtissues recapitulate key biochemical and mechanical properties of both healthy and fibrotic tissues, they allow cell-level phenotypic and tissue-level functional screening in a relatively high-throughput manner. For these reasons, microtissues are a compelling approach to conduct fibrosis research [282]. Here we aimed to investigate myofibroblast activation and deactivation under cyclic stretching in a microtissue model using our MVAS-force device. Importantly this approach allowed us to link changes to protein expression to mechanical behaviors that directly reflect the clinical manifestation of fibrotic disease.

As expected, TGF-β1 treatment led to fibroblast to myofibroblast differentiation, indicated by positive α-SMA staining, and increased microtissue contractility and stiffness. These changes were consistent with a previous publication that assessed microtissues populated with human lung fibroblasts [282]. Our findings are further in accordance with multiple studies have shown that increased tissue stiffness is a characteristic feature of fibrosis, albeit, the changes we observed over a relatively short experimental time were less than those previously reported in fibrotic lungs (increases from ~2kPa to ~17kPa) [26,289,290] and liver (~1kpa to 3-22kPa) [27]. In organs with established fibrosis, stiffness changes are thought to arise from extracellular protein deposition, particularly fibrillar collagen, and matrix crosslinking [27,291]. Increased deposition of collagen fibers upon myofibroblast activation has already been reported in microtissues [282], and thus, likely contributed to our results. Altered cell (as opposed to matrix) stiffness may also have made a significant contribution to the change in tissue mechanics. In that regard, it has been previous argued that differences between decellularized matrices cannot fully account for differences in stiffness between normal and fibrotic tissue samples [289]. Although the contribution from altered cell properties to fibrotic tissue stiffness has yet to be established, it may be considerable [274].

A stiffer ECM is well accepted to encourage myofibroblast activation through mechanosensing at focal adhesions and Rho/ROCK signaling [111,112]. Therefore, it was not surprising that we found that concurrent ROCK inhibition during TGF-β1 treatment prevented fibrotic functional changes and helped preserve the fibroblastic phenotype. Accordingly the Rho/ROCK pathway has become an attractive target for anti-fibrotic pharmaceutical treatments [292–294], and from our demonstration here, the MVAS-force may offer a method for testing and developing such treatments in tissue-like structures prior to clinical trials.

In addition to mechanosensing through focal adhesions, α-SMA itself is beginning to be considered mechanosensitive, as it only localizes to stress fibers when cells are subjected to considerable mechanical loads [176]. For example, α-SMA expression in stress fibers requires a substrate stiffness around 20kPa and reducing cellular tension by inhibiting myosin contraction leads to disassembly of α-SMA stress fibers [295,296]. This could provide a direct explanation as to the tight coupling between tissue mechanics and α-SMA staining intensity that we generally observed outside of ROCK inhibition.

Although it is generally agreed that increased substrate stiffness favors fibroblast differentiation into myofibroblasts [28,184], the role of cyclic mechanical stretch, as cells would encounter in airways and vasculature, is less clear. There have been conflicting reports as to whether cyclic stretch promotes myofibroblast differentiation [185,187,188] or serves as a protective role promoting a quiescent fibroblastic phenotype [186,297]. In contrast to those reports, we did not find that stretch had any effect on myofibroblast activation in microtissues. Differences in ECM stiffness may partially explain these conflicting reports, since stretching of lung fibroblasts cultured on stiff (30kPa) gels has been shown to augment myofibroblastic phenotype, while stretching on soft (2kPa) gels had no affect [188]. Differences in the strain field may also contribute as enhanced anisotropy when under biaxial loading has been shown to augment myofibroblast activation from valve interstitial cells [187].

Following stimulation with TGF-β1, subsequent withdrawal partially reversed the myofibroblastic phenotype and mechanical behavior. Classically in the paradigm for tissue repair, terminally differentiated myofibroblasts are removed from healing tissue through apoptosis [298]. However, opposed to earlier investigations which suggested that TGF-β1 induces a relatively stable alteration in cell phenotype [276], more recent work has found that myofibroblasts have the capacity for de-differentiation back into a quiescent fibroblast phenotype [283,299–301].

Importantly in contrast to microtissues kept under static conditions, we found that cyclic stretching maintained the myofibroblastic phenotype and tissue mechanics during TGF-β1 withdrawal. This can likely be accounted by autocrine signaling involving mechanical activation of latent TGF-β1 since blocking TGF-β1 receptors while stretching led to identical behaviors as in static conditions. We further demonstrated that stretching microtissues could activate latent TGF-β1 to promote differentiation towards a myofibroblast phenotype and to increase tissue stiffness.

These results add to an already large precedent that TGF-β1 can be mechanically activated from extracellular stores. For example, contractile forces from lung fibroblasts have been shown to directly activate

latent TGF-β1 from ECM independent of proteolytic activity [189]. Furthermore, tensile loading of fibrotic lung strips respond by releasing active TGF-β1, and subsequently increasing Smad2/3 signaling [192]. Lastly, using single molecule force spectroscopy to pull directly on LAP has been shown to induce a conformation change that frees active TGF-β1 in a pure mechanical process [193,194]. Admittedly we found no difference in deactivation with and without a TGF-β1 receptor block under static conditions, and exogenous latent TGF-β1 treatment had no effect on static cultures. Together these results indicate that endogenous latent TGF-β1 did not contribute to responses under static culturing. Although contractile forces produced by myofibroblasts during wound contraction are thought to be strong enough to open up the LAP to liberate active TGF-β1 [189], passive remodeling force may not be or at least do not happen at an appreciable occurrence to significantly change myofibroblast activation in established microtissues. On the other hand, external stretching that simulates breathing in the lung and pulsatile flow in vasculature is capable of maintaining myofibroblast behavior in microtissues through this autocrine-signaling pathway.

6.6 Conclusions

In this article we demonstrated the effectiveness of MVAS-force devices to investigate fibrosis by showing that microtissues are able to recapitulate characteristic mechanical and biological features that occur in fibrotic disease, namely increased contractility, stiffness and α-SMA expression. These changes were partially reversible, upon exogenous TGF-β1 withdrawal. In addition to its ability for relatively high throughput mechanical assessment of tissue-level mechanics, the MVAS-force permitted long-term conditioning of fibrotic microtissues to mimic the stretch cells experience in lung and vasculature tissue. Importantly stretch inhibited the partial myofibroblast deactivation that occurred following exogenous TGF-β1 withdrawal likely through endogenous latent TGF-β1 activation. Therefore external mechanical stretch might be a powerful stimulus for continued myofibroblast activation to progress fibrotic development. To conclude, further research into this pathway, which links mechanical forces to soluble mediators, may have important implications in the development of therapeutic treatments urgently needed to stop the advancement of fibrosis.

CHAPTER 7| CONCLUSIONS & FUTURE DIRECTIONS

Over the last couple of decades, an extensive body of research has intimately linked mechanical forces to cell biology. For instance, dynamic physical remodeling of the cytoskeleton and active force generation through motor proteins are known to drive various fundamental cellular functions, such as crawling, dividing, and contracting. On the other hand, mechanical stimuli from the extracellular microenvironment have been shown to influence cell behavior through several force-sensing mechanisms, which involve physical deformations of adhesion and cytoskeletal proteins [1–3]. Importantly, these mechanosensing pathways play crucial roles in maintaining homeostasis in the body, and their dysregulation often contributes to disease development [4–6]. For these reasons, a great effort is being carried out to characterize the physical properties of our cells and their behavior in response to mechanical loading. Large strides in our understanding have been made, largely in part, by studying isolated cells grown on 2D substrates with locally applied compressive and shear loads [58,65,66,68,115]. In contrast to these approaches, however, cells in the body associate with a 3D ECM, and many are stretched along their entire length. These differences may have critical consequences to our interpretations of cellular mechanobiology research. Accordingly, this thesis explored the mechanics and responses of cells in 3D microtissue cultures under dynamic tensile loading. Our results have raised prominent questions on how we currently characterize the mechanical properties of cells and the biological relevance of these approaches to studying cell behavior *in vitro*.

To shed new insights into cellular mechanobiology, it is necessary that we continue to develop platforms for cell mechanics that precisely replicate biochemical and physical aspects of the *in vivo* cellular environment [171]. Recent progress in experimental approaches has lead to a better understanding of diseases, discovery of new treatments, and improved predictions of drug efficacy prior to clinical trials [34,123]. To add to those platforms, in this thesis, we developed a microfabricated microtissue stretcher that replicates the tensile loading that cells experience in the body and their 3D ECM. Using a lab-on-a-chip approach, we were able to study the biophysical properties of cells and visualize cytoskeletal remodeling within microtissues with high resolution imaging techniques. In addition our approach allowed assessments of long-term mechanical loading with a relatively high throughput because of the array format. We demonstrated that our device supports microtissues formed out of fibroblast, airway smooth muscle, skeletal muscle and myofibroblast cells with an initial collagen matrix. To further establish our approach, continued investigations should be carried out with additional cell types, co-cultures of multiple cells, and a more physiologically complex, tissue-specific assortment of matrix proteins. This future work will better recapitulate the cellular and environmental diversity of specific organs. It may also be possible to connect multiple devices to each other through microfluidic channels to simulate the communication within a system of organs, and perhaps one-day, an entire human-on-a-chip may be created [302]. Further progress in this area will undoubtedly advance our understanding of how the behavior of cells is regulated by their microenvironment.

Prior to this work, investigations of cell mechanics using microtissues were mainly limited to measurements of static contractile force and quasi-static stiffness [120,124,126–129]. In comparison, this thesis assessed their dynamic behaviors for important two reasons: first, the mechanical behavior of cells is known to be dynamically regulated by stretch; and second, cells exhibit a broad spectrum of time-dependent physical properties.

In regards to the first reason, we quantitatively linked force-induced mechanical softening in microtissues to remodeling in the cytoskeleton. These results further support the hypothesis that the actin cytoskeleton is a mechanosensor of stretch and rapidly depolymerizes under fluctuating stresses [91,92]. Characterizing this dynamic mechanical response of microtissue cultures marks an important contribution to the field as it connects our understanding of mechanobiology from 2D experimental approaches to a physiologically relevant environment. With that said, unlike cells in 2D culture [92], softening in microtissues was not accompanied by a more fluid-like response. This observation brings to question how the physical behavior of cells is determined by the investigative approach (2D vs. 3D culture and local vs. global deformation).

As for the second reason, by characterizing the behavior of microtissues over a broad spectrum of timescales, we quantified the dynamics of various cytoskeletal-remodeling processes. In that regard both the time and frequency domain responses of microtissues gave stretched exponential behaviors with power law exponents that tended to agree with theoretical 3D trap models dominated by Brownian forces. The time constants indicated that stress relaxation was a nonlinear process, while recovery was typically slower and linear - being independent of step size and strain. Furthermore, the characteristic time constant of the frequency response corresponded to the difference between these time constants, suggesting that, under cyclic stretch, microtissues reach an equilibrium state set by the difference in the dynamics of these processes. Since pharmacologically induced actin depolymerization eliminated these time-dependences, stress relaxation and recovery probably heavily reflect the depolymerization and repolymerization of actin microfilaments, respectively. With that said, the relaxation spring constants in our model remained tightly coupled throughout an assortment of pharmacological treatments and strain amplitudes. This collapse of microtissue mechanics down to a single relationship suggests that cells do not achieve their physical behavior through individual proteins, but actually through the interactions between cytoskeletal proteins. Further evidence in support of this conjecture has previously been brought forward through several universal mechanical behaviors found in 2D cell cultures [76,77,92]. Importantly it means that opposed to a traditional reductionist bottom-up approach to studying cell mechanics, our field should contemplate more complex models that involve the exchanges of stress within a network of different cytoskeletal elements.

In contrast to the characteristic timescale behaviors that we reported in 3D microtissues, cells in 2D culture have largely been observed to follow featureless weak power laws [65,66,68,99]. However, by plating cells on a 2D substrate, adhesion proteins, and in turn, a large majority of the cytoskeleton, are unnaturally polarized to the bottom of the cell [31]. It is, therefore, reasonable to suspect that the interactions between cytoskeletal proteins, and thus the mechanical behavior of the cell are affected to a degree by this dramatic change to the cytoskeletal

distribution and structure. Another explanation for the distinct rheological behaviors may lie in the different length-scales of the measurements (local vs. global deformations). If this is the case, then local shear and compressive loading used in previous approaches may not accurately reflect properties under comparably longer length-scale tensile forces because of the complex, inhomogeneous cytoskeleton. Whether the rheological differences arose out of the dimensionality of the microenvironment or are an effect from the length-scale of the measurement are important considerations for future studies.

When we considered both mechanically induced cytoskeletal remodeling and the rheological behavior cells, we discovered that the degree of strain softening in microtissues increased with the rate of stretch. This finding demonstrates that a cell's perception of strain, and its remodeling response, is time-scale dependent. Continued exploration of the dynamic response of microtissues to stretch, may further tie the rheological behavior of cells in tissues to time-dependencies in other mechanotransduction pathways. Among which, force-sensing and downstream signaling at focal adhesions should be made a central focus of future investigations in 3D microtissues. Carrying out these investigations in conjunction with future advancements in high temporal and spatial resolution imaging, and gene editing with CRISPR to systematically create mutations in key force-sensing proteins will invaluably progress our understanding of cells and mechanotransduction pathways.

The final manuscript in this thesis further showed the importance of integrating a 3D ECM and physical loading into medical research by investigating the maintenance of myofibroblast phenotype and function that characterizes fibrotic disease. In that way, this chapter adds to an already extensive body of literature that has shown how the microenvironment is critical in controlling cellular behaviors in our bodies and is an especially important consideration in the context of studying diseases. More specifically the ECM is known to sequester numerous signaling molecules and, in itself, it can act as a force sensor by releasing these molecules upon mechanical loading [189–191]. In that regard, we demonstrated that latent TGF-β1 could be mechanically activated to sustain myofibroblast differentiation. Further investigation into this pathway may reveal new drug targets that lead to improved therapeutic treatments for fibrosis.

To conclude, through the technological developments in this thesis, we have built upon the link between mechanics and cell biology. Our investigations further our field's understanding of how mechanical stretch delivered to cells within a physiologically relevant 3D ECM controls their biological function, and as well as their physical properties. For reasons that are not currently fully understood, cells in 3D microtissues displayed rheological behaviors and responses to stretch that differed from our understanding of their behavior when grown on 2D substrates. As all good research ends with more questions, we hope that other investigators build upon our work in the same manner as we were inspired by a vast number of prior studies. The answers to these questions posed by our findings may further unravel 'the beads, buttons, pins and threads of Mother's work basket', and thereby enlighten the pathways of how cells sense and dynamically respond to their mechanical surroundings.

APPENDIX A| SUPPLEMENTARY INFORMATION OF CHAPTER 2

Supplementary information for the manuscript: “A vacuum-actuated microtissue stretcher for long-term exposure to oscillatory strain within a 3D matrix”.

Supplementary note

A.1: Microtissue strain field example calculation.

Using a four level pyramid based Lucas and Kanade algorithm, inter-frame displacements were estimated across a region of interest at five-pixel spacing. Representative interframe displacements in the x and y directions, U and V respectively, are below.

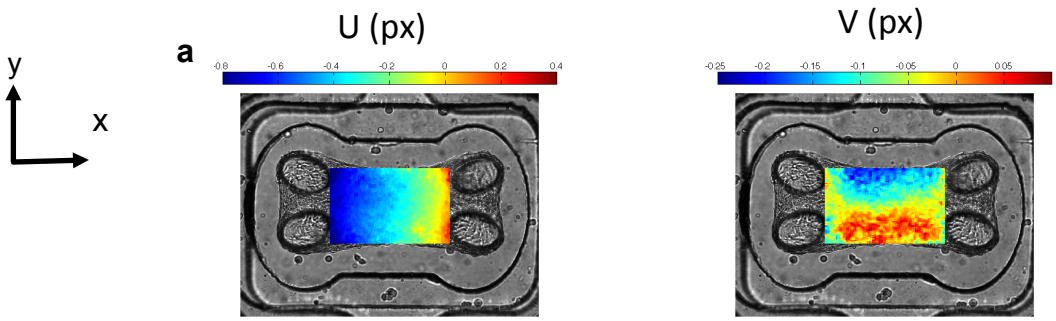

The inter-frame displacements were filtered to remove errant estimations and fitted with a LOWESS surface-fitting algorithm in Matlab to smooth the data. Representative interframe smoothed displacements are below.

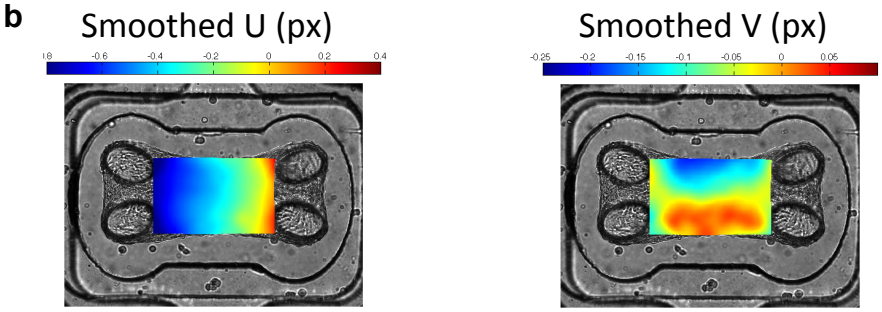

The strain tensor was calculated from the displacement field with the following set of equations:

$$E_{xx} = \frac{dU}{dx} \tag{A.1}$$

$$Exy = \frac{1}{2}\left(\frac{dU}{dy} + \frac{dV}{dx}\right) \tag{A.2}$$

$$Eyy = \frac{dV}{dy} \tag{A.3}$$

Representative inter-frame strain fields are below.

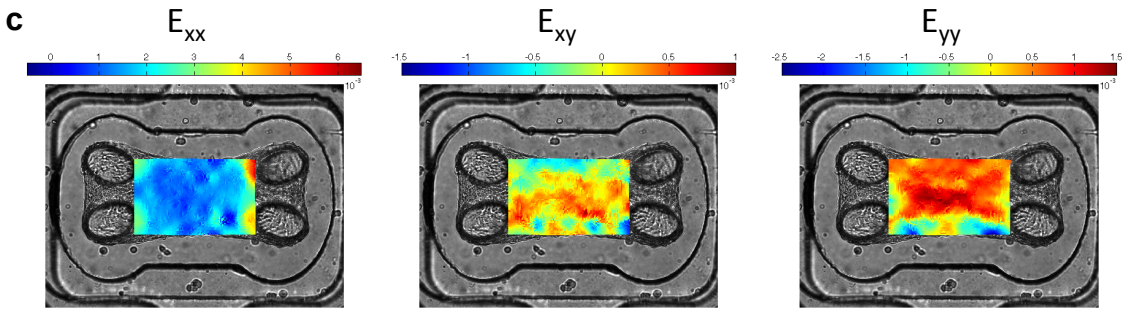

Interframe strain fields were integrated through time to estimate the local total strain field. Representative inter-frame strain fields are below.

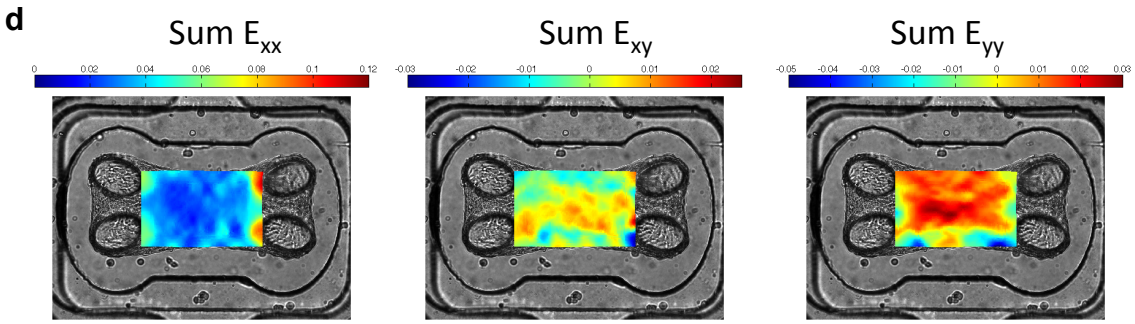

Additional figures

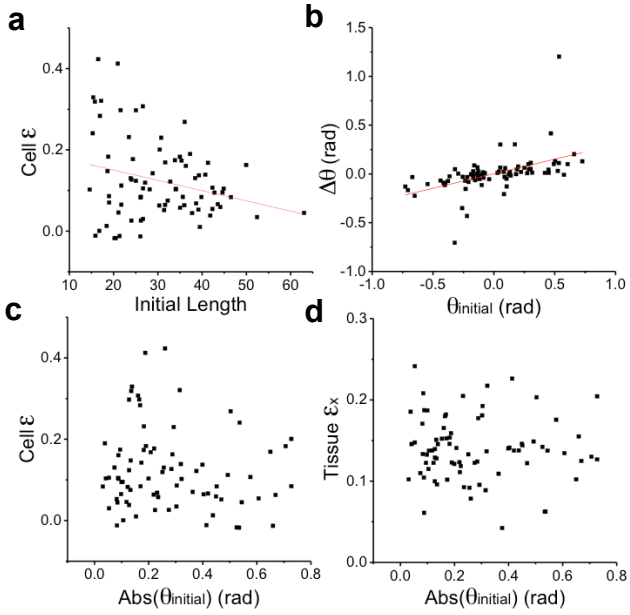

Fig. A.2: Single cell strain at 90kPa. Cell strain (n=79) was weakly related to initial cell length with shorter cells experiencing greater strain (R^2=0.07, p<0.05) (a). During a single stretch, the cells better aligned with the longitudinal axis of the microtissue. The degree of rotation was weakly related to the initial cell angle with poorly

aligned cells undergoing a greater angular change (R^2=0.26, p<0.001) (b). There were no relationships between initial cell angle and the cell or tissue strains (P>0.05) (c,d).

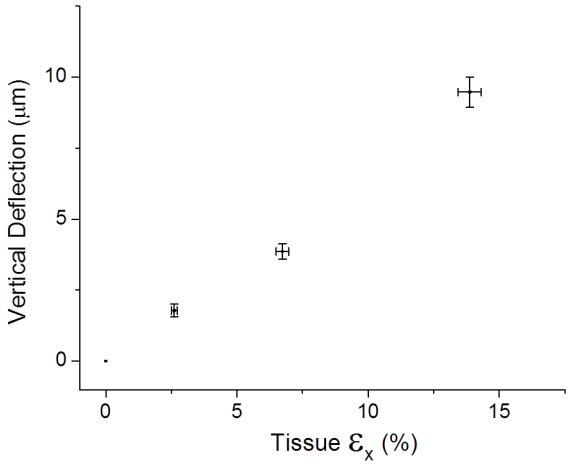

Fig. A.3: Out of plane motion. Out of plane motion was quantified by tracking the vertical deflection of GFP-labeled cells (n=124) in confocal image Z-stacks. For each cell, XY intensities were integrated over the cell's projected area at each Z step (5μm interval) and fit with a Gaussian distribution. The vertical deflection was measured as a change in the location of the peak of the Gaussian distribution.

Electronic supplementary information

Movie A.1: Representative microtissues stretching at 0.1hz.

Movie A.2: The average (n=10) axial strain field of a 345x187μm region between the cantilevers. Strain is unitless.

Movie A.3: The standard deviation of axial strain fields.

Movie A.4: The average (n=10) transverse strain field of a 345x187μm region between the cantilevers. Strain is unitless.

Movie A.5: The standard deviation of transverse strain fields.

Movie A.6: The average (n=10) shear strain field of a 345x187μm region between the cantilevers. Strain is unitless.

Movie A.7: The standard deviation of shear strain fields.

APPENDIX B| SUPPLEMENTARY INFORMATION OF CHAPTER 3

Supplementary information for the manuscript: "Structural and mechanical remodeling of the cytoskeleton studied in 3D microtissues under acute dynamic stretch".

Additional figures

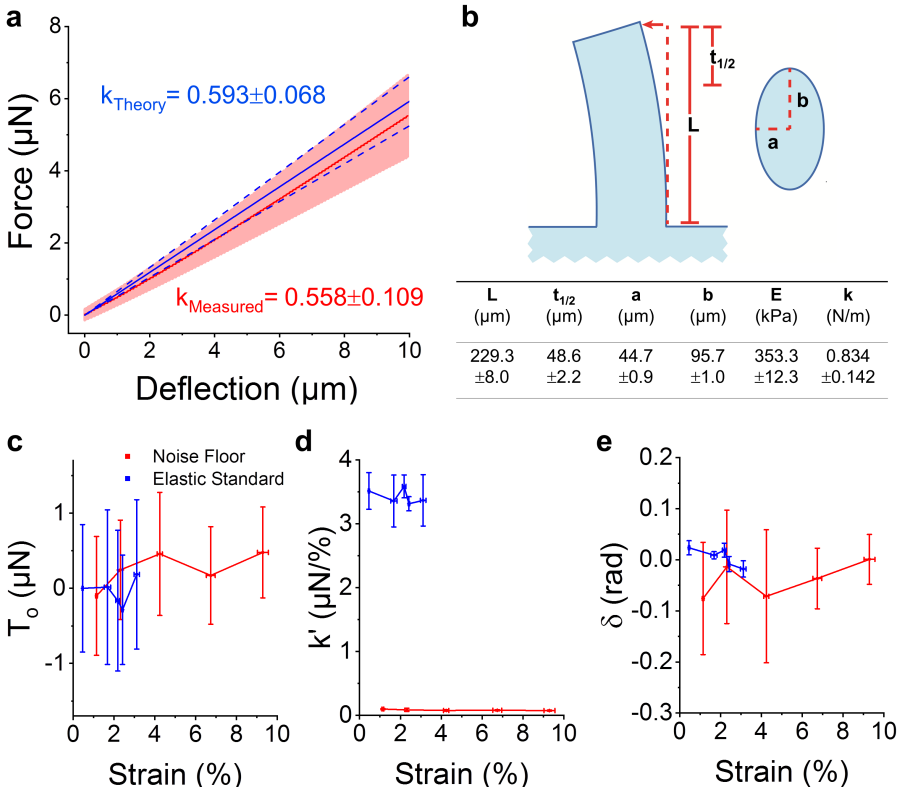

L (μm)	$t_{1/2}$ (μm)	a (μm)	b (μm)	E (kPa)	k (N/m)
229.3 ±8.0	48.6 ±2.2	44.7 ±0.9	95.7 ±1.0	353.3 ±12.3	0.834 ±0.142

Fig. B.1: The force-sensing cantilever spring constant and validation of MVAS-Force. Force measurements were calculated from the visible deflection of the sensing cantilever and its spring constant. (a) The spring constant of the cantilever under a tip load was theoretically calculated using the moment of inertia of an ellipse (equation B.1) and Euler-Bernoulli beam theory (equation B.2) with constants from (b), and validated with AFM (N=6). The length constants were measured from calibrated images (N>5). The elastic modulus of PDMS, E, was measured with AFM (N=6). For measurements of microtissue force, the spring constant was calculated according to equations B.1 and B.3 to model the load at half the tissue thickness, $t_{1/2}$, from the top of the cantilever. The prestress, storage stiffness and phase lag measured without a load (ie. the noise floor) and with an elastic standard (a polymerized 70x15μm strip of PDMS) are shown in c-e, respectively. The noise floor was much smaller than microtissue force measurements and remained unaltered throughout the examined strain range (N=6, linear regression, p>0.5).

Measurements of the elastic standard were also invariant on the tested strain range (N=5, linear regression, p>0.5), and as expected, had near zero internal friction. Error bars represent the standard deviation.

$$I = \frac{\pi a b^3}{4} \tag{B.1}$$

$$k = \frac{3EI}{L^3} \tag{B.2}$$

$$k = \frac{6EI}{(L - t_{1/2})^2 (2L + t_{1/2})} \tag{B.3}$$

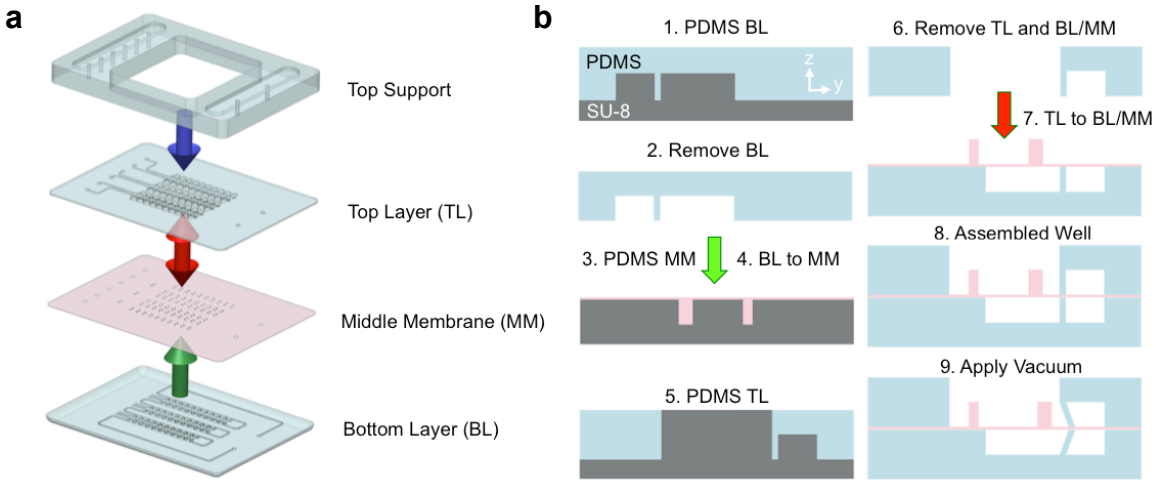

Fig. B.2: MVAS-force assembly. The device consists of a top support and three photolithographic layers: 1) a top layer comprising the open-top microtissue wells and enclosed vacuum chambers; 2) a middle membrane with cantilevers; and 3) a bottom layer containing vacuum and empty bottom chambers. An exploded view is shown in (a) and cross-sections of fabrication steps of one well are illustrated in (b). For the bottom layer, PDMS is applied over top of the features on the SU-8 photolithography master and removed. For the middle membrane, PDMS, doped with Rhodamine B, is spin coated to a thickness of 30µm. Lastly, for the top layer, PDMS is spin coated to the top of the features on the SU-8 master. The bottom layer is then plasma bonded onto the middle membrane (green arrow) and the top support layer is bonded onto the top layer (blue arrow, not shown in (b)). The two are then removed from the middle membrane and top layer masters, respectively, and bonded together (red arrows). When a vacuum is applied, the middle membrane is deformed moving the cantilevers apart stretching the microtissue in plane.

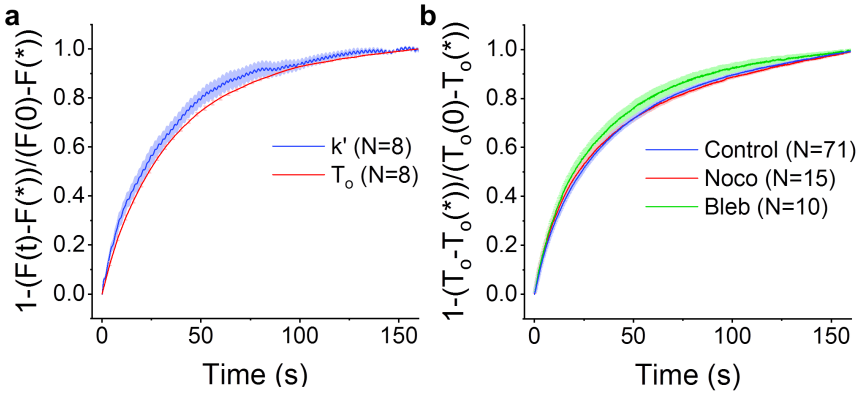

	a	τ (s)	β	d	r²
T$_o$	-1.9 ± 0.2 µN	38 ± 1	0.87 ± 0.01	1.9 ± 0.1 µN	0.9991 ± 0.0003
k'	-0.73 ± 0.08 µN/%	35 ± 6	0.92 ± 0.08	1.8 ± 3 µN/%	0.995 ± 0.002

	a (% Control)	τ (s)	β	d (% Control)	r²
Control	-	43 ± 2	0.79 ± 0.01	-	0.9988 ± 0.0003
Noco	85 ± 13 ***	42 ± 3	0.71 ± 0.02 **	83 ± 13 ***	0.995 ± 0.002
Bleb	-31 ± 5 ***	38 ± 7	0.79 ± 0.02	31 ± 5 ***	0.9989 ± 0.0003

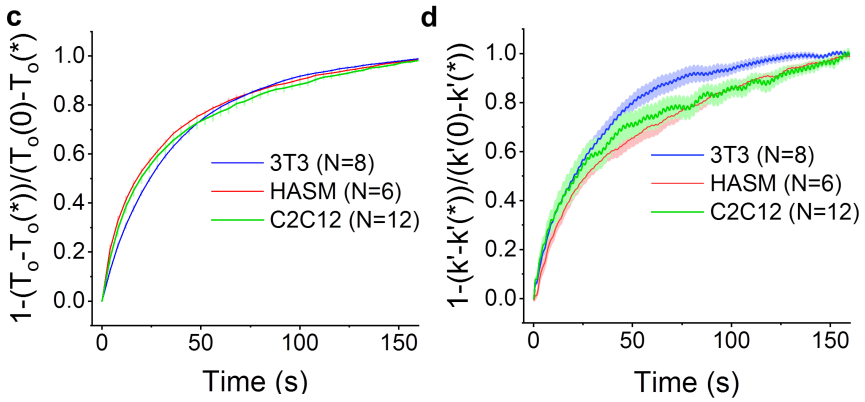

	a (µN)	τ (s)	β	d (µN)	r²
3T3	-1.9 ± 0.2	38 ± 1	0.87 ± 0.01	1.9 ± 0.1	0.9991 ± 0.0003
HASM	-2.0 ± 0.1	36 ± 2	0.66 ± 0.03	2.0 ± 0.1	0.9988 ± 0.0004
C2C12	-1.0 ± 0.1	43 ± 6	0.67 ± 0.04	1.0 ± 0.1	0.9971 ± 0.0004

	a (%)	τ (s)	β	d (%)	r²
3T3	-42 ± 2	35 ± 6	0.92 ± 0.08	100 ± 4	0.995 ± 0.002
HASM	-56 ± 12	138 ± 48	0.7 ± 0.1	110 ± 13	0.9955 ± 0.0008
C2C12	-42 ± 3	41 ± 7	1.0 ± 0.1	96 ± 3	0.985 ± 0.006

Fig. B.3: Microtissue recovery shares similar dynamics across pharmacological treatments and cell types. For microtissues composed of 3t3 cells, tension and stiffness recovery followed similar trajectories. They both fit well to stretch exponentials with agreeing time (τ) and power (β) constants (a). Microtubule depolymerization (Noco) or myosin inhibition (Bleb) did not change the time constant and only microtubule depolymerization changed the power law constant (repeated measures t-tests). The tension recoveries for 3T3, HASM, and C2C12 microtissues are shown in (c). The tension recovery in C2C12 microtissues was significantly less than 3T3 ($P<0.01$) and HASM ($P<0.001$) (1-way ANOVA). There was no change in the time constant. The power law constant for 3T3 microtissues was greater ($P<0.001$) than C2C12 or HASM. The stiffness recoveries for 3T3, HASM, and C2C12 microtissues are shown in (d). The time constant for HASM recovery was greater than either 3T3 or C2C12 microtissues ($p<0.05$). There were no other significant differences.

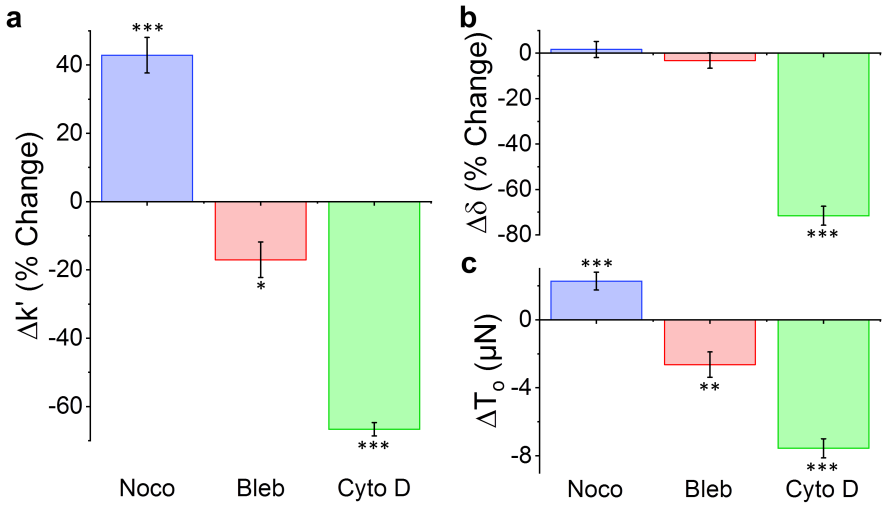

Fig. B.4: Pharmacological responses. Microtissue storage stiffness (a), phase lag (b) and prestress (c) change in response to microtubule depolymerization (noco) (N=15), myosin inhibition (bleb) (N=10) and actin depolymeriza5ion (cytoD) (N=16). Microtubule depolymerization significantly increased storage stiffness and prestress. Myosin inhibition or actin depolymerization decreased storage stiffness and prestress. Actin depolymerization also significantly reduced the phase lag. (*P<0.05; **P<0.01; ***P<0.001; repeated measures t-tests).

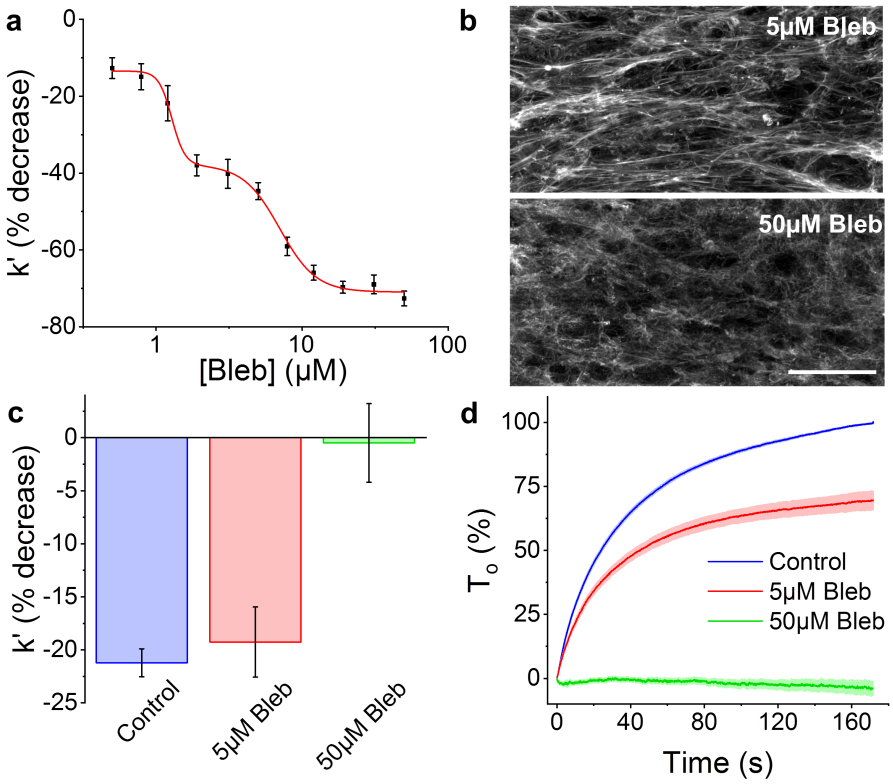

Fig. B.5: Strain softening does not depend upon myosin activity. The dose-response curve for blebbistatin is biphasic (a). Biphasic responses result from multiple mechanisms of action. Blebbistatin is a selective myosin-II inhibitor but at higher concentrations other changes to structural proteins may occur. For example following a treatment with 5μM blebbistatin, the f-actin cytoskeleton is largely intact, whereas following a 50μM dose f-actin is more unorganized and not densely polymerized into stress fibers (b). Therefore it is reasonable to suspect that the first plateau of the dose-response curve, which ends roughly at 5μM, represents myosin-II inhibition, while at greater concentrations the response is more inline with actin depolymerization. At 5μM there was no change in softening in terms of percent stiffness change (c) (1-way ANOVA). Only the absolute value of prestress recovery changed (d), which is to be expected because blebbistatin decreases the prestress on its own. On the other hand, at 50μM, and because of its action to depolymerize f-actin, the response reflects changes seen in Fig. 3.3 with cytochalasin D- no softening and no recovery. The scale bar in (b) represents 50um.

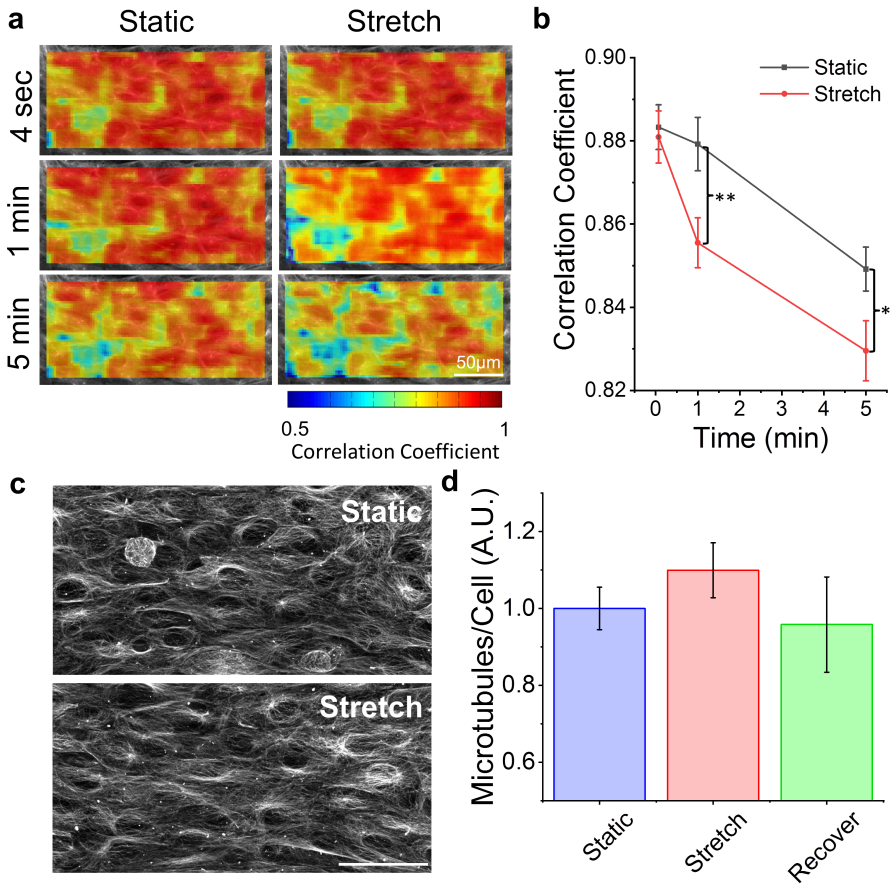

Fig. B.6: Microtubules remodel under oscillatory stretching but polymerization does not change. Representative heat maps of microtubule remodeling after various durations under static and stretching conditions are shown in (a). The average correlation coefficients are in (b). At 1min and 5min there was significantly more remodeling in microtubules when under oscillatory loading than in static (*P<0.05, **P<0.01; N=7, Paired t-tests). This was not unexpected especially considering we saw similar strain-dependent remodeling in f-actin filaments and microtubule and actin dynamics have been previously linked in the literature.[303] Unlike actin, however, stretching caused no observable change in microtubule distribution/organization (c) and there was no difference in the amount of polymerization per cell after 5min of stretching (N=15) or 5min of recovery (N=14) compared to static (N=16) (d) (1-way ANOVA). The scale bar in (c) represents 50um.

Supplementary note

B.7: Advantages and limitations of the MVAS-force

The main advantage of our device over previous methods (ie. atomic force microscopy (AFM), optical magnetic twisting cytometry (OMTC) and optical/magnetic tweezers) used to assess micro-rheology of cells is that in our device cell mechanics are assessed within a 3D physiologically relevant environment, whereas in previous methods, cells are grown on 2D substrates. Although direct mechanical comparisons between cells grown on 2D and in 3D environments are lacking, a third dimension for cell adhesion is known to significantly affect the

distribution and structure of the cytoskeleton.[31] In addition to possibly affecting mechanical properties, we are starting to appreciate that the dimensionality of the extracellular environment may influence how cells respond to mechanical stimuli.

Another advantage of our device over previous micro-rheology methods is that the uniaxial tensile deformation used to measure mechanical properties resembles the deformation a cell would experience in airways during inspiration or in blood vessels during systole. In comparison local shear from magnetic beads in OMTC or compressive deformation from an AFM tip have limited relevance. In our device the length-scale of deformation is the size of the cell whereas the deformation during OMTC or with a fine AFM tip is very local and volumetrically relatively small compared to the size of a cell. This difference has important consequences when comparing mechanical properties between microrheology methods. First, the measurement of elasticity can vary over four magnitudes depending upon the length scale of deformation.[67] Secondly, stress dissipation from a volumetrically small deformation may arise solely from frictional stress between cytoskeletal filaments, and thus follows the structural damping law,[66,68] whereas at the length scale of the entire cell, dissipation may arise from both the cytoskeleton and viscous damping through cytosolic fluid movement.[86]

Static measurements of microtissue elasticity have been previously investigated using a magnetic actuation system.[128,129] In this closely related method, a ferrous bead is fixed to one of the cantilevers and moved by magnetic tweezers while the other cantilever is used as a force sensor. Although this method has provided valuable insights into how tissue-level forces are generated from cells, actuation through magnetic tweezers is not suitable for long-term simultaneous conditioning of multiple microtissues and the device fabrication throughput is limited. Our vacuum actuation approach overcomes these disadvantages.

Perhaps one limitation of the MVAS-Force device is that it requires specialized equipment for master fabrication and bonding device layers together. The equipment (plasma machine, mask aligner, and spin coater) is, however, common to microfabrication facilities and presently available on most university campuses.

In this article we reported, for the first time, on cytoskeletal remodeling in response to dynamic stretching in living cells in 3D cell cultures. Although we believe that the ability of our device to allow high resolution imaging of living cells in a physiologically relevant environment marks a significant improvement over previous methods, there is some difficulties that remain. Firstly, despite our best efforts to make a device with minimal out of plane motion, there is a vertical deflection of roughly 0.5µm/ % strain. Although this is not a great deal of vertical motion, admittedly it is enough to change focal planes when imaging with high numerical aperture objectives. This was not a problem for the work in this article because all imaging was done at 0% strain. If in future work, images would like to be compared at different strains, this limitation could be overcome by programing a z-stage to work in conjunction with the MVAS-force. Secondly, although microtissues are far easier to image than centimeter scale 3D cultures, imaging does still suffer from fluorescence attenuation and longer acquisition times when capturing z-stacks compared to imaging cells on 2D glass or plastic surfaces. For this reason, imaging cells in 2D culture will likely remain for now the most common method for assessing cytoskeletal remodeling. However, the MVAS-force

is a suitable alternative for answering whether or not similar remodeling occurs in a more relevant 3D environment.

Electronic supplementary information

Movie B.1: The MVAS-force device enables high throughput mechanical stimulation and force measurements of microtissues. In this movie, two microtissue cultures are simultaneously stretched in the MVAS-force device with a 0.25Hz sinusoidal vacuum. When a vacuum is applied, the cantilevers (on the left side) closest to the vacuum chamber move to stretch the microtissues while changes in microtissue tension are simultaneously measured by tracking the passive deflection in the opposing cantilevers (on the right side).

APPENDIX C| SUPPLEMENTARY INFORMATION OF CHAPTER 4

Supplementary information for the manuscript: “Time dependencies in the dynamical mechanical behavior of 3D microtissue cell cultures”.

Additional figures

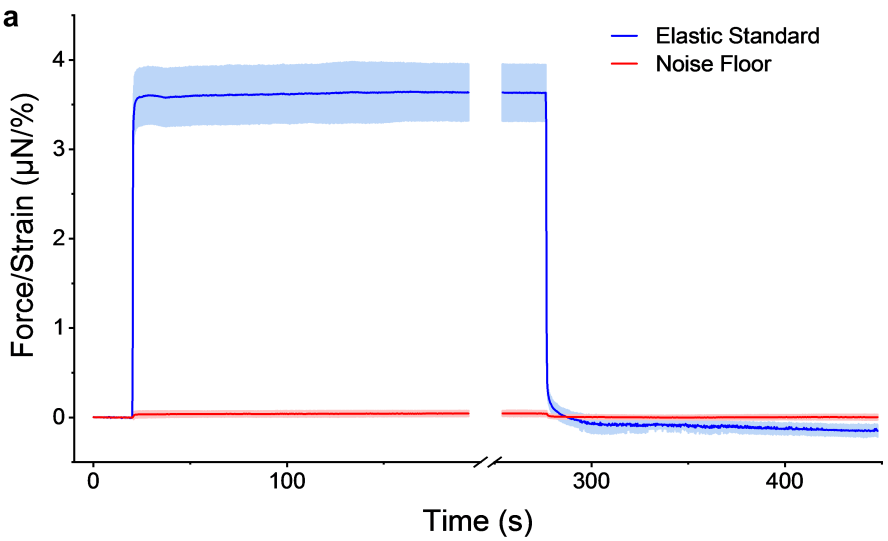

Fig. C.1: MVAS-force validation for step strain measurements. Step strain experiments were performed without an attached load (N=5), to measure the noise floor, and with a polymerized 70x15µm strip of PDMS (N=3), to act as an elastic standard (a). The noise floor was much smaller than microtissue force measurements. Furthermore, as expected, there was no relaxation or recovery response with measurements of the elastic standard or the noise floor. The errors represent the standard deviation.

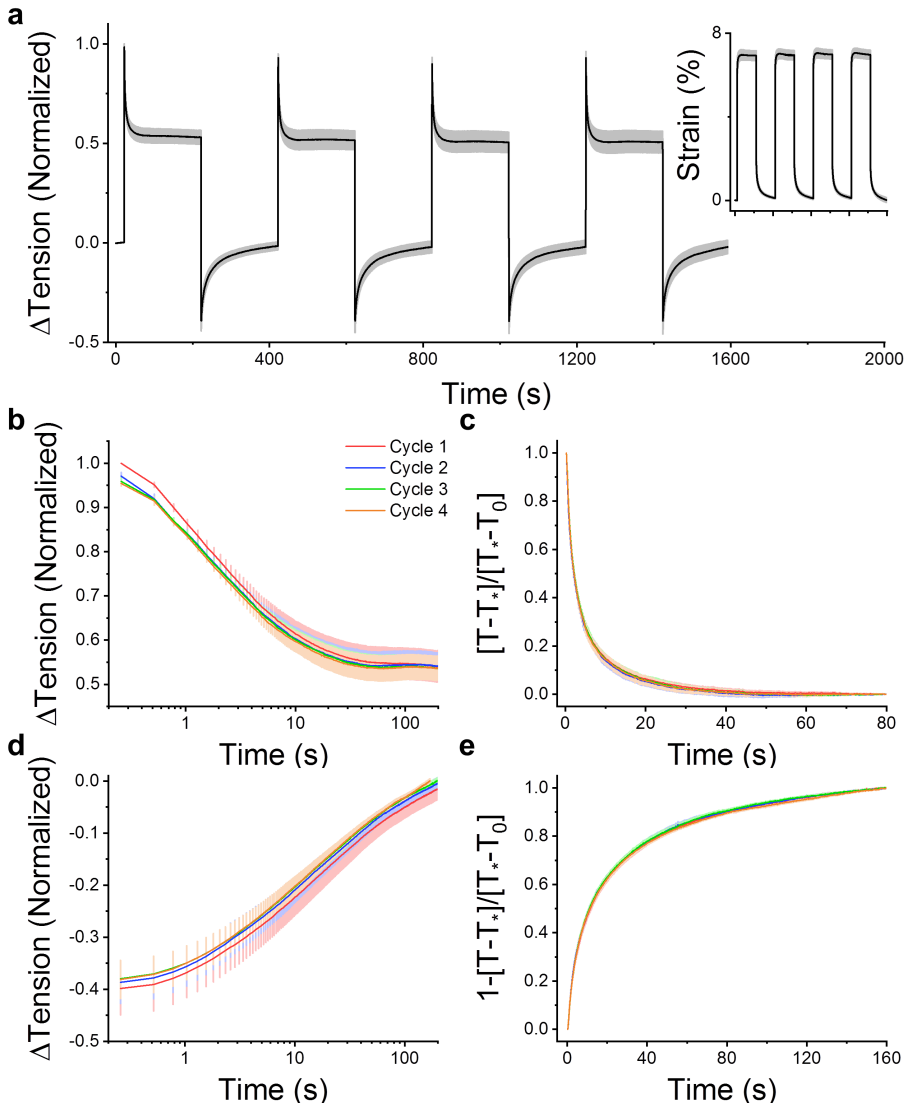

Fig. C.2: Microtissue viscoelastic behavior is highly repeatable. Four step strain experiments were completed sequentially on the same microtissues (N=6) (a). Stress relaxations shared similar amplitudes (b) and rates (c) and so did stress recoveries (d and e). There were no significant differences to any of the fitting constants (k_1, k_2, τ, or β) for relaxation or recovery (repeated measures 1-way ANOVA; $P>0.05$).

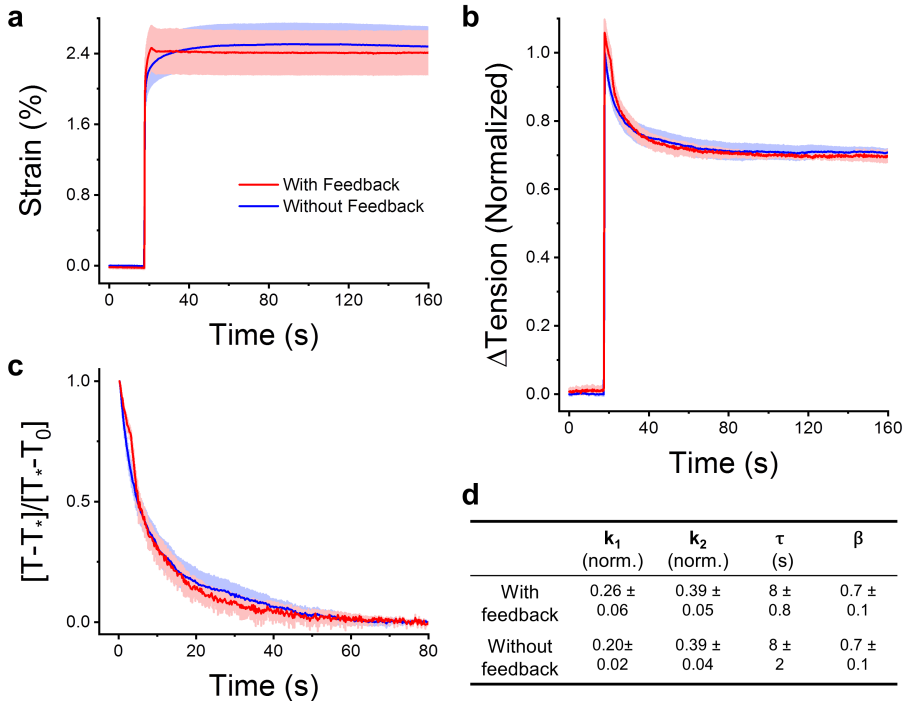

d

	k_1 (norm.)	k_2 (norm.)	τ (s)	β
With feedback	0.26 ± 0.06	0.39 ± 0.05	8 ± 0.8	0.7 ± 0.1
Without feedback	0.20± 0.02	0.39 ± 0.04	8 ± 2	0.7 ± 0.1

Fig. C.3: Microtissue creep does not effect assessment of stress relaxation behavior. Because our method of measuring tissue tension through cantilever deflection inherently causes some creep in the tissue length, we assessed how our measurements were affected by first doing a step strain experiment as normal (without feedback) and then by redoing the step strain experiment on the same microtissues but while modulating the vacuum pressure so to get rid of the creep response in the original experiment (with feedback) (a) (N=4). The changes to tension (b) and the rate of relaxation (c) were comparable without and with modulating the vacuum pressure to remove creep. Furthermore both relaxation responses followed stretched exponential trajectories; the fitting constants are in (d). As expected, the k_1 constant was slight higher, but not significantly ($P>0.05$, repeated measures t-test), when there was no creep in microtissue length. There was no change in k_2, the time constant, or the power law constant (repeated measures t-tests; $P>0.05$).

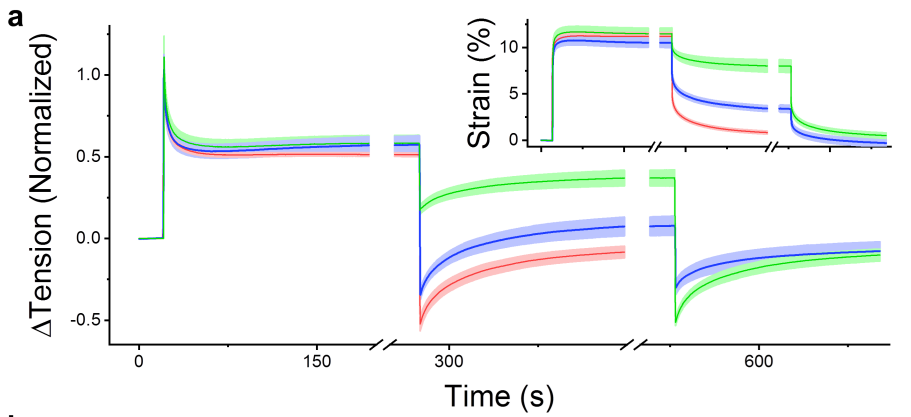

d

	a (μN)	d (μN)	τ (s)	β
0%	-5.6 ± 0.5	-0.6 ± 0.3	42 ± 3	0.68 ± 0.02
3.4%	-5.3 ± 0.5	1.2 ± 0.6	40 ± 2	0.689 ± 0.008
8.0%	-2.6 ± 0.4	2.8 ± 0.5	39 ± 3	0.67 ± 0.03

e

	a (μN)	d (μN)	τ (s)	β
0%	-5.6 ± 0.5	-0.6 ± 0.3	42 ± 3	0.68 ± 0.02
3.4%	-2.8 ± 0.3	-0.7 ± 0.6	40 ± 3	0.67 ± 0.02
8.0%	-5.2 ± 0.5	-0.8 ± 0.4	42 ± 4	0.64 ± 0.02

Fig. C.4: Microtissue stress recovery rate is strain independent. Large step strains (insert) were applied and microtissues (N=6) were allowed to fully relax (a). In the next part of the experiment, microtissue recovery was assessed at a full return to initial length (red), and at large (blue) and small (green) intermediate steps. Recovery rates at 0%, 3.4% or 8.0% strain were identical (b). In the last part of the experiment, tissues at intermediary steps were returned to their initial lengths. These recoveries also shared the same rates (c). Panels (d) and (e) contain the average fitting constants for the intermediate steps and the later recoveries to initial length, respectively. There were no significant differences in either the time or power law constants (repeated measures 1-way ANOVA; P>0.05) despite large changes to the step size and the strain at which the tissues recovered.

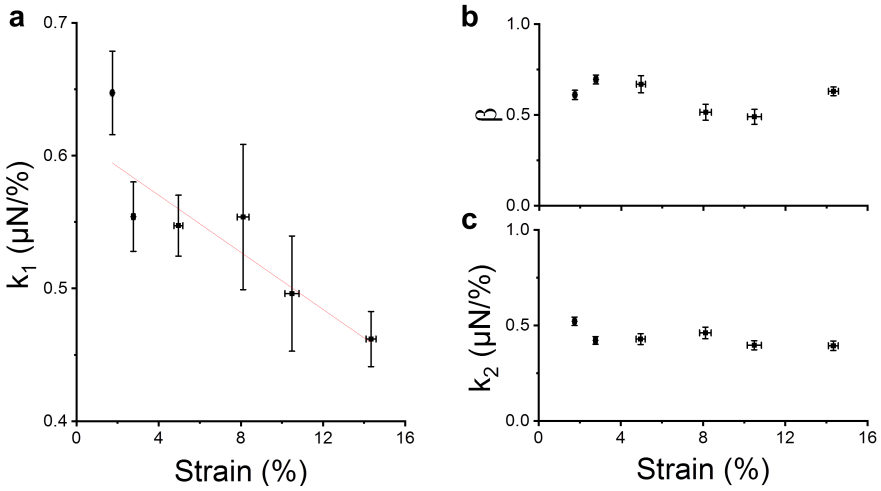

Fig. C.5: The fitting constants for microtissue stress relaxation at various step sizes. The microtissue k1 spring constant, describing the amplitude of the relaxation response normalized to microtissue strain, linearly decreased with step size (a) (linear regression; R^2=0.78 P<0.001). In contrast, the power law constant and the k_2 spring constant, describing the residual elasticity, were invariant with step size.

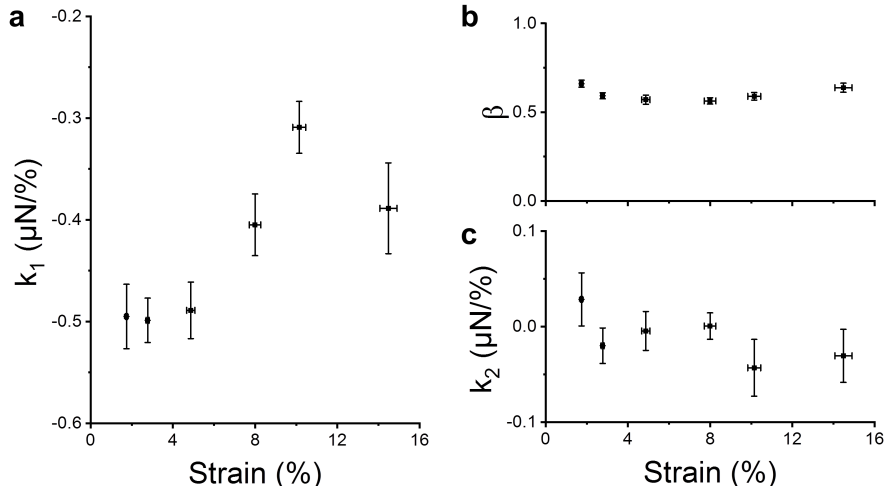

Fig. C.6: The fitting constants for microtissue stress recovery at various step sizes. The microtissue k_1 spring constant, describing the amplitude of the recovery response normalized to microtissue strain, decreased with step size (linear regression; R^2=0.66 P<0.05). The power law constant was invariant with step size. The k_2 spring constant was also invariant and was near zero, indicating that there was no difference between residual stresses before and after the step strain experiment.

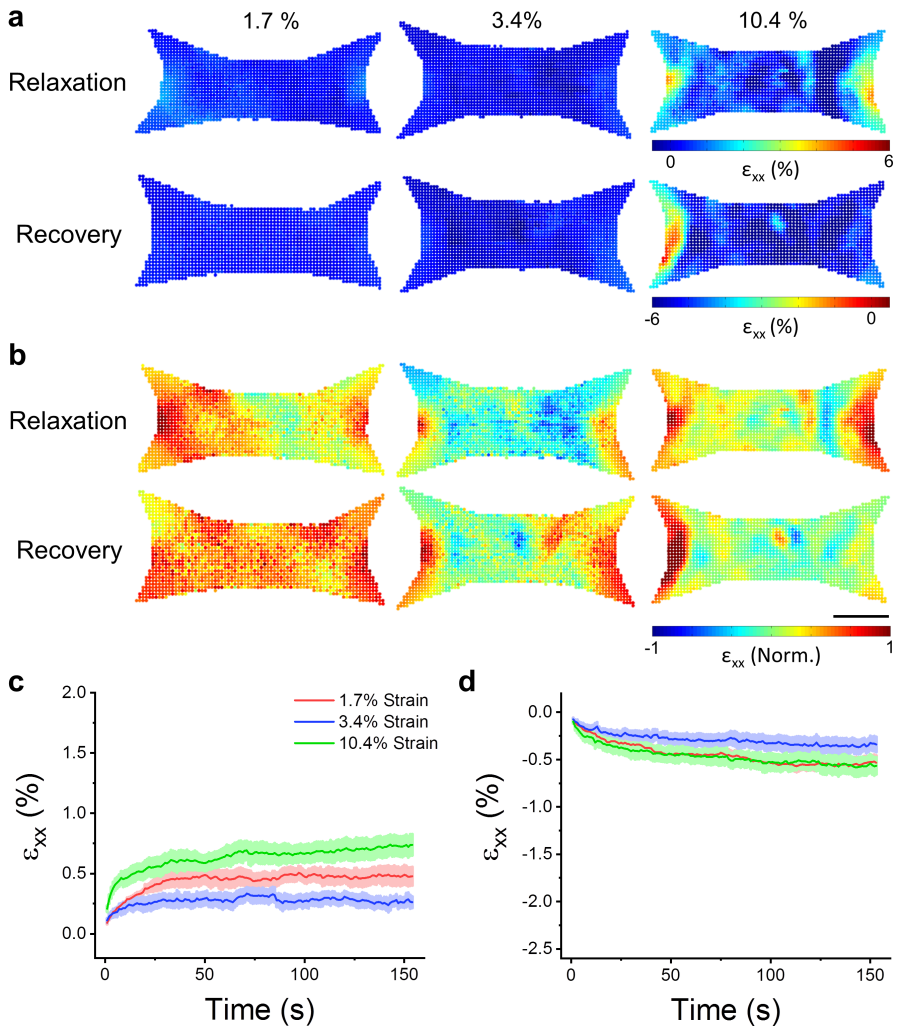

Fig. C.7: Remodeling in the longitudinal direction following changes to microtissue length. Spatial distributions of relaxation and recovery in the longitudinal direction after various step sizes are shown in (a). The distributions are normalized to three standard deviations outside the absolute mean value in (b). The scale bar represents 100µm. The average (N=6) strain in the x-direction during stress relaxation is shown in (c). The remodeling during stress recovery is shown in (d).

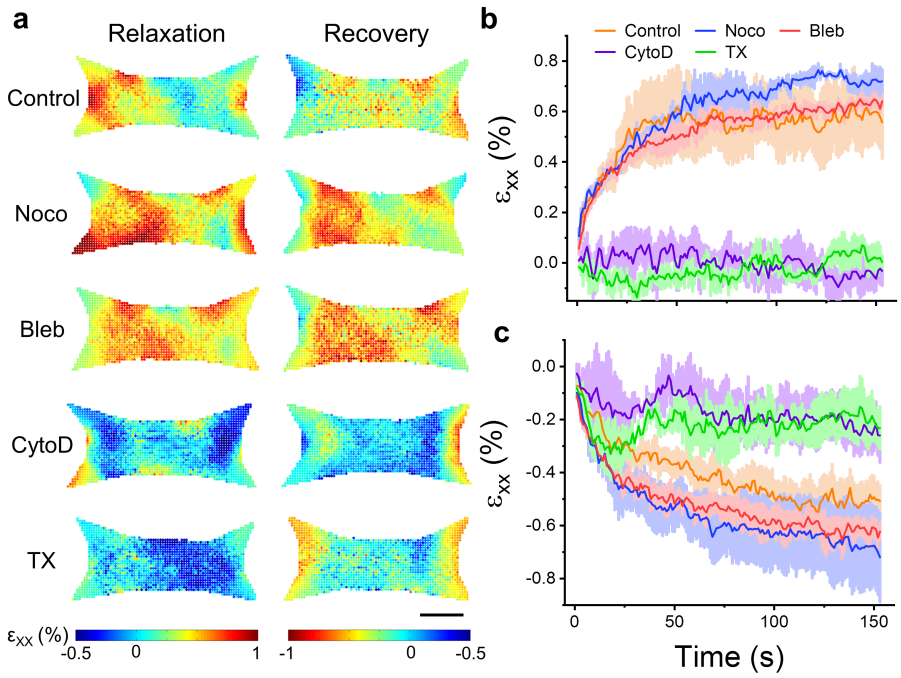

Fig. C.8: Remodeling in the longitudinal direction following changes to microtissues length varies with pharmacological treatments. Spatial distributions of relaxation and recovery in the longitudinal direction after pharmacological treatments are shown in (a). The scale bar represents 100µm. The average (N=3) strain in the x-direction during stress relaxation is shown in (b). The remodeling during stress recovery is shown in (c).

APPENDIX D| SUPPLEMENTARY INFORMATION OF CHAPTER 5

Supplementary information for the manuscript: “Time dependencies in the dynamical mechanical behavior of 3D microtissue cell cultures”.

Additional figures

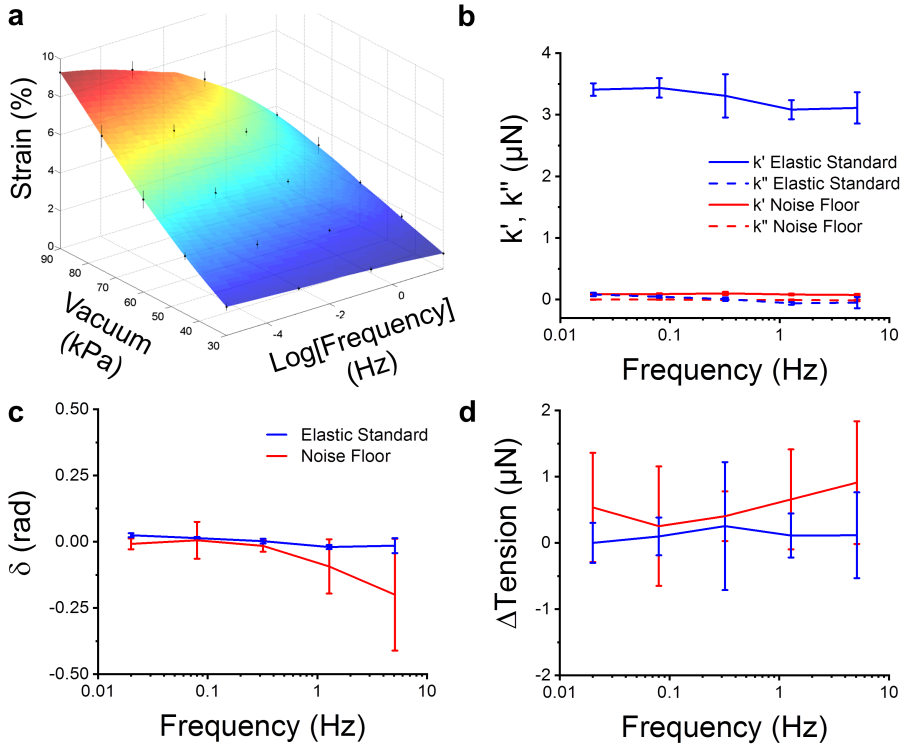

Fig. D.1: Strain amplitude characterization and validation of dynamic mechanical measurements with the MVAS-Force. To account for different oscillatory frequencies leading to different tissue strain amplitudes, microtissue strain was assessed over a range of vacuum pressures and frequencies (the scatter plot in a). A lower frequency and higher vacuum pressure led to greater microtissue strain. The vacuum pressure needed to drive the MVAS-force at a specific strain across the tested frequency range was calculated by modeling the average (N=3) response with a LOWESS surface algorithm. To determine the noise floor of our technique, measurements were taken without an attached microtissue (N=6). Noise floor measurements were all relatively low compared to microtissue measurements and were invariant across the tested frequency range. To further validate our method, an elastic standard (a 70x15μm strip of PDMS) was measured (N=3). As expected, the phase lag was near zero, indicating low internal friction and measurements were also frequency invariant. Error bars represent the standard deviation.

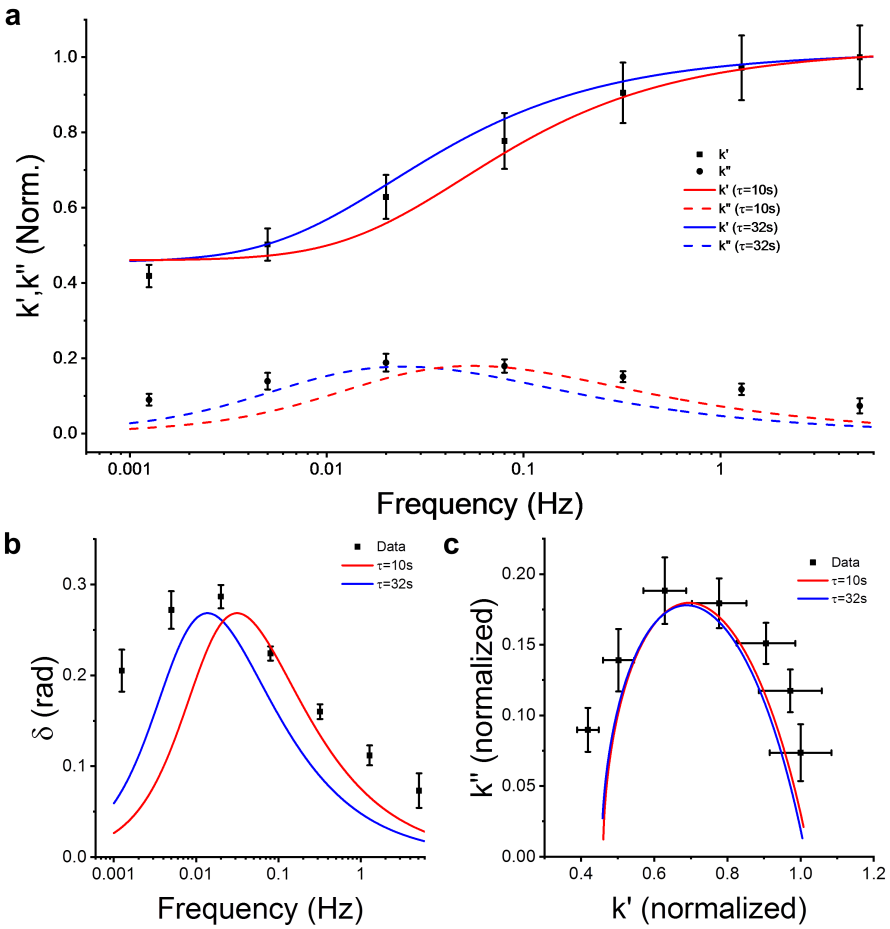

Fig. D.2: The characteristic timescale of oscillatory measurements lies between the characteristic timescales of stress relaxation and recovery. The frequency responses of the average microtissue storage and loss stiffness and phase lag are shown in (a) and (b), respectively. Also plotted are fits with time constants that were obtained after similar amplitude step changes in length in our previous report. The other constants in the models were kept consistent with figure 3c. Stress relaxation occurred at a rate that is too quick while recovery occurs at rate that is too slow compared to explain the dynamic behavior of microtissues when under oscillatory loading.

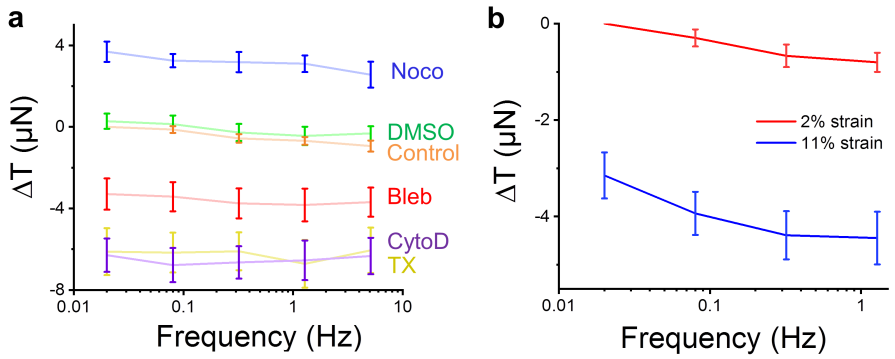

Fig. D.3: The timescale behavior of microtissue prestress under various pharmacological treatments and strain amplitudes. The changes to prestress following pharmacological treatments are shown in (a). Microtubule depolymerization (Noco) increased microtissue prestress while myosin inhibition (Bleb), actin depolymerization (CytoD) and decellularization (TX) decreased the prestress. DMSO, a loading control had no effect compared to the non-treated control. The differences from the control were fairly consistent across the tested frequency range. The change in the prestress under 2% and 11% strain amplitudes are shown in (b). Increasing the strain amplitude decreased the prestress across the entire tested frequency range, and in both cases, the prestress fell with the oscillation rate.

APPENDIX E| SUPPLEMENTARY INFORMATION OF CHAPTER 6

Supplementary information for the manuscript: “Mechanical stretch sustains myofibroblast phenotype and function in microtissues through latent TGF-β1 activation”.

Additional figures

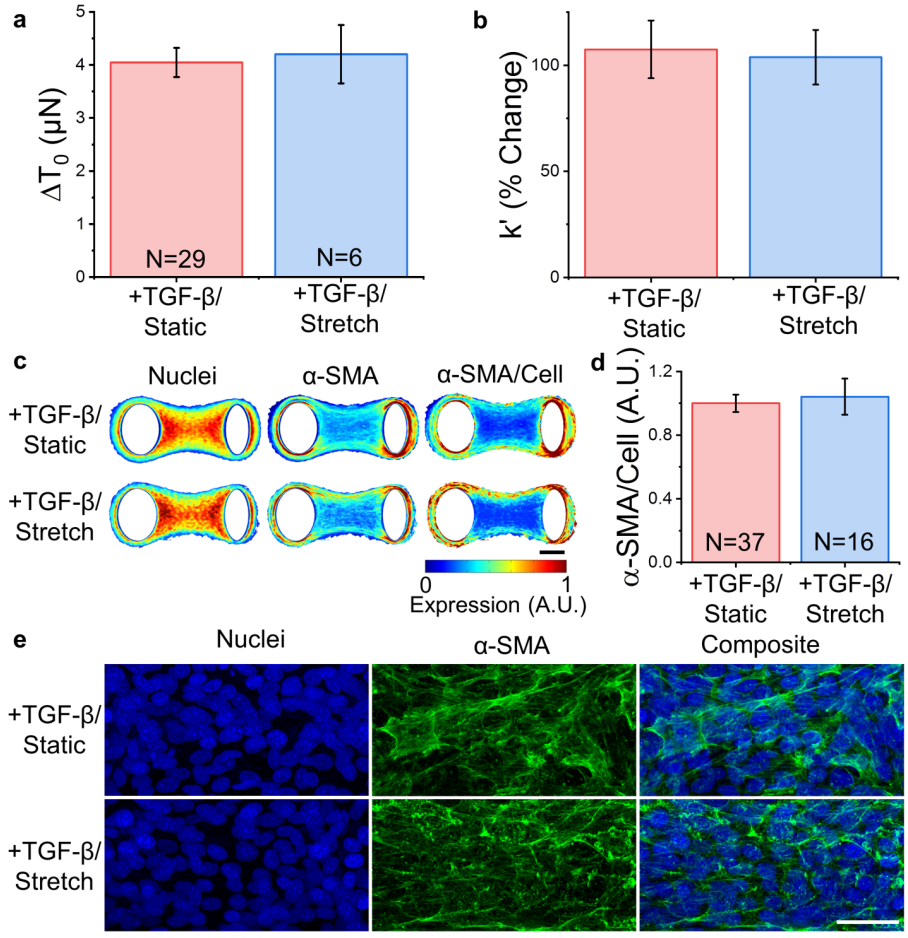

Fig. E.1: Cyclic stretch does not contribute to myofibroblast differentiation in microtissues. Stretching microtissues during TGF-β treatment did not change contractility (a), stiffness (b) or α-SMA staining intensity (c-e) compared to a static control group (t-tests, P>0.05).

REFERENCES

1. Ingber, D. E. Cellular mechanotransduction: putting all the pieces together again. *FASEB J.* **20**, 811–27 (2006).
2. Wang, J. H. C. & Thampatty, B. P. An introductory review of cell mechanobiology. *Biomechanics and Modeling in Mechanobiology* **5**, 1–16 (2006).
3. Kamm, R. D. & Kaazempur-Mofrad, M. R. On the molecular basis for mechanotransduction. *Mech. Chem. Biosyst.* **1**, 201–9 (2004).
4. Mammoto, T., Mammoto, A. & Ingber, D. E. Mechanobiology and developmental control. *Annual review of cell and developmental biology* **29**, 27–61 (2013).
5. Ingber, D. E. Mechanobiology and diseases of mechanotransduction. *Ann. Med.* **35**, 564–77 (2003).
6. Jaalouk, D. E. & Lammerding, J. Mechanotransduction gone awry. *Nature Reviews Molecular Cell Biology* **10**, 63–73 (2009).
7. Fredberg, J. J. *et al.* Airway smooth muscle, tidal stretches, and dynamically determined contractile states. *Am J Respir Crit Care Med* **156**, 1752–1759 (1997).
8. Fredberg, J. J., Inouye, D. S., Mijailovich, S. M. & Butler, J. P. Perturbed equilibrium of myosin binding in airway smooth muscle and its implications in bronchospasm. *Am J Respir Crit Care Med* **159**, 959–967 (1999).
9. Huh, D. *et al.* Reconstituting Organ-Level Lung Functions on a Chip. *Science (80-.).* **328**, (2010).
10. Albinsson, S., Nordström, I. & Hellstrand, P. Stretch of the vascular wall induces smooth muscle differentiation by promoting actin polymerization. *J. Biol. Chem.* **279**, 34849–55 (2004).
11. Jufri, N. F., Mohamedali, A., Avolio, A. & Baker, M. S. Mechanical stretch: physiological and pathological implications for human vascular endothelial cells. *Vasc. Cell* **7**, 8 (2015).
12. Kim, E. H., Oh, N., Jun, M., Ko, K. & Park, S. Effect of cyclic stretching on cell shape and division. *Biochip J.* **9**, 306–312 (2015).
13. Lele, T. P., Thodeti, C. K. & Ingber, D. E. Force meets chemistry: analysis of mechanochemical conversion in focal adhesions using fluorescence recovery after photobleaching. *J. Cell. Biochem.* **97**, 1175–83 (2006).
14. Lele, T. P., Thodeti, C. K., Pendse, J. & Ingber, D. E. Investigating complexity of protein-protein interactions in focal adhesions. *Biochem. Biophys. Res. Commun.* **369**, 929–34 (2008).
15. Vogel, V. & Sheetz, M. Local force and geometry sensing regulate cell functions. *Nat. Rev. Mol. Cell Biol.* **7**, 265–275 (2006).
16. Youm, J. B. *et al.* Role of Stretch-activated Channels in the Heart: Action Potential and Ca2+ Transients. *Mechanosensitivity in Cells and Tissues* **12**, 1–20 (2005).
17. Eyckmans, J., Boudou, T., Yu, X. & Chen, C. S. A Hitchhiker's Guide to Mechanobiology. *Dev. Cell* **21**, 35–47 (2011).
18. Heisenberg, C.-P. & Bellaïche, Y. Forces in tissue morphogenesis and patterning. *Cell* **153**, 948–62 (2013).
19. Hove, J. R. *et al.* Intracardiac fluid forces are an essential epigenetic factor for embryonic cardiogenesis. *Nature* **421**, 172–177 (2003).
20. Engler, A. J., Sen, S., Sweeney, H. L. & Discher, D. E. Matrix elasticity directs stem cell lineage specification. *Cell* **126**, 677–89 (2006).
21. Vining, K. H. & Mooney, D. J. Mechanical forces direct stem cell behaviour in development and regeneration. *Nature Reviews Molecular Cell Biology* **18**, 728–742 (2017).
22. Viswanathan, P. *et al.* 3D surface topology guides stem cell adhesion and differentiation. *Biomaterials* **52**, 140–147 (2015).
23. Elsaadany, M. *et al.* Equiaxial Strain Modulates Adipose-derived Stem Cell Differentiation within 3D Biphasic Scaffolds towards Annulus Fibrosus. *Sci. Rep.* **7**, (2017).
24. Chen, J. H., Liu, C., You, L. & Simmons, C. A. Boning up on Wolff's Law: Mechanical regulation of the cells that make and maintain bone. *J. Biomech.* **43**, 108–118 (2010).
25. Chatterjee, S. Endothelial mechanotransduction, redox signaling and the regulation of vascular inflammatory pathways. *Frontiers in Physiology* **9**, (2018).
26. Liu, F. *et al.* Feedback amplification of fibrosis through matrix stiffening and COX-2 suppression. *J. Cell Biol.* **190**, 693–706 (2010).

27. Georges, P. C. *et al.* Increased stiffness of the rat liver precedes matrix deposition: Implications for fibrosis. *Am. J. Physiol. - Gastrointest. Liver Physiol.* **293**, (2007).
28. Huang, X. *et al.* Matrix stiffness-induced myofibroblast differentiation is mediated by intrinsic mechanotransduction. *Am. J. Respir. Cell Mol. Biol.* **47**, 340–348 (2012).
29. Maksym, G. N., Deng, L., Fairbank, N. J., Lall, C. A. & Connolly, S. C. Beneficial and harmful effects of oscillatory mechanical strain on airway smooth muscle. *Can J Physiol Pharmacol* **83**, 913–922 (2005).
30. Johnson, P. R. A. *et al.* Extracellular matrix proteins modulate asthmatic airway smooth muscle cell proliferation via an autocrine mechanism. *J. Allergy Clin. Immunol.* **113**, 690–696 (2004).
31. Hakkinen, K. M., Harunaga, J. S., Doyle, A. D. & Yamada, K. M. Direct comparisons of the morphology, migration, cell adhesions, and actin cytoskeleton of fibroblasts in four different three-dimensional extracellular matrices. *Tissue Eng. Part A* **17**, 713–24 (2011).
32. Birgersdotter, A., Sandberg, R. & Ernberg, I. Gene expression perturbation in vitro - A growing case for three-dimensional (3D) culture systems. *Seminars in Cancer Biology* **15**, 405–412 (2005).
33. Griffith, L. G. & Swartz, M. A. Capturing complex 3D tissue physiology in vitro. *Nat Rev Mol Cell Biol* **7**, 211–224 (2006).
34. Pampaloni, F., Reynaud, E. G. & Stelzer, E. H. K. K. *The third dimension bridges the gap between cell culture and live tissue*. *Nature Reviews Molecular Cell Biology* **8**, 839–845 (Nature Publishing Group, 2007).
35. Janmey, P. A. Mechanical properties of cytoskeletal polymers. *Curr. Opin. Cell Biol.* **3**, 4–11 (1991).
36. Goode, B. L. & Eck, M. J. Mechanism and Function of Formins in the Control of Actin Assembly. *Annu. Rev. Biochem.* **76**, 593–627 (2007).
37. Korenbaum, E. *et al.* The role of profilin in actin polymerization and nucleotide exchange. *Biochemistry* **37**, 9274–9283 (1998).
38. Bamburg, J. R. & Bernstein, B. W. Roles of ADF/cofilin in actin polymerization and beyond. *F1000 Biology Reports* **2**, (2010).
39. Bernstein, B. W. & Bamburg, J. R. Actin-ATP hydrolysis is a major energy drain for neurons. *J. Neurosci.* **23**, 1–6 (2003).
40. Pollard, T. D. & Borisy, G. G. Cellular motility driven by assembly and disassembly of actin filaments. *Cell* **112**, 453–465 (2003).
41. Gardel, M. L. *et al.* Prestressed F-actin networks cross-linked by hinged filamins replicate mechanical properties of cells. *Proc. Natl. Acad. Sci. U. S. A.* **103**, 1762–1767 (2006).
42. Mitchison, T. & Kirschner, M. Dynamic instability of microtubule growth. *Nature* **312**, 237–242 (1984).
43. Walker, R. A. *et al.* Dynamic instability of individual microtubules analyzed by video light microscopy: rate constants and transition frequencies. **107**, (1988).
44. Kent, I. A. & Lele, T. P. Microtubule-based force generation. *Wiley Interdisciplinary Reviews: Nanomedicine and Nanobiotechnology* **9**, (2017).
45. Ingber, D. E., Heidemann, S. R., Lamoureux, P. & Buxbaum, R. E. controversies in physiology Opposing views on tensegrity as a structural framework for understanding cell mechanics. *J Appl Physiol* **89**, 1663–1678 (2000).
46. Rape, A., Guo, W. & Wang, Y. Microtubule depolymerization induces traction force increase through two distinct pathways. *J. Cell Sci.* **124**, 4233–4240 (2011).
47. Stamenović, D., Mijailovich, S. M., Tolić-Nørrelykke, I. M., Chen, J. & Wang, N. Cell prestress. II. Contribution of microtubules. *Am. J. Physiol. Physiol.* **282**, C617–C624 (2002).
48. Buehler, M. J. Mechanical players - The role of intermediate filaments in cell mechanics and organization. *Biophysical Journal* **105**, 1733–1734 (2013).
49. Herrmann, H., Bär, H., Kreplak, L., Strelkov, S. V. & Aebi, U. Intermediate filaments: From cell architecture to nanomechanics. *Nature Reviews Molecular Cell Biology* **8**, 562–573 (2007).
50. Qin, Z., Kreplak, L. & Buehler, M. J. Hierarchical Structure Controls Nanomechanical Properties of Vimentin Intermediate Filaments. *PLoS One* **4**, e7294 (2009).
51. Vicente-Manzanares, M., Ma, X., Adelstein, R. S. & Horwitz, A. R. *Non-muscle myosin II takes centre stage in cell adhesion and migration*. *Nature Reviews Molecular Cell Biology* **10**, 778–790 (2009).
52. Tojkander, S. *et al.* A molecular pathway for myosin II recruitment to stress fibers. *Curr. Biol.* **21**, 539–550 (2011).
53. Wang, H. B., Dembo, M., Hanks, S. K. & Wang, Y. Focal adhesion kinase is involved in mechanosensing

during fibroblast migration. *Proc. Natl. Acad. Sci. U. S. A.* **98**, 11295–300 (2001).
54. Prager-Khoutorsky, M. *et al.* Fibroblast polarization is a matrix-rigidity-dependent process controlled by focal adhesion mechanosensing. *Nat. Cell Biol.* **13**, 1457–65 (2011).
55. Schwarz, U. S., Erdmann, T. & Bischofs, I. B. Focal adhesions as mechanosensors: the two-spring model. *Biosystems.* **83**, 225–32 (2006).
56. Plotnikov, S. V, Pasapera, A. M., Sabass, B. & Waterman, C. M. Force fluctuations within focal adhesions mediate ECM-rigidity sensing to guide directed cell migration. *Cell* **151**, 1513–27 (2012).
57. Wozniak, M. A., Modzelewska, K., Kwong, L. & Keely, P. J. Focal adhesion regulation of cell behavior. *Biochim. Biophys. Acta* **1692**, 103–19 (2004).
58. Wang, N., Butler, J. P. & Ingber, D. E. Mechanotransduction across the cell surface and through the cytoskeleton. *Science (80-.).* **260**, 1124–1127 (1993).
59. Geiger, B., Spatz, J. P. & Bershadsky, A. D. Environmental sensing through focal adhesions. *Nature Reviews Molecular Cell Biology* **10**, 21–33 (2009).
60. Ciobanasu, C., Faivre, B. & Le Clainche, C. Actomyosin-dependent formation of the mechanosensitive talin-vinculin complex reinforces actin anchoring. *Nat. Commun.* **5**, 3095 (2014).
61. Humphries, J. D. *et al.* Vinculin controls focal adhesion formation by direct interactions with talin and actin. *J. Cell Biol.* **179**, 1043–1057 (2007).
62. Goldmann, W. H. Role of vinculin in cellular mechanotransduction. *Cell Biol. Int.* **40**, 241–256 (2016).
63. Provenzano, P. P. & Keely, P. J. Mechanical signaling through the cytoskeleton regulates cell proliferation by coordinated focal adhesion and Rho GTPase signaling. *J. Cell Sci.* **124**, 1195–1205 (2011).
64. Haase, K. & Pelling, A. E. Investigating cell mechanics with atomic force microscopy. *J. R. Soc. Interface* **12**, 20140970 (2015).
65. Alcaraz, J. *et al.* Microrheology of human lung epithelial cells measured by atomic force microscopy. *Biophys. J.* **84**, 2071–2079 (2003).
66. Fabry, B. *et al.* Scaling the microrheology of living cells. *Phys Rev Lett* **87**, 148102 (2001).
67. Maksym, G. N. *et al.* Mechanical properties of cultured human airway smooth muscle cells from 0.05 to 0.4 Hz. *J. Appl. Physiol.* **89**, 1619–1632 (2000).
68. Fabry, B. *et al.* Time scale and other invariants of integrative mechanical behavior in living cells. *Phys Rev E Stat Nonlin Soft Matter Phys* **68**, 41914 (2003).
69. Schmidt, C. E., Horwitz, A. F., Lauffenburger, D. A. & Sheetz, M. P. Integrin-cytoskeletal interactions in migrating fibroblasts are dynamic, asymmetric, and regulated. *J. Cell Biol.* **123**, 977–991 (1993).
70. Balland, M. *et al.* Power laws in microrheology experiments on living cells: Comparative analysis and modeling. *Phys. Rev. E - Stat. Nonlinear, Soft Matter Phys.* **74**, (2006).
71. Bausch, A. R., Ziemann, F., Boulbitch, A. A., Jacobson, K. & Sackmann, E. Local measurements of viscoelastic parameters of adherent cell surfaces by magnetic bead microrheometry. *Biophys. J.* **75**, 2038–2049 (1998).
72. Kollmannsberger, P. & Fabry, B. High-force magnetic tweezers with force feedback for biological applications. *Rev. Sci. Instrum.* **78**, (2007).
73. Thoumine, O. & Ott, A. Time scale dependent viscoelastic and contractile regimes in fibroblasts probed by microplate manipulation. *J. Cell Sci.* **110 (Pt 17)**, 2109–16 (1997).
74. Desprat, N., Guiroy, A. & Asnacios, A. Microplates-based rheometer for a single living cell. *Rev. Sci. Instrum.* **77**, 055111 (2006).
75. Fernández, P., Pullarkat, P. A. & Ott, A. A master relation defines the nonlinear viscoelasticity of single fibroblasts. *Biophys. J.* **90**, 3796–3805 (2006).
76. Kollmannsberger, P. & Fabry, B. Linear and Nonlinear Rheology of Living Cells. *Annu. Rev. Mater. Res.* **41**, 75–97 (2011).
77. Moeendarbary, E. & Harris, A. R. Cell mechanics: principles, practices, and prospects. *Wiley Interdiscip. Rev. Syst. Biol. Med.* **6**, 371–88 (2014).
78. Pender, N. & McCulloch, C. A. A. Quantitation of actin polymerization in two human fibroblast sub-types responding to mechanical stretching. *J. Cell Sci.* **100**, 187–93 (1991).
79. Costa, K. D., Hucker, W. J. & Yin, F. C.-P. Buckling of actin stress fibers: A new wrinkle in the cytoskeletal tapestry. *Cell Motil. Cytoskeleton* **52**, 266–274 (2002).
80. Chen, C. *et al.* Fluidization and Resolidification of the Human Bladder Smooth Muscle Cell in Response to Transient Stretch. *PLoS One* **5**, e12035 (2010).

81. Semmrich, C. *et al.* Glass transition and rheological redundancy in F-actin solutions. *Proc. Natl. Acad. Sci. U. S. A.* **104**, 20199–203 (2007).
82. Humphrey, D., Duggan, C., Saha, D., Smith, D. & Käs, J. Active fluidization of polymer networks through molecular motors. *Nature* **416**, 413–416 (2002).
83. Smith, D. *et al.* Molecular Motor-Induced Instabilities and Cross Linkers Determine Biopolymer Organization. *Biophys. J.* **93**, 4445–4452 (2007).
84. Heilbronn, A. Eine neue methode zur bestimmung der viskosität lebender protoplasten. *Jahrb. Wiss. Bot* **61**, 284 (1922).
85. Crick, F. & Hughes, A. F. W. The Physical Properties of Cytoplasm: A Study by Means of the Magnetic Particle Method, Part I. Experimental. *Exp Cell Res* (1950).
86. Moeendarbary, E. *et al.* The cytoplasm of living cells behaves as a poroelastic material. *Nat. Mater.* **12**, 253–261 (2013).
87. Wang, N. *et al.* Cell prestress. I. Stiffness and prestress are closely associated in adherent contractile cells. *Am. J. Physiol. Cell Physiol.* **282**, C606-16 (2002).
88. Ingber, D. E. Tensegrity: the architectural basis of cellular mechanotransduction. *Annu. Rev. Physiol.* **59**, 575–599 (1997).
89. Ingber, D. E. Tensegrity and mechanotransduction. *J. Bodyw. Mov. Ther.* **12**, 198–200 (2008).
90. Brangwynne, C. P. *et al.* Microtubules can bear enhanced compressive loads in living cells because of lateral reinforcement. *J. Cell Biol.* **173**, 733–741 (2006).
91. Krishnan, R. *et al.* Reinforcement versus fluidization in cytoskeletal mechanoresponsiveness. *PLoS One* **4**, e5486 (2009).
92. Trepat, X. *et al.* Universal physical responses to stretch in the living cell. *Nature* **447**, 592–595 (2007).
93. Fung, Y. C. *Biomechanics: Mechanical Properties of Living Tissues*. (Springer-Verlag, 1981).
94. Sato, M., Ohshima, N. & Nerem, R. M. Viscoelastic properties of cultured porcine aortic endothelial cells exposed to shear stress. *J. Biomech.* **29**, 461–467 (1996).
95. Krishnan, R. *et al.* Fluidization, resolidification, and reorientation of the endothelial cell in response to slow tidal stretches. *Am. J. Physiol. Cell Physiol.* **303**, C368-75 (2012).
96. Storm, C., Pastore, J. J., MacKintosh, F. C., Lubensky, T. C. & Janmey, P. A. Nonlinear elasticity in biological gels. *Nature* **435**, 191–194 (2005).
97. Bates, J. H. T. A Recruitment Model of Quasi-Linear Power-Law Stress Adaptation in Lung Tissue. *Ann. Biomed. Eng.* **35**, 1165–1174 (2007).
98. Bates, J. H. T. & Ma, B. A Progressive Rupture Model of Soft Tissue Stress Relaxation. *Ann. Biomed. Eng.* **41**, 1129–1138 (2013).
99. Hoffman, B. D. *et al.* The consensus mechanics of cultured mammalian cells. *Proc. Natl Acad. Sci. Usa* **103**, 10259–10264 (2006).
100. Fredberg, J. J. *et al.* Friction in airway smooth muscle: mechanism, latch, and implications in asthma. *J. Appl. Physiol.* **81**, 2703–2703 (1996).
101. Lenormand, G., Bursac, P., Butler, J. P. & Fredberg, J. J. Out-of-equilibrium dynamics in the cytoskeleton of the living cell. *Phys. Rev. E* **76**, 041901 (2007).
102. Bursac, P. *et al.* Cytoskeletal remodelling and slow dynamics in the living cell. *Nat. Mater.* **4**, 557–561 (2005).
103. Yap, B. & Kamm, R. D. Mechanical deformation of neutrophils into narrow channels induces pseudopod projection and changes in biomechanical properties. *J. Appl. Physiol.* **98**, 1930–1939 (2005).
104. Goto, M., VanBavel, E., Giezeman, M. J. & Spaan, J. A. Vasodilatory effect of pulsatile pressure on coronary resistance vessels. *Circ. Res.* **79**, 1039–45 (1996).
105. Fish, J. E., Ankin, M. G., Kelly, J. F. & Peterman, V. I. Regulation of bronchomotor tone by lung inflation in asthmatic and nonasthmatic subjects. *J Appl Physiol* **50**, 1079–1086 (1981).
106. Fredberg, J. & Fabry, B. The cytoskeleton as a soft glassy material. in *Cytoskeletal Mechanics* (eds. Mofrad, M. R. K. & Kamm, R. D.) 50–70 (Cambridge University Press, 2006). doi:10.1017/CBO9780511607318.004
107. Sollich, P., Lequeux, F., Hebraud, P. & Cates, M. E. Rheology of soft glassy materials. *Phys. Rev. Lett.* **78**, 2020–2023 (1997).
108. Sollich, P. Rheological constitutive equation for a model of soft glassy materials. *Phys. Rev. E* **58**, 738–759 (1998).

109. Biot, M. A. General theory of three-dimensional consolidation. *J. Appl. Phys.* **12**, 155–164 (1941).
110. Biernacka, A., Dobaczewski, M. & Frangogiannis, N. G. TGF-β signaling in fibrosis. *Growth Factors* **29**, 196–202 (2011).
111. Hinz, B. The myofibroblast: Paradigm for a mechanically active cell. *J. Biomech.* **43**, 146–155 (2010).
112. Saums, M. K. *et al.* Mechanically and chemically tunable cell culture system for studying the myofibroblast phenotype. *Langmuir* **30**, 5481–7 (2014).
113. Thorne, J. T. *et al.* Dynamic Reciprocity Between Cells and Their Microenvironment in Reproduction1. *Biol. Reprod.* **92**, (2015).
114. Bissell, M. J. & Aggeler, J. Dynamic reciprocity: how do extracellular matrix and hormones direct gene expression? *Prog. Clin. Biol. Res.* **249**, 251–262 (1987).
115. Lau, A. W., Hoffman, B. D., Davies, A., Crocker, J. C. & Lubensky, T. C. Microrheology, stress fluctuations, and active behavior of living cells. *Phys. Rev. Lett.* **91**, 198101 (2003).
116. Billiar, K. L. The Mechanical Environment of Cells in Collagen Gel Models. in 201–245 (Springer, Berlin, Heidelberg, 2010). doi:10.1007/8415_2010_30
117. Canty, E. G. & Kadler, K. E. Procollagen trafficking, processing and fibrillogenesis. *Journal of Cell Science* **118**, 1341–1353 (2005).
118. Boraschi-Diaz, I., Wang, J., Mort, J. S. & Komarova, S. V. Collagen type i as a ligand for receptor-mediated signaling. *Frontiers in Physics* **5**, (2017).
119. Pedersen, J. A. & Swartz, M. A. Mechanobiology in the Third Dimension. *Ann. Biomed. Eng.* **33**, 1469–1490 (2005).
120. West, A. R. *et al.* Development and characterization of a 3D multicell microtissue culture model of airway smooth muscle. *Am J Physiol Lung Cell Mol Physiol* **304**, L4-16 (2013).
121. Souza, A. G. *et al.* Comparative Assay of 2D and 3D Cell Culture Models: Proliferation, Gene Expression and Anticancer Drug Response. *Curr. Pharm. Des.* **24**, 1689–1694 (2018).
122. Jia, W. *et al.* Effects of three-dimensional collagen scaffolds on the expression profiles and biological functions of glioma cells. *Int. J. Oncol.* **52**, 1787–1800 (2018).
123. Edmondson, R., Broglie, J. J., Adcock, A. F. & Yang, L. Three-dimensional cell culture systems and their applications in drug discovery and cell-based biosensors. *Assay Drug Dev. Technol.* **12**, 207–18 (2014).
124. Legant, W. R. *et al.* Microfabricated tissue gauges to measure and manipulate forces from 3D microtissues. *Proc. Natl. Acad. Sci. U. S. A.* **106**, 10097–10102 (2009).
125. Afshar, M. E. *et al.* A 96-well culture platform enables longitudinal analyses of engineered human skeletal muscle microtissue strength. *bioRxiv* 562819 (2019). doi:10.1101/562819
126. Boudou, T. *et al.* A microfabricated platform to measure and manipulate the mechanics of engineered cardiac microtissues. *Tissue Eng. - Part A* **18**, 910–919 (2012).
127. Boudou W. R.; Mu, A.; Borochin, M. A.; Thavandiran, N.; Radisic, M.; Zandstra, P. W.; Epstein, J. A.; Margulies, K. B.; Chen, C. S., T. . L. A microfabricated platform to measure and manipulate the mechanics of engineered cardiac microtissues. *Tissue Eng. Part A* **18**, 910–919 (2012).
128. Zhao, R. *et al.* Decoupling Cell and Matrix Mechanics in Engineered Microtissues Using Magnetically Actuated Microcantilevers. *Adv. Mater.* **25**, 1699–1705 (2013).
129. Liu, A. S. *et al.* Matrix viscoplasticity and its shielding by active mechanics in microtissue models: experiments and mathematical modeling. *Sci. Rep.* **6**, 33919 (2016).
130. Frantz, C., Stewart, K. M. & Weaver, V. M. The extracellular matrix at a glance. *Journal of Cell Science* **123**, 4195–4200 (2010).
131. Hosoyama, K. *et al.* Electroconductive materials as biomimetic platforms for tissue regeneration. *Biotechnology Advances* **37**, 444–458 (2019).
132. Klezovitch, O. & Vasioukhin, V. Cadherin signaling: Keeping cells in touch. *F1000Research* **4**, (2015).
133. Vaday, G. G. & Lider, O. Extracellular matrix moieties, cytokines, and enzymes: dynamic effects on immune cell behavior and inflammation. *J. Leukoc. Biol.* **67**, 149–159 (2000).
134. Discher, D. E., Janmey, P. & Wang, Y. Tissue cells feel and respond to the stiffness of their substrate. *Science* **310**, 1139–43 (2005).
135. Yeung, T. *et al.* Effects of substrate stiffness on cell morphology, cytoskeletal structure, and adhesion. *Cell Motil. Cytoskeleton* **60**, 24–34 (2005).
136. Pelham, R. J. & Wang, Y. -l. Cell locomotion and focal adhesions are regulated by substrate flexibility. *Proc.*

Natl. Acad. Sci. **94**, 13661–13665 (1997).
137. Lo, C. M., Wang, H. B., Dembo, M. & Wang, Y. L. Cell movement is guided by the rigidity of the substrate. *Biophys. J.* **79**, 144–52 (2000).
138. Chagnon-Lessard, S., Jean-Ruel, H., Godin, M. & Pelling, A. E. Cellular orientation is guided by strain gradients. *Integr. Biol.* **66**, 409–422 (2017).
139. Chen, K. *et al.* Role of boundary conditions in determining cell alignment in response to stretch. *Proc. Natl. Acad. Sci. U. S. A.* **115**, 986–991 (2018).
140. Geiger, B. & Bershadsky, A. Exploring the neighborhood: Adhesion-coupled cell mechanosensors. *Cell* **110**, 139–142 (2002).
141. Qiu, X. & Müller, U. Mechanically gated ion channels in mammalian hair cells. *Frontiers in Cellular Neuroscience* **12**, (2018).
142. Sachs, F. Stretch-activated ion channels: What are they? *Physiology* **25**, 50–56 (2010).
143. Lele, T. P. *et al.* Mechanical forces alter zyxin unbinding kinetics within focal adhesions of living cells. *J. Cell. Physiol.* **207**, 187–94 (2006).
144. Van Aelst, L. & D'Souza-Schorey, C. Rho GTPases and signaling networks. *Genes and Development* **11**, 2295–2322 (1997).
145. Fukata, M. & Kaibuchi, K. Rho-family GTPases in cadherin-mediated cell-cell adhesion. *Nature Reviews Molecular Cell Biology* **2**, 887–897 (2001).
146. Hoon, J., Tan, M. & Koh, C.-G. The Regulation of Cellular Responses to Mechanical Cues by Rho GTPases. *Cells* **5**, 17 (2016).
147. Totsukawa, G. *et al.* Distinct roles of ROCK (Rho-kinase) and MLCK in spatial regulation of MLC phosphorylation for assembly of stress fibers and focal adhesions in 3T3 fibroblasts. *J. Cell Biol.* **150**, 797–806 (2000).
148. Ohashi, K. *et al.* Rho-associated kinase ROCK activates LIM-kinase 1 by phosphorylation at threonine 508 within the activation loop. *J. Biol. Chem.* **275**, 3577–3582 (2000).
149. Lessey, E. C., Guilluy, C. & Burridge, K. From mechanical force to RhoA activation. *Biochemistry* **51**, 7420–7432 (2012).
150. Guilluy, C. *et al.* The Rho GEFs LARG and GEF-H1 regulate the mechanical response to force on integrins. *Nat. Cell Biol.* **13**, 722–728 (2011).
151. Gawlak, G. *et al.* Paxillin mediates stretch-induced Rho signaling and endothelial permeability via assembly of paxillin-p42/44MAPK-GEF-H1 complex. *FASEB J.* **28**, 3249–3260 (2014).
152. Peng, F. *et al.* Mechanical stretch-induced RhoA activation is mediated by the RhoGEF Vav2 in mesangial cells. *Cell. Signal.* **22**, 34–40 (2010).
153. Abiko, H. *et al.* Rho guanine nucleotide exchange factors involved in cyclic-stretch-induced reorientation of vascular endothelial cells. *J. Cell Sci.* **128**, 1683–1695 (2015).
154. Burridge, K. & Wittchen, E. S. The tension mounts: stress fibers as force-generating mechanotransducers. *J. Cell Biol.* **200**, 9–19 (2013).
155. Deng, L., Fairbank, N. J., Fabry, B., Smith, P. G. & Maksym, G. N. Localized mechanical stress induces time-dependent actin cytoskeletal remodeling and stiffening in cultured airway smooth muscle cells. *Am J Physiol Cell Physiol* **287**, C440-8 (2004).
156. Ehrlicher, A. J., Nakamura, F., Hartwig, J. H., Weitz, D. A. & Stossel, T. P. Mechanical strain in actin networks regulates FilGAP and integrin binding to filamin A. *Nature* **478**, 260–263 (2011).
157. Greenberg, M. J., Arpağ, G., Tüzel, E. & Ostap, E. M. A Perspective on the Role of Myosins as Mechanosensors. *Biophys. J.* **110**, 2568–2576 (2016).
158. Le, S. *et al.* Mechanotransmission and Mechanosensing of Human alpha-Actinin 1. *Cell Rep.* **21**, 2714–2723 (2017).
159. Krendel, M., Zenke, F. T. & Bokoch, G. M. Nucleotide exchange factor GEF-H1 mediates cross-talk between microtubules and the actin cytoskeleton. *Nat. Cell Biol.* **4**, 294–301 (2002).
160. Fujiwara, S., Ohashi, K., Mashiko, T., Kondo, H. & Mizuno, K. Interplay between Solo and keratin filaments is crucial for mechanical forceinduced stress fiber reinforcement. *Mol. Biol. Cell* **27**, 954–966 (2016).
161. Jiu, Y. *et al.* Vimentin intermediate filaments control actin stress fiber assembly through GEF-H1 and RhoA. *J. Cell Sci.* **130**, 892–902 (2017).
162. Leckband, D. E. & de Rooij, J. Cadherin Adhesion and Mechanotransduction. *Annu. Rev. Cell Dev. Biol.* **30**,

291–315 (2014).
163. Liu, Z. *et al.* Mechanical tugging force regulates the size of cell-cell junctions. *Proc. Natl. Acad. Sci. U. S. A.* **107**, 9944–9949 (2010).
164. Tabdili, H. *et al.* Cadherin-dependent mechanotransduction depends on ligand identity but not affinity. *J. Cell Sci.* **125**, 4362–4371 (2012).
165. Thomas, W. A. *et al.* α-Catenin and vinculin cooperate to promote high E-cadherin-based adhesion strength. *J. Biol. Chem.* **288**, 4957–4969 (2013).
166. Ladoux, B. *et al.* Strength dependence of cadherin-mediated adhesions. *Biophys. J.* **98**, 534–542 (2010).
167. Le Duc, Q. *et al.* Vinculin potentiates E-cadherin mechanosensing and is recruited to actin-anchored sites within adherens junctions in a myosin II-dependent manner. *J. Cell Biol.* **189**, 1107–1115 (2010).
168. Haupt, B. J., Pelling, A. E. & Horton, M. A. Integrated Confocal and Scanning Probe Microscopy for Biomedical Research. *Sci. World J.* **6**, 1609–1618 (2006).
169. Haase, K., Shendruk, T. N. & Pelling, A. E. Rapid dynamics of cell-shape recovery in response to local deformations. *Soft Matter* **13**, 567–577 (2017).
170. Guck, J. Some thoughts on the future of cell mechanics. *Biophysical Reviews* **11**, 667–670 (2019).
171. Mohammed, D. *et al.* Innovative tools for mechanobiology: Unraveling outside-in and inside-out mechanotransduction. *Frontiers in Bioengineering and Biotechnology* **7**, 162 (2019).
172. Schönfelder, J., De Sancho, D. & Perez-Jimenez, R. The Power of Force: Insights into the Protein Folding Process Using Single-Molecule Force Spectroscopy. *J. Mol. Biol.* **428**, 4245–4257 (2016).
173. Charrier, E. E., Pogoda, K., Wells, R. G. & Janmey, P. A. Control of cell morphology and differentiation by substrates with independently tunable elasticity and viscous dissipation. *Nat. Commun.* **9**, 449 (2018).
174. Hinz, B. The myofibroblast in connective tissue repair and regeneration. in *Regenerative Medicine and Biomaterials for the Repair of Connective Tissues* 39–80 (Elsevier, 2010). doi:10.1533/9781845697792.39
175. Desmoulière, A., Chaponnier, C. & Gabbiani, G. Tissue repair, contraction, and the myofibroblast. *Wound Repair and Regeneration* **13**, 7–12 (2005).
176. Hinz, B. Formation and function of the myofibroblast during tissue repair. *Journal of Investigative Dermatology* **127**, 526–537 (2007).
177. Hinz, B. *et al.* The myofibroblast: one function, multiple origins. *Am. J. Pathol.* **170**, 1807–1816 (2007).
178. Tomasek, J. J., Gabbiani, G., Hinz, B., Chaponnier, C. & Brown, R. A. Myofibroblasts and mechano: Regulation of connective tissue remodelling. *Nature Reviews Molecular Cell Biology* **3**, 349–363 (2002).
179. Gabbiani, G. The myofibroblast in wound healing and fibrocontractive diseases. *J. Pathol.* **200**, 500–503 (2003).
180. Friedlander, M. Fibrosis and diseases of the eye. *Journal of Clinical Investigation* **117**, 576–586 (2007).
181. Travers, J. G., Kamal, F. A., Robbins, J., Yutzey, K. E. & Blaxall, B. C. Cardiac fibrosis: The fibroblast awakens. *Circulation Research* **118**, 1021–1040 (2016).
182. Hinz, B. Myofibroblasts. *Exp. Eye Res.* **142**, 56–70 (2016).
183. Dreier, B. *et al.* Substratum Compliance Modulates Corneal Fibroblast to Myofibroblast Transformation. *Investig. Opthalmology Vis. Sci.* **54**, 5901 (2013).
184. SHI, Y. *et al.* Substrate stiffness influences TGF-β1-induced differentiation of bronchial fibroblasts into myofibroblasts in airway remodeling. *Mol. Med. Rep.* **7**, 419–424 (2013).
185. Merryman, W. D. *et al.* Synergistic effects of cyclic tension and transforming growth factor-β1 on the aortic valve myofibroblast. *Cardiovasc. Pathol.* **16**, 268–276 (2007).
186. Waxman, A. S., Kornreich, B. G., Gould, R. A., Sydney Moïse, N. & Butcher, J. T. Interactions between TGFβ1 and cyclic strain in modulation of myofibroblastic differentiation of canine mitral valve interstitial cells in 3D culture. *J. Vet. Cardiol.* **14**, 211–221 (2012).
187. Gould, R. A. *et al.* Cyclic strain anisotropy regulates valvular interstitial cell phenotype and tissue remodeling in three-dimensional culture. *Acta Biomater.* **8**, 1710–1719 (2012).
188. Thomas Freeberg, M., Thatcher, T. H. & Sime, P. J. Assessment of Myofibroblast Phenotype with Cellular Stretch on Substrates of Different Stiffness. in *A107. ENGINEERED AND REMODELLED MATRIX COMPARTMENTS* A2560–A2560 (American Thoracic Society, 2019). doi:10.1164/ajrccm-conference.2019.199.1_MeetingAbstracts.A2560
189. Wipff, P. J., Rifkin, D. B., Meister, J. J. & Hinz, B. Myofibroblast contraction activates latent TGF-β1 from the extracellular matrix. *J. Cell Biol.* **179**, 1311–1323 (2007).

190. Annes, J. P., Munger, J. S. & Rifkin, D. B. Making sense of latent TGFβ activation. *Journal of Cell Science* **116**, 217–224 (2003).
191. Miyazono, K., Olofsson, A., Colosetti, P. & Heldin, C. H. A role of the latent TGF-beta 1-binding protein in the assembly and secretion of TGF-beta 1. *EMBO J.* **10**, 1091–1101 (1991).
192. Froese, A. R. *et al.* Stretch-induced Activation of Transforming Growth Factor-β_1 in Pulmonary Fibrosis. *Am. J. Respir. Crit. Care Med.* **194**, 84–96 (2016).
193. Buscemi, L. *et al.* The single-molecule mechanics of the latent TGF-β1 complex. *Curr. Biol.* **21**, 2046–2054 (2011).
194. Shi, M. *et al.* Latent TGF-β structure and activation. *Nature* **474**, 343–351 (2011).
195. Tremblay, D., Chagnon-Lessard, S., Mirzaei, M., Pelling, A. E. & Godin, M. A microscale anisotropic biaxial cell stretching device for applications in mechanobiology. *Biotechnol. Lett.* **36**, 657–665 (2014).
196. Walker, M., Godin, M. & Pelling, A. E. A vacuum-actuated microtissue stretcher for long-term exposure to oscillatory strain within a 3D matrix. *Biomed. Microdevices* **20**, 43 (2018).
197. Lee, J., Cuddihy, M. J. & Kotov, N. A. Three-Dimensional Cell Culture Matrices: State of the Art. *Tissue Eng. Part B Rev.* **14**, 61–86 (2008).
198. Seliktar, D., Black, R. A., Vito, R. P. & Nerem, R. M. Dynamic Mechanical Conditioning of Collagen-Gel Blood Vessel Constructs Induces Remodeling In Vitro. *Ann. Biomed. Eng.* **28**, 351–362 (2000).
199. Tomei, A. A., Boschetti, F., Gervaso, F. & Swartz, M. A. 3D collagen cultures under well-defined dynamic strain: A novel strain device with a porous elastomeric support. *Biotechnol. Bioeng.* **103**, 217–225 (2009).
200. Stegemann, J. P. & Nerem, R. M. Phenotype modulation in vascular tissue engineering using biochemical and mechanical stimulation. *Ann. Biomed. Eng.* **31**, 391–402 (2003).
201. Kanda, K., Matsuda, T. & Oka, T. Mechanical stress induced cellular orientation and phenotypic modulation of 3-D cultured smooth muscle cells. *ASAIO J.* **39**, M686-90
202. Kim, B.-S., Nikolovski, J., Bonadio, J. & Mooney, D. J. Cyclic mechanical strain regulates the development of engineered smooth muscle tissue. *Nat. Biotechnol.* **17**, 979–983 (1999).
203. Martin, I., Wendt, D. & Heberer, M. The role of bioreactors in tissue engineering. *Trends Biotechnol.* **22**, 80–86 (2004).
204. Xu, F. *et al.* A microfabricated magnetic actuation device for mechanical conditioning of arrays of 3D microtissues. *Lab Chip* **15**, 2496–503 (2015).
205. Cui, Y. *et al.* Cyclic stretching of soft substrates induces spreading and growth. **6**, 6333 (2015).
206. Lucas T., B. D. . K., Lucas, B. D. & Kanade, T. An iterative image registration technique with an application to stereo vision. in *Proceedings of the International Joint Conference on Artificial Intelligence* 674–679 (Morgan Kaufmann Publishers Inc., 1981).
207. Shyu, K.-G. Cellular and molecular effects of mechanical stretch on vascular cells and cardiac myocytes. *Clin. Sci.* **116**, (2009).
208. Williams, B. Mechanical influences on vascular smooth muscle cell function. *J. Hypertens.* **16**, 1921–9 (1998).
209. Smith, P. G., Garcia, R. & Kogerman, L. Strain reorganizes focal adhesions and cytoskeleton in cultured airway smooth muscle cells. *Exp Cell Res* **232**, 127–136 (1997).
210. Smith, P. G., Deng, L., Fredberg, J. J. & Maksym, G. N. Mechanical strain increases cell stiffness through cytoskeletal filament reorganization. *Am J Physiol Lung Cell Mol Physiol* **285**, L456-63 (2003).
211. Yoshigi, M., Hoffman, L. M., Jensen, C. C., Yost, H. J. & Beckerle, M. C. Mechanical force mobilizes zyxin from focal adhesions to actin filaments and regulates cytoskeletal reinforcement. *J. Cell Biol.* **171**, (2005).
212. Hirata, H., Tatsumi, H. & Sokabe, M. Mechanical forces facilitate actin polymerization at focal adhesions in a zyxin-dependent manner. *J. Cell Sci.* **121**, 2795–2804 (2008).
213. Riehl, B. D., Park, J.-H., Kwon, I. K. & Lim, J. Y. Mechanical stretching for tissue engineering: two-dimensional and three-dimensional constructs. *Tissue Eng. Part B. Rev.* **18**, 288–300 (2012).
214. Han, W. M. *et al.* Macro- to microscale strain transfer in fibrous tissues is heterogeneous and tissue-specific. *Biophys. J.* **105**, 807–17 (2013).
215. LaPrad, A. S., Szabo, T. L., Suki, B. & Lutchen, K. R. Tidal stretches do not modulate responsiveness of intact airways in vitro. *J. Appl. Physiol.* **109**, 295–304 (2010).
216. Wakatsuki, T., Kolodney, M. S., Zahalak, G. I. & Elson, E. L. Cell mechanics studied by a reconstituted model tissue. *Biophys. J.* **79**, 2353–68 (2000).

217. Barocas A. G.: Moon, Tranquillo, R. T., V. H. . M. The fibroblast-populated collagen microsphere assay of cell traction force—part 2: measurement of the cell traction parameter. *J. Biomech. Eng.* **117**, 161–170 (1995).
218. Tranquillo, R. T., Durrani, M. A. & Moon, A. G. Tissue engineering science: consequences of cell traction force. *Cytotechnology* **10**, 225–50 (1992).
219. Brown, R. A., Prajapati, R., McGrouther, D. A., Yannas, I. V. & Eastwood, M. Tensional homeostasis in dermal fibroblasts: Mechanical responses to mechanical loading in three-dimensional substrates. *J. Cell. Physiol.* **175**, 323–332 (1998).
220. Eastwood, M., McGrouther, D. A. & Brown, R. A. Fibroblast responses to mechanical forces. *Proc. Inst. Mech. Eng. H.* **212**, 85–92 (1998).
221. Nekouzadeh, A., Pryse, K. M., Elson, E. L. & Genin, G. M. Stretch-activated force shedding, force recovery, and cytoskeletal remodeling in contractile fibroblasts. *J. Biomech.* **41**, 2964–2971 (2008).
222. Lee, S.-L. *et al.* Physically-Induced Cytoskeleton Remodeling of Cells in Three-Dimensional Culture. *PLoS One* **7**, e45512 (2012).
223. Wille, J. J., Elson, E. L. & Okamoto, R. J. Cellular and Matrix Mechanics of Bioartificial Tissues During Continuous Cyclic Stretch. *Ann. Biomed. Eng.* **34**, 1678–1690 (2006).
224. Gosens, R. *et al.* Role of caveolin-1 in p42/p44 MAP kinase activation and proliferation of human airway smooth muscle. *Am. J. Physiol. Cell. Mol. Physiol.* **291**, L523–L534 (2006).
225. Wang, N. *et al.* Mechanical behavior in living cells consistent with the tensegrity model. *Proc. Natl. Acad. Sci. U. S. A.* **98**, 7765–70 (2001).
226. Andrews, G. F. The living substance as such; and as organism. *J Morph* **12**, 1–179 (1897).
227. Mathews, A. P. & Whitcher, B. R. The importance of mechanical shock in protoplasmic activity. *Am. J. Physiol. Content* **8**, 300–306 (1903).
228. Angerer, C. A. The effects of mechanical agitation on the relative viscosity of amoeba protoplasm. *J Cell Comp Physiol* **8**, 329–345 (1936).
229. Kohlrausch, R. Theorie des elektrischen Rückstandes in der Leidner Flasche. *Ann. der Phys. und Chemie* **91**, 179–213 (1854).
230. Williams, G. & Watts, D. C. Non-symmetrical dielectric relaxation behaviour arising from a simple empirical decay function. *Trans. Faraday Soc.* **66**, 80 (1970).
231. Lindsey, C. P. & Patterson, G. D. Detailed comparison of the Williams–Watts and Cole–Davidson functions. *J. Chem. Phys.* **73**, 3348–3357 (1980).
232. Hoppin, F. G. Parenchymal mechanics and asthma. in *Chest* **107**, 140S-144S (American College of Chest Physicians, 1995).
233. Wolff, L., Fernández, P. & Kroy, K. Resolving the Stiffening-Softening Paradox in Cell Mechanics. *PLoS One* **7**, e40063 (2012).
234. Gardel, M. L. *et al.* Elastic behavior of cross-linked and bundled actin networks. *Science (80-.).* **304**, 1301–1305 (2004).
235. Trepat, X. *et al.* Viscoelasticity of human alveolar epithelial cells subjected to stretch. *Am. J. Physiol. Lung Cell. Mol. Physiol.* **287**, L1025-34 (2004).
236. Marquez, J. P., Genin, G. M., Zahalak, G. I. & Elson, E. L. The relationship between cell and tissue strain in three-dimensional bio-artificial tissues. *Biophys. J.* **88**, 778–89 (2005).
237. Matthews, B. D., Overby, D. R., Mannix, R. & Ingber, D. E. Cellular adaptation to mechanical stress: role of integrins, Rho, cytoskeletal tension and mechanosensitive ion channels. *J. Cell Sci.* **119**, 508–518 (2006).
238. Glogauer, M. *et al.* Calcium ions and tyrosine phosphorylation interact coordinately with actin to regulate cytoprotective responses to stretching. 11–21 (1997).
239. Giannone, G., Jiang, G., Sutton, D. H., Critchley, D. R. & Sheetz, M. P. Talin1 is critical for force-dependent reinforcement of initial integrin–cytoskeleton bonds but not tyrosine kinase activation. *J. Cell Biol.* **163**, 409–419 (2003).
240. Choquet, D., Felsenfeld, D. P. & Sheetz, M. P. Extracellular matrix rigidity causes strengthening of integrin-cytoskeleton linkages. *Cell* **88**, 39–48 (1997).
241. Bershadsky, A. D., Balaban, N. Q. & Geiger, B. Adhesion-Dependent Cell Mechanosensitivity. *Annu. Rev. Cell Dev. Biol.* **19**, 677–695 (2003).
242. Balaban, N. Q. *et al.* Force and focal adhesion assembly: a close relationship studied using elastic

micropatterned substrates. *Nat. Cell Biol.* **3**, 466–72 (2001).
243. Lan, B. *et al.* Transient stretch induces cytoskeletal fluidization through the severing action of cofilin. *Am. J. Physiol. Lung Cell. Mol. Physiol.* **314**, L799–L807 (2018).
244. Pernier, J. *et al.* Myosin 1b is an actin depolymerase. *Nat. Commun.* **10**, (2019).
245. Rosner, S. R. *et al.* The actin regulator zyxin reinforces airway smooth muscle and accumulates in airways of fatal asthmatics. *PLoS One* **12**, e0171728 (2017).
246. Tang-Schomer, M. D., Patel, A. R., Baas, P. W. & Smith, D. H. Mechanical breaking of microtubules in axons during dynamic stretch injury underlies delayed elasticity, microtubule disassembly, and axon degeneration. **24**, (2010).
247. McElhaney, J. *Biomechanics* . *Mechanical Properties of Living Tissues* by Y. C. Fung. *Med. Phys.* **9**, 788–789 (1982).
248. Wang, N. & Ingber, D. E. Control of cytoskeletal mechanics by extracellular matrix, cell shape, and mechanical tension. *Biophys. J.* **66**, 2181–2189 (1994).
249. Schmid-Schönbein, G. W., Sung, K. L., Tözeren, H., Skalak, R. & Chien, S. Passive mechanical properties of human leukocytes. *Biophys. J.* **36**, 243–56 (1981).
250. Wagenseil, J. E., Wakatsuki, T., Okamoto, R. J., Zahalak, G. I. & Elson, E. L. One-Dimensional Viscoelastic Behavior of Fibroblast Populated Collagen Matrices. *J. Biomech. Eng.* **125**, 719 (2003).
251. Eyckmans, J. & Chen, C. S. 3D culture models of tissues under tension. *Comment. Spec. ISSUE 3D CELL Biol.* (2017). doi:10.1242/jcs.198630
252. Hildebrandt, J. Comparison of mathematical models for cat lung and viscoelastic balloon derived by Laplace transform methods from pressure-volume data. *Bull. Math. Biophys.* **31**, 651–67 (1969).
253. Fung, Y. *Elasticity of soft tissues in simple elongation*. *AMERICAN JOURNAL OF PHYSIOLOGY* **213**, 1532–1544 (1967).
254. Rambousky, R., Moske, M. & Samwer, K. Structural relaxation and viscous flow in amorphous ZrAlCu. *Zeitschrift für Phys. B Condens. Matter* **99**, 387–391 (1995).
255. Schröter, K. & Donth, E. Comparison of shear response with other properties at the dynamic glass transition of different glassformers. *J. Non. Cryst. Solids* **307–310**, 270–280 (2002).
256. Wiechert, E. Gesetze der elastischen Nachwirkung für constante Temperatur. *Ann. Phys.* **286**, 546–570 (1893).
257. Meng, F., Pritchard, R. H. & Terentjev, E. M. Stress Relaxation, Dynamics, and Plasticity of Transient Polymer Networks. *Macromolecules* **49**, 2843–2852 (2016).
258. Naumis, G. G. & Phillips, J. C. Bifurcation of stretched exponential relaxation in microscopically homogeneous glasses. *J. Non. Cryst. Solids* **358**, 893–897 (2012).
259. Phillips, J. C. Stretched exponential relaxation in molecular and electronic glasses. *Reports Prog. Phys.* **59**, 1133–1207 (1996).
260. Fredberg, J. J. & Dimitrije, A. On the imperfect elasticity of lung tissue. *J Appl Physiol* **67**, 2408–19 (1989).
261. Fredberg, J. J., Bunk, D., Ingenito, E. & Shore, S. A. Tissue resistance and the contractile state of lung parenchyma. *J. Appl. Physiol.* **74**, 1387–1397 (1993).
262. Trepat, X., Lenormand, G. & Fredberg, J. J. Universality in cell mechanics. *Soft Matter* **4**, 1750 (2008).
263. Bates, J. H., Maksym, G. N., Navajas, D. & Suki, B. Lung tissue rheology and 1/f noise. *Ann. Biomed. Eng.* **22**, 674–81 (1994).
264. Doehring, T. C., Carew, E. O. & Vesely, I. The effect of strain rate on the viscoelastic response of aortic valve tissue: a direct-fit approach. *Ann. Biomed. Eng.* **32**, 223–32 (2004).
265. Provenzano, P., Lakes, R., Keenan, T. & Vanderby, Jr., R. Nonlinear Ligament Viscoelasticity. *Ann. Biomed. Eng.* **29**, 908–914 (2001).
266. Navajas, D., Mijailovich, S., Glass, G. M., Stamenovic, D. & Fredberg, J. J. Dynamic response of the isolated passive rat diaphragm strip. *J. Appl. Physiol.* **73**, 2681–2692 (1992).
267. Smith, B. A., Tolloczko, B., Martin, J. G. & Grütter, P. Probing the viscoelastic behavior of cultured airway smooth muscle cells with atomic force microscopy: stiffening induced by contractile agonist. *Biophys. J.* **88**, 2994–3007 (2005).
268. MacKintosh, F. C. & Schmidt, C. F. Active cellular materials. *Current Opinion in Cell Biology* **22**, 29–35 (2010).
269. Walker, M., Rizzuto, P., Godin, M. & Pelling, A. E. Structural and mechanical remodeling of the cytoskeleton

studied in 3D microtissues under acute dynamic stretch. *bioRxiv* 780312 (2019). doi:10.1101/780312
270. Walker, M., Godin, M., Harden, J. & Pelling, A. Time dependencies in the dynamic mechanical behavior of 3D microtissue cell cultures. *bioRxiv* 2020.01.25.916874 (2020). doi:10.1101/2020.01.25.916874
271. Shen, X., Wu, M. F., Tepper, R. S. & Gunst, S. J. Mechanisms for the mechanical response of airway smooth muscle to length oscillation. *J Appl Physiol* **83**, 731–738 (1997).
272. Brown, R. A., Talas, G., Porter, R. A., McGrouther, D. A. & Eastwood, M. Balanced mechanical forces and microtubule contribution to fibroblast contraction. *J. Cell. Physiol.* **169**, 439–447 (1996).
273. Darby, I. A. & Hewitson, T. D. Fibroblast Differentiation in Wound Healing and Fibrosis. *Int. Rev. Cytol.* **257**, 143–179 (2007).
274. Wells, R. G. Tissue mechanics and fibrosis. *Biochimica et Biophysica Acta - Molecular Basis of Disease* **1832**, 884–890 (2013).
275. Meng, X. M., Nikolic-Paterson, D. J. & Lan, H. Y. TGF-β: The master regulator of fibrosis. *Nature Reviews Nephrology* **12**, 325–338 (2016).
276. Evans, R. A., Tian, Y. C., Steadman, R. & Phillips, A. O. TGF-β1-mediated fibroblast-myofibroblast terminal differentiation - The role of Smad proteins. *Exp. Cell Res.* **282**, 90–100 (2003).
277. Desmouliere, A., Geinoz, A., Gabbiani, F. & Gabbiani, G. Transforming growth factor-β1 induces α-smooth muscle actin expression in granulation tissue myofibroblasts and in quiescent and growing cultured fibroblasts. *J. Cell Biol.* **122**, 103–111 (1993).
278. Sime, P. J., Xing, Z., Graham, F. L., Csaky, K. G. & Gauldie, J. Adenovector-mediated gene transfer of active transforming growth factor- β1 induces prolonged severe fibrosis in rat lung. *J. Clin. Invest.* **100**, 768–776 (1997).
279. Zhao, J. *et al.* Spatial-specific TGF-beta1 adenoviral expression determines morphogenetic phenotypes in embryonic mouse lung. *Eur. J. Cell Biol.* **78**, 715–25 (1999).
280. Zhang, Y. E. Non-Smad pathways in TGF-β signaling. *Cell Research* **19**, 128–139 (2009).
281. Haycock, J. W. 3D cell culture: a review of current approaches and techniques. *Methods Mol Biol* **695**, 1–15 (2011).
282. Asmani, M. *et al.* Fibrotic microtissue array to predict anti-fibrosis drug efficacy. *Nat. Commun.* **9**, 2066 (2018).
283. Vaughan, M. B., Howard, E. W. & Tomasek, J. J. Transforming growth factor-β1 promotes the morphological and functional differentiation of the myofibroblast. *Exp. Cell Res.* **257**, 180–189 (2000).
284. Lee, S. H. & Dominguez, R. Regulation of actin cytoskeleton dynamics in cells. *Molecules and cells* **29**, 311–325 (2010).
285. Amano, M. *et al.* Phosphorylation and activation of myosin by Rho-associated kinase (Rho- kinase). *J. Biol. Chem.* **271**, 20246–20249 (1996).
286. Zhou, H. *et al.* Fasudil hydrochloride hydrate, a Rho-kinase inhibitor, suppresses high glucose-induced proliferation and collagen synthesis in rat cardiac fibroblasts. *Clin. Exp. Pharmacol. Physiol.* **38**, 387–394 (2011).
287. Fukushima, M. *et al.* Fasudil hydrochloride hydrate, a Rho-kinase (ROCK) inhibitor, suppresses collagen production and enhances collagenase activity in hepatic stellate cells. *Liver Int.* **25**, 829–838 (2005).
288. Itoh, Y., Kimoto, K., Imaizumi, M. & Nakatsuka, K. Inhibition of RhoA/Rho-kinase pathway suppresses the expression of type I collagen induced by TGF-β2 in human retinal pigment epithelial cells. *Exp. Eye Res.* **84**, 464–472 (2007).
289. Booth, A. J. *et al.* Acellular normal and fibrotic human lung matrices as a culture system for in vitro investigation. *Am. J. Respir. Crit. Care Med.* **186**, 866–876 (2012).
290. Brown, A. C., Fiore, V. F., Sulchek, T. A. & Barker, T. H. Physical and chemical microenvironmental cues orthogonally control the degree and duration of fibrosis-associated epithelial-to-mesenchymal transitions. *J. Pathol.* **229**, 25–35 (2013).
291. Perepelyuk, M. *et al.* Hepatic stellate cells and portal fibroblasts are the major cellular sources of collagens and lysyl oxidases in normal liver and early after injury. *Am. J. Physiol. - Gastrointest. Liver Physiol.* **304**, (2013).
292. Bond, J. E. *et al.* Wound contraction is attenuated by fasudil inhibition of Rho-associated kinase. *Plast. Reconstr. Surg.* **128**, (2011).
293. Ho, T. J., Huang, C. C., Huang, C. Y. & Lin, W. T. Fasudil, a Rho-kinase inhibitor, protects against excessive

endurance exercise training-induced cardiac hypertrophy, apoptosis and fibrosis in rats. *Eur. J. Appl. Physiol.* **112**, 2943–2955 (2012).
294. Huang, X. *et al.* Relaxin Regulates Myofibroblast Contractility and Protects against Lung Fibrosis. *Am. J. Pathol.* **179**, 2751–2765 (2011).
295. Goffin, J. M. *et al.* Focal adhesion size controls tension-dependent recruitment of alpha-smooth muscle actin to stress fibers\njcb.200506179 [pii] 10.1083/jcb.200506179. *J Cell Biol* **172**, 259–268 (2006).
296. Hinz, B. Masters and servants of the force: The role of matrix adhesions in myofibroblast force perception and transmission. *European Journal of Cell Biology* **85**, 175–181 (2006).
297. Blaauboer, M. E., Smit, T. H., Hanemaaijer, R., Stoop, R. & Everts, V. Cyclic mechanical stretch reduces myofibroblast differentiation of primary lung fibroblasts. *Biochem. Biophys. Res. Commun.* **404**, 23–27 (2011).
298. Desmouliere, A., Redard, M., Darby, I. & Gabbiani, G. Apoptosis mediates the decrease in cellularity during the transition between granulation tissue and scar. *Am. J. Pathol.* **146**, 56–66 (1995).
299. Kollmannsberger, P., Bidan, C. M., Dunlop, J. W. C., Fratzl, P. & Vogel, V. Tensile forces drive a reversible fibroblast-to-myofibroblast transition during tissue growth in engineered clefts. *Sci. Adv.* **4**, (2018).
300. Nagaraju, C. K. *et al.* Myofibroblast Phenotype and Reversibility of Fibrosis in Patients With End-Stage Heart Failure. *J. Am. Coll. Cardiol.* **73**, 2267–2282 (2019).
301. Hecker, L., Jagirdar, R., Jin, T. & Thannickal, V. J. Reversible differentiation of myofibroblasts by MyoD. *Exp. Cell Res.* **317**, 1914–1921 (2011).
302. Abaci, H. E. & Shuler, M. L. Human-on-a-chip design strategies and principles for physiologically based pharmacokinetics/pharmacodynamics modeling. *Integr. Biol. (United Kingdom)* **7**, 383–391 (2015).
303. Wehrle-Haller, B. & Imhof, B. A. Actin, microtubules and focal adhesion dynamics during cell migration. *Int. J. Biochem. Cell Biol.* **35**, 39–50 (2003).